UNIVERSITY OF CALIFORNIA,
IRVINE

Optical Properties and Chemical Composition of Brown Carbon Aerosols

DISSERTATION

submitted in partial satisfaction of the requirements
for the degree of

DOCTOR OF PHILOSOPHY

in Chemistry

by

Paige Kuuipo Aiona

Dissertation Committee:
Professor Sergey Nizkorodov, Chair
Professor Barbara Finlayson-Pitts
Professor Craig Murray

2018

ProQuest Page

Dedication

To my family

"Without deviation from the norm, progress is not possible."

-Frank Zappa

"Whatever You Are, Be A Good One."

-Abraham Lincoln

Table of Contents

Table of Figures

Table of Tables

Acknowledgements

First I would like to thank my advisor Professor Sergey Nizkorodov. He has been extremely helpful since before I even started at the University of California, Irvine (UCI). He was willing to meet with me while I was applying to graduate schools and show me his lab. He was the one to call and inform me that I had gotten accepted. I knew before rotations that his group would be the right fit for me and my graduate career. From helping me with my NSF and Ford Foundation essays, which got me funding for the past four years, to getting me through my qualifying exam, Sergey was always supportive and willing to do whatever he could to help me be successful. He was also very understanding of the ups and downs I experienced throughout graduate school, which is what I am most thankful for. I know there were times that I was frustrating to work with, but he remained patient through it all. Without his guidance the past nearly six years I may not have ended up working my dream job at the SCAQMD.

I would also like to thank my committee members Professor Finlayson-Pitts and Professor Murray. I enjoyed working with you throughout my qualifying exams and my defense. Some of your questions may have been challenging but they helped me be a better scientist. Julie Lee, a previous post-doc in our group also deserves my thanks. She helped trained me when I first started at UCI and collaborated with me for a large portion of my time here.

The other graduate student members of our group also deserve thanks. Groups meetings, lunches, game nights, and BBQs were always enjoyable with all of you around. Thank you Mallory Hinks for sharing an office with me all these years. Thank you Kurtis Malecha for always dealing with all my questions, especially about preparing for my dissertation the past few months. Thank you Amanda MacMillan and Sandy Blair for always being great friends and

research group. She got me into environmental research working with samples from different water systems. I worked with Dr. Clark and Dr. de Bruyn all four years I was at Chapman and enjoyed every minute of it. I was able to get experience in the laboratory, writing manuscripts, and presenting at conference. Working for them really set me up for success and for that I could not be more grateful.

Last, but certainly not least, I need to thank my friends and family. I've made many friends throughout my college career here in California, most of them through cat rescue. I would like to thank each and every one of them for every time they put up with me being stressed out about school or changing plans because I was too busy to hang out. Thank you all for being my family while I was away from my family. I also want to give a special shout out to my friends back in Hawaii for dealing with me growing up and being the most unique group of people I've had the honor of knowing.

And of course my actual family. So many of you have been there for me my whole life that I do not have enough time or space to thank all of you individually for everything you have done for me, but I am going to try. Aunty Tania, thank you for pushing me to go to Kamehameha and get my education jump started and for everything you have done to help me since I've been in California. Thank you Jo for giving me a place to stay when I first moved out here and for always being a blast to spend time with. Ashlee, you are the greatest cousin and have given me so much relief being able to enjoy life, even through all the stressful times I've had. Aunty Donna, even though you live so far away you have always related to me and everything I was going through. To all me other aunts, uncles, and cousins, you all deserve thanks as well. Isaiah, you and I don't always relate, but I have enjoyed that we have gotten closer the past few years and that we are able to have meaningful conversations now. No matter how much taller than me

you are you'll still always be my little brother. Thank you to my grandparents, with a special thank you to my Grandma Pearl. You helped raise me into a strong and independent woman and have been there for me every step of the way. Getting to spend time with you through all the hustle and bustle of work and school is such a relief and brings me so much happiness. I am so happy that you get to see me finally become a doctor.

Now for the real MVPs, my parents. I know I haven't always been the easiest daughter to raise, being as stubborn, hard-headed, and impatient as I am, but thank you so much for the way you raised me. You were always supportive in everything I did and made sure I had everything I needed and so much more. You put up with all my temper tantrums, OCD, anxiety, and all the times I wanted to spend time with my friends instead of being at home. I never appreciated all of that back then, but I sure do now. Dad, you were always a strong and hard-working father figure. You always provided for us and I will always remember you sticking up for me when the boys would push me around in elementary school. You helped me learn to stick up for myself. Mom, you are the hardest one to write to because you gave me all your emotionality and now I can't get through this without crying. But that's not a bad thing. You taught me to be caring, loving, and compassionate. Although it is difficult sometimes to not be able to keep my emotions contained, it is much better than being an emotionless person. You always said I was my worst critic and you were always right. You let me push myself because you knew that is what would get me the furthest in life and look at me now. Thank you for every time you told me that if it wasn't hard that it wasn't worth it and that being challenged just meant I was getting my money's worth in school. Thank you for every late night phone call freaking out over something silly and for all the tears you've dealt with. I could not have gotten to where I am without either of you being there for me every step of the way and for that I will always be eternally gratefully.

Curriculum Vitae
Paige Aiona

Education:

Ph.D. in Chemistry, University of California, Irvine. Anticipated Graduation June 2018.

M.S. in Chemistry, University of California, Irvine. Awarded Fall 2016.

B.S. in Chemistry, Chapman University, Minor in Mathematics. Graduated May 2012.

Research Experience:

Graduate Research Assistant, February 2013 – Present
Department of Chemistry, University of California, Irvine

Undergraduate Research Manager, August 2011 – May 2012
Schmid College of Science and Technology; Chemistry, Chapman University

Undergraduate Research Assistant, February 2009 – August 2011
Schmid College of Science and Technology; Chemistry, Chapman University

Teaching Experience:

General Chemistry Laboratory Lecturer, August 2016 – May 2017
Schmid College of Science and Technology; Chemistry, Chapman University

Graduate Mentor, June – September 2013 and June – August 2015
Department of Chemistry, University of California, Irvine

Graduate Teaching Assistant, September 2012 – June 2013
Department of Chemistry, University of California, Irvine

AirUCI Workshop Teaching Assistant, June 2013
Department of Chemistry, University of California, Irvine

Undergraduate Student Grader, August 2011 – May 2012
Schmid College of Science and Technology; Chemistry, Chapman University

Work Experience:

Assistant Air Quality Chemist, September 2017 – Present
South Coast Air Quality Management District

Office Assistant, August 2011 – May 2012
Schmid College of Science and Technology; Chemistry, Chapman University

Publications:

- **Aiona, P. K.,** Luek, H. L., Timko, S. A., Powers, L. C., Gonsior, M., Nizkorodov, S. A., Effect of photolysis on absorption and fluorescence spectra of light-absorbing secondary organic aerosols. ACS Earth Space Chem., 2, 235-245, 2018.
- Montoya-Aguilera, J., Hinks, M. L., **Aiona, P. K.**, Wingen, L. M., Horne, J. R., Zhu, S., Dabdub, D., Laskin, A., Laskin, J., Lin, P., Nizkorodov, S. A., Reactive uptake of ammonia by biogenic and anthropogenic organic aerosols. In *Multiphase Environmental Chemistry in the Atmosphere (ACS Symposium Series)*; Hunt, S., Laskin, A., Nizkorodov, S. A., Eds.; 2018.
- **Aiona, P. K.**, Lee, H. J., Leslie, R., Lin, P., Laskin, A., Laskin, J., Nizkorodov, S. A., Photochemistry of products of the aqueous reaction of methylglyoxal with ammonium sulfate. ACS Earth Space Chem., 1, 522-532, 2017.
- **Aiona, P. K.**, Lee, H. J., Lin, P. Heller, F., Laskin, A., Laskin, J., Nizkorodov, S., A role for 2-methyl pyrrole in the browning of 4-oxopentanal and limonene secondary organic aerosol. Environ. Sci. Technol., 51, 11048-11056, 2017.
- Lin, P., **Aiona, P. K.**, Li, Y., Shiraiwa, M., Laskin, J., Nizkorodov, S. A., Laskin, A., Molecular characterization of brown carbon in biomass burning aerosol. Environ. Sci. Technol., 50, 11815-11824, 2016.
- Romonosky, D. E., Ali, N. N., Saiduddin, M. N., Wu, M., Lee, H. J., **Aiona, P. K.**, Nizkorodov, S. A., Effective absorption cross sections and photolysis rates of anthropogenic and biogenic secondary organic aerosols. Atmos. Environ., 130, 172-179, 2016.
- Clark, C.D., De Bruyn, W. J., **Aiona, P.**, Temporal variation in optical properties of chromophoric dissolved organic matter (CDOM) in Southern California coastal waters with near-shore kelp and seagrass. Limnol. Oceanogr., *61*(1), 32-46, 2016.
- Fooshee, D. R., **Aiona, P. K.**, Laskin, A., Laskin, J., Nizkorodov, S. A., Baldi, P., Atmospheric oxidation of squalene: Molecular study using cobra modeling and high-resolution mass spectrometry. Environ. Sci. Technol., 49, 13304-13313, 2015.
- Lee, H. J., **Aiona, P. K.**, Laskin, A., Laskin, J., Nizkorodov, S. A., Effect of solar radiation on the optical properties and molecular composition of laboratory proxies of atmospheric brown carbon. Environ. Sci. Technol., *48*(17), 10217-10226, 2014.
- Clark, C. D., **Aiona, P.**, Keller, J. K., De Bruyn, W. J., Optical characterization and distribution of chromophoric dissolved organic matter (CDOM) in soil porewater from a salt marsh ecosystem. Mar. Ecol.: Prog. Ser., 516, 71-83, 2014.
- De Bruyn, W.J., Clark, C.D., Ottelle, K., **Aiona, P.**, Photodegradation of phenanthrene as a function of natural water variables modeling fresh to marine environments. Mar. Pollut. Bull., *64*(3), 532-538, 2012.
- Clark, C.D., De Bruyn, W. J., Hirsch, C.M., **Aiona, P.**, Diel cycles of hydrogen peroxide in marine bathing waters in Southern California, USA: in situ surf-zone measurements. Mar. Pollut. Bull., 60, 2284-2288, 2010.
- **Aiona, P. K**., MacMillan, A. C., Lee, H. J., Zhang, X., Helgestad, T., Novak, G., Lin, P., Laskin, J., Laskin, A., Bertram, T. H., Cappa, C., Nizkorodov, S. A., Effects of Humidity, NOx, and Ammonia on the Optical Properties and Molecular Composition of Photo-oxidized Naphthalene Secondary Organic Aerosols. ACS Earth Space Chem.. In Prep.
- Clark, C.D., **Aiona, P.**, De Bruyn, W. J., Brahm, B., Optical properties of chromophoric dissolved organic matter in the surface waters and sediment porewaters of a Southern California freshwater natural treatment wetland system. Environ. Sci. Technol., In Prep.

Oral Presentations:

- Conference of Ford Fellows, Irvine, CA, Sept. 2014. *Analysis of brown carbon in aerosols and the aqueous phase.*
- 248th American Chemical Society National Meeting, San Francisco, CA, Aug. 2014. *Analysis of brown carbon in aerosols and the aqueous phase.*

Poster Presentations:

- 35th Annual American Association for Aerosol Research Conference, Portland, OR, Oct. 2016. *Exploring potential brown carbon chromophores with mass spectrometry and NMR.*
- 33nd Informal Symposium on Kinetics and Photochemical Processes in the Atmosphere, Irvine, CA, March 2016. *Effects of humidity, NO_x, and ammonia on the optical properties and molecular composition of photo-oxidized naphthalene secondary organic aerosols.*
- International Chemical Congress of Pacific Basin Societies, Honolulu, HI, Dec. 2015. *Effects of humidity, NO_x, and ammonia on the optical properties and molecular composition of photo-oxidized naphthalene secondary organic aerosols.*
- Conference of Ford Fellows, Washington, D.C., Sept. 2015. *Effects of ammonia on aerosol composition.*
- 32nd Informal Symposium on Kinetics and Photochemical Processes in the Atmosphere, Northridge, CA, April 2015. *Absorption coefficient, molecular composition, and photodegradation of different types of brown carbon aerosols.*
- 243rd American Chemical Society National Meeting, San Diego, CA, March 2012. *Association of optical properties of chromophoric dissolved organic matter in soil porewaters with seasonal variations in dated sediment cores.*
- 43rd American Chemical Society Western Regional Meeting, Pasadena, CA, Nov. 2011. *Analysis of Chromophoric Dissolved organic matter (CDOM) in a Southern California freshwater natural treatment wetland system (NTWS).*
- Fourth International Water Association Specialty Conference on "Natural Organic Matter: From Source to Tap and Beyond," Costa Mesa, CA, July 2011. *Optical characterization of NOM in surface water and sediment porewater in Southern California wetlands: comparison of a restored salt marsh to a natural treatment wetland system.*
- Schmid College of Science Student Research Fair and Student Undergraduate Research Fair and Creative Scholars, Orange, CA, May 2011. *Biological influences and photodegradation of chromophoric dissolved organic matter (CDOM) produced by sea grass and kelp in Southern California coastal waters.*
- Southern California Undergraduate Research Conference in Chemistry and Biochemistry, Santa Barbara, CA, April 2011. *Analysis of chromophoric dissolved organic matter (CDOM) in a Southern California salt marsh with relationship to sediment depth.*
- 241st American Chemical Society National Meeting, Anaheim, CA, March 2011. *Optical characterization of chromophoric dissolved organic matter in sediment pore waters of a Southern Californian salt marsh.*
- Schmid College of Science and Technology Research Fair, Orange, CA, April 2010. *Diel studies of hydrogen peroxide production and cycling in urban-impacted Southern California coastal receiving waters.*
- Schmid College of Science and Technology Research Day, Orange, CA, April 2009. *Spatial and temporal measurements of hydrogen peroxide concentrations in recreational marine bathing waters in Southern California.*

Fellowships:
- Graduate Research Fellowship, National Science Foundation: Awarded 2014
- Ford Foundation Pre-doctoral Fellowship: Awarded 2014

Honors, Awards, and Scholarships:
- Associated Graduate Students (AGS) Travel Grant, University of California, Irvine: Fall 2015
- Cheverton Award Finalist, Chapman University: May 2012
- Graduated Magna Cum Laude, Chapman University: May 2012
- Outstanding Leadership as President of American Chemical Society, Chapman University and the Faculty of Chemistry: April 2012
- Special Recognition and Special Achievement-American Chemical Society, Chapman University and the Faculty of Chemistry: April 2012
- Outstanding Senior Chemistry, Chapman University and the Faculty of Chemistry: April 2012
- Program Honors, Chapman University and the Faculty of Chemistry: April 2012
- The Om and Saraswati Bahethi Scholarship, American Meteorological Society: 2011-2012
- Outstanding Chemistry Student at Chapman University, American Chemical Society Orange County Section: 2011-2012
- Shuichi, Katsu & Itsuyo Suga Scholarship, Hawaii Community Foundation: 2011-2012
- Chancellors List, Chapman University: Fall 2008, Spring 2009, Spring 2011, Spring 2012
- Deans Scholarship, Chapman University: 2008-2009, 2009-2010, 2010-2011, 2011-2012
- Chapman Grant, Chapman University: 2008-2009, 2009-2010, 2010-2011, 2011-2012
- Office of Hawaiian Affairs Higher Education Scholarship Program, Hawaii Community Foundation: 2009-2012
- Kaiulani Home for Girls Trust Scholarship, Hawaii Community Foundation: 2009-2012
- Gamma Beta Phi Scholarship, Chapman University: Fall 2011
- Norris Foundation Scholarship, Chapman University: 2010-2011
- National Science and Mathematics Access to Retain Talent (SMART) Grant: 2010-2011
- Na Ho`okama a Pauahi Scholarship, Kamehameha Schools: 2008-2011

Associations and Leadership Experience:
- American Association for Aerosol Research (AAAR), May 2016 – present
- Iota Sigma Pi National Honor Society for Women in Chemistry, February 2013 – present
- American Chemical Society, August 2009 – present
- Gamma Beta Phi Honor Society, May 2009 – May 2012
- American Society of Limnologists and Oceanographers (ASLO), 2010 – 2011

Outreach/Volunteer Work:
- UCI Chemistry Outreach Program: November 2015
- Guide for AirUCI Lab Tours: April 2015 and October 2015
- Scientist in the Room at the Boys and Girls Club: June 2015
- Organized Lab Tour for Lennox Math, Science & Technology Academy: October 2014
- Science Day at the Santa Ana Zoo: October 2009, October 2010, and October 2011
- Magic @ the Library: December 2009, April 2010, and December 2010
- Relay for Life: March 2010
- Science and Nature at the Park (SNAP): February 2010
- Caring Friends Cat Rescue: November 2008 – present

Abstract of the Dissertation

Optical Properties and Chemical Composition of Brown Carbon Aerosols

By

Paige Kuuipo Aiona

Doctor of Philosophy in Chemistry

University of California, Irvine, 2018

Professor Sergey A. Nizkorodov, Chair

Organic aerosols in the atmosphere range in color from white to brown to black and each type contributes differently to the atmospheric radiative energy budget. White aerosols scatter radiation causing a cooling effect, while black aerosols reduce this cooling by absorbing radiation and converting it into heat. The contribution of brown aerosols, also known as "brown carbon" (BrC), to this radiative forcing carries the most uncertainty due to its unique light-absorbing properties and chemical composition. Primary BrC is produced by biomass burning and other combustion processes, while secondary BrC is formed by a variety of atmospheric processes. To better quantify the ability of BrC to absorb near-UV and visible radiation, methods like UV-Vis and fluorescence spectroscopy are used to analyze its optical properties. In this dissertation, UV-Vis spectroscopy is used to determine the mass absorption coefficient of secondary BrC formed via the reaction of nitrogen-containing compounds, such as ammonia and amines, with several dicarbonyls, as well as through gas-phase photooxidation of a variety of aromatic precursors via the hydroxyl radical. Fluorescence spectroscopy is also used to characterize fluorescence yields and spectra of BrC. Additionally, different high-resolution mass spectrometry techniques have been used in order to characterize the different compounds that could be consider chromophores that contribute to this type of aerosols brown color. This color can be compromised by atmospheric aging, such as exposure to sunlight. By combining spectroscopy and mass spectrometry methods, the loss of BrC's ability to absorb radiation upon UV exposure is used to determine its kinetics, as well as pin-point specific compounds that may be responsible for light absorption. This dissertation provides a comparison of the properties of BrC produced by different atmospherically-relevant systems and precursors, aiding in a better overall understanding of the influence of BrC on the climate.

Chapter 1 Introduction

1.1. Background and Motivation

1.1.1. Organic Aerosols

An aerosol is composed of a liquid or solid that is suspended in a gas, usually in air. Atmospheric aerosols can cause population health issues, decrease visibility, and influence climate and weather. Photochemical reactions in cities such as Los Angeles and coal burning and pollution in places like Beijing result in large concentrations of aerosol particles referred to as "smog," which significantly reduces visibility in these areas.[1, 2] Health issues arise from the stress that inhalation of foreign particulates exerts on the body, and include cardiovascular and respiratory problems, as well as possible effects on the central nervous and reproductive systems.[3-5] Direct effects on climate are related to the interaction of aerosols with solar radiation. Scattering of incoming solar radiation reduces the amount of solar energy that reaches the Earth's surfaces causing a predominantly cooling effect. The opposing absorption traps this radiation in the lower atmosphere and converts it into heat. Aerosols also have an indirect effect on climate by altering cloud properties, for example, by making the cloud droplets more numerous and smaller in droplet diameter, which results in an increased cloud albedo.[6-8] While the basic physical principles of the climate effects of aerosols are understood, the complexity of these processes and multiple unaccounted feedbacks between them result in large uncertainties in calculating the effect of aerosols on the radiative energy budget in the atmosphere. For this reason, optical and hygroscopic properties of aerosol particles are actively investigated by atmospheric scientists.

Aerosols in the atmosphere are produced by both primary and secondary sources and have been found to contain mineral species, primary biological aerosol particles, black carbon, inorganic species, and organic species.[7, 9] Particles that predominantly contain organic species

are referred to as organic aerosols (OA) and are the main type of aerosol discussed within this thesis. Primary organic aerosols (POA) are emitted directly into the atmosphere by vehicle exhaust, fossil fuel combustion, biomass burning, and sea salt spray. Secondary organic aerosols (SOA) are produced by biogenic and anthropogenic volatile organic compounds (VOCs) undergoing different types of atmosphere processes, including: heterogeneous uptake of VOC precursors onto the surface of particles, gas-phase VOC reactions with oxidants, such as ozone (O_3), the nitrate radical (NO_3), and the hydroxyl radical (OH), followed by condensation into particles, and aqueous photochemical processing of VOCs in fog and cloud droplets followed by evaporation. Once formed, POA and SOA can then undergo further aging processes that alter their chemical and physical properties. [10-13]

1.1.2. Brown Carbon Aerosols

OA have a range of optical properties, from predominantly scattering to strongly absorbing, that are related to their direct effects on climate. Particles that do not contain strongly-absorbing species, such as sea-spray or forest haze scatter radiation and produce a cooling effect. In contrast, strongly-absorbing aerosols, such as black carbon formed by incomplete combustion and certain types of mineral dust, scatter and absorb radiation. An aerosols scattering ability can be represented using a single-scattering albedo (SSA), the ratio of its scattering to its total extinction.[14] The larger the albedo the greater the scattering, for example, values greater than ~0.85 are expected to result in cooling, while smaller values have significant absorption abilities and may cause warming.[15] "White," strongly scattering aerosols have and SSA near one, while "black," strongly absorbing aerosols, such as freshly emitted soot, fall closer to 0.3 to 0.4.[16-18]

Brown carbon (BrC) refers to a type of light-absorbing organic material found in various aerosols.[11] These aerosols have a characteristic yellow-brown coloring and have the ability to

both scatter and absorb radiation to different degrees.[11, 19, 20] Primary BrC is emitted from combustion sources like biomass and biofuels burning, residential coal burning, and forest fires,[7, 11, 19, 21-23] while secondary BrC is produced by different SOA formation and aging processes.[24-33] OA, including BrC, have a tropospheric lifetime of about one week, with dry and wet deposition being a primary sink.[7] Throughout its lifetime, BrC can undergo different aging processes, such as photolysis and oxidation, which change its physicochemical properties, making quantification of its contributions more complicated than other organic aerosols.[7, 10]

The mass absorption coefficient (MAC) of BrC is an order of magnitude smaller than that of black carbon[21] and its light-absorption coefficient has a stronger wavelength dependence.[11, 12, 34] However, BrC is believed to be more abundant in the atmosphere than BC, making its overall contributions to the absorption of radiation by aerosol particles comparable. BrC is able to absorb radiation in the visible (400 – 700 nm) and near-UV (300 – 400 nm) regions of the solar spectrum, usually with a steep increase occurring between the visible and UV region.[11, 35] Since a large fraction of BrC is water-soluble (up to ~70%),[36, 37] it can dissolve into cloud droplets. Within these droplets, the light-absorbing abilities of BrC also contribute to radiative forcing indirectly by causing cloud dispersion and droplet evaporation.[38] For example, global simulations by Feng *et al.* (2013) estimate that BrC may contribute 19% (with radiative forcing up to 0.25 Wm^{-2}) to total anthropogenic aerosol absorption,[39] while Lin *et al*. (2014) calculated the global absorption of BrC to fall within 0.22 to 0.57 Wm^{-2}.[40]

1.1.3. Measurements of Brown Carbon

A main focus of BrC research is the correlation between its optical and chemical properties, in hopes of identifying mechanism of formation and aging of distinct light-absorbing chromophores. Optical properties of aerosols are typically determined by online methods,

including photoacoustic spectroscopy (PAS, measures absorption coefficient),[41-49] cavity ring down spectroscopy (CRDS, measures extinction coefficient),[41, 42, 45, 47, 49-51] and nephelometry (measures scattering coefficient).[21, 52-54] The absorption coefficient of the material from which the particles are made can also be measured by offline methods, by extracting the particle compounds in an appropriate solution, and doing standard spectrophotometry (the method used in this thesis). Molecular characterization is done most commonly using various types of online and offline mass spectrometry (MS), with high-resolution mass spectrometry (HRMS) becoming a dominant method in BrC research. Different ionization sources are used, depending on the types of compounds that are being detected, including electron impact (EI), chemical ionization (CI), electrospray ionization (ESI), nanospray desorption electrospray ionization (nano-DESI), direct analysis in real time (DART), atmospheric pressure chemical ionization (APCI), and atmospheric pressure photoionization (APPI).[10] Different separation techniques are also used to separate the complex BrC mixture into fractions before the analysis, such as gas (GC), liquid (LC), and high-performance liquid (HPLC) chromatography. An in depth discussion on these methods is not in the scope of this introduction, but methods that are directly relevant to this thesis are discussed in a later section and within respective chapters.

High resolution mass spectrometry (HRMS) has become a front runner in the field of aerosol mass spectrometry. HRMS is an offline technique that utilizes linear ion trap (LIT)/Orbitrap[55-57] and Fourier transform ion cyclotron resonance (FT-ICR)[58-60] mass analyzers. The mass resolving power of HRMS methods is very high compared to more conventional MS methods ($\sim 10^5 - 10^6$ vs $\sim 10^3$), resulting in the separation of peaks with the same nominal mass. The difference between measured and exact *m/z* values is also minimal due to its high mass

accuracy. This combination of mass accuracy and resolving power is ideal for the unambiguous identification of the numerous compounds found in complex BrC aerosols.[61]

1.1.4. Brown Carbon Systems

As previously mentioned, BrC is produced by both primary and secondary sources in the atmosphere. This section will summarize studies done to explore different BrC systems, emphasizing the different pathways secondary BrC may be formed, starting with a brief overview of primary BrC sources. Different types of combustion are the primary source of BrC in the atmosphere, but extensive research has shown that the properties of BrC differ when produced from varying fuel types and burning conditions. Multiple controlled burns of different fuel sources have been done in order to explore the influence of burning conditions on the optical and molecular properties of primary BrC. [36, 52, 62-67] Studies have also been done during biomass burning and haze events to see how the increased production of BrC affects the optical and chemical properties of ambient aerosols.[63, 68-77]

There is an extensive list of secondary sources of BrC. Since some BrC is water soluble, one production pathway is different aqueous reactions within cloud and fog waters. Gelencser *et. al.* (2003) used Fenton chemistry to produce hydroxyl radicals (OH) that then oxidized aromatic hydroxyacids,[78] resulting in elevated light absorption in the products, resembling those of humic-like substances.[37] This process was also found to produce oligomeric products when applied to levoglucosan.[79] The photolysis of hydrogen peroxide (H_2O_2) has also been used as a source of OH used for the oxidation of phenolic compounds, which produces light-absorbing, high molecular weight compounds.[80-82] Pyruvic acid has also been found to produce BrC via aqueous photochemistry when certain electrolytes are also in solution.[83, 84] Simple aldehydes and ketones are able to undergo acid-catalyzed aldol condensation to may also produce light-absorbing

products due to oligomerization.[85-89] Oligomerization products can also be formed by α-dicarbonyls by the same process at pH 4 – 5, or by hydration followed by hemiacetal formation at pH 3.5.[90]

Another key aqueous-phase reaction of dicarbonyls that produces BrC is the reaction with nitrogen species such as NH_4^+, amino acids, and ammonia.[28, 30, 51, 91-103] The mechanism of this reaction will be explained in Chapters 2 and 3 of this thesis. Glyoxal (G) and methylglyoxal (MG) are α-dicarbonyls produced during oxidation of many VOCs, such as isoprene and toluene. Both G and MG are highly water-soluble and easily partition into clouds, fogs, and wet aerosols.[10] These compounds can then react with reduced nitrogen species in the atmosphere to produce BrC. Oligomerization products and nitrogen-containing compounds are commonly formed by this reaction.[93, 97] Although both G and MG produce BrC, Powelson *et al.* (2014) found that MG was more efficient at browning and that amines and ammonia result in very different UV-Vis spectra.[95] This reaction can also proceed by the reactive uptake of these carbonyls onto ammonium sulfate seed particles.[28, 29, 98, 103-106] Lastly, although this has been found to be a significant BrC production pathway, the lifetime of this type of BrC is on the order of minutes when exposed to sunlight so its contribution to radiative forcing is likely minimal.[107]

BrC can also be form in the gas-phase by photooxidation of VOCs to form SOA. Photooxidation of biogenic precursors, like isoprene and its derivatives, produces SOA with a small absorption coefficient not representative of BrC.[27, 32, 108-111] This is due to their composition being dominated by carbonyl, carboxyl, and hydroxyl functional groups, which do not have low-energy electronic transitions.[10] However, if highly acidic seed particles are present under dry conditions they can promote the formation of biogenic SOA with increased absorption coefficients, likely due to potential adol condensation reactions of the uptake of carbonyls onto

the particles.[10, 26, 33, 112, 113] Biogenic SOA from both photooxidation and ozonolysis can also undergo the aging by ammonia, amines, and amino acids to produce BrC SOA. Absorption coefficients of biogenic SOA are also significantly increase by exposure to nitrogen species like ammonia, amines, and amino acids.[27, 109, 114-117] The carbonyl products of this oxidation react with ammonia (or other nitrogen-containing compound) to form primary amines and imines that continue reacting with carbonyls and condensing to form oligomeric products containing secondary imines, with the potential to form N-heterocyclic structures via intramolecular cyclization.[10] Since this reaction is not proceeding through adol condensation, it is not strongly pH dependent, unlike the reactions of MG and G discussed above. Additionally, polycyclic aromatic hydrocarbons can undergo nitration to form BrC.[118-120]

Photooxidation of aromatic VOCs, such as toluene, trimethylbenzene, naphthalene, and xylene, produces BrC SOA without any additional aging processes. This browning is accentuated by high-NO_x conditions.[31, 32, 42, 49, 81, 108, 111, 113, 121-125] Although aging is not necessary, exposure of these BrC SOA to ammonia has also been found to increase the magnitude of its light absorbing properties.[27, 126, 127] Nitroaromatic compound have large absorption cross sections in the regions where BrC SOA have been found to absorb, suggesting that these species are like contributing chromophores.[118, 128] Several studies have identified nitroaromatics, such as nitrophenols and ntirocresols, as products of toluene photooxidation.[129-131] Cloud water and $PM_{2.5}$ biomass burning samples have also been found to contain nitrophenols and nitrocatechols as primary light-absorbing species.[132, 133] Overall, both aqueous and gas-phase reactions are important secondary sources for BrC in the atmosphere.

1.2.   Goals

The overall purpose of this thesis is to achieve a better understanding of composition and properties of BrC aerosols from different secondary sources. Optical properties are analyzed to quantify light-absorbing abilities as mass absorption coefficients (MAC) and fluorescence excitation-emission matrices (EEMs). High-resolution mass spectrometry methods are also used in order to characterize the molecular composition of different secondary BrC. Additionally, the effect of photolysis on these properties is explored.

Chapter 2 investigates the browning of aqueous solutions of 4-oxopentanal (4-OPA) and different nitrogen-containing compounds, including ammonium sulfate (AS), amines, and amino acids. Based on previous aging studies of SOA with AS, 4-OPA was selected as a representative 1,4-dicarbonyl to investigate the chemistry and possible pyrrole intermediates produced by this type of reaction. UV-Vis spectroscopy was used to monitor the growth of characteristic BrC peaks as a function of reaction time and gas chromatography confirmed the presence of a 2-methyl pyrrole reaction intermediate. Evaporation of the solution was also performed to determine if dehydration processes can contribute to BrC formation and accelerate browning in this type of system.

Chapter 3 moves on to BrC produced by evaporating aqueous solutions of methyl glyoxal (MG), a 1,2-dicarbonyl, mixed with AS. The resulting BrC was then exposed to radiation to explore the effects of photolysis in the atmosphere, as well as sodium borohydride to determine if carbonyls in the system would be chemically reduced. MAC values were determined using UV-Vis spectroscopy and were monitored as a function of photolysis time to determine reaction kinetics and the effective photolysis quantum yield. Fluorescence spectroscopy was used to create EEMs before and after photolysis and to determine the fluorescence quantum yield. The

effect of NaBH$_4$ reduction on both of these optical properties is also discussed. Electrospray ionization high-resolution mass spectrometry (ESI-HRMS) was used to collect mass spectra of samples before and after irradiation to identify compounds affected by photolysis. High-performance liquid chromatography paired with a photodiode array detector and high-resolution mass spectrometry (HPLC-PDA-HRMS) was used to compare BrC reduced by either photolysis of NaBH$_4$ to a dark control in order to determine what species were responsible for the loss of light-absorption at distinct PDA peaks.

In Chapter 4 there is a shift to BrC produced by VOC oxidation in the aerosol smog chamber. Naphthalene is used as a precursor for SOA formed via photooxidation of the hydroxyl radical under high-NO$_x$ conditions. SOA extracted into aqueous solutions was once again exposed to radiation to model NAP SOA being photolyzed within cloud and fog droplets. Once again, spectroscopy methods were used to determine MAC, create pre- and post-irradiation EEMs, and calculate the effective photolysis rate for this BrC system. ESI-HRMS was used to investigate the effect of photolysis on the molecular composition of NAP SOA, specifically its average molecular formula.

Chapter 5 continues the work with NAP SOA, while determining the influences of different atmospheric conditions on its optical and chemical properties. In chamber studies NAP SOA was formed under high- vs low-NO$_x$ conditions, in the absence or presence of ammonia (NH$_3$), and in a humid (high relative humidity) or dry (low relative humidity) chamber. In this study, offline analysis was done on extracts of NAP SOA collected on filters. Absorptions measurements were done using UV-Vis spectroscopy and nanospray desorption electrospray ionization high-resolution mass spectrometry (nano-DESI-HRMS) was used to collect mass

spectra of the extracts to determine the different environmental conditions on molecular composition.

Lastly, Chapter 6 focuses on the effect of photolysis on the optical properties on BrC formed by the photooxidation of different aromatic precursors. A novel photolysis system was used to take semi-continuous fluorescence and absorption measurements of pH controlled SOA extracts. The effects of photolysis and pH on the absorption coefficients and kinetics were determined. EEMs were created to show the change in fluorescence due to photolysis and to compare them to those of chromophoric dissolved organic matter found in water samples. Fluorescence data was also used to calculate the apparent quantum yield of each SOA system.

1.3. General Methods

1.3.1. Generation and Collection of SOA in the Aerosol Smog Chamber

Different types of BrC SOA were produced in Chapters 4 through 6 of this dissertation using an aerosol smog chamber. This section described the general process of SOA production, with specific details pertinent to each study included in the respective chapter. Prior to each study, the 5 m^3 Teflon chamber was flushed with clean air from a FTIR purge air generator (Parker Balston, Model 75-62). Oxidation of VOCs in the chamber can occur through either ozonolysis or photooxidation with the hydroxyl radical (OH). For this thesis all SOA were formed via photooxidation using hydrogen peroxide (H_2O_2, Aldrich, 30% by volume in water) as the OH precursor. H_2O_2 was injected into a glass injection port and introduced to the sealed chamber through stainless steel tubing via evaporation with dry air. Once the H_2O_2 was fully evaporated, liquid VOC precursors were added to the chamber in the same manner.

Experiments in Chapters 5 and 6 were performed under both dry (<2% relative humidity (RH)) and humid (40 – 90% RH) conditions. The RH and temperature were monitored using a

11

Vaisala HMT330 probe sealing within the bottom of the chamber. For studies done under humid conditions, the chamber was humidified prior to the addition of any precursors. Introduction of water vapor into the chamber was done by flowing purge air through a Nafion membrane humidifier connected to a 35°C water bath circulator. Studies in Chapters 4 and 6, and some studies in Chapter 5, were conducted under high-NO_x (200 – 400 ppb of NO/NO_2 added) conditions. For these types of studies a calculated volume of NO primary gas standard (Parxair. 5000 ppm NO in N_2) was added to the sealed chamber after the addition of H_2O_2, but before VOCs. Some of the NO is oxidized into NO_2 during the addition.

All reagents were mixed with a fan sealed within the chamber for several minutes, which was then turned off to prevent wall loss. At this point the photooxidation process was initiated by turning on the UV-B lamps (FS40T12/UVB, Solarc System Inc.) with emissions centered at 310 nm that surround the sides of the chamber. After several hours of oxidation, SOA were passed through an activated charcoal denuder (Sunset Laboratories Inc.) and collected onto PTFE filters (Millipore 0.2 μm pore size). These filters were with directly extracted or vacuumed sealed and frozen for offline analyses. Throughout the SOA formation and collection processes the concentration of NO/NO_y and ozone were respectively tracked using model 42i-Y and 49i Thermo Scientific monitors, while the size distribution and particle concentration were measured using a scanning mobility particle sizer (SMPS, TSI model 3936).
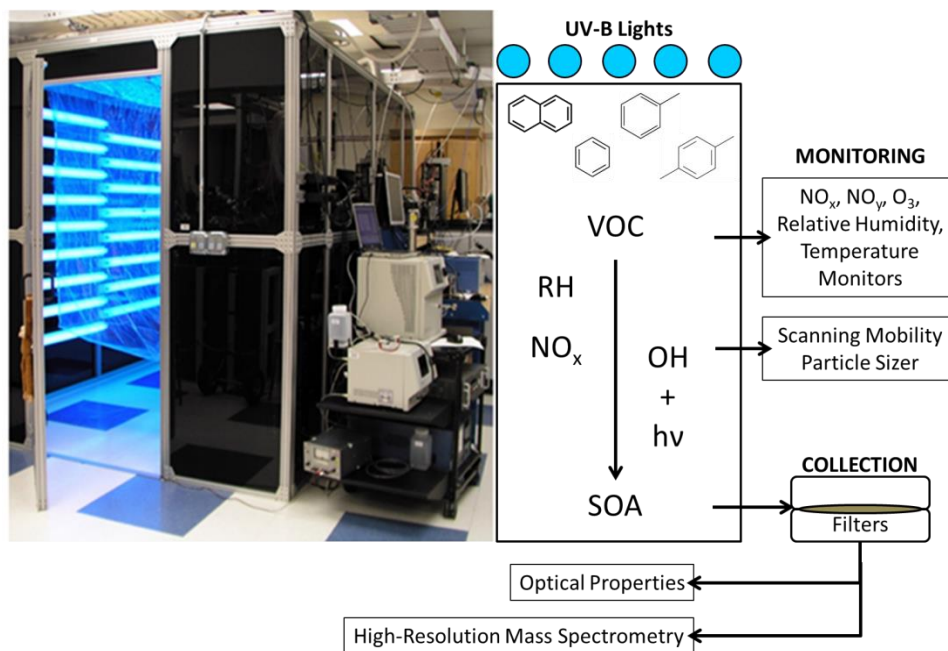
Figure 1.1: Photo and diagram of chamber setup

1.3.2. High-Resolution Mass Spectrometry for Chemical Composition

The molecular composition of BrC samples was determined using high-resolution mass spectrometry performed at the Wiley Environmental Molecular Sciences Laboratory (EMSL) at Pacific Northwest Nation Laboratory (PNNL) in collaboration with Drs. Alexander Laskin and Julia Laskin. Samples were analyzed using a high-resolution linear ion trap (LTQ) Orbitrap (Thermo Corp.) mass spectrometer connected to either an electrospray ionization (ESI) or nanospray-desorption electrospray ionization (nano-DESI) source. Each day the instrument was calibrated with a mixture of caffeine, MRFA, and Ultramark 1621. All samples were with a mass resolving power of 10^5 (m/Δm) at *m/z* 400 and in positive ion mode, producing either protonated (M-H$^+$) or sodiated (M-Na$^+$) analytes. Subtraction of the mass of a proton or sodium, respectively, was done in order to determine the neutral chemical formula of identified compounds.

13

In Chapters 3 and 4 solutions of BrC were photolyzed at PNNL then analyzed using the LTQ Orbitrap mass spectrometer equipped with a direct-infusion ESI. This soft ionization technique results in minimal fragmentation of ionized species, making it well suited for identifying different species in complex samples such as BrC. In both studies sample solutions were diluted in a 1:1 ratio with acetonitrile before being injected into the ESI source in order to increase the stability of the source. The solution is drawn to a conical tip through a fused-silica capillary where a high voltage is applied and a spray of highly charged droplets is formed. In Chapter 3 a subset of studies was done with a high-performance liquid chromatography pump and photodiode array detector setup prior to the ESI source in order to separate the species in each sample and pair absorption events with specific compounds.

In Chapter 5 a nano-DESI source was used for soft ionization.[134, 135] This technique ionizes directly from the surface of the filter instead of a solution, preventing preparation discrepancies and possible solvent effects. A primary silica capillary directs a flow of solvent to the substrate, which then creates a solvent bridge to a secondary capillary used to transfer the analyte into the mass spectrometer. After several minutes of contact with the sample the filter is then repositioned in order to collect a background reading from an area that is sample free. Due to the reduced amount of solvent used in this ionization technique the limit of detection is very low, on the order of nanograms.

1.3.3. Processing of High-Resolution Mass Spectrometry Data

Mass spectra for all studies in Chapters 3 through 5 were analyzed based on the following procedure. Raw data were collected from the LTQ Orbitrap mass spectrometer and evaluated in the Xcalibur program to determine the best data set. ESI data contained both sample and solvent files, while nano-DESI data had to be integrated to produce a background file from when the

edge of the filter was used and a sample file for the actual analyte. Files were then grouped accordingly and a list of peak positions and intensities was extracted using the Decon2SL program developed by PNNL. Batches of samples and corresponding background or solvent files were then aligned using a custom written program in Labview 7.0. Peaks that appeared in both the sample and solvent data sets were removed, as well as peaks that had a significantly high ratio of solvent-to-sample. In addition to aligning the peaks of inputted files, Labview also flagged peaks containing the ^{13}C isotope, which were also removed.

Once sample peaks were isolated, they were ran through another Labview 7.0 program for assignment of their protonated (M-H$^+$) or sodiated (M-Na$^+$) molecular formula based on their *m/z* value. Tolerance of *m/*z was specified and constraints were placed on the number of specific atoms (C, H, O, N, and Na) and elemental ratios (H/C and O/C). Details of restrictions are listed in subsequent chapters. These assignments were then used to assess the calibration of the *m/z* axis and if noticeable deviations were present the masses were recalibrated based on a best-fit line through the data set. Once the masses were adjusted they were reran through the Labview 7.0 assignment program and reassessed. Once the deviation in *m/z* was minimal the ionized masses were converted to neutral masses, which were then used to calculate elemental ratios, double-bond equivalents, and average molecular formulas, as well as to plot the mass spectra discussed within this thesis.

1.4. References

1.   Hidy, G. M., An historical experiment: Los Angeles smog evolution observed by blimp. *J. Air Waste Manag. Assoc.* **2018**.

2.   Zhang, R.; Wang, G.; Guo, S.; Zamora, M. L.; Ying, Q.; Wang, W.; Hu, M.; Wang, Y., Formation of urban fine particulate matter. *Chem. Rev.* **2015,** *115*, (10), 3803-55.

3.   Tositti, L., The Relationship Between Health Effects and Airborne Particulate Constituents. In *Clinical Handbook of Air Pollution-Related Diseases*, Capello, F.; Gaddi, A., Eds. Springer, Cham: 2018.

4.   EPA., U. S., Provisional Assessment of Recent Studies on Health Effects of Particulate Matter Exposure. In Agency, U. S. E. P., Ed. EPA: Washington, DC, 2012.

5.   Mauderly, J. L.; C., C. J., Health effects of organic aerosols. *Inhal. Toxicol.* **2008,** *20*, (3), 257-88.

6.   Charlson, R. J.; Schwartz, S. E., Climate forcing by anthropogenic aerosols. *Science* **1992,** *255*, (5043), 423-30.

7.   Boucher, O.; Randall, D.; Artaxo, P.; Bretherton, C.; Feingold, G.; Forster, P.; Kerminen, V.-M.; Kondo, Y.; Liao, H.; Lohmann, U.; Rasch, P.; Satheesh, S. K.; Sherwood, S.; Stevens, B.; Zhang, X. Y., Clouds and Aerosols. In *Climate Change 2013: The Physical Science Basis. Contribution of Working Group I to the Fifth Assessment Report of the Intergovernmental Panel on Climate Change*, Stocker, T. F.; Qin, D.; Plattner, G.-K.; Tignor, M.; Allen, S. K.; Boschung, J.; Nauels, A.; Xia, Y.; Bex, V.; Midgley, P. M., Eds. Cambridge University Press: Cambridge, United Kingdom and New York, NY, USA, 2013.

8.   Twomey, S., Aerosols, clouds and radiation. *Atmos. Environ., Part A: General Topics* **1991,** *25A*, (11), 2435-42.

9.   Glasius, M.; Goldstein, A. H., Recent discoveries and future challenges in atmospheric organic chemistry. *Environ. Sci. Technol.* **2016,** *50*, (6), 2754-64.

10.   Laskin, A.; Laskin, J.; Nizkorodov, S. A., Chemistry of atmospheric brown carbon. *Chem. Rev.* **2015,** *115*, (10), 4335-82.

11.   Andreae, M. O.; Gelencser, A., Black carbon or brown carbon? The nature of light-absorbing carbonaceous aerosols. *Atmos. Chem. Phys.* **2006,** *6*, (10), 3131-48.

12.   Moosmüller, H.; Chakrabarty, R. K.; Arnott, W. P., Aerosol light absorption and its measurement: a review. *J. Quant. Spectrosc. Radiat. Transfer* **2009,** *110*, (11), 844-78.

13.   Bond, T. C.; Bergstrom, R. W., Light absorption by carbonaceous particles: an investigative review. *Aerosol Sci. Technol.* **2006,** *40*, (1), 27-67.

14.   Kokhanovsky, A. A., *Aerosol optics: light absorption and scattering by particles in the atmosphere*. Springer Science & Business Media: 2008.

15.   Takemura, T.; Nakajima, T., Single-scattering albedo and radiative forcing of various aerosol species with a global three-dimensional model. *J. Clim.* **1983,** *15*, (4), 333-52.

16.   Ma, L.; Thompson, J. E., Optical properties of dispersed aerosols in the near ultraviolet (355 nm): measurement approach and initial data. *Anal. Chem.* **2012,** *84*, (13), 5611-17.

17.   Hopkins, R. J.; Lewis, K.; Desyaterik, Y.; Wang, Z.; Tivanski, A. V.; Arnott, W. P.; Laskin, A.; Gilles, M. K., Correlations between optical, chemical and physical properties of biomass burn aerosols. *Geophys. Res. Lett.* **2007,** *34*.

18.   Bruce, C. W.; Stromberg, T. F.; Gurton, K. P.; Mozer, J. B., Trans-spectral absorption and scattering of electromagnetic radiation by diesel soot. *Appl. Opt* **1991,** *30*, 1537-46.

19.   Bond, T. C., Spectral dependence of visible light absorption by carbonaceous particles emitted from coal combustion *Geophys. Res. Lett.* **2001,** *28*, (21), 4075-78.

20.   Bond, T. C.; Charlson, R. J.; Heintzenberg, J., Quantifying the emission of light-absorbing particles: Measurements tailored to climate studies. *Geophys. Res. Lett.* **1998,** *25*, 337-40.

21.   Yang, M.; Howell, S. G.; Zhuang, J.; Huebert, B. J., Attribution of aerosol light absorption to black carbon, brown carbon, and dust in China – interpretations of atmospheric measurements during EAST-AIRE *Atmos. Chem. Phys.* **2009,** *9*, 2035-50.

22.   Saleh, R.; Robinson, E. S.; Tkacik, D. S.; Ahern, A. T.; Liu, S.; Aiken, A. C.; Sullivan, R. C.; Presto, A. A.; Dubey, M. K.; Yokelson, R. J.; Donahue, N. M.; Robinson, A. L., Brownness of organics in aerosols from biomass burning linked to their black carbon content. *Nat. Geosci.* **2014,** *7*, 647-50.

23.   Washenfelder, R. A.; Attwood, A. R.; Brock, C. A.; Guo, H.; Xu, L.; Weber, R. J.; Ng, N. L.; Allen, H. M.; Ayres, B. R.; Baumann, K.; Cohen, R. C.; Draper, D. C.; Duffey, K. C.; Edgerton, E.; Fry, J. L.; Hu, W. W.; Jimenez, J. L.; Palm, B. B.; Romer, P.; Stone, E. A.; Wooldridge, P. J.; Brown, S. S., Biomass burning dominates brown carbon absorption in the rural southeastern United States *Geophys. Res. Lett.* **2015,** *42*, (2), 653-64.

24.   Zhang, X.; Lin, Y. H.; Surratt, J. D.; Zotter, P.; Prevot, A. S. H.; Weber, R. J., Light-absorbing soluble organic aerosol in Los Angeles and Atlanta: A contrast in secondary organic aerosol. *Geophys. Res. Lett.* **2011,** *38*, L21810.

25.   Zhang, X.; Liu, Z.; Hecobian, A.; Zheng, M.; Frank, N. H.; Edgerton, E.; Weber, R. J., Spatial and seasonal variations of fine particle water-soluble organic carbon (WSOC) over the southeastern United States: implications for secondary organic aerosol formation. *Atmos. Chem. Phys.* **2012,** *12*, 6593-6607.

26.   Limbeck, A.; Kulmala, M.; Puxbaum, H., Secondary organic aerosol formation in the atmosphere via heterogeneous reaction of gaseous isoprene on acidic particles. *Geophys. Res. Lett.* **2003,** *30*, (19), 1996, 10.1029/2003GL017738.

27.   Updyke, K. M.; Nguyen, T. B.; Nizkorodov, S. A., Formation of brown carbon via reactions of ammonia with secondary organic aerosols from biogenic and anthropogenic precursors. *Atmos. Environ.* **2012,** *63*, 22-31.

28.   De Haan, D. O.; Hawkins, L. N.; Welsh, H. G.; Pednekar, R.; Casar, J. R.; Pennington, E. A.; de Loera, A.; Jimenez, N. G.; Symons, M. A.; Zauscher, M.; Pajunoja, A.; Caponi, L.; Cazaunau, M.; Formenti, P.; Gratien, A.; Pangui, E.; Doussin, J. F., Brown carbon production in ammonium- or amine-containing aerosol particles by reactive uptake of methylglyoxal and photolytic cloud cycling. *Environ. Sci. Technol.* **2017,** *51*, (13), 7458-66.

29.   De Haan, D. O.; Tapavicza, E.; Riva, M.; Cui, T.; Surratt, J. D.; Smith, A. C.; Jordan, M. C.; Nilakantan, S.; Almodovar, M.; Stewart, T. N.; de Loera, A.; De Haan, A. C.; Cazaunau, M.; Gratien, A.; Pangui, E.; Doussin, J. F., Nitrogen-containing, light-absorbing oligomers produced in aerosol particles exposed to methylglyoxal, photolysis, and cloud cycling. *Environ. Sci. Technol.* **2018,** *52*, (7), 4061-71.

30.   Lin, P.; Laskin, J.; Nizkorodov, S. A.; Laskin, A., Revealing brown carbon chromophores produced in reactions of methylglyoxal with ammonium sulfate. *Environ. Sci. Technol.* **2015,** *49*, (24), 14257-66.

31.   Lin, P.; Liu, J.; Shilling, J. E.; Kathmann, S. M.; Laskin, J.; Laskin, A., Molecular characterization of brown carbon (BrC) chromophores in secondary organic aerosol generated from photo-oxidation of toluene. *Phys. Chem. Chem. Phys.* **2015,** *17*, 23312-25.

32.   Liu, J.; Lin, P.; Laskin, A.; Laskin, J.; Kathmann, S. M.; Wise, M.; Caylor, R.; Imholt, F.; Selimovic, V.; Shilling, J. E., Optical properties and aging of light-absorbing secondary organic aerosol. *Atmos. Chem. Phys.* **2016,** *16*, 12815-27.

33.   Song, C.; Gyawali, M.; Zaveri, R. A.; Shilling, J. E.; Arnott, W. P., Light absorption by secondary organic aerosol from α-pinene: effects of oxidants, seed aerosol acidity, and relative humidity. *J. Geophys. Res. Atmos.* **2013,** *118*, 11741-49.

34.   Lack, D. A.; Langridge, J. M., On the attribution of black and brown carbon light absorption using the Ångström exponent *Atmos. Chem. Phys.* **2013,** *13*, 10535-43.

35.   Gustafsson, O.; Krusa, M.; Zencak, Z.; Sheesley, R. J.; Granat, L.; Engstrom, E.; Praveen, P. S.; Rao, P. S. P.; Leck, C.; Rodhe, H., Brown clouds over South Asia: biomass or fossil fuel combustion? *Science* **2009,** *323*, (5913), 495-98.

36.   Chen, Y.; Bond, T. C., Light absorption by organic carbon from wood combustion. *Atmos. Chem. Phys.* **2010,** *10*, (4), 1773-87.

37.   Hoffer, A.; Kiss, G.; Blazso, M.; Gelencser, A., Chemical characterization of humic-like substances (HULIS) formed from a lignin-type precursor in model cloud water. *Geophys. Res. Lett.* **2004,** *31*, L06115, 10.1029/2003GL018962.

38.   Hansen, J.; Sato, M.; Ruedy, R., Radiative forcing and climate response. *J. Geophys. Res.* **1997,** *102*, (D6), 6831-64.

39.   Feng, Y.; Ramanathan, V.; Kotamarthi, V., Brown carbon: a significant atmospheric absorber of solar radiation? *Atmos. Chem. Phys.* **2013,** *13*, 8607-21.

40.   Lin, G.; Penner, J. E.; Flanner, M. G.; Sillman, S.; Xu, L.; Zhou, C., Radiative forcing of organic aerosol in the atmosphere and on snow: Effects of SOA and brown carbon *J. Geophys. Res. Atmos.* **2014,** *119*, (12), 7453-76.

41.   Lack, D. A.; Langridge, J. M.; Bahreini, R.; Cappa, C. D.; Middlebrook, A. M.; Schwarz, J. P., Brown carbon and internal mixing in biomass burning particles. *PNAS* **2012,** *109*, (37), 14802-07.

42.   Lambe, A. T.; Cappa, C. D.; Massoli, P.; Onasch, T. B.; Forestieri, S. D.; Martin, A. T.; Cummings, M. J.; Croasdale, D. R.; Brune, W. H.; Worsnop, D. R.; Davidovits, P., Relationship between oxidation level and optical properties of secondary organic aerosol. *Environ. Sci. Technol.* **2013,** *47*, (12), 6349-57.

43.   Arnott, W. P.; Moosmüller, H.; Sheridan, P. J.; Ogren, J. A.; Raspet, R.; Slaton, W. V.; Hand, J. L.; Kreidenweis, S. M.; Collett, J. L. J., Photoacoustic and filter-based ambient aerosol light absorption measurements: Instrument comparisons and the role of relative humidity. *J. Geophys. Res. Atmos.* **2002,** *108*, (D1), AAC 15-1 - 15-11.

44.   Lack, D. A.; Lovejoy, E. R.; Baynard, T.; Pettersson, A.; Ravishankara, A. R., Aerosol absorption measurement using photoacoustic spectroscopy: sensitivity, calibration, and uncertainty developments. *Aerosol Sci. Technol.* **2006,** *40*, (9), 697-708.

45.   Langridge, J. M.; Richardson, M. S.; Lack, D. A.; Brock, C. A.; Murphy, D. M., Limitations of the photoacoustic technique for aerosol absorption measurement at high relative humidity. *Aerosol Sci. Technol.* **2013,** *47*, (11), 1163-73.

46.   Pokhrel, R. P.; Beamesderfer, E. R.; Wagner, N. L.; Langridge, J. M.; Lack, D. A.; Jayarathne, T.; Stone, E. A.; Stockwell, C. E.; Yokelson, R. J.; Murphy, S. M., Relative importance of black carbon, brown carbon, and absorption enhancement from clear coatings in biomass burning emissions *Atmos. Chem. Phys.* **2017,** *17*, 5063-78.

47.   Zhang, X.; Kim, H.; Parworth, C. L.; Young, D. E.; Zhang, Q.; Metcalf, A. R.; Cappa, C. D., Optical properties of wintertime aerosols from residential wood burning in Fresno, CA: Results from DISCOVER-AQ 2013. *Environ. Sci. Technol.* **2016,** *50*, (4), 1681-90.

48.   Healy, R. M.; Wang, J. M.; Jeong, C.-H.; Lee, A. K. Y.; Willis, M. D.; Jaroudi, E.; Zimmerman, N.; Hilker, N.; Murphy, M.; Eckhardt, S.; Stohl, A.; Abbatt, J. P. D.; Wenger, J. C.; Evans, G. J., Light-absorbing properties of ambient black carbon and brown carbon from fossil fuel and biomass burning sources. *J. Geophys. Res. Atmos.* **2015**, *120*, (13), 6619-33.

49.   Nakayama, T.; Sato, K.; Matsumi, Y.; Imamura, T.; Yamazaki, A.; Uchiyama, A., Wavelength and NO$_x$ dependent complex refractive index of SOAs generated from the photooxidation of toluene *Atmos. Chem. Phys.* **2013,** *13*, 531-45.

50.   Zarzana, K. J.; De Haan, A. C.; Freedman, M. A.; Hasenkopf, C. A.; Tolbert, M. A., Optical properties of the products of α-dicarbonyl and amine reactions in simulated cloud droplets. *Environ. Sci. Technol.* **2012,** *46*, (9), 4845-51.

51.   Kwon, D.; Or, V. W.; Sovers, M. J.; Tang, M.; Kleiber, P. D.; Grassian, V. H., Optical property measurements and single particle analysis of secondary organic aerosol produced from the aqueous-phase reaction of ammonium sulfate with methylglyoxal. *ACS Earth Space Chem.* **2018,** *2*, (4), 356-65.

52.   Lewis, K. A.; Arnott, W. P.; Moosmüller, H.; Chakrabarty, R. K.; Carrico, C. M.; Kreidenweis, S. M.; Day, D. A.; Malm, W. C.; Laskin, A.; Jimenez, J. L.; Ulbrich, I. M.; Huffman, J. A.; Onasch, T. B.; Trimborn, A.; Liu, L.; Mishchenko, M. I., Reduction in biomass burning aerosol light absorption upon humidification: roles of inorganically-induced hygroscopicity, particle collapse, and photoacoustic heat and mass transfer. *Atmos. Chem. Phys.* **2009,** *9*, 8949-66.

53.   Chakrabarty, R. K.; Arnold, I. J.; Francisco, D. M.; Hatchett, B.; Hosseinpour, F.; Loria, M.; Pokharel, A.; Woody, B. M., Black and brown carbon fractal aggregates from combustion of two fuels widely used in Asian rituals. *J. Quant. Spectrosc. Radiat. Transfer* **2013,** *122*, 25-30.

54.   Heintzenberg, J.; Charlson, R. J., Design and applications of the integrating nephelometer: A review *J. Atmos. Oceanic Tech* **1996,** *13*, (987-1000).

55.   Perry, R. H.; Cooks, R. G.; Noll, R. J., Orbitrap mass spectrometry: instrumentation, ion motion and applications. *Mass Spectrom. Rev.* **2008,** *27*, (6), 661-99.

56.   Makarov, A.; Denisov, E.; Lange, O., Performance evaluation of a high-field Orbitrap mass analyzer. *J. Am. Soc. Mass Spectrom.* **2009,** *20*, (8), 1391-96.

57.   Makarov, A.; Denisov, E.; Kholomeev, A.; Balschun, W.; Lange, O.; Strupat, K.; Horning, S., Performance evaluation of a hybrid linear Iin trap/Orbitrap mass spectrometer. *Anal. Chem.* **2006,** *78*, (7), 2113-20.

58.   Marshall, A. G.; Hendrickson, C. L.; Jackson, G. S., Fourier Transform Ion Cyclotron Resonance Mass Spectrometry. In *Encyclopedia of Analytical Chemistry*, John Wiley & Sons, Ltd: 2006.

59.	Marshall, A. G., Milestones in fourier transform ion cyclotron resonance mass spectrometry technique development. *Int. J. Mass Spectrom.* **2000,** *200*, 331-56.

60.	Zhang, L. K.; Rempel, D.; Pramanik, B. N.; Gross, M. L., Accurate mass measurements by Fourier transform mass spectrometry. *Mass Spectrom. Rev.* **2005,** *24*, 286-309.

61.	Nizkorodov, S. A.; Laskin, J.; Laskin, A., Molecular chemistry of organic aerosols through the application of high resolution mass spectrometry. *Phys. Chem. Chem. Phys.* **2011,** *13*, 3612-29.

62.	Radney, J. G.; You, R.; Zachariah, M. R.; Zangmeister, C. D., Direct in situ mass specific absorption spectra of biomass burning particles generated from smoldering hard and softwoods. *Environ. Sci. Technol.* **2017,** *51*, (10), 5622-29.

63.	Budisulistiorini, S. H.; Riva, M.; Williams, M.; Chen, J.; Itoh, M.; Surratt, J. D.; Kuwata, M., Light-absorbing brown carbon aerosol constituents from combustion of indonesian peat and biomass. *Environ. Sci. Technol.* **2017,** *51*, (8), 4415-23.

64.	Rathod, T. D.; Sahu, S. K.; Tiwari, M.; Pandit, G. G., Direct radiative effect due to brownness in organic carbon aerosols generated from biomass combustion. *J. Quant. Spectrosc. Radiat. Transfer* **2016,** *185*, 101-09.

65.	Lin, P.; Aiona, P. K.; Li, Y.; Shiraiwa, M.; Laskin, J.; Nizkorodov, S. A.; Laskin, A., Molecular characterization of brown carbon in biomass burning aerosol particles. *Environ. Sci. Technol.* **2016,** *50*, 11815-24.

66.	Zhong, M.; Jang, M., Dynamic light absorption of biomass-burning organic carbon photochemically aged under natural sunlight. *Atmos. Chem. Phys.* **2014,** *14*, 1517-25.

67.	Chakrabarty, R. K.; Moosmüller, H.; Chen, L. W. A.; Lewis, K.; Arnott, W. P.; Mazzoleni, C.; Dubey, M. K.; Wold, C. E.; Hao, W. M.; Kreidenweis, S. M., Brown carbon in tar balls from smoldering biomass combustion *Atmos. Chem. Phys.* **2010,** *10*, (6363-70).

68.	Lin, P.; Bluvshtein, N.; Rudich, Y.; Nizkorodov, S. A.; Laskin, J.; Laskin, A., Molecular chemistry of atmospheric brown carbon inferred from a nationwide biomass burning event. *Environ. Sci. Technol.* **2017,** *51*, (20), 11561-70.

69.	Di Lorenzo, R. A.; Washenfelder, R. A.; Attwood, A. R.; Guo, H.; Xu, L.; Ng, N. L.; Weber, R. J.; Baumann, K.; Edgerton, E.; Young, C. J., Molecular-size-separated brown carbon absorption for biomass-burning aerosol at multiple field sites. *Environ. Sci. Technol.* **2017,** *51*, (6), 3128-37.

70.	Selimovic, V.; Yokelson, R. J.; Warneke, C.; Roberts, J. M.; de Gouw, J.; Reardon, J.; Griffith, D. W. T., Aerosol optical properties and trace gas emissions by PAX and OP-FTIR for laboratory-simulated western US wildfires during FIREX. *Atmos. Chem. Phys.* **2018,** *18*, (4), 2929-48.

71.   Di Lorenzo, R. A.; Place, B. K.; VandenBoer, T. C.; Young, C. J., Composition of size-resolved aged boreal fire aerosols: brown carbon, biomass burning tracers, and reduced nitrogen. *ACS Earth Space Chem.* **2018,** *2*, (3), 278-85.

72.   Sumlin, B. J.; Heinson, Y. W.; Shetty, N.; Pandey, A.; Pattison, R. S.; Baker, S.; Hao, W. M.; Chakrabarty, R. K., UV–Vis–IR spectral complex refractive indices and optical properties of brown carbon aerosol from biomass burning. *J. Quant. Spectrosc. Radiat. Transfer* **2018,** *206*, 392-98.

73.   Bluvshtein, N.; Lin, P.; Flores, J. M.; Segev, L.; Mazar, Y.; Tas, E.; Snider, G.; Weagle, C.; Brown, S. S.; Laskin, A.; Rudich, Y., Broadband optical properties of biomass-burning aerosol and identification of brown carbon chromophores *J. Geophys. Res. Atmos.* **2017,** *122*, (10), 5441-56.

74.   Chakrabarty, R. K.; Gyawali, M.; Yatavelli, R. L. N.; Pandey, A.; Watts, A. C.; Knue, J.; Chen, L.-W. A.; Pattison, R. R.; Samburova, V.; Moosmüller, H., Brown carbon aerosols from burning of boreal peatlands: microphysical properties, emission factors, and implications for direct radiative forcing. *Atmos. Chem. Phys.* **2016,** *16*, 3033-40.

75.   Liu, J.; Scheuer, E.; Dibb, J.; Diskin, G. S.; Ziemba, L. D.; Thornhill, K. L.; Anderson, B. E.; Wisthaler, A.; Mikoviny, T.; Devi, J. J.; Bergin, M.; Perring, A. E.; Markovic, M. Z.; Schwarz, J. P.; Campuzano-Jost, P.; Day, D. A.; Jimenez, J. L.; Weber, R. J., Brown carbon aerosol in the North American continental troposphere: sources, abundance, and radiative forcing. *Atmos. Chem. Phys.* **2015,** *15*, 7841-58.

76.   Forrister, H.; Liu, J.; Scheuer, E.; Dibb, J.; Ziemba, L. D.; Thornhill, K. L.; Anderson, B. E.; Diskin, G. S.; Perring, A. E.; Schwarz, J. P.; Campuzano-Jost, P.; Day, D. A.; Palm, B. B.; Jimenez, J. L.; Nenes, A.; Weber, R. J., Evolution of brown carbon in wildfire plumes. *Geophys. Res. Lett.* **2015,** *42*, (11), 4623-30.

77.   Hoffer, A.; Gelencser, A.; Guyon, P.; Kiss, G.; Schmid, O.; Frank, G. P.; Artaxo, P.; Andreae, M. O., Optical properties of humic-like substances (HULIS) in biomass-burning aerosols. *Atmos. Chem. Phys.* **2006,** *6*, 3563-70.

78.   Gelencser, A.; Hoffer, A.; Kiss, G.; Tombacz, E.; Kurdi, R.; Bencze, L., In-situ formation of light-absorbing organic matter in cloud water. *J. Atmos. Chem.* **2003,** *45*, (1), 25-33.

79.   Holmes, B. J.; Petrucci, G. A., Water-soluble oligomer formation from acid-catalyzed reactions of levoglucosan in proxies of atmospheric aqueous aerosols. *Environ. Sci. Technol.* **2006,** *40*, (16), 4983-89.

80.   Chang, J. L.; Thompson, J. E., Characterization of colored products formed during irradiation of aqueous solutions containing H_2O_2 and phenolic compounds. *Atmos. Environ.* **2010,** *44*, (4), 541-51.

81.   Li, Y. J.; Huang, D. D.; Cheung, H. Y.; Lee, A. K. Y.; Chan, C. K., Aqueous-phase photochemical oxidation and direct photolysis of vanillin – a model compound of methoxy phenols from biomass burning *Atmos. Chem. Phys.* **2014,** *14*, 2871-85.

82.   Sun, Y. L.; Zhang, Q.; Anastasio, C.; Sun, J., Insights into secondary organic aerosol formed via aqueous-phase reactions of phenolic compounds based on high resolution mass spectrometry *Atmos. Chem. Phys.* **2010,** *10*, 4809-22.

83.   Rincon, A. G.; Guzmán, M. I.; Hoffmann, M. R.; Colussi, A. J., Optical absorptivity versus molecular composition of model organic aerosol matter. *J. Phys. Chem. A* **2009,** *113*, (39), 10512-20.

84.   Rincon, A. G.; Guzmán, M. I.; Hoffmann, M. R.; Colussi, A. J., Thermochromism of model organic aerosol matter. *J. Phys. Chem. Lett.* **2010,** *1*, (1), 368-73.

85.   Yi, Y.; Zhou, X.; Xue, L.; Wang, W., Air pollution: formation of brown, lighting-absorbing, secondary organic aerosols by reaction of hydroxyacetone and methylamine. *Environ. Chem. Lett.* **2018**, 1-6.

86.   Casale, M.; Richman, A.; Elrod, M.; Garland, R.; Beaver, M.; Tolbert, M., Kinetics of acid-catalyzed aldol condensation reactions of aliphatic aldehydes. *Atmos. Environ.* **2007,** *41*, (29), 6212-24.

87.   Noziere, B.; Esteve, W., Organic reactions increasing the absorption index of atmospheric sulfuric acid aerosols. *Geophys. Res. Lett.* **2005,** *32*, L03812, 10.1029/2004GL021942.

88.   Noziere, B.; Esteve, W., Light-absorbing aldol condensation products in acidic aerosols: spectra, kinetics, and contribution to the absorption index. *Atmos. Environ.* **2007,** *41*, (6), 1150-63.

89.   Noziere, B.; Voisin, D.; Longfellow, C. A.; Friedli, H.; Henry, B. E.; Hanson, D. R., The uptake of methyl vinyl ketone, methacrolein, and 2-methyl-3-butene-2-ol onto sulfuric acid solutions. *J. Phys. Chem. A* **2006,** *110*, (7), 2387-95.

90.   Yasmeen, F.; Sauret, N.; Gal, J.-F.; Maria, P.-C.; Massi, L.; Maenhaut, W.; Claeys, M., Characterization of oligomers from methylglyoxal under dark conditions: a pathway to produce secondary organic aerosol through cloud processing during nighttime *Atmos. Chem. Phys.* **2010,** *10*, 3803-12.

91.   Kampf, C. J.; Jakob, R.; Hoffmann, T., Identification and characterization of aging products in the glyoxal/ammonium sulfate system - implications for light-absorbing material in atmospheric aerosols. *Atmos. Chem. Phys.* **2012,** *12*, (14), 6323-33.

92.   Shapiro, E. L.; Szprengiel, J.; Sareen, N.; Jen, C. N.; Giordano, M. R.; McNeill, V. F., Light-absorbing secondary organic material formed by glyoxal in aqueous aerosol mimics. *Atmos. Chem. Phys.* **2009,** *9*, (7), 2289-2300.

93.   Sareen, N.; Schwier, A. N.; Shapiro, E. L.; Mitroo, D.; McNeill, V. F., Secondary organic material formed by methylglyoxal in aqueous aerosol mimics. *Atmos. Chem. Phys.* **2010,** *10*, (3), 997-1016.

94.   De Haan, D. O.; Tolbert, M. A.; Jimenez, J. L., Atmospheric condensed-phase reactions of glyoxal with methylamine. *Geophys. Res. Lett.* **2009,** *36*, L11819, 10.1029/2009gl037441.

95.   Powelson, M. H.; Espelien, B. M.; Hawkins, L. N.; Galloway, M. M.; De Haan, D. O., Brown carbon formation by aqueous-phase carbonyl compound reactions with amines and ammonium sulfate. *Environ. Sci. Technol.* **2014,** *48*, (2), 985-93.

96.   Rodriguez, A. A.; de Loera, A.; Powelson, M. H.; Galloway, M. M.; De Haan, D. O., Formaldehyde and acetaldehyde increase aqueous-phase production of imidazoles in methylglyoxal/amine mixtures: quantifying a secondary organic aerosol formation mechanism. *Environ. Sci. Technol. Lett.* **2017,** *4*, (6), 234-39.

97.   Noziere, B.; Dziedzic, P.; Cordova, A., Products and kinetics of the liquid-phase reaction of glyoxal catalyzed by ammonium ions (NH_4^+). *J. Phys. Chem. A* **2009,** *113*, (1), 231-37.

98.   Trainic, M.; Abo Riziq, A.; Lavi, A.; Flores, J. M.; Rudich, Y., The optical, physical and chemical properties of the products of glyoxal uptake on ammonium sulfate seed aerosols. *Atmos. Chem. Phys.* **2011,** *11*, (18), 9697-9707.

99.   Yu, G.; Bayer, A. R.; Galloway, M. M.; Korshavn, K. J.; Fry, C. G.; Keutsch, F. N., Glyoxal in aqueous ammonium sulfate solutions: products, kinetics and hydration effects. *Environ. Sci. Technol.* **2011,** *45*, (15), 6336-42.

100.   Tang, M.; Alexander, J. M.; Kwon, D.; Estillore, A. D.; Laskina, O.; Young, M. A.; Kleiber, P. D.; Grassian, V. H., Optical and physicochemical properties of brown carbon aerosol: light scattering, FTIR extinction spectroscopy, and hygroscopic growth. *J. Phys. Chem. A* **2016,** *120*, (24), 4155-66.

101.   Kampf, C. J.; Filippi, A.; Zuth, C.; Hoffmann, T.; Opatz, T., Secondary brown carbon formation via the dicarbonyl imine pathway: nitrogen heterocycle formation and synergistic effects. *Phys. Chem. Chem. Phys.* **2016,** *18*, 18353-64.

102.   Zhao, R.; Lee, A. K. Y.; Huang, L.; Li, X.; Yang, F.; Abbatt, J. P. D., Photochemical processing of aqueous atmospheric brown carbon. *Atmos. Chem. Phys.* **2015,** *15*, (11), 6087-6100.

103.   Galloway, M. M.; Chhabra, P. S.; Chan, A. W. H.; Surratt, J. D.; Flagan, R. C.; Seinfeld, J. H.; Keutsch, F. N., Glyoxal uptake on ammonium sulphate seed aerosol: reaction products and

reversibility of uptake under dark and irradiated conditions. *Atmos. Chem. Phys.* **2009,** *9*, (10), 3331-45.

104.   Trainic, M.; Riziq, A. A.; Lavi, A.; Rudich, Y., Role of interfacial water in the heterogeneous uptake of glyoxal by mixed glycine and ammonium sulfate aerosols. *J. Phys. Chem. A* **2012,** *116*, (24), 5948-57.

105.   Galloway, M. M.; Loza, C. L.; Chhabra, P. S.; Chan, A. W. H.; Yee, L. D.; Seinfeld, J. H.; Keutsch, F. N., Analysis of photochemical and dark glyoxal uptake: Implications for SOA formation *Geophys. Res. Lett.* **2011,** *38*, L17811.

106.   Hamilton, J. F.; Baeza-Romero, M. T.; Finessi, E.; Rickard, A. R.; Healy, R. M.; Peppe, S.; Adams, T. J.; Daniels, M. J. S.; Ball, S. M.; Goodall, I. C. A.; Monks, P. S.; Borras, E.; Munoz, A., Online and offline mass spectrometric study of the impact of oxidation and ageing on glyoxal chemistry and uptake onto ammonium sulfate aerosols *Faraday Discuss.* **2013,** *165*, (447-72).

107.   Sareen, N.; Moussa, S. G.; McNeill, V. F., Photochemical aging of light-absorbing secondary organic aerosol material. *J. Phys. Chem. A* **2013,** *114*, (14), 2987-96.

108.   Xie, M.; Chen, X.; Hays, M. D.; Lewandowski, M.; Offenberg, J.; Kleindienst, T. E.; Holder, A. L., Light absorption of secondary organic aerosol: composition and contribution of nitroaromatic compounds *Environ. Sci. Technol.* **2017,** *51*, (20), 11607-16.

109.   Flores, J. M.; Washenfelder, R. A.; Adler, G.; Lee, H. J.; Segev, L.; Laskin, J.; Laskin, A.; Nizkorodov, S. A.; Brown, S. S.; Rudich, Y., Complex refractive indices in the near-ultraviolet spectral region of biogenic secondary organic aerosol aged with ammonia. *Phys. Chem. Chem. Phys.* **2014,** *16*, (22), 10629-42.

110.   Nakayama, T.; Sato, K.; Matsumi, Y.; Imamura, T.; Yamazaki, A.; Uchiyama, A., Wavelength dependence of refractive index of secondary organic aerosols generated during the ozonolysis and photooxidation of α-pinene. *Sola* **2012,** *8*, (119-23).

111.   Nakayama, T.; Matsumi, Y.; Sato, K.; Imamura, T.; Yamazaki, A.; Uchiyama, A., Laboratory studies on optical properties of secondary organic aerosols generated during the photooxidation of toluene and the ozonolysis of α-pinene *J. Geophys. Res. Atmos.* **2010,** *115*, (D24), D24204.

112.   Lin, Y. H.; Budisulistiorini, S. H.; Chu, K.; Siejack, R. A.; Zhang, H.; Riva, M.; Zhang, Z.; Gold, A.; Kautzman, K. E.; Surratt, J. D., Light-absorbing oligomer formation in secondary organic aerosol from reactive uptake of isoprene epoxydiols. *Environ. Sci. Technol.* **2014,** *48*, (20), 12012–21.

113.   Zhong, M.; Jang, M., Light absorption coefficient measurement of SOA using a UV–Visible spectrometer connected with an integrating sphere. *Atmos. Environ.* **2011,** *45*, (25), 4263-71.

114.   Nguyen, T. B.; Lee, P. B.; Updyke, K. M.; Bones, D. L.; Laskin, J.; Laskin, A.; Nizkorodov, S. A., Formation of nitrogen- and sulfur-containing light-absorbing compounds accelerated by evaporation of water from secondary organic aerosols. *J. Geophys. Res.* **2012,** *117*, D01207, 10.1029/2011jd016944.

115.   Lee, H. J.; Laskin, A.; Laskin, J.; Nizkorodov, S. A., Excitation-emission spectra and fluorescence quantum yields for fresh and aged biogenic secondary organic aerosols. *Environ. Sci. Technol.* **2013,** *47*, (11), 5763-70.

116.   Bones, D. L.; Henricksen, D. K.; Mang, S. A.; Gonsior, M.; Bateman, A. P.; Nguyen, T. B.; Cooper, W. J.; Nizkorodov, S. A., Appearance of strong absorbers and fluorophores in limonene-O_3 secondary organic aerosol due to NH_4^+-mediated chemical aging over long time scales. *J. Geophys. Res.* **2010,** *115*, D05203, 10.1029/2009jd012864.

117.   Mang, S. A.; Henricksen, D. K.; Bateman, A. P.; Sulbaek Andersen, M. P.; Blake, D. R.; Nizkorodov, S. A., Contribution of carbonyl photochemistry to aging of atmospheric secondary organic aerosol. *J. Phys. Chem. A* **2008,** *112*, (36), 8337-44.

118.   Jacobson, M. Z., Isolating nitrated and aromatic aerosols and nitrated aromatic gases as sources of ultraviolet light absorption. *J. Geophys. Res.* **1999,** *104*, (D3), 3527-42.

119.   Kwamena, N. O. A.; Abbatt, J. P. D., Heterogeneous nitration reactions of polycyclic aromatic hydrocarbons and n-hexane soot by exposure to $NO_3/NO_2/N_2O_5$. *Atmos. Environ.* **2008,** *42*, (35), 8309-14.

120.   Pitts Jr., J. N.; Van Cauwenberghe, K. A.; Grosjean, D.; Schmid, J. P.; Fitz, D. R.; Belser Jr., W. L.; Knudson, G. B.; Hynds, P. M., Atmospheric reactions of polycyclic aromatic hydrocarbons: facile formation of mutagenic nitro derivatives. *Science* **1978,** *202*, (4367), 515-19.

121.   Kim, H.; Paulson, S. E., Real refractive indices and volatility of secondary organic aerosol generated from photooxidation and ozonolysis of limonene, α-pinene and toluene *Atmos. Chem. Phys.* **2013,** *13*, 7711-23.

122.   Romonosky, D. E.; Laskin, A.; Laskin, J.; Nizkorodov, S. A., High-resolution mass spectrometry and molecular characterization of aqueous photochemistry products of common types of secondary organic aerosols. *J. Phys. Chem. A* **2014,** *119*, (11), 2594-2606.

123.   Forstner, H. J. L.; Flagan, R. C.; Seinfeld, J. H., Secondary organic aerosol from the photooxidation of aromatic hydrocarbons: Molecular composition. *Environ. Sci. Technol.* **1997,** *31*, (5), 1345-58.

124.   Liu, S.; Shilling, J. E.; Song, C.; Hiranuma, N.; Zaveri, R. A.; Russell, L. M., Hydrolysis of organonitrate functional groups in aerosol particles. *Aerosol Sci. Technol.* **2012,** *46*, (1359-69).

125.   Liu, P. F.; Abdelmalki, N.; Hung, H.-M.; Wang, Y.; Brune, W. H.; Martin, S. T., Ultraviolet and visible complex refractive indices of secondary organic material produced by photooxidation of the aromatic compounds toluene and m-xylene *Atmos. Chem. Phys.* **2015,** *15*, (1435-46).

126.   Huang, M.; Xu, J.; Cai, S.; Liu, X.; Zhao, W.; Hu, C.; Gu, X.; Fang, L.; Zhang, W., Characterization of brown carbon constituents of benzene secondary organic aerosol aged with ammonia. *J. Atmos. Chem.* **2017**, 1-14.

127.   Liu, Y.; Liggio, J.; Staebler, R.; Li, S.-M., Reactive uptake of ammonia to secondary organic aerosols: kinetics of organonitrogen formation. *Atmos. Chem. Phys.* **2015,** *15*, 13569-84.

128.   Chen, J.; Wenger, J. C.; Venables, D. S., Near-ultraviolet absorption cross sections of nitrophenols and their potential influence on tropospheric oxidation capacity. *J. Phys. Chem. A* **2011,** *115*, (44), 12235-42.

129.   Jang, M.; Kamens, R. M., Characterization of secondary aerosol from the photooxidation of toluene in the presence of NO_x and 1-Propene. *Environ. Sci. Technol.* **2001,** *35*, (18), 3626-39.

130.   Sato, K.; Hatakeyama, S.; Imamura, T., Secondary organic aerosol formation during the photooxidation of toluene: NO_x dependence of chemical composition. . *J. Phys. Chem. A* **2007,** *111*, (39), 9796-808.

131.   White, S. J.; Jamie, I. M.; Angove, D. E., Chemical characterisation of semi-volatile and aerosol compounds from the photooxidation of toluene and NO_x. *Atmos. Environ.* **2014,** *83*, 237-44.

132.   Desyaterik, Y.; Sun, Y.; Shen, X.; Lee, T.; Wang, X.; Collett, J. L., Speciation of "brown" carbon in cloud water impacted by agricultural biomass burning in eastern China. *J. Geophys. Res. Atmos.* **2013,** *118*, (13), 7389-99.

133.   Claeys, M.; Vermeylen, R.; Yasmeen, F.; Gomez-Gonzalez, Y.; Chi, X.; Maenhaut, W.; Meszaros, T.; Salma, I., Chemical characterisation of humic-like substances from urban, rural and tropical biomass burning environments using liquid chromatography with UV/vis photodiode array detection and electrospray ionisation mass spectrometry. *Environ. Chem.* **2012,** *9*, (3), 273-84.

134.   Roach, P. J.; Laskin, J.; Laskin, A., Molecular Characterization of Organic Aerosols Using Nanospray-Desorption/Electrospray Ionization-Mass Spectrometry. *Analyt. Chem.* **2010,** *82*, (19), 7979-86.

135.   Roach, P. J.; Laskin, J.; Laskin, A., Nanospray desorption electrospray ionization: an ambient method for liquid-extraction surface sampling in mass spectrometry. *Analyst* **2010,** *135*, (9), 2233-36.

Chapter 2   A Role for 2-Methyl Pyrrole in the Browning of 4-Oxopentanal and Limonene Secondary Organic Aerosol

2.1. Abstract

Reactions of ammonia or ammonium sulfate (AS) with carbonyls in secondary organic aerosol (SOA) produced from limonene are known to form brown carbon (BrC) with a distinctive absorption band at 505 nm. This study examined the browning processes in aqueous solutions of AS and 4-oxopentanal (4-OPA), which has a 1,4-dicarbonyl structural motif present in many limonene SOA compounds. Aqueous reactions of 4-OPA with AS were found to produce 2-methyl pyrrole (2-MP), which was detected by gas chromatography. While 2-MP does not absorb visible radiation, it can further react with 4-OPA eventually forming BrC compounds. This was demonstrated by reacting 2-MP with 4-OPA or limonene SOA, both of which produced BrC with absorption bands at 475 and 505 nm, respectively. The formation of BrC in the reaction of 4-OPA with AS and ammonium nitrate was greatly accelerated by evaporation of the solution suggesting an important role of the dehydration processes in BrC formation. 4-OPA was also found to produce BrC in aqueous reactions with a broad spectrum of amino acids and amines. These results suggest that 4-OPA may be the smallest atmospherically relevant compound capable of browning by the same mechanism as limonene SOA.

2.2. Introduction

Atmospheric particles have a significant direct effect on the global radiative budget due to scattering and absorption of solar radiation and an indirect effect due to the altering of cloud properties.[1] Light scattering by particles is the dominant direct effect, resulting in a negative forcing on climate (cooling). Light absorption reduces the cooling effect of particles by transforming a fraction of the solar energy into trapped heat.[2-4] There is an uncertainty in the sign and magnitude of the overall radiative forcing by aerosols[1, 2] because a majority of atmospheric particles scatter radiation, but a highly variable fraction of light-absorbing particles, namely mineral dust, black carbon, and brown carbon, have the ability to reduce the cooling effect of aerosols.[5-11]

Brown carbon (BrC) refers to light-absorbing carbonaceous matter in atmospheric particles capable of absorbing visible and near-UV radiation.[6, 12] BrC is attributed to primary sources, such as emissions from combustion and biomass burning, as well as secondary formation through multi-phase chemistry involving particles, cloud micro-droplets, and gases during atmospheric aging.[5-7, 13] Secondary sources of BrC include: OH oxidation of aromatic hydroxyacids and phenols in cloud water,[14-16] reactive uptake of gaseous isoprene and its derivatives on acidic atmospheric particles,[17, 18] aqueous photochemistry of pyruvic acid in the presence of common atmospheric electrolytes,[19, 20] acid-catalyzed aldol condensation of volatile aldehydes,[21-28] nitration of polycyclic aromatic hydrocarbons,[29-31] and formation of secondary organic aerosol (SOA) on highly acidic seed particles.[17, 32] Secondary BrC can also be formed by the reactions of carbonyls with aqueous NH_4^+, amino acids, and gaseous ammonia. For example, aqueous and multi-phase reactions of 1,2-dicarbonyls (glyoxal and methylglyoxal) with ammonium sulfate (AS) or amino acids have been found to produce BrC.[33-44]

Particular interest has been given to secondary BrC formed by the reaction of SOA with ammonia (NH_3) or AS, which may occur in geographic areas with large emissions of NH_3. SOA formed by the ozonolysis of limonene (LSOA) was found to be surprisingly effective in producing BrC by this mechanism,[45-50] in stark contrast with SOA formed by ozonolysis of α-pinene.[51] This aging process results in minor changes in the overall chemical composition of SOA, but a dramatic change in optical properties due to chromophores that give BrC its color.[45, 47, 48, 51, 52] Nguyen et al. (2013) investigated possible precursors responsible for the production of these chromophores in LSOA, specifically pinonaldehyde, limonoaldehyde, and ketolimononaldehyde (KLA). It was found that KLA, a secondary product of limonene ozonolysis, was the only precursor to produce brown products upon exposure to reduced nitrogen compounds, demonstrating a remarkable sensitivity of this process to the molecular structure of the precursor.[52]

The mechanism for the production of BrC chromophores via NH_3-mediated aging is actively being investigated.[12] It has been proposed that carbonyls react with NH_3 to form primary amines, which then undergo further reactions with unreacted carbonyls to form more stable secondary amines.[51, 52] These reactions are reversible, with the equilibrium shifted towards the carbonyl reactants. However, in the presence of multiple carbonyl groups within the same molecule, intramolecular cyclization may occur to form a stable N-heterocyclic compound. For example, formation of pyrrole-based compounds was recently observed in reaction of 1,4-dicarbonyl compound 2,5-hexanedione with AS or glycine.[53] The N-heterocyclic compounds can then undergo intermolecular carbonyl-imine condensation reactions to form the larger, conjugated oligomers.[51]

While the general features of the reaction mechanism are established, the molecular structures of the actual chromophores have not been determined. Even in the case of a single KLA precursor reacting with NH_3, a number of products were observed and the structures of the chromophores could not be confidently assigned.[52] Therefore, it is important to identify simpler model systems that lead to browning by closely related mechanisms. This study attempts to simplify the search for BrC chromophores by focusing on the 1,4-dicarbonyl substructure of KLA, using 4-oxopentanal (4-OPA) as a representative model system. To highlight the importance of the aldehyde group in 4-OPA we also examined a structurally related compound 6-methyl-hepten-2-one (6-MHO), which differs from 4-OPA by the lack of the reactive aldehyde group (Figure 2.1). 6-MHO is often co-produced with 4-OPA in the environment. For example, squalene, a compound commonly found in plant and animal lipids, undergoes ozonolysis to form 6-MHO as a primary product and 4-OPA as a secondary product.[54] Both 6-MHO and 4-OPA can also be produced via oxidation of common fragrance compounds, such as limonene, α-terpineol, and geraniol, with ozone or the hydroxyl radical.[55] The presence of 6-MHO and 4-OPA in the atmosphere has been confirmed in several field studies.[56-59] Additionally, the reaction of ozone with human skin lipids has been found to produce 6-MHO and 4-OPA in indoor environments at concentrations that may be hazardous to human health.[60, 61]
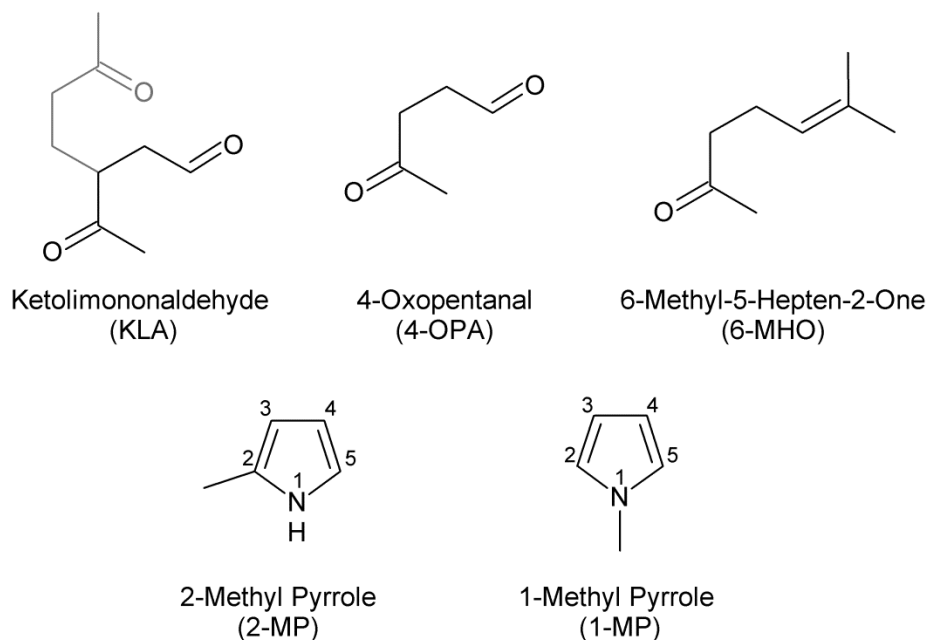
Figure 2.1: Structures of ketolimononaldehyde (KLA), 4-oxopentanal (4-OPA), 6-methyl-5-hepten-2-one (6-MHO), 2-methyl pyrrole (2-MP), and 1-methyl pyrrole (1-MP). KLA is a known BrC precursor. A portion of its structure is shown in gray to emphasize the structural similarity between KLA and 4-OPA. The browning potential of 4-OPA and 6-MHO are tested in this work, while 2-MP and 1-MP are investigated as possible reaction intermediates.

In this work, we show that the reaction of 4-OPA with AS results in carbonyl-imine conversion of the aldehyde group, followed by intramolecular cyclization to form a 2-methyl pyrrole (2-MP) intermediate, as shown in Figure 2.2. The proposed mechanism is consistent with the work of Kampf et al. (2016), who observed pyrrole derivative in reactions 2,5-hexanedione with AS.[53] The resulting 2-MP further reacts with 4-OPA to form oligomerization products, such as the dimer shown in Figure 2.2 (the identification of the actual chromophoric products will be described in a follow-up paper).
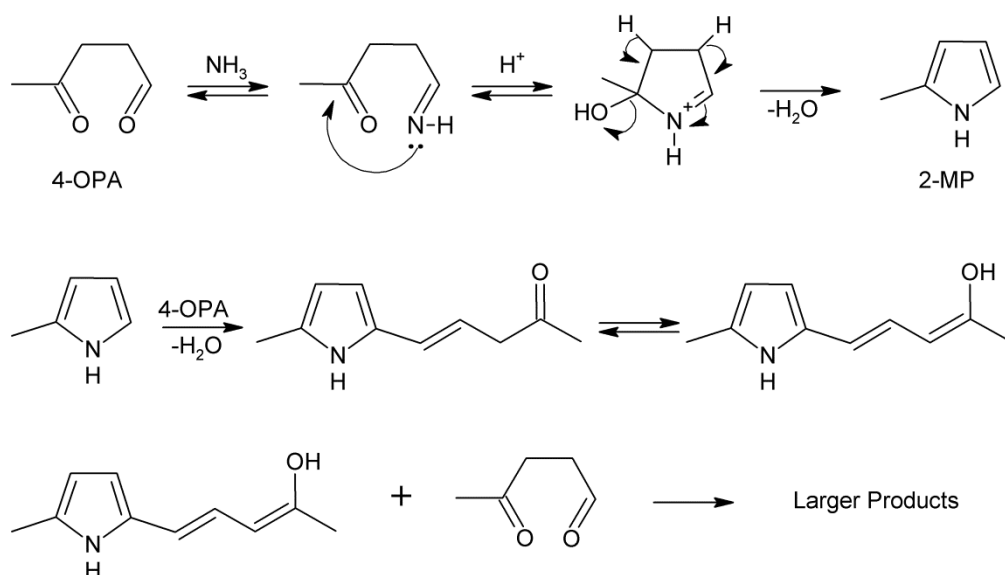
Figure 2.2: (Top) 4-OPA reacting with NH₃ to form 2-MP, an intermediate to the production of BrC chromophores. (Bottom) 2-MP further reacting with 4-OPA to form dimer products. A series of such reactions can produce larger, conjugated products potentially capable of absorbing visible light.

To confirm this hypothesis, we carried out bulk aqueous phase studies of 4-OPA mixed with AS or with 2-MP. Control experiments were also done using 6-MHO instead of 4-OPA and 1-methyl pyrrole (1-MP) instead of 2-MP, in order to examine molecular selectivity of this browning mechanism. The browning in 4-OPA + AS mixtures and lack of browning in 6-MHO + AS mixtures confirmed the importance of the presence of both carbonyl groups in 4-OPA. In addition, we found that browning in 4-OPA + AS and LSOA + AS aqueous mixtures leads to similar types of chromophores with distinctive absorption bands in the visible spectrum. Experiments were also done to examine acceleration in browning reactions during the evaporation of water in comparison to those undergoing slow aging in solution; a phenomenon that has been observed in the LSOA + AS BrC systems.[46] Lastly, 4-OPA reacting with a broad range of amino acids and amines resulted in the formation of BrC. We conclude that 4-OPA may be the smallest atmospherically relevant compound capable of browning by the same mechanism as LSOA, and a convenient model system for studying secondary BrC formation.

2.3. Experimental Methods

2.3.1. Aqueous Phase Reactions of 4-OPA with AS, 2-MP, and 1-MP

Experiments were performed to examine slow aging of aqueous phase 4-OPA in AS solution as a function of time. Liquid 4-OPA (>98% purity) was custom synthesized by commercial vendors DevirChim, Inc. (Roissy, France) and Richman Chemical Inc. (Lower Gwynedd, PA, USA). Solutions of AS were made by dissolving solid AS (Fisher Scientific, ≥99%) in deionized water. The reaction was initiated by adding a desired amount of 4-OPA to the AS solution and placing the mixture in a 1 cm quartz cuvette with a sealed top at room temperature (~23 °C). UV-Vis spectra ranging from 200-700 nm were recorded every 1-2 hours to monitor the progress of reaction for 36 to 100 hours, using a Shimadzu 1800 spectrophotometer with a distilled water reference. The three concentration combinations of 4-OPA in AS were: 0.2 M 4-OPA in 0.1 M AS, 0.06 M 4-OPA in 0.1 M AS and 0.03 M 4-OPA in 0.06 M AS. The UV-Vis experiments were repeated with 6-MHO (Sigma-Aldrich, 99%), a known precursor of 4-OPA in the atmosphere, to determine whether the aldehyde group of 4-OPA, which is absent in 6-MHO (Figure 2.1), is required for browning.

In order to positively confirm the formation of the 2-MP intermediate in the browning reaction, the 4-OPA + AS mixture was extracted with dichloromethane, and the brown extract was analyzed by gas chromatography electron impact ionization mass spectrometry (GC-EI-MS). A 2-MP standard in dichloromethane was analyzed as well and compared to samples taken from the 4-OPA + AS reaction mixture.

2-MP (Ark Pharm Inc., >95%) or 1-MP (Sigma-Aldrich, 99%) were used in place of AS to determine whether browning can occur through reactions with the 2-MP intermediate, without direct involvement of AS, and to determine whether the placement of the methyl group on the

pyrrole ring has an influence on browning. Concentrations of 4-OPA and MP were: 0.2 M 4-OPA in 0.1 M 1-MP or 2-MP and 0.06 M 4-OPA in 0.1 M 2-MP. The initial aqueous mixtures were opaque due to the presence of a colloid. To keep the reactants and products dissolved, 1 mL of each mixture and 1 mL of acetonitrile were combined, resulting in a transparent solution (implying that the reaction products were more soluble in acetonitrile than in water). The measurements were done with a Shimadzu 2450 spectrophotometer collecting a spectrum every 15 to 30 minutes over 5 to 24 hours while stirring and water cooling at 20 °C to minimize acetonitrile evaporation.

In order to compare the results with a previously studied LSOA +AS system,[47] LSOA was generated in a 14 L flow tube by a gas-phase reaction between limonene and ozone. Liquid limonene was injected into 5 SLM (standard liters per minute) air flow via a syringe pump at a rate of 25 µL/h. Ozone produced by flowing oxygen (Airgas; 99.994%) through an ozone generator at 0.7 SLM was injected downstream of the limonene injection. The initial mixing ratios of the limonene and ozone were 11 ppm and 9 ppm respectively, and the flow tube residence time was 2.5 min. The aerosol exited the flow tube, passed through a charcoal filter to remove excess ozone, and was collected on a foil substrate using a Sioutas Cascade Impactor. Several milligrams of LSOA were collected and dissolved in 1:1 acetonitrile in nanopure water to achieve a mass concentration comparable to the 0.06 M 4-OPA solution. The resulting solution was mixed with 0.1 M 2-MP and allowed to react. The UV-Vis spectra of the LSOA + 2-MP sample were recorded every 15 minutes for 22 hours.

2.3.2. Reactions of 4-OPA in Evaporating Solutions

The combination of 0.06 M 4-OPA + 0.1 M AS was selected to examine the possible acceleration of the browning process by evaporation. Solutions were mixed in a scintillation vial

to create a total mixture volume of 2 mL. The vial was connected to a Buchi Rotavapor R-215 at 30°C and evaporated under rough vacuum (< 10 mbar) for 10 minutes until all of the water was removed and a only a brown residue remained. Subsequently, 2 mL of distilled water was added to the vial to dissolve the residue and a UV-Vis spectrum of the resulting solution was acquired. This evaporation and dissolving process was repeated three times, until the change in the measured absorbance was minimal. Similar evaporation experiments were done with ammonium nitrate (AN; Fisher Scientific, ≥99%) in place of AS for comparison. A control experiment was also done in the absence of ammonium ions, by evaporating the solution of 4-OPA alone. The UV-Vis spectra obtained in this set of evaporation experiments were compared to the spectrum acquired for the aqueous 0.06 M 4-OPA + 0.1 M AS sample aged for 48 hours at room temperature.

2.3.3. Reactions of 4-OPA with Amines and Amino Acids

Additional studies were performed to investigate the reactions of 4-OPA with a variety of other reduced-nitrogen species, including amines, amides and the nitroso functional group. The following reactions were conducted by undergraduate student Forest Heller at the Pacific Northwest National Laboratory in Richland, WA. The reagents were purchased from Sigma-Aldrich at the highest available purities (typically >98%) and used without further purification. Based on qualitative observations, only certain amines formed brown products while the amides (acetamide, N,N-dimethylacetamide, N,N-dimethylformamide) and N-Nitrosodiethylamine did not. In order to quantitatively test the amines and compare them to reactions with ammonia, stock solutions of 0.09 M were prepared using the following reagents: 2-amino-2-methyl-1-propanol (AMP), AS, diethylamine (DEA), dimethylamine (DMA), ethylenediamine (EDA), glycine (GLY), methylamine (MA), methyldiethanolamine (MDEA), ethanolamine (MEA),

ammonium hydroxide (NH₄OH), AN, propylamine (PA), piperazine (PIP), and trimethylamine

(TMA). A stock solution of 0.03 M 4-OPA was also prepared. A fixed volume of 4-OPA stock

solution and varying volume fractions of nitrogen-containing stock solutions were mixed

together and diluted to a total volume of 1.0 mL, resulting in 0.015 M 4-OPA and 0.0-0.045 M

nitrogen-containing compound. The UV-Vis spectrum of the initial mixture was recorded with a

UV-Vis spectrophotometer (USB 2000+, Ocean Optics). Each sample was aged at an elevated

temperature of 40°C to increase the reaction rate. After a 75 minute interval, the sample was

removed from the incubator and its UV-Vis spectrum was recorded. The procedure was repeated

until the observed absorption spectrum stopped changing.

2.3.4. Mass Absorption Coefficient (MAC)

The effective mass absorption coefficient (*MAC*) was used to quantify the extent of

browning in all studied mixtures. The *MAC* was calculated using the base-10 absorbance A_{10} of

the sample with the total organic carbon mass concentration of the solution C_{mass} (g cm^{-3}) and the

path length of the cuvette *b* (cm):[62]

$$MAC(\lambda) = \frac{A_{10}(\lambda)*\ln(10)}{b*C_{mass}}$$
(**Equation 2.1**)

C$_{mass}$ was the mass concentration of the carbonyl reactant (4-OPA, 6-MHO or LSOA). The

change in the mass of organics resulting from the ammonia reaction is minor based on results of

previous studies of KLA[52] and LSOA.[51] GC-EI-MS experiments confirmed that only a small

fraction of 4-OPA was converted into BrC products. Therefore, the nitrogen-containing

reactants (AS, AN, 2-MP, 1-MP, amino acids, amines, etc.) were not included in *C*$_{mass}$ to make it

easier to compare results of different experiments. For aqueous reactants (4-OPA and 6-MHO),

C$_{mass}$ was calculated by converting the measured volume of the reactant to mass using its density

and dividing it by the total volume of solution. For LSOA, the mass of SOA on the filter was divided by the volume of solvent used for extraction.

2.4. Results and Discussion

2.4.1. Role of Pyrrole Compounds in Browning Reactions of 4-OPA and LSOA with AS

Figure 2.3a shows time-dependent *MAC* spectra for a mixture containing 0.06 M 4-OPA and 0.1 M AS. In this mixture, as well as all other 4-OPA in AS mixtures examined in this work, a well-defined absorption peak at 475 nm increased in intensity as time progressed, accompanied by a visible browning of the solutions. The initial growth rate of the 475 nm peak increased with the concentration of 4-OPA and AS in solution (Figure 2.3c). However, the extent of browning at longer time scales did not correlate with 4-OPA concentration.

LSOA was also mixed with AS and aged in a similar way, resulting in browning of the solution as observed in previous experiments.[45] Figure 2.3b compares the *MAC* spectra of the aged 4-OPA + AS and LSOA + AS solutions after 22 hours. Both systems generated prominent absorption peaks at similar wavelengths (475 mm for 4-OPA and 505 nm for LSOA) and with comparable *MAC* values. These results suggest that browning of 4-OPA and LSOA occurs by a similar mechanism. In addition, these results support our assumption that the 1,4-dicarbonyl motif of KLA contributes to the browning of LSOA.[52] The shift of the 505 nm peak in the LSOA + AS system to 475 nm in the 4-OPA + AS system may be due the smaller molecular size of chromophores formed in the latter system. LSOA is a rather complex mixture of different compounds, which contains molecules with structurally similar motifs to 4-OPA, but also with other functional groups that may lead to the observed spectral shift. Mixtures of 6-MHO with AS did not produce a significant growth of new bands in the absorption spectra. This confirms that

39

the aldehyde group in 4-OPA, which is absent in 6-MHO, is required for browning to occur, further supporting the assumption in Figure 2.2 that both carbonyl groups in 4-OPA are essential for its browning chemistry.
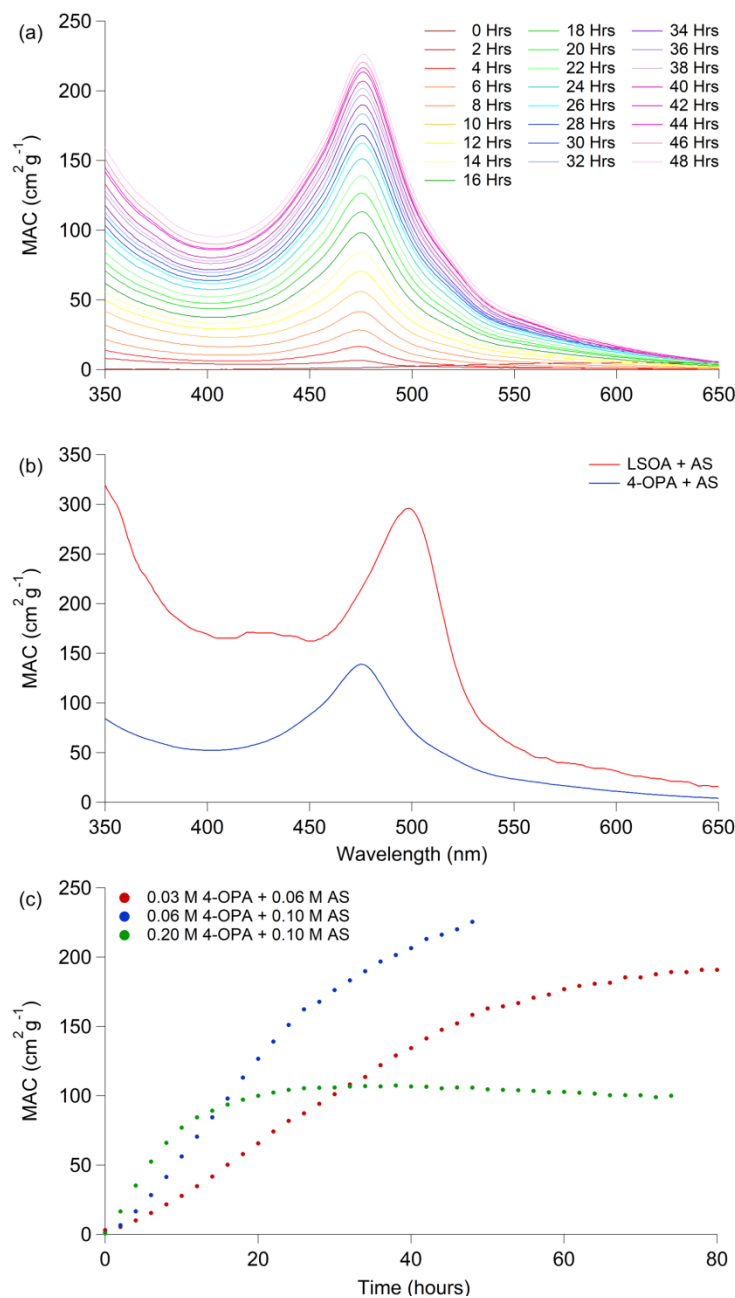
Figure 2.3: (a) Time-dependent *MAC* of 0.06 M 4-OPA in 0.1 M AS showing the growth of an absorption peak at 475 nm, accompanied by browning of the solution. (b) A comparison of *MAC* spectra for 4-OPA and LSOA after slow aging with AS for 22 hours. (c) Comparison of peak growth at 475 nm for each combination of 4-OPA + AS concentrations tested.

Our hypothesis is that browning begins by reaction of 4-OPA with dissolved NH_3 resulting in the formation of a 2-MP intermediate after intramolecular cyclization. Formation of more complex compounds (Figure 2.2), some of which may be light absorbing, is initiated by oligomerization reactions between 2-MP with 4-OPA. To prove that 2-MP is actually produced in the 4-OPA + AS aqueous reaction, we compared the GC-MS chromatograms of the reaction mixture with that of a 2-MP solution in dichloromethane. The 2-MP standard eluted at 3.8 min and had three distinct peaks in the EI mass spectrum, at m/z 53, 80 and 81, in agreement with the mass spectrum of 2-MP in the NIST library. 4-OPA eluted at 4.1 min and had strong peaks at m/z 57, 72, an 85, as well as a number of weaker peaks, including one at m/z 81 (but no peak at m/z 80). A selected ion chromatogram for the extracted 4-OPA + AS mixture observed at m/z 80 produced a chromatographic peak at the same retention time (3.8 min) as in the 2-MP standard. In addition to the unreacted 4-OPA and 2-MP, the mixture contained a number of other compounds eluting between 2-30 min, suggesting complex secondary chemistry leading to BrC formation. None of these compounds could be identified using the NIST mass spectral library.

To further demonstrate the important role of 2-MP in browning of 4-OPA, we acquired UV-Vis spectra of 0.2 M 4-OPA and 0.06 M 4-OPA in 0.1 M 2-MP mixtures. Figure 2.4a shows results of the 0.2 M 4-OPA + 0.1 M 2-MP experiment, in which a peak growth occurs at 475 nm, a wavelength pertinent to the browning of 4-OPA + AS mixtures. Browning was found to occur more quickly at 0.2 M in comparison to 0.06 M 4-OPA. To investigate the importance of methyl group placement on the pyrrole ring, 0.2 M 4-OPA was reacted with 0.1 M 1-MP in place of 2-MP. The mixture of 4-OPA and 1-MP did not produce absorption peaks in the visible range (Figure 2.4b), indicating that the formation of light-absorbing products is sensitive to the position of the methyl group in the pyrrole ring under these reaction conditions. Under other reaction

conditions, such as the heating described in the amine and amino acid section below, 1-MP may potentially lead to browning by a different chemical mechanism.

The experiments were also carried out for LSOA with 2-MP, in absence of NH_3. Similarly to the 4-OPA + 2-MP mixtures, LSOA reaction with 0.1 M 2-MP resulted in efficient browning evidenced by the growth of a peak at 482 nm in the UV-Vis spectrum (Figure 2.4c). At a similar mass concentration to 4-OPA, LSOA in 0.1 M 2-MP browned more slowly than 4-OPA. In the LSOA mixture only a fraction of species have the necessary structure for efficient browning, so the overall concentration of compounds capable of browning is lower compared to solutions containing only 4-OPA.
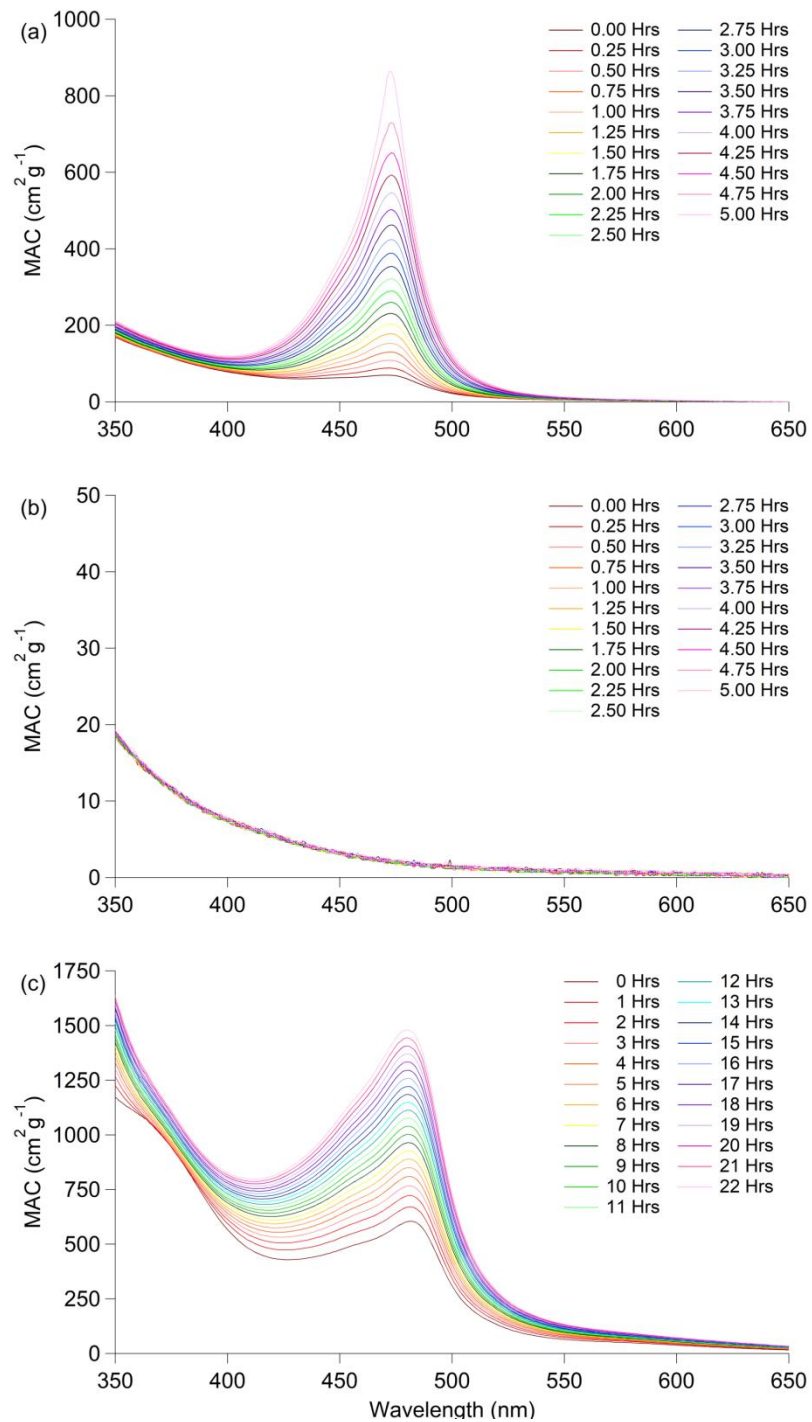
Figure 2.4: (a) *MAC* of 0.2 M 4-OPA in 0.1 M 2-MP verses time showing the growth of a peak at 475 nm. (b) *MAC* of 0.2 M 4-OPA in 0.1 M 1-MP over time showing no peak growth. (c) *MAC* of LSOA reacted with 0.1 M 2-MP with a peak growing in at 482 nm. *MAC* was calculated using Eq. (1). Y-axis is scaled differently in each panel to show differences between each system.

Collectively, these experiments confirm that the conversion of 4-OPA into 2-MP may be an important initial step in the browning process. They also suggest that similar pyrrole-based intermediates may be important in browning chemistry of LSOA. The 2-MP absorbs only in the UV range, so it cannot be responsible for the brown color of the solution. However, oligomerization reactions involving 2-MP as an intermediate may produce more complex, conjugated compounds capable of absorbing visible radiation. A unique feature of the pyrrole ring is that nitrogen donates its nonbonding electrons to the ring by resonance. Increased electron density at C atoms makes them accessible for electrophilic substitution, such as reactions with aldehydes and ketones, with the C_5 carbon of the pyrrole ring being the most reactive (Figure 2.2). The presence of more than one reactive site in the 2-MP ring (C_3, C_4, C_5) and two carbonyl groups in 4-OPA provides multiple cross-oligomerization pathways that may lead to the formation of larger light-absorbing species. The molecular identity of the chromophores responsible for the appearance of the distinctive 475 nm absorption band in the 4-OPA + AS and 4-OPA + 2-MP is outside of the scope of this study, and will be discussed in detail in a follow-up publication.

2.4.2. Browning of 4-OPA Accelerated by Evaporation

The mechanism outlined in Figure 2.2 suggests that the browning process may be accelerated by actively removing water from the 4-OPA + AS system. In the evaporation experiments, 0.1 M AS or AN was mixed with 0.06 M 4-OPA and the solution was evaporated. The reaction products were subsequently re-dissolved in water and the evaporation process was repeated until the change in *MAC* values was minimal between the successive evaporations. Figure 2.5 shows that the evaporation of 4-OPA + AS and 4-OPA + AN solutions resulted in *MAC* values comparable to those obtained in the much slower reaction in unevaporated aqueous

solutions. The reaction appears to be very fast and limited by the evaporation rate. For example, a comparison of Figure 2.3 (*MAC* of ~100 cm^2g^{-1} achieved after about 24 hours of aqueous reaction) and Figure 2.5 (*MAC* of ~100 cm^2g^{-1} achieved after 10 min in the first evaporation) suggests that BrC formation reactions occur at least 2-3 orders of magnitude faster during the evaporation process.

Figure 2.5 shows that the evaporation of AS yields a *MAC* value nearly two times higher than AN (180 cm^2g^{-1} for AS and 100 cm^2g^{-1} for AN). The initial solution pH was very similar (5.2 in 0.1 M AS and 5.1 in 0.1 M AN based on the E-AIM model II: http://www.aim.env.uea.ac.uk/aim/aim.php).[63] However, the solution of AS has twice as many ammonium ions than AN, and the extent of browning occurring in the reaction with 4-OPA may be dependent on the total amount of ammonium ions present in the system. Additionally, AN is more likely to volatilize as $HNO_3 + NH_3$ during the evaporation process leaving less nitrogen available for the reaction. The absorption spectra are slightly different for the 4-OPA + AS and 4-OPA + AN cases: the 4-OPA + AN spectrum is slightly red shifted and has more pronounced additional bands between 550 and 600 nm. This difference suggests that the anion also affects the structures of the products, possibly by altering the ionic strength and pH of the evaporating solution as well as solubility of 4-OPA. For example, glyoxal hydration equilibrium is known to be strongly and selectively affected by the sulfate anions;[44, 64] similar effects may occur for the hydration of 4-OPA. A control experiment was performed with 4-OPA in deionized water to examine the reactivity of 4-OPA undergoing evaporation in the absence of ammonium ions. This experiment did not result in the growth of any peaks in the *MAC* spectrum, confirming that the ammonium ions are needed for the browning.

The evaporation of 4-OPA + AS and 4-OPA + AN solutions resulted in smaller *MAC* values compared to *MAC* values after 48 hours of reaction in unevaporated aqueous solution (Figure 2.5). In the previous studies of LSOA + AS[46] and glyoxal + AS,[65] the evaporation was found to produce larger *MAC* values than the slower aqueous reaction. It is possible that some 4-OPA was lost during the evaporation step because it is a fairly volatile molecule. Although the *MAC* values of the evaporated mixtures were somewhat lower, they may be more atmospherically relevant because they produce BrC at a much faster rate and are less likely to compete with the photobleaching of BrC by sunlight that has been observed in several studies.[36, 66]
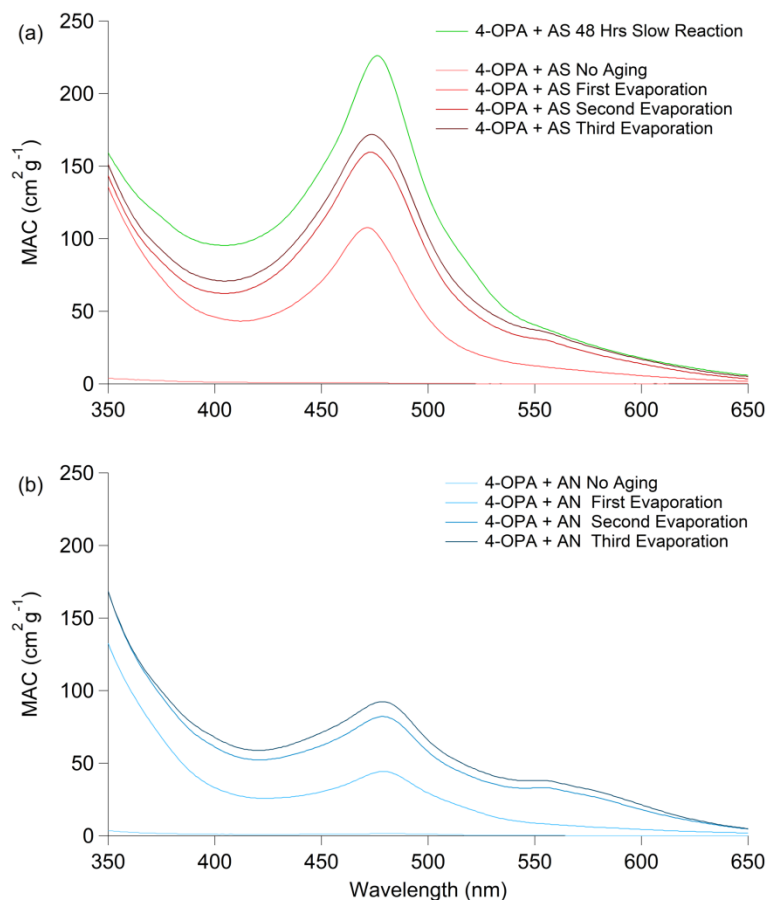
Figure 2.5: *MAC* after evaporation and dissolution for 0.1 M AS (a) and AN (b) reacting with 0.06 M 4-OPA. For the 4-OPA + AS case, the result of slow aging in aqueous unevaporated solution is also shown.

2.4.3. Browning Reactions of 4-OPA Reacting with Amines and Amino Acids

In order to further explore the BrC-forming potential of 4-OPA, additional studies were conducted with 4-OPA reacted with a variety of nitrogen-containing organic compounds. The amines and amino acids produced visible browning of the solutions, but this was not the case for nitroso and amide compounds. The concentration and time dependence of the reaction was then further quantified by keeping the 4-OPA concentration constant and varying the concentration of the nitrogen-containing species. This generally shows that 4-OPA has the ability to react with these nitrogen-containing compounds and over time form products that have the ability to absorb in the UV and more importantly the visible region. This is not to say that these amines and amino acids proceed by the same mechanism as AS and 2-MP. For example, secondary and tertiary amines cannot undergo the intramolecular reaction shown in Figure 2.2 to form pyrrole structures. A possible pathway for brown carbon formation with secondary amines and 4-OPA is the production of an enamine followed by an intermolecular reaction with a second 4-OPA molecule, similar to a Stork enamine alkylation, leading to oligomerization. Tertiary amines and 4-OPA can undergo aldol condensation reactions promoted by the basicity of the amines.

Figure 2.6 compares the *MAC* values after nine 75-minute heating intervals (675 minutes; the concentration of all nitrogen-containing species is 0.035 M). In all cases, there is an increase in *MAC* values in the UV region with a broad absorption tail extending into the visible region. The largest *MAC* values in the visible range were observed for secondary amines DMA, DEA, and PIP. In several cases specific peaks are observed, such as for MA at 325 nm and for PA near 350 nm. The *MAC* values in the visible region were considerably larger for amines and amino acids compared to NH_4OH, AN, and AS, which have the lowest *MAC* values in Figure 2.6. The much larger *MAC* values resulting from reaction of amines and amino acids with 4-OPA can

compensate for the fact that amines and amino acids are less abundant in the atmosphere compared to AS.
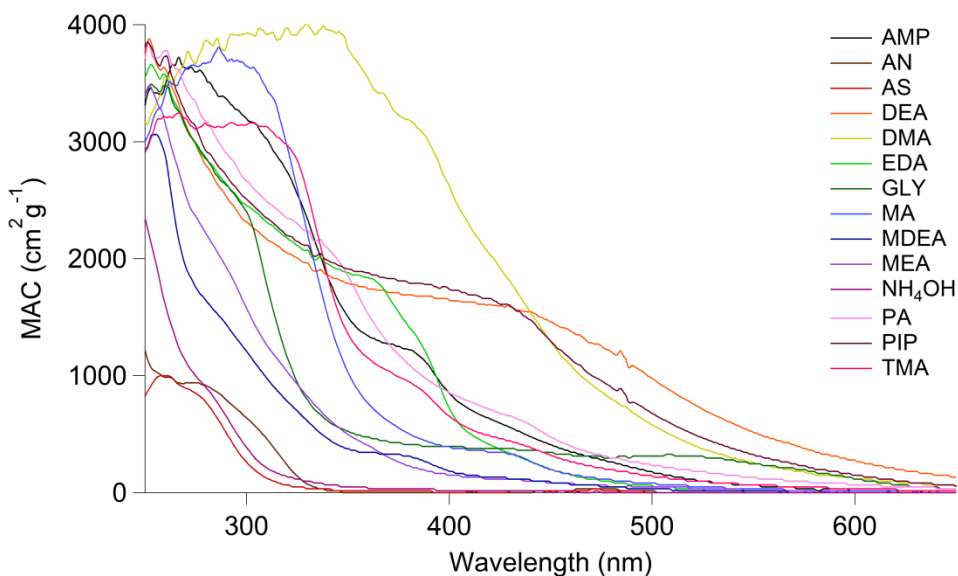
Figure 2.6: *MAC* after 675 minutes of aging at 40°C. The concentration of 4-OPA was 0.015 M and the concentration of each nitrogen-containing compound was 0.035 M. Abbreviations of nitrogen-containing compounds: 2-amino-2-methyl-1-propanol (AMP), ammonium nitrate (AN), ammonium sulfate (AS), diethylamine (DEA), dimethylamine (DMA), ethylenediamine (EDA), glycine (GLY), methylamine (MA), methyldiethanolamine (MDEA), ethanolamine (MEA), ammonium hydroxide (NH4OH), propylamine (PA), piperazine (PIP), and trimethylamine (TMA).

2.5. Atmospheric Implications

The experiments described in this paper demonstrate that 4-OPA may be the smallest atmospherically relevant molecule that undergoes browning by the same general mechanism as previously observed in LSOA. This assertion is based on the fact that browning of 4-OPA in an aqueous solution in the presence of AS produces remarkably similar absorption spectra to those observed for the LSOA + AS system. Furthermore, similar spectra are observed in reactions of 4-OPA with 2-MP and of LSOA with 2-MP, supporting the hypothesis that pyrrole-based compounds act as probable intermediates in this browning chemistry. Pyrroles are reactive

towards carbonyls, and they may continue to react with 4-OPA or structurally related compounds in LSOA to produce larger, light-absorbing products. The *MAC* values from the 4-OPA + AS reaction products are modest, and not large enough to compete with primary BrC from biomass burning, but reactions of 4-OPA could provide important insights into the chemical mechanisms of secondary BrC formation in reactions of SOA. Although the aqueous reaction of 4-OPA with either AS or AN is relatively slow, it is greatly accelerated by condensation reactions promoted by evaporation. This reinforces the suggestion from previous studies that BrC can be produced efficiently in evaporation of cloud and fog droplets. Finally, the browning of 4-OPA is not limited to reactions with AN and AS. It can also react with a variety of other nitrogen-containing species including amines, amino acids, and compounds containing ammonium ions. Of these, secondary amines produce the highest *MAC* values in the visible region. We conclude that 4-OPA is a convenient model system for studying secondary BrC formation in reactions of carbonyls and reduced nitrogen compounds.

2.6. References

1.   Boucher, O.; Randall, D.; Artaxo, P.; Bretherton, C.; Feingold, G.; Forster, P.; Kerminen, V. M.; Kondo, Y.; Liao, H.; Lohmann, U.; Rasch, P.; Satheesh, S. K.; Sherwood, S.; Stevens, B.; Zhang, X. Y., Climate Change 2013: The Physical Science Basis. Contribution of Working Group I to the Fifth Assessment Report of the Intergovernmental Panel on Climate Change. In Cambridge University Press: New York, NY, USA, 2013.

2.   Climate Change 2007: The Physical Science Basis. Contribution of Working Group I to the Fourth Assessment Report of the Intergovernmental Panel on Climate Change. In *IPCC*, Solomon, S.; Qin, D.; Manning, M.; Chen, Z.; Marquis, M.; Averyt, K. B.; Tignor, M.; Miller, H. L., Eds. Cambridge University Press: Cambridge, United Kingdom and New York, NY, USA, 2007.

3.   Finlayson-Pitts, B. J.; Pitts Jr, J. N., *Chemistry of the Upper and Lower Atmosphere: Theory, Experiments, and Applications*. Academic Press: San Diego, CA, 2000.

4.   Forster, P.; Ramaswamy, V.; Artaxo, P.; Berntsen, T.; Betts, R.; Fahey, D. W.; Haywood, J.; Lean, J.; Lowe, D. C.; Myhre, G.; Nganga, J.; Prinn, R.; Raga, G.; Schulz, M.; Van Dorland, R., Changes in Atmospheric Constituents and in Radiative Forcing. In *Climate Change 2007: The Physical Science Basis. Contribution of Working Group I to the Fourth Assessment Report of the Intergovernmental Panel on Climate Change*, Cambridge University Press: Cambridge, United Kingdom and New York, NY, USA, 2007; pp 129-243.

5.   Alexander, D. T.; Crozier, P. A.; Anderson, J. R., Brown carbon spheres in East Asian outflow and their optical properties. *Science* **2008,** *321*, (5890), 833-36.

6.   Andreae, M. O.; Gelencser, A., Black carbon or brown carbon? The nature of light-absorbing carbonaceous aerosols. *Atmos. Chem. Phys.* **2006,** *6*, (10), 3131-48.

7.   Bond, T. C.; Bergstrom, R. W., Light absorption by carbonaceous particles: an investigative review. *Aerosol Sci. Technol.* **2006,** *40*, (1), 27-67.

8.   Bahadur, R.; Praveen, P. S.; Xu, Y.; Ramanathan, V., Solar absorption by elemental and brown carbon determined from spectral observations. *Proc. Natl. Acad. Sci. U. S. A.* **2012,** *109*, (43), 17366-71.

9.   Chunga, C. E.; Ramanathan, V.; Decremera, D., Observationally constrained estimates of carbonaceous aerosol radiative forcing. *Proc. Natl. Acad. Sci. U. S. A.* **2012,** *109*, (29), 11624-29.

10.   Ramanathan, V.; Li, F.; Ramana, M. V.; Praveen, P. S.; Kim, D.; Corrigan, C. E.; Nguyen, H.; Stone, E. A.; Schauer, J. J.; Carmichael, G. R.; Adhikary, B.; Yoon, S. C., Atmospheric brown clouds: hemispherical and regional variations in long-range transport, absorption, and radiative forcing. *J. Geophys. Res.* **2007,** *112*, D22S21, 10.1029/2006JD008124.

11.   Usher, C. R.; Michel, A. E.; Grassian, V. H., Reactions on mineral dust. *Chem. Rev.* **2003,** *103*, (12), 4883-4940.

12.   Laskin, A.; Laskin, J.; Nizkorodov, S. A., Chemistry of atmospheric brown carbon. *Chem. Rev.* **2015,** *115*, (10), 4335-82.

13.   Moosmüller, H.; Chakrabarty, R. K.; Arnott, W. P., Aerosol light absorption and its measurement: a review. *J. Quant. Spectrosc. Radiat. Transfer* **2009,** *110*, (11), 844-78.

14.   Chang, J. L.; Thompson, J. E., Characterization of colored products formed during irradiation of aqueous solutions containing H_2O_2 and phenolic compounds. *Atmos. Environ.* **2010,** *44*, (4), 541-51.

15.   Gelencser, A.; Hoffer, A.; Kiss, G.; Tombacz, E.; Kurdi, R.; Bencze, L., In-situ formation of light-absorbing organic matter in cloud water. *J. Atmos. Chem.* **2003,** *45*, (1), 25-33.

16.   Hoffer, A.; Kiss, G.; Blazso, M.; Gelencser, A., Chemical characterization of humic-like substances (HULIS) formed from a lignin-type precursor in model cloud water. *Geophys. Res. Lett.* **2004,** *31*, L06115, 10.1029/2003GL018962.

17.   Lin, Y. H.; Budisulistiorini, S. H.; Chu, K.; Siejack, R. A.; Zhang, H.; Riva, M.; Zhang, Z.; Gold, A.; Kautzman, K. E.; Surratt, J. D., Light-absorbing oligomer formation in secondary organic aerosol from reactive uptake of isoprene epoxydiols. *Environ. Sci. Technol.* **2014,** *48*, (20), 12012–21.

18.   Limbeck, A.; Kulmala, M.; Puxbaum, H., Secondary organic aerosol formation in the atmosphere via heterogeneous reaction of gaseous isoprene on acidic particles. *Geophys. Res. Lett.* **2003,** *30*, (19), 1996, 10.1029/2003GL017738.

19.   Rincon, A. G.; Guzmán, M. I.; Hoffmann, M. R.; Colussi, A. J., Optical absorptivity versus molecular composition of model organic aerosol matter. *J. Phys. Chem. A* **2009,** *113*, (39), 10512-20.

20.   Rincon, A. G.; Guzmán, M. I.; Hoffmann, M. R.; Colussi, A. J., Thermochromism of model organic aerosol matter. *J. Phys. Chem. Lett.* **2010,** *1*, (1), 368-73.

21.   Casale, M.; Richman, A.; Elrod, M.; Garland, R.; Beaver, M.; Tolbert, M., Kinetics of acid-catalyzed aldol condensation reactions of aliphatic aldehydes. *Atmos. Environ.* **2007,** *41*, (29), 6212-24.

22.   Noziere, B.; Esteve, W., Light-absorbing aldol condensation products in acidic aerosols: spectra, kinetics, and contribution to the absorption index. *Atmos. Environ.* **2007,** *41*, (6), 1150-63.

23.   Esteve, W.; Noziere, B., Uptake and reaction kinetics of acetone, 2-butanone, 2,4-pentanedione, and acetaldehyde in sulfuric acid solutions. *J. Phys. Chem. A* **2005,** *109*, (48), 10920-28.

24.   Garland, R. M.; Elrod, M. J.; Kincaid, K.; Beaver, M. R.; Jimenez, J. L.; Tolbert, M. A., Acid-catalyzed reactions of hexanal on sulfuric acid particles: identification of reaction products. *Atmos. Environ.* **2006,** *40*, (35), 6863-78.

25.   Krizner, H. E.; De Haan, D. O.; Kua, J., Thermodynamics and kinetics of methylglyoxal dimer formation: a computational study. *J. Phys. Chem. A* **2009,** *113*, (25), 6994-7001.

26.   Noziere, B.; Esteve, W., Organic reactions increasing the absorption index of atmospheric sulfuric acid aerosols. *Geophys. Res. Lett.* **2005,** *32*, L03812, 10.1029/2004GL021942.

27.   Noziere, B.; Voisin, D.; Longfellow, C. A.; Friedli, H.; Henry, B. E.; Hanson, D. R., The uptake of methyl vinyl ketone, methacrolein, and 2-methyl-3-butene-2-ol onto sulfuric acid solutions. *J. Phys. Chem. A* **2006,** *110*, (7), 2387-95.

28.   Zhao, J.; Levitt, N. P.; Zhang, R., Heterogeneous chemistry of octanal and 2,4-hexadienal with sulfuric acid. *Geophys. Res. Lett.* **2005,** *32*, L09802, 10.1029/2004GL022200.

29.   Jacobson, M. Z., Isolating nitrated and aromatic aerosols and nitrated aromatic gases as sources of ultraviolet light absorption. *J. Geophys. Res.* **1999,** *104*, (D3), 3527-42.
30.   Kwamena, N. O. A.; Abbatt, J. P. D., Heterogeneous nitration reactions of polycyclic aromatic hydrocarbons and n-hexane soot by exposure to $NO_3/NO_2/N_2O_5$. *Atmos. Environ.* **2008,** *42*, (35), 8309-14.

31.   Pitts Jr., J. N.; Van Cauwenberghe, K. A.; Grosjean, D.; Schmid, J. P.; Fitz, D. R.; Belser Jr., W. L.; Knudson, G. B.; Hynds, P. M., Atmospheric reactions of polycyclic aromatic hydrocarbons: facile formation of mutagenic nitro derivatives. *Science* **1978,** *202*, (4367), 515-19.

32.   Song, C.; Gyawali, M.; Zaveri, R. A.; Shilling, J. E.; Arnott, W. P., Light absorption by secondary organic aerosol from α-pinene: effects of oxidants, seed aerosol acidity, and relative humidity. *J. Geophys. Res. Atmos.* **2013,** *118*, 11741-49.

33.   Powelson, M. H.; Espelien, B. M.; Hawkins, L. N.; Galloway, M. M.; De Haan, D. O., Brown carbon formation by aqueous-phase carbonyl compound reactions with amines and ammonium sulfate. *Environ. Sci. Technol.* **2014,** *48*, (2), 985-93.

34.   Lin, P.; Laskin, J.; Nizkorodov, S. A.; Laskin, A., Revealing brown carbon chromophores produced in reactions of methylglyoxal with ammonium sulfate. *Environ. Sci. Technol.* **2015,** *49*, (24), 14257-66.

35.   Tang, M.; Alexander, J. M.; Kwon, D.; Estillore, A. D.; Laskina, O.; Young, M. A.; Kleiber, P. D.; Grassian, V. H., Optical and physicochemical properties of brown carbon aerosol: light scattering, FTIR extinction spectroscopy, and hygroscopic growth. *J. Phys. Chem. A* **2016,** *120*, (24), 4155-66.

36.   Zhao, R.; Lee, A. K. Y.; Huang, L.; Li, X.; Yang, F.; Abbatt, J. P. D., Photochemical processing of aqueous atmospheric brown carbon. *Atmos. Chem. Phys.* **2015,** *15*, (11), 6087-6100.

37.   Galloway, M. M.; Chhabra, P. S.; Chan, A. W. H.; Surratt, J. D.; Flagan, R. C.; Seinfeld, J. H.; Keutsch, F. N., Glyoxal uptake on ammonium sulphate seed aerosol: reaction products and reversibility of uptake under dark and irradiated conditions. *Atmos. Chem. Phys.* **2009,** *9*, (10), 3331-45.

38.   Noziere, B.; Dziedzic, P.; Cordova, A., Products and kinetics of the liquid-phase reaction of glyoxal catalyzed by ammonium ions (NH_4^+). *J. Phys. Chem. A* **2009,** *113*, (1), 231-37.

39.   Sareen, N.; Schwier, A. N.; Shapiro, E. L.; Mitroo, D.; McNeill, V. F., Secondary organic material formed by methylglyoxal in aqueous aerosol mimics. *Atmos. Chem. Phys.* **2010,** *10*, (3), 997-1016.

40.   De Haan, D. O.; Tolbert, M. A.; Jimenez, J. L., Atmospheric condensed-phase reactions of glyoxal with methylamine. *Geophys. Res. Lett.* **2009,** *36*, L11819, 10.1029/2009gl037441.

41.   Shapiro, E. L.; Szprengiel, J.; Sareen, N.; Jen, C. N.; Giordano, M. R.; McNeill, V. F., Light-absorbing secondary organic material formed by glyoxal in aqueous aerosol mimics. *Atmos. Chem. Phys.* **2009,** *9*, (7), 2289-2300.

42.   Trainic, M.; Abo Riziq, A.; Lavi, A.; Flores, J. M.; Rudich, Y., The optical, physical and chemical properties of the products of glyoxal uptake on ammonium sulfate seed aerosols. *Atmos. Chem. Phys.* **2011,** *11*, (18), 9697-9707.

43.   Kampf, C. J.; Jakob, R.; Hoffmann, T., Identification and characterization of aging products in the glyoxal/ammonium sulfate system - implications for light-absorbing material in atmospheric aerosols. *Atmos. Chem. Phys.* **2012,** *12*, (14), 6323-33.

44.   Yu, G.; Bayer, A. R.; Galloway, M. M.; Korshavn, K. J.; Fry, C. G.; Keutsch, F. N., Glyoxal in aqueous ammonium sulfate solutions: products, kinetics and hydration effects. *Environ. Sci. Technol.* **2011,** *45*, (15), 6336-42.

45.   Bones, D. L.; Henricksen, D. K.; Mang, S. A.; Gonsior, M.; Bateman, A. P.; Nguyen, T. B.; Cooper, W. J.; Nizkorodov, S. A., Appearance of strong absorbers and fluorophores in limonene-O_3 secondary organic aerosol due to NH_4^+-mediated chemical aging over long time scales. *J. Geophys. Res.* **2010,** *115*, D05203, 10.1029/2009jd012864.

46.   Nguyen, T. B.; Lee, P. B.; Updyke, K. M.; Bones, D. L.; Laskin, J.; Laskin, A.; Nizkorodov, S. A., Formation of nitrogen- and sulfur-containing light-absorbing compounds accelerated by evaporation of water from secondary organic aerosols. *J. Geophys. Res.* **2012,** *117*, D01207, 10.1029/2011jd016944.

47.   Updyke, K. M.; Nguyen, T. B.; Nizkorodov, S. A., Formation of brown carbon via reactions of ammonia with secondary organic aerosols from biogenic and anthropogenic precursors. *Atmos. Environ.* **2012,** *63*, 22-31.

48.   Lee, H. J.; Laskin, A.; Laskin, J.; Nizkorodov, S. A., Excitation-emission spectra and fluorescence quantum yields for fresh and aged biogenic secondary organic aerosols. *Environ. Sci. Technol.* **2013,** *47*, (11), 5763-70.

49.   Flores, J. M.; Washenfelder, R. A.; Adler, G.; Lee, H. J.; Segev, L.; Laskin, J.; Laskin, A.; Nizkorodov, S. A.; Brown, S. S.; Rudich, Y., Complex refractive indices in the near-ultraviolet spectral region of biogenic secondary organic aerosol aged with ammonia. *Phys. Chem. Chem. Phys.* **2014,** *16*, (22), 10629-42.

50.   Laskin, J.; Laskin, A.; Roach, P. J.; Slysz, G. W.; Anderson, G. A.; Nizkorodov, S. A.; Bones, D. L.; Nguyen, L. Q., High-resolution desorption electrospray ionization mass spectrometry for chemical characterization of organic aerosols. *Anal. Chem.* **2010,** *82*, (5), 2048-58.

51.   Laskin, J.; Laskin, A.; Nizkorodov, S. A.; Roach, P.; Eckert, P.; Gilles, M. K.; Wang, B.; Lee, H. J.; Hu, Q., Molecular selectivity of brown carbon chromophores. *Environ. Sci. Technol.* **2014,** *48*, (20), 12047-55.

52.   Nguyen, T. B.; Laskin, A.; Laskin, J.; Nizkorodov, S. A., Brown carbon formation from ketoaldehydes of biogenic monoterpenes. *Faraday Discuss.* **2013,** *165*, 473-94.

53.   Kampf, C. J.; Filippi, A.; Zuth, C.; Hoffmann, T.; Opatz, T., Secondary brown carbon formation via the dicarbonyl imine pathway: nitrogen heterocycle formation and synergistic effects. *Phys. Chem. Chem. Phys.* **2016,** *18*, (27), 18353-64.

54.   Fruekilde, P.; Hjorth, J.; Jensen, N. R.; Kotzias, D.; Larsen, B., Ozonolysis at vegetation surfaces: a source of acetone, 4-oxopentanal, 6-methyl-5-hepten-2-one, and geranyl acetone in the troposphere. *Atmos. Environ.* **1998,** *32*, (11), 1893-1902.

55.   Forester, C. D.; Wells, J. R., Yields of carbonyl products from gas-phase reactions of fragrance compounds with OH radical and ozone. *Environ. Sci. Technol.* **2009,** *43*, (10), 3561-68.

56.   Matsunaga, S.; Michihiro, M.; Kimitaka, K., Variation on the atmospheric concentrations of biogenic carbonyl compounds and their removal processes in the northern forest at Moshiri, Hokkaido Island in Japan. *J. Geophys. Res.* **2004,** *109*, D04302, 10.1029/2003JD004100.

57.   Matsunaga, S.; Mochida, M.; Kawamura, K., High abundance of gaseous and particulate 4-oxopentanal in the forestal atmosphere. *Chemosphere* **2004,** *55*, (8), 1143-47.

58.   Helmig, D.; Pollock, W.; Greenberg, J.; Zimmerman, P., Gas chromatography mass spectrometry analysis of volatile organic trace gases at Mauna Loa Observatory, Hawaii. *J. Geophys. Res.* **1996,** *101*, (D9), 14697-710.

59.   Ciccioli, P.; Brancaleoni, E.; Frattoni, M.; Cecinato, A.; Brachetti, A., Ubiquitous occurrence of semi-volatile carbonyl compounds in tropospheric samples and their possible sources. *Atmos. Environ., Part A* **1993,** *27*, (12), 1891-1901.

60.   Anderson, S. E.; Franko, J.; Jackson, L. G.; Wells, J. R.; Ham, J. E.; Meade, B. J., Irritancy and allergic responses induced by exposure to the indoor air chemical 4-oxopentanal. *Toxicol. Sci.* **2012,** *127*, (2), 371-81.

61.   Weschler, C. J.; Wisthaler, A.; Cowlin, S.; Tamás, G.; Strøm-Tejsen, P.; Hodgson, A. T.; Destaillats, H.; Herrington, J.; Zhang, J.; Nazaroff, W. W., Ozone-initiated chemistry in an occupied simulated aircraft cabin. *Environ. Sci. Technol.* **2007,** *41*, (17), 6177-84.

62.   Chen, Y.; Bond, T. C., Light absorption by organic carbon from wood combustion. *Atmos. Chem. Phys.* **2010,** *10*, (4), 1773-87.

63.   Friese, E.; Ebel, A., Temperature dependent thermodynamic model of the system H^+ - NH_4^+ - Na^+ - SO_4^{2-} - NO_3^- - Cl^- - H_2O. *J. Phys. Chem. A* **2010,** *114*, (43), 11595-11631.

64.   Kampf, C. J.; Waxman, E. M.; Slowik, J. G.; Dommen, J.; Pfaffenberger, L.; Praplan, A. P.; Prévôt, A. S. H.; Baltensperger, U.; Hoffmann, T.; Volkamer, R., Effective Henry's law partitioning

and the salting constant of glyoxal in aerosols containing sulfate. *Environmental science & technology* **2013,** *47*, (9), 4236-44.

65.   Lee, A. K.; Zhao, R.; Li, R.; Liggio, J.; Li, S. M.; Abbatt, J. P., Formation of light absorbing organo-nitrogen species from evaporation of droplets containing glyoxal and ammonium sulfate. *Environmental science & technology* **2013,** *47*, (22), 12819-26.

66.   Lee, H. J.; Aiona, P. K.; Laskin, A.; Laskin, J.; Nizkorodov, S. A., Effect of solar radiation on the optical properties and molecular composition of laboratory proxies of atmospheric brown carbon. *Environmental science & technology* **2014,** *48*, (17), 10217-26.

Chapter 3   Photochemistry of Products of the Aqueous Reaction of Methylglyoxal with Ammonium Sulfate

3.1. Abstract

Aqueous reactions of methyl glyoxal (MG) and glyoxal with ammonium sulfate (AS) produce light-absorbing compounds (chromophores) and may serve as a source of atmospheric secondary "brown carbon" (BrC). The molecular composition of these chromophores is ambiguous and their transformation due to exposure to solar UV radiation is not well understood. We examined the molecular composition, mass absorption coefficients, and fluorescence spectra of BrC samples produced by the evaporation of aqueous MG/AS solutions. Chromatograms of BrC produced by evaporation were different from those of BrC produced by slow MG/AS reaction in water, highlighting the substantial sensitivity of BrC to its formation conditions. The BrC samples were characterized before and after their exposure to broadband (270-390 nm) UV radiation. Irradiation led to rapid photobleaching, a decrease in the characteristic 280 nm absorption band, a complete loss of fluorescence, and a dramatic change in molecular composition. By comparing the composition before and after the irradiation, we identified several structural motifs that may contribute to the light absorbing properties of MG/AS BrC. For example, a family of oligomers built from an imidazole carbonyl and repetitive MG units was prominent in the initial sample, and decreased in abundance after photolysis. More complex oligomers containing both imidazole and pyrrole rings in their structures also appeared to contribute to the pool of BrC chromophores. The selective reduction of carbonyl functional groups by sodium borohydride diminished the absorption, but had little effect on the fluorescence of MG/AS BrC samples, suggesting that absorption in this system is dominated by individual chromophores as opposed to supramolecular charge-transfer complexes. Due to the efficient photolysis of the BrC chromophores, this MG/AS BrC system has limited impact on the

direct radiative forcing of climate, but may have an effect on atmospheric photochemistry in

aerosol particles.

3.2. Introduction

Methylglyoxal (MG) is produced by gas-phase oxidation of many anthropogenic and biogenic volatile organic compounds (VOC) including: benzene, toluene, ethylbenzene, xylenes, C_3-C_5 alkanes, isoprene, acetone, monoterpenes, and methylbutenol (see Fu et al.[1] and references therein). Biofuel and biomass burning are also known to directly emit MG into the atmosphere. As a result, MG is commonly observed in urban, rural, and remote environments, with an estimated global annual production of about 140 Tg/year.[1]

Several laboratory and field studies have shown that the uptake of MG (and of the structurally related glyoxal, G) by wet aerosols and cloud droplets and its subsequent aging proceed through several competing aqueous-phase chemical processes, including: 1) aqueous oxidation, which in the case of MG produces water soluble glyoxylic, pyruvic, and oxalic acids; 2) formation of gem-diols followed by oligomerization into high molecular weight products; and 3) ammonium-catalyzed condensation and formation of imidazole compounds.[1-3] Some of these processes result in the formation of light-absorbing compounds that may affect the optical properties of secondary organic aerosols (SOA) formed in the aqueous phase.[1, 2, 4, 5] Specifically, the products of MG reacting with ammonium sulfate (AS) have an absorption band at 280 nm, as well as a weak absorption tail that extends into the visible range. The presence of this absorption tail makes MG + AS and G + AS reactions a potential source of "brown carbon" (BrC).[2]

A number of recent studies have characterized the products formed in aqueous reactions of MG and G (see Ref. [2] for a comprehensive review of the recent literature). For example, De Hann et al. performed structural analysis of the products of MG reactions with AS, amino acids, and methyl amine and observed nitrogen-containing oligomers of imidazole.[6, 7] Figure 3.1 adopted from De Haan et al. (2011) shows some of the processes relevant for this work.[7] Sareen

et al. (2010) used chemical ionization mass spectrometry to study the reaction of MG with AS and observed aldol condensation products, high-molecular-weight oligomers, and sulfur- and nitrogen-containing compounds.[8] Maxut et al. (2015) measured molar extinction coefficients of several expected products of G and AS.[9] The imidazole carbonyl (IC) shown in Figure 3.1 likely makes the dominant contribution to the 280 nm absorption peak; however, the molecular identities of the absorbers in the red tail of the spectrum remain ambiguous.[9-11]
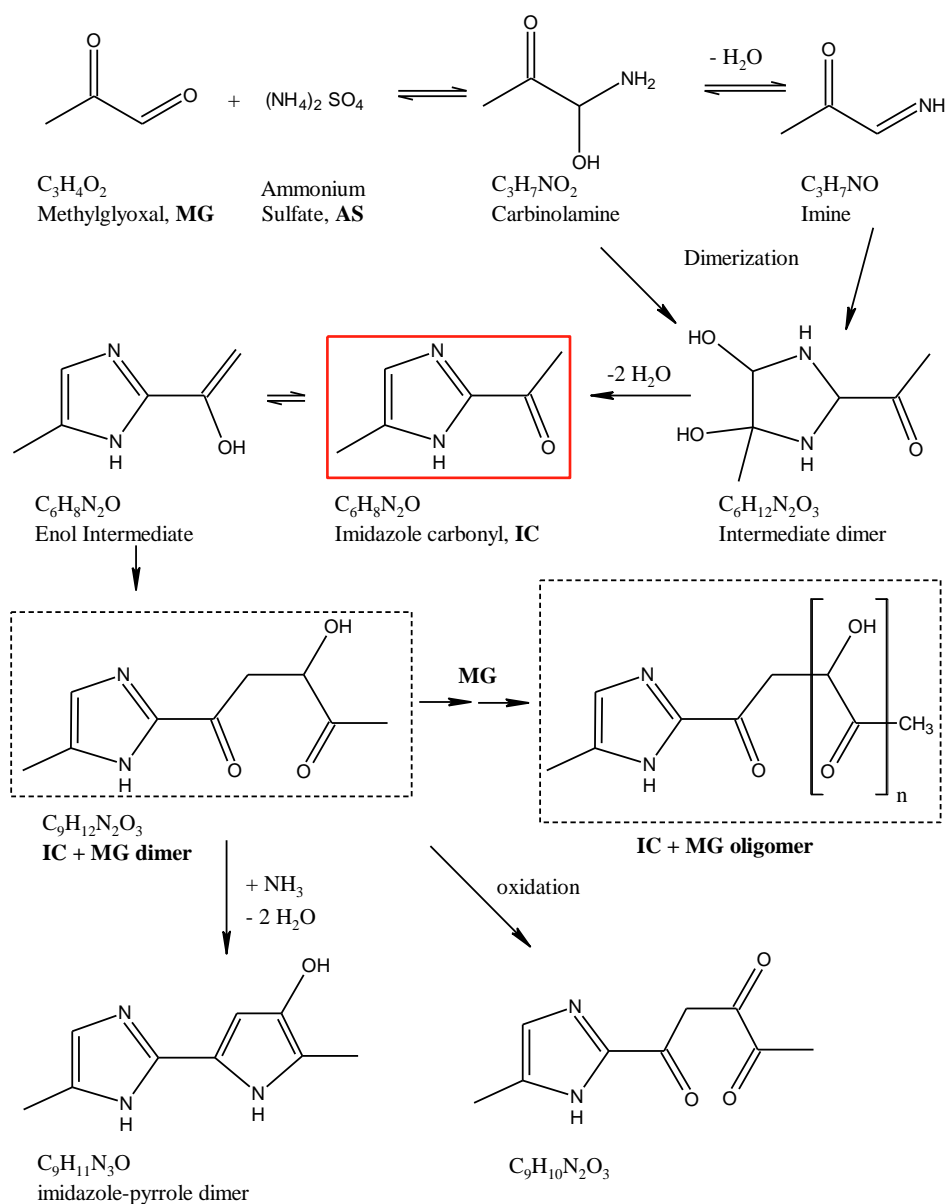
Figure 3.1: MG + AS reactions leading to the formation of the imidazole carbonyl (IC) and its oligomers, adopted from De Haan et al. (2011).[7] IC is the well-known product of the MG + AS reaction; the dashed boxes indicate possible structures of the oligomers observed in this work. The bottom part of the scheme shows possible reactions of IC + MG oligomers including pyrrole ring formation and oxidation.

Although numerous studies have examined MG/AS reactions under dark conditions,[2] much less is known about the photochemical properties of the resulting BrC products (referred to as MG/AS BrC for the rest of the manuscript). Sareen et al. (2013) examined the stability of

MG/AS BrC with respect to UV photolysis and oxidative aging by O_3 and/or OH radicals and concluded that photolysis is the primary daytime sink of this type of BrC in the atmosphere, with a characteristic lifetime on the order of minutes.[12] This short lifetime suggests that MG/AS BrC accumulating in aqueous reactions overnight is quickly removed upon sunrise and is not likely to have a strong effect on direct radiative forcing.[12-14] Similarly, Zhao et al. (2012) reported that MG/AS BrC exhibits rapid photochemical bleaching in the aqueous phase by a combination of direct photolysis and OH oxidation. They estimated that the atmospheric lifetime of MG/AS BrC ranges from minutes to a few hours.[15]

Concentrated aqueous solutions of MG and AS develop brown color on a time scale of hours to days,[8] but this process can be dramatically accelerated by evaporating the solution. For example, Lee et al. demonstrated that evaporation of aerosolized G/AS aqueous solutions produces BrC orders of magnitude faster than observed in bulk solutions.[16] In our previous work, we used high-performance liquid chromatography paired with a photodiode array detector and high-resolution mass spectrometry (HPLC-PDA-HRMS) to characterize MG/AS BrC formed via slow aqueous reaction.[17] In this work, we characterized the molecular composition, absorption spectra, and fluorescence spectra of MG/AS BrC accelerated by evaporation of MG solutions containing AS. The changes in molecular composition of MG/AS BrC, before and after UV photolysis, were analyzed by high-resolution mass spectrometry (HRMS). We found that aqueous photolysis of MG/AS BrC not only decreases its absorption and fluorescence intensity but also results in a significant change in molecular composition. We explored the response of selected BrC species to photolysis using HPLC-PDA-HRMS. We carried out a reduction of MG/AS BrC compounds by sodium borohydride (NaBH$_4$), which is commonly used to selectively reduce carbonyl groups into alcohols and disrupt charge-transfer (CT) complexes

formed by the interaction between donor (-OH) and acceptor (=O) groups.[18, 19] The absorption

peak at 280 nm was eliminated by NaBH$_4$ reduction, but the fluorescence was mostly unaffected,

implying that CT complexes do not strongly contribute to light-absorption properties in the

MG/AS system. Additionally, this reduction eliminated all but one chromophore seen in the

MG/AS BrC chromatogram. Our results support the conclusion that MG/AS BrC is a highly

dynamic system that is quite unstable under solar irradiation, as previously concluded by Sareen

et al.(2013)[12] and Zhao et al. (2012)[15] Although this BrC system will have a marginal impact on

the direct radiative forcing of climate, it may have a profound effect on atmospheric

photochemistry occurring in fog droplets and wet aerosols.

3.3. Experimental Methods

3.3.1. Methylglyoxal and Ammonium Sulfate Mixtures

A 0.1 M stock solution of MG was prepared by diluting a commercial MG solution in

deionized water (Sigma-Aldrich, 40% in H$_2$O). A 0.1 M stock solution of AS was prepared by

dissolving 1.32 grams of AS (Fisher Scientific, ≥99%) in 100 mL of deionized water. The two

stock solutions were mixed in a 1:1 ratio by volume resulting in a 0.05 M concentration of each

reactant in the initial solution (corresponding to 3.6 g/L MG and 6.6 g/L AS). The browning of

this mixture occurs fairly slowly at room temperature, over the course of several days. In order to

speed up the browning process,[7, 16, 20] the mixed sample was immediately evaporated in a

scintillation vial attached to a Buchi Rotavapor® R-215 at 30°C until all solvent was removed.

While the full evaporation process took ~ 20 min, the residue acquired brown color only at the

end of the evaporation process, in the las minute, when most of the water was evaporated from

the sample. Evaporation could have been done faster at a higher evaporation temperature but we

did not want to deviate too much from typical ambient temperatures. The brown residue formed

during the evaporation was then re-dissolved in the same amount of deionized water as the initial volume of the mixed MG and AS solutions. This re-dissolution process may lead to a partial reversal of the reactions occurring upon evaporation, but the brown color of the final solution suggests that at least some of the BrC compounds produced in evaporation are stable with respect to hydrolysis. It is also possible that some MG was lost during the evaporation step but we had no easy way of quantifying this loss. The products formed during the evaporation differ from those formed in the slower browning process, as implied by the difference in the HPLC-PDA-HRMS data for samples obtained by these two methods. The evaporation-driven products are likely to be more environmentally relevant because they can be produced faster, after a single cloud processing cycle.

3.3.2. Optical Properties and Photolysis of MG/AS BrC

Following evaporation and re-dissolution, each MG/AS BrC sample was diluted to achieve an absorbance less than one at 280 nm in order to avoid deviations from Beer's law. The resulting concentrations of organics in the diluted solutions (0.5-0.8 g/L) listed in Table 3.1 are based on the mass of MG used in the initial reaction mixture and the total volume used to reach an absorbance less than one at 280 nm.

Table 3.1: Summary of photolysis experiments. [a]

Sample #	Concentration of BrC (g/L)	Absorbance decay rate (s^{-1})	QY
1	0.60	1.5×10^{-3}	0.46
2	0.60	2.3×10^{-3}	0.59
3	0.80	2.2×10^{-3}	0.98
4	0.54	1.2×10^{-3}	0.33
Average			0.59
(SD)			0.28

[a] For each MG/AS sample, the estimated BrC mass concentration (taken to be equal to the mass concentration MG would have had after re-dissolution and dilution if it was not reactive), the measured 280 nm absorbance decay rate, and the effective quantum yield (QY) value calculated from Eq. 3.1 are listed. The average QY and its standard deviation (SD) are listed as well.

This calculation neglects the possible MG mass loss by evaporation and mass gain due to aqueous chemistry. A dual-beam spectrophotometer (Shimadzu UV-2450) was used to record the UV/Vis absorption spectra of the diluted samples in the 200-700 nm range. Three-dimensional excitation-emission matrix (EEM) spectra were acquired with a Hitachi F-4500 fluorescence instrument.[16] The excitation wavelength spanned the 200 – 500 nm range in 5 nm steps, and the emission was recorded over the 300 – 600 nm range in 2 nm increments. Deionized water served as the background for the absorption and EEM measurements. For all samples, back-to-back absorption and fluorescence measurements were conducted before and after photolysis.

The procedure for photolysis of the MG/AS BrC samples was similar to that described by Epstein et al.[21] Briefly, the sample in a standard 1.0 cm cuvette was placed in a temperature-controlled cuvette holder. The cuvette was irradiated from the top with broadband UV radiation delivered from a xenon arc lamp housing (Newport model 6256) through a 0.95 cm liquid light guide. Before entering the light guide, the UV radiation was reflected with a 90-degree dichroic mirror and filtered with a U-330 band-pass filter (Edmund optics #46-438). The height of the irradiated samples was kept consistent by using a constant volume of 2.5 mL in the cuvette. No

change in solution volume was visible throughout the photolysis experiments. A small magnetic stir bar mixed the sample during photolysis. For the MG/AS BrC samples, the absorbance at 280 nm was continuously measured through the side of the cuvette to determine the effective photolysis rate, listed in Table 3.1. This experiment was repeated four times with four independently prepared samples. In addition, a complete absorption spectrum was periodically recorded (the stir bar was stopped during these measurements).

The spectral flux density of the UV radiation was determined by photolyzing a 0.1 M solution of azoxybenzene (Fisher Scientific, 98 %) in ethanol in the presence of 0.1 M potassium hydroxide, as described by Lee et al.[22] Azoxybenzene is a convenient actinometer because its photolysis quantum yield (QY_{azo} ~0.020) is not strongly dependent on temperature and concentration.[23] The actinometer measurements were conducted prior to and after photolysis of the MG/AS BrC samples. The radiation flux density was determined from the increase in absorption of the azoxybenzene photoisomer (molar absorption coefficient of 7600 L mol^{-1}cm^{-1} at 458 nm) as a function of irradiation time.[22] Most of the photolyzing radiation fell within the 270 – 390 nm range with a peak flux of ~1.5×10^{14} photon cm^{-2} s^{-1} nm^{-1} occurring near 320 nm (Figure 3.2). Based on the measured flux, the effective quantum yield (QY) of MG/AS BrC photolysis was calculated, as described in the next section. For direct comparison, similar analysis was done for the photolysis of brown compounds produced by the reaction of limonene ozonolysis SOA with ammonia (aged-LIM/O$_3$ SOA). Details of the aged-LIM/O$_3$ SOA production and measurements were described in Lee et al.[22]
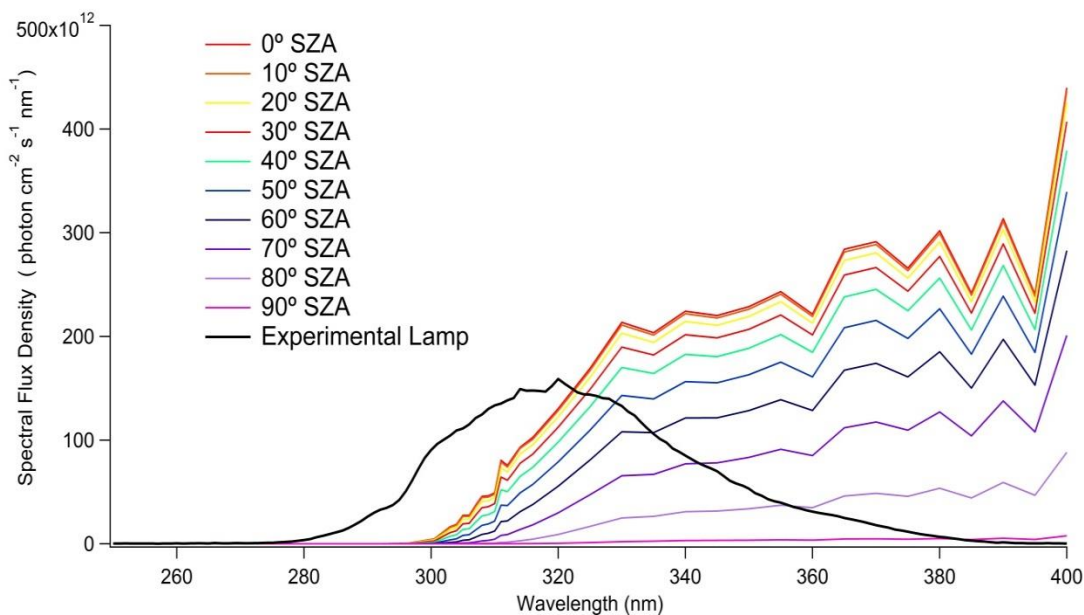
Figure 3.2: Spectral flux density of radiation, $D_0(\lambda)$, from the irradiation source compared to that from the sun at different solar zenith angles (SZA).

3.3.3. Calculation of the Effective Quantum Yield of Photolysis

The effective photolysis quantum yield was calculated as the ratio of the rate of photolysis ($Rate_{photolysis}$) to the effective rate of photon absorption ($Rate_{absorption}$):

$$QY = \frac{Rate_{photolysis}}{Rate_{absorption}} \qquad \textbf{(Equation 3.1)}$$

$Rate_{absorption}$ by the solution was calculated from the base-10 wavelength-dependent absorbance $A_{vertical}(\lambda)$ through the solution of height $h_{solution}$, and from the spectral flux density of the photolyzing radiation, $D_0(\lambda)$, as described in Lee et al. (2014).[22]

$Rate_{photolysis}$ can be determined from the rate of change of absorbance of the solution at a chosen probe wavelength. However, this is complicated by the fact that both the initially present BrC compounds and their photolysis products also absorb at the probe wavelength. It is instructive to first consider what happens in the case of a single absorbing compound R producing a single product P with a photolysis rate constant k. We assume that both R and P

67

absorb at the probe wavelength with molar extinction coefficients ε_R and ε_P, respectively. In this case, the absorbance changes with time as follows:

$$A(t) = b[R]_0 \left[\varepsilon_P + \left(\varepsilon_R - \varepsilon_P \right) e^{-kt} \right] \qquad \textbf{(Equation 3.2)}$$

Fitting the absorbance to function

$$A(t) = c_1 + c_2 e^{-kt} \qquad \textbf{(Equation 3.3)}$$

with c_1, c_2, and k as fitting parameters should give us the effective rate constant, k, and therefore the photolysis rate:

$$Rate_{photolysis} = k[R]\frac{N_A}{1000} \qquad \textbf{(Equation 3.4)}$$

The Avogadro number and the factor of 1000 appearing in this equation are for converting the molar concentrations into molecular units compatible with Eq. 3.1.

To avoid complications associated with the rate of absorption changing with photolysis time, both absorption and photolysis rates were evaluated at t=0 when the initial molar concentration of the reactant and the absorbance of the solution are related via:

$$A_0 = b\varepsilon_R[R]_0 \qquad \textbf{(Equation 3.5)}$$

The BrC extract contains a number of compounds, and there is no reason to expect that the absorbance of the solution should follow first-order kinetics expected from equation (Eq. 3.2). However, the observed decay in absorbance appeared to fit an exponential decay reasonably well, as shown in Figure 3.3. Therefore, in this work, we approximated the BrC mixture as a solution of a single organic compound with an average formula and average optical properties of BrC. Taking the average molecular weight (*MW*) for the BrC molecules from the HR-MS data we converted the mass concentration (C_{mass}) of the dissolved BrC into the effective molar concentration:

$$[R]_0 = \frac{C_{mass}}{MW} \qquad\qquad \textbf{(Equation 3.6)}$$

The concentration in the above equations was then used to calculate the effective quantum yield of photolysis at t=0.

3.3.4. Electrospray Ionization High-Resolution Mass Spectrometry (ESI-HRMS)

A separate set of aged and photolyzed MG/AS BrC samples was analyzed using a high–resolution (m/Δm ~ 10^5 at m/z 450) linear-ion-trap-Orbitrap^{TM} (Thermo Corp.) electrospray ionization mass spectrometer (ESI-HRMS) operated in positive ion mode. The dissolved analytes were detected as sodiated $[M + Na]^+$ and protonated $[M + H]^+$ species. A calibration mixture of caffeine MRFA and Ultramark 1621 (LTQ ESI Positive Ion Calibration Solution, Thermo Scientific, Inc.) was used to calibrate the m/z axis at the beginning and end of each day. In each set of the experiments, a MG/AS BrC sample was prepared, as described in section 2.1. Half of the sample was photolyzed for 40 minutes while the other half was kept in the dark as a control. Photolysis led to a complete loss of the brown color of the sample. After the photolysis, both the control and photolyzed samples were diluted with acetonitrile (Aldrich, HPLC grade) in a 1:1 ratio to improve the ESI source stability. A blank sample, corresponding to a 1:1 mixture of acetonitrile and water, was also prepared. The control, photolyzed, and blank samples were then analyzed using ESI-HRMS. This type of photolysis experiment was repeated twice for reproducibility.

The data analysis protocol was similar to that used by Lee et al.[22] Briefly, internal calibration of the m/z axis, with respect to the expected MG/AS BrC products, resulted in a mass accuracy of better than ± 0.0005 Da in the m/z range of 100 – 800. Peaks that appeared in the blank sample and peaks corresponding to ^{13}C isotopes were filtered out. Only peaks that reproducibly appeared in both sets of independent measurements were retained. The peaks were

assigned molecular formulas with the atomic restrictions of $C_{2-42}H_{2-80}O_{0-35}N_{0-4}Na_{0-1}^{+}$ and a tolerance of 0.00075 *m/z* while constraining the H/C and O/C ratios to 0 – 1.0 and 0.3 – 2.0, respectively, and only permitting closed-shell ions (no ion-radicals). For ambiguous assignments, the preference was to assign peaks to a formula with fewer N-atoms. This preference is based on the prevalence of compounds containing low N-atom numbers for the unambiguously assigned peaks. For clarity, all of the formulas discussed in this paper correspond to neutral analytes (with H^{+} or Na^{+} removed from the ion formula).

3.3.5. Selective Reduction of Carbonyls by NaBH₄

Sharpless and Blough reported that NaBH₄ selectively reduces carbonyl groups that act as acceptors in the charge-transfer (CT) process.[19] To test for the potential contribution of the CT complexes to the measured absorption and fluorescence, a new set of MG/AS BrC samples was prepared as described in section 2.1, diluted to achieve a 280 nm absorbance of less than one, and reacted with solid NaBH₄.[18] Prior to the NaBH₄ addition, absorbance, fluorescence, and pH of the diluted MG/AS BrC solutions were measured. At this point the pH of the MG/AS solution was around 4. After the addition of ~0.6 mg of NaBH₄ to 3.5 mL of the diluted sample, the absorption spectrum was continuously measured every 5 minutes for about 20 hours. We observed an increase, as opposed to the anticipated decrease, in the absorbance. Once the increase in the absorbance slowed down, about ~4.7 mg of additional NaBH₄ was added and the absorption spectrum was continuously measured again for 2 – 4 hours. This second addition of NaBH₄ led to the anticipated decrease in absorbance. After taking the last absorption spectrum, the pH of the samples was around 9. In order to match the starting pH of the MG/AS BrC solution before the NaBH₄ addition, the pH was adjusted from 9 back to 4 using dropwise addition of 1 M HCl. Once corrected, the absorbance and fluorescence were measured. The study

was repeated twice, both under O_2 and N_2 purging conditions. While the reduction was taking place, an identical control sample without $NaBH_4$ was left in the dark for comparison. Absorbance and fluorescence spectra of this sample were taken at the beginning and end of the study.

3.3.6. HPLC-PDA-HRMS

Both the photolysis and $NaBH_4$ reduction samples were analyzed using a HPLC-PDA-HRMS platform, along with a dark control sample. Analysis was done using procedures identical to those used by Lin et al.[17] The HPLC pump and PDA detector were part of the Surveyor Plus system and the high-resolution mass spectrometer was a LTQ-Orbitrap with a standard IonMAX electrospray ionization (ESI) source (all modules are from Thermo Electron, Inc.). The separation was done with a SM-C18 column (Imtakt Scherzo SM-C18, SM035, 130 Å pore size, 3 μm particles, 150 x 3.0 mm). The column was operated at a CH_3CN/H_2O binary mobile phase with a 200 μL min^{-1} flow rate using the following elution protocol: a 3 min hold at 10% of CH_3CN, a 43 min linear gradient to 90% CH_3CN, a 7 min hold at this level, a 1 min return to 10% CH_3CN, and another hold until the total scan time of 80 min. No desalting processing was done before the separation. The PDA detector was used to take UV-Vis spectra from 250 to 700 nm, while the ESI settings were: positive ionization mode, + 4 kV spray potential, 35 units of sheath gas flow, 10 units of auxiliary gas flow, and 8 units of sweep gas flow. Data were analyzed using Xcalibur software (Thermo Scientific) and formulas were assigned with a Molecular Formula Calculator (http://magnet.fsu.edu/~midas/).

3.4. Results and Discussion

3.4.1. Mass Absorption Coefficients of MG/AS BrC

The initial solution before evaporation contained 3.6 g/L MG and 6.6 g/L AS. These values are considerably higher than concentrations of organics and ammonium sulfate in cloud/fog water but lower than to the concentrations expected for aerosol liquid water.[24] Table 3.1 summarizes the effective BrC concentrations (0.5-0.8 g/L) of the solutions obtained after the evaporation, re-dissolution and dilution, and subsequently used for the photolysis experiments. The effective BrC mass concentration in these solutions was assumed to be equal to what the mass concentration of MG would have been if it was unreactive towards AS. This is an approximation because we do not know how much MG was lost during the evaporation of the MG/AS samples and how much MG reacted in the browning process. Furthermore, we do not account for NH_3 and water that may have been incorporated into the organic products during the evaporative aging.
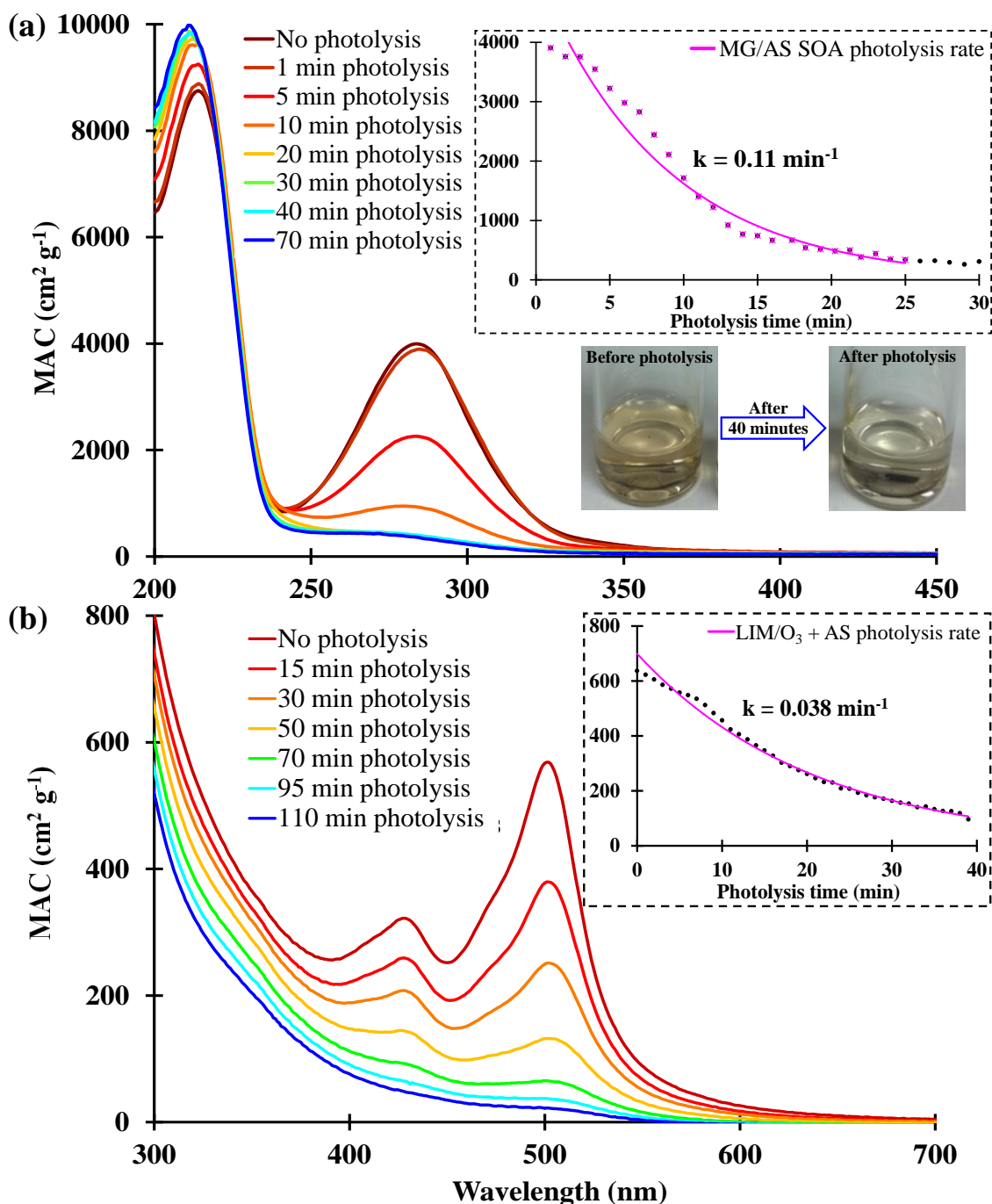
Figure 3.3: Wavelength-dependent mass absorption coefficients (*MAC*, calculated from Eq. 3.7) of (a) MG/AS BrC and (b) aged-LIM/O₃ SOA taken at different photolysis times. The right corner of each panel shows the time dependence of *MAC* for MG/AS BrC at 280 nm and for aged-LIM/O₃ SOA at 500 nm. The photo illustrates the change in the MG/AS BrC sample color from brown to colorless during photolysis.

Figure 3.3(a) shows the bulk mass absorption coefficient (*MAC*) of MG/AS BrC as a function of wavelength calculated using Eq. 3.7 from the measured base-10 absorbance, A_{10}, mass concentration, C_{mass}, and path length, $b = 1$ cm.[25]

$$MAC(\lambda) = \frac{A_{10}^{solution}(\lambda) \times \ln(10)}{b \times C_{mass}}$$

(Equation 3.7)

The *MAC* values shown in Figure 3.3(a) represent an average of the data for the four samples listed in Table 3.1, using the MG concentration as C_{mass} in Eq. 3.7. Because of the uncertainty in the mass concentrations of BrC, the *MAC* values should be regarded as order-of-magnitude estimates. Nevertheless, the maximum *MAC* value of 0.4 m^2 g^{-1} at 280 nm is quite high and comparable to *MAC* for biomass burning organic aerosols (0.2 – 3 m^2 g^{-1}).[2] The *MAC* values for the aged LIM/O_3 SOA shown in Figure 3.3(b) for comparison are an order of magnitude lower. However, unlike the MG/AS reaction products, which only absorbs in the near-UV range, the aged-LIM/O_3 SOA absorbs throughout the visible range where it can have a much stronger effect on direct radiative forcing.

3.4.2. Effective Quantum Yield of Photolysis

The inset of Figure 3.3(a) shows the effect of photolysis on *MAC* at 280 nm, i.e., at the peak of the BrC absorption spectrum. *MAC* was efficiently decreased by photolysis, and the decay rate in *MAC* was approximately exponential with a first order rate constant of 0.11 min^{-1}. After ~30 min of photolysis, the solution became colorless, as shown in the inset of Figure 3.3(a), and the *MAC* at visible wavelengths ($\lambda = 400$-700 nm) dropped below the limit of detection. The corresponding *MAC* values of aged-LIM/O_3 SOA, and the effect of photolysis on that system, are shown in Figure 3.3(b) for comparison. The loss of the characteristic absorption band at 500 nm occurred at a slower rate of 0.038 min^{-1} under comparable experimental conditions.

Quantitative interpretation of these measurements is complicated because of the large number of individual absorbers in the BrC solution. One possible approach is to expand the usual definition of photolysis quantum yield for a single absorber to a complex mixture of absorbing compounds (Eq. 3.1). In this case, multiple compounds absorb radiation, with some of them breaking or isomerizing and others disposing of the excitation energy without undergoing a reaction. The rate of absorption by the mixture can be calculated without making any approximations by measuring the known spectral flux density and wavelength dependent absorbance, as described in Lee et al.[22] The rate of photolysis can be obtained from the measured absorbance decay rates (e.g., Figure 3.3(a)) using an assumption that all molecules in the mixture have the same average formula and identical photophysical properties. In this approach, the application of Eq. 3.1 to our data generates an *effective photolysis quantum yield*. This QY shows what fraction of the absorbed photons would result in photolysis if all the BrC molecules were the same.

Table 3.1 lists all of the calculated absorbance decay rates used in the QY calculation for MG/AS BrC samples using Eq. 3.1. The inferred QY values ranged from 0.33 to 0.98 suggesting that the result may be sensitive to the distribution of BrC chromophores. The average QY for the four measurements was 0.59 ± 0.28, which means that a large fraction of photons that are absorbed lead to the loss of the MG/AS BrC chromophores. The high QY value implies a very short lifetime of the electronically excited state, suggesting a direct photolysis process occurring in a singlet excited state. We carried out similar analysis for the photobleaching of the aged-LIM/O_3 SOA solution shown in Figure 3.3(b). The effective QY for the aged-LIM/O_3 SOA was ~0.26, which is also quite high. Therefore, we expect that both types of BrC will be photobleached promptly by sunlight lowering their potential impact on climate.

3.4.3. Photolysis Effect on Fluorescence of Aged MG/AS

In order to determine the effect of photolysis on fluorescence and the fluorescence quantum yield for the MG/AS BrC samples, EEM spectra were generated. The EEM in Figure 3.4(a) shows that MG/AS BrC is weakly fluorescent. The EEM observed in this work is qualitatively similar to the EEM reported in Refs.[26, 27], with the peak occurring at λ_{ex}~330 nm and λ_{ex}~400 nm. The fluorescence quantum yield (QY_F) was analyzed as described in Lee et al.[16] Compared to previously studied BrC model systems, such as aged-LIM/O_3 SOA with QY_F of 0.002 and naphthalene/OH SOA with QY_F of 0.003, the QY_F for MG/AS BrC was an order of magnitude higher, at 0.02.[22] This value is comparable to the QY_F of ~0.02 in ambient samples reported by Phillips et al.[18] The fluorescence disappeared almost completely after 40 minutes of photolysis. This behavior is similar to that in aged-LIM/O_3 SOA, but opposite to SOA produced by photooxidation of naphthalene, for which the fluorescence intensity increased with photolysis.[22] Our results confirm that fluorescence of secondary BrC is highly dependent on the structures of BrC chromophores.[8, 15, 18, 22]
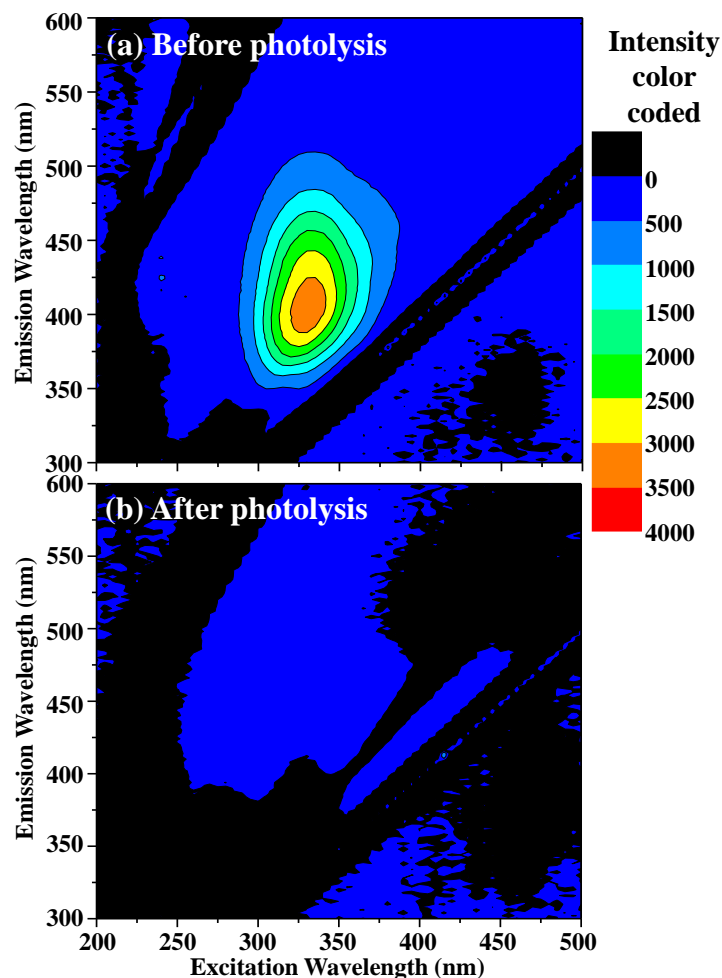
Figure 3.4: EEMs recorded (a) before and (b) after 40 minutes of photolysis of a MG/AS BrC sample. The relative fluorescence intensity is indicated with the color bar.

3.4.4. Molecular Composition of MG/AS BrC

Figure 3.5 compares direct infusion ESI mass spectra acquired before and after photolysis of aqueous MG/AS BrC samples and Table 3.2 provides a list of all the reproducibly observed formulas. The mass spectrum of the unphotolyzed sample is qualitatively consistent with the ESI mass spectrum of products of reactions of MG and AS in evaporating droplets reported by De Haan et al. (2011).[7] The most abundant peak in Figure 3.5 corresponds to the imidazole carbonyl (IC, $C_6H_8N_2O$), observed as a protonated ion at *m/z* 125.0709, which is also one of the major peaks in the mass spectrum in Figure 1 of De Haan et al. (2011). The second most abundant peak

in the unphotolyzed sample is $C_9H_{15}NO_6$, appearing as a protonated ion at *m/z* 234.0972, which is the largest peak in the De Haan et al. (2011) mass spectrum. Other prominent peaks of protonated ions in Figure 3.5 include $C_8H_{14}N_4O_7$ at *m/z* 279.0935, $C_{12}H_{19}NO_8$ at *m/z* 306.183, and $C_{12}H_{21}NO_9$ at *m/z* 324.1289. A series of IC + MG oligomers, formed by the reaction of enol forms of IC with *n* MG molecules, were also observed. Figure 3.1, adopted from De Haan et al. (2011),[7] presents a possible mechanism for the formation of these IC + MG oligomers. Scheme S1 shows possible structures for larger oligomers not included in Figure 3.1.
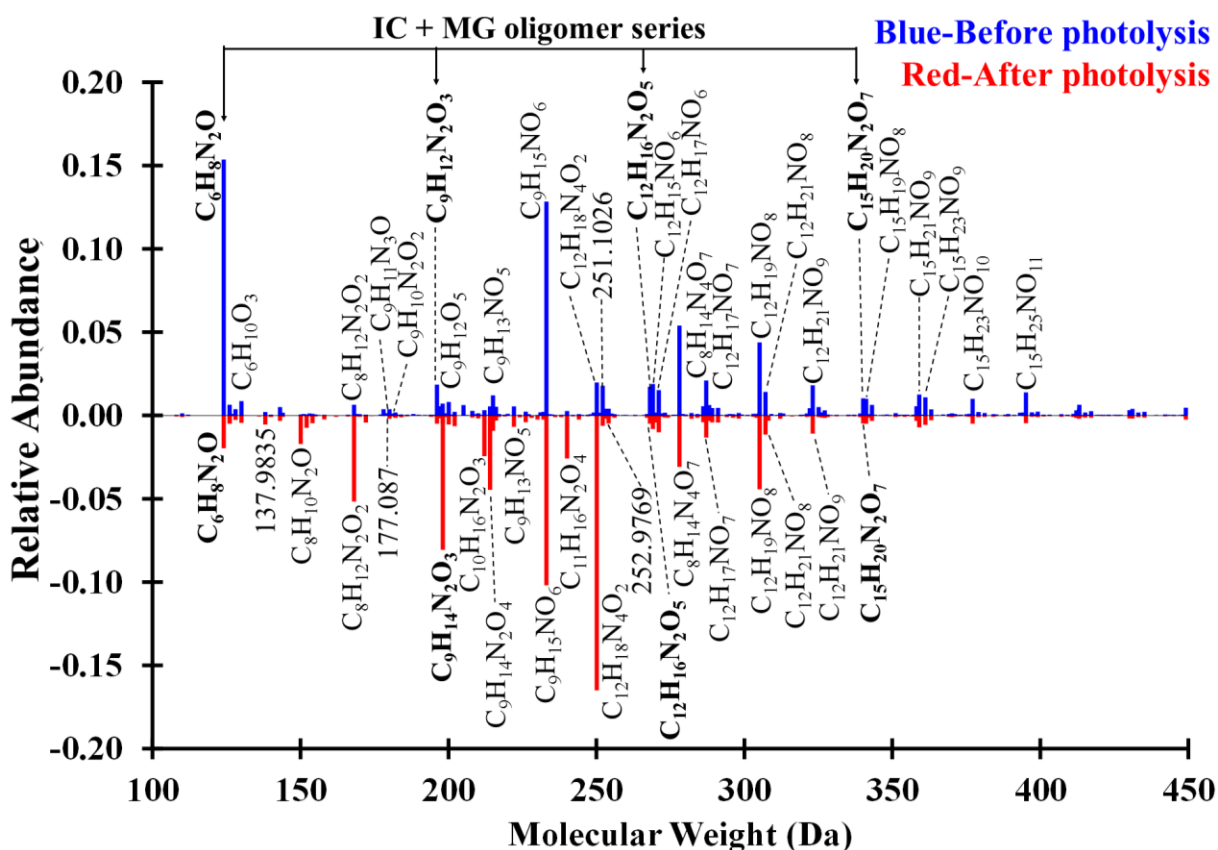
Figure 3.5: Reconstructed mass spectra of assigned peaks in the MG/AS BrC samples before (positive signal) and after (negative signal) photolysis. The peak abundances are normalized with respect to the total ion current, with the normalized abundances of all the peaks adding up to 1. Abundant peaks are labelled with the corresponding neutral formulas. The removal of higher molecular weight compounds during photolysis is clearly evident from the spectra. The IC + MG oligomers (Scheme 1) are highlighted in bold and shown with an arrow on the 'before photolysis' side.

Table 3.2: List of assigned HR-ESI-MS peaks with significant abundance. Molecular weights, MW, in Dalton (Da) and the formulas are listed for all assigned peaks. In the "Trend" column, decrease in intensity ($\downarrow$), increase in intensity ($\uparrow$), and no change ($-$) in response to photolysis are listed. Also, peaks found only before or after photolysis are listed as B or A, respectively. The IC + MG oligomers highlighted are bolded and labelled with letter "O" in the last column.

MW (Da)	C	H	N	O	Trend	Olig
124.0637	**C_6**	**H_8**	**N_2**	**O_1**	$\downarrow$	**O**
126.0317	C_6	H_6		O_3	$\downarrow$	
127.0633	C_6	H_9	N_1	O_2	$\downarrow$	
128.0473	C_6	H_8		O_3	$\downarrow$	
130.0630	C_6	H_{10}		O_3	$\downarrow$	
140.0586	C_6	H_8	N_2	O_2	A	
143.0582	C_6	H_9	N_1	O_3	$\downarrow$	
150.0793	C_8	H_{10}	N_2	O_1	$\uparrow$	
151.0633	C_8	H_9	N_1	O_2	$\downarrow$	
152.0950	C_8	H_{12}	N_2	O_1	$\uparrow$	
168.0899	C_8	H_{12}	N_2	O_2	$\uparrow$	
170.0579	C_8	H_{10}		O_4	$\downarrow$	
177.0902	C_9	H_{11}	N_3	O_1	$\downarrow$	O
178.0742	C_9	H_{10}	N_2	O_2	$\uparrow$	O
186.0528	C_8	H_{10}		O_5	$\downarrow$	
194.0691	C_9	H_{10}	N_2	O_3	$\downarrow$	O
196.0848	**C_9**	**H_{12}**	**N_2**	**O_3**	$\downarrow$	**O**
197.0688	C_9	H_{11}	N_1	O_4	$\downarrow$	
198.0528	C_9	H_{10}		O_5	$\downarrow$	
198.1004	C_9	H_{14}	N_2	O_3	$\uparrow$	
200.0685	C_9	H_{12}		O_5	$\downarrow$	
202.0954	C_8	H_{14}	N_2	O_4	A	
212.1161	C_{10}	H_{16}	N_2	O_3	$\uparrow$	
214.0954	C_9	H_{14}	N_2	O_4	$\uparrow$	
215.0794	C_9	H_{13}	N_1	O_5	$-$	
222.1004	C_{11}	H_{14}	N_2	O_3	$\uparrow$	
231.1008	C_{12}	H_{13}	N_3	O_2	$\downarrow$	O
232.0848	C_{12}	H_{12}	N_2	O_3	$\uparrow$	O
233.0899	C_9	H_{15}	N_1	O_6	$-$	
240.1110	C_{11}	H_{16}	N_2	O_4	$\uparrow$	
248.1273	C_{12}	H_{16}	N_4	O_2	$\downarrow$	
249.1113	C_{12}	H_{15}	N_3	O_3	$\downarrow$	O
250.0954	C_{12}	H_{14}	N_2	O_4	$\downarrow$	O
250.1430	C_{12}	H_{18}	N_4	O_2	$\uparrow$	
252.1110	C_{12}	H_{16}	N_2	O_4	$\downarrow$	
266.0903	C_{12}	H_{14}	N_2	O_5	$\downarrow$	O

m/z	Formula			
268.1059	**$C_{12}H_{16}N_2O_5$**	↓		O
269.0899	$C_{12}H_{15}N_1O_6$	↓		
271.1056	$C_{12}H_{17}N_1O_6$	↓		
278.0862	$C_8H_{14}N_4O_7$		↑	
286.1165	$C_{12}H_{18}N_2O_6$	↓		
287.1005	$C_{12}H_{17}N_1O_7$	↓		
288.0845	$C_{12}H_{16}O_8$	↓		
289.1162	$C_{12}H_{19}N_1O_7$		↑	
304.1271	$C_{12}H_{20}N_2O_7$		B	O
305.1111	$C_{12}H_{19}N_1O_8$		↑	
305.1376	$C_{15}H_{19}N_3O_4$	↓		O
307.1267	$C_{12}H_{21}N_1O_8$	↓		
313.1162	$C_{14}H_{19}N_1O_7$	↓		
322.1165	$C_{15}H_{18}N_2O_6$	↓		O
323.1216	$C_{12}H_{21}N_1O_9$	↓		
340.1271	$C_{15}H_{20}N_2O_7$	↓		
341.1111	**$C_{15}H_{19}N_1O_8$**	↓		O
358.1376	$C_{15}H_{22}N_2O_8$	↓		
359.1216	$C_{15}H_{21}N_1O_9$	↓		
361.1373	$C_{15}H_{23}N_1O_9$	↓		
376.1271	$C_{18}H_{20}N_2O_7$	↓		O
377.1322	$C_{15}H_{23}N_1O_{10}$	↓		
393.1536	$C_{18}H_{23}N_3O_7$	↓		O
394.1376	$C_{18}H_{22}N_2O_8$	↓		O
395.1428	$C_{15}H_{25}N_1O_{11}$	↓		
412.1482	**$C_{18}H_{24}N_2O_9$**	↓		O
466.1587	$C_{21}H_{26}N_2O_{10}$	↓		O
484.1693	**$C_{21}H_{28}N_2O_{11}$**	↓		O

In addition to the imidazole-based compounds containing two nitrogen atoms, and imidazole-based dimers containing four nitrogen atoms, compounds containing three nitrogen atoms were also observed. Such compounds can be readily produced by replacing any of the carbonyl groups in the primary products by an imine group. The imine-carbonyl equilibrium usually strongly favors the carbonyl, but the imines may be stabilized by intramolecular reactions leading to stable aromatic rings. For example, the IC + MG oligomers have multiple carbonyl groups in 1,4 arrangement, which can form stable pyrrole-based ring structures in NH_3-mediated

reactions.[10] Figure 3.1 shows a plausible pathway for IC + MG dimer ($C_9H_{12}N_2O_3$) to undergo such a reaction. A formula corresponding to the expected $C_9H_{11}N_3O$ product was found in the ESI-HRMS spectrum and is listed in Table 3.2. Finally, the distribution of observed formulas implies that oxidation of the hydroxyl groups to carbonyl groups was occurring in solution. For example, the IC + MG dimer ($C_9H_{12}N_2O_3$) can be oxidized to ($C_9H_{10}N_2O_3$) as shown in Figure 3.1.

The 40 minutes of photolysis, during which MG/AS BrC lost its brown color, resulted in a substantial change in the mass spectrum. Table 3.2 provides a list of the observed formulas, and indicates whether peaks decreased or increased in relative abundance after photolysis. Some peaks were completely removed during photolysis and several new peaks appeared in the photolyzed sample. The peak intensities of the IC + MG oligomers decreased greatly with photolysis, as shown in Figure 3.6. Nitrogen-containing heterocyclic oligomers have been identified as the plausible light-absorbing compounds in the MG/AS mixture;[17] the loss of the IC + MG oligomers occurring in parallel with photobleaching suggests that they may contribute to the visible light absorption of the mixture. All of the imidazole-pyrrole complex oligomers (compounds with 3 nitrogen atoms) also decreased in peak abundance with photolysis, suggesting that they may contribute to the light-absorbing properties of MG/AS BrC.
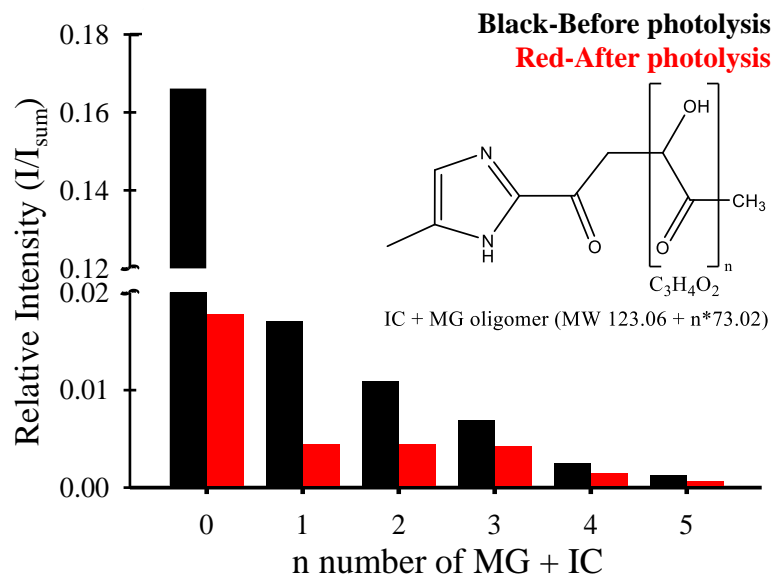
Figure 3.6: Effect of photolysis on the relative intensity of the IC + MG oligomers that are shown in Scheme 1, for n = 0-5.

For compounds, $C_cH_hO_oN_n$, containing c carbon, h hydrogen, o oxygen, and n nitrogen atoms, the double bond equivalent (DBE), which is equal to the total number of double bonds and rings, can be calculated as follows:

$$DBE = 1 + \frac{n-h}{2} + c \qquad \textbf{(Equation 3.8)}$$

Nitrogen is assumed to have a valence of 3 in this formula, which is consistent with its anticipated chemistry. The distribution of DBE values in the MG/AS BrC is shown in Figure 3.7. Average elemental ratios are commonly used to express bulk composition for comparing the complexity of the SOA. Using the assigned molecular formulas, the average elemental composition (C, H, N, and O), ratios (H/C, O/C, N/C, and N/O), and DBE are estimated based on the following equations:

$$\langle Y \rangle = \frac{\sum_i x_i Y_i}{\sum_i x_i} \quad \text{where Y= c, h, o, n, DBE} \qquad \textbf{(Equation 3.9)}$$

$$\frac{\langle Y \rangle}{\langle Z \rangle} = \frac{\sum_i x_i Y_i}{\sum_i x_i Z_i} \quad \text{where } Y/Z = \text{H/C, O/C, N/C, and N/O} \qquad \textbf{(Equation 3.10)}$$

Peak abundance, x_i, is used as the weighing factor. Table 3.3 lists all the calculated average

elemental ratios and DBE for MG/AS BrC samples before and after photolysis. Table 3.4 focuses

on the fraction of N-containing compounds and the N/C ratios for the subgroups of the

compounds containing n = 0, 1, 2, 3, and 4 N-atoms.
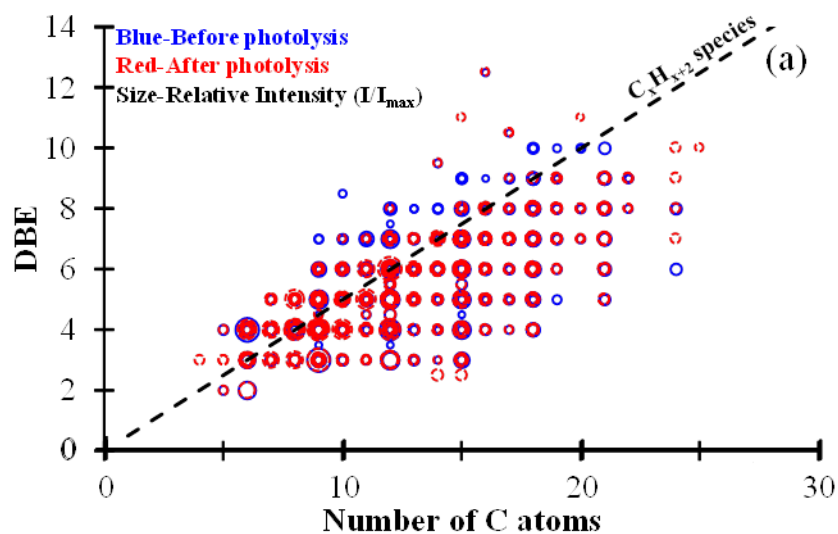
Figure 3.7: DBE of MG/AS BrC products. DBE is plotted as a function of the carbon number before and after photolysis. The size of the points represents relative intensity. The dashed line corresponds to the expected DBE for linear polyenes (C_xH_x+2).

Table 3.3: Average elemental ratios and double-bond equivalents (DBE) before and after photolysis.

	<H/C>	<O/C>	<N/C>	<N/O>	<DBE>
Before	1.47	0.51	0.14	0.28	3.9
(SD)	(0.03)	(0.03)	(0.03)	(0.07)	(0.5)
After	1.53	0.50	0.15	0.32	3.7
(SD)	(0.04)	(0.10)	(0.04)	(0.1)	(0.7)
After - Before	0.06	-0.01	0.003	0.04	-0.2

Table 3.4: Percent of N-containing compounds and the average N/C ratio for each subset of N-containing compounds (with n=0, 1, 2, 3, and 4) before and after photolysis.

# N	%		<N/C>	
	Before	**After**	**Before**	**After**
0	22.6	20.7		
1	43.5	42.9	0.08	0.08
2	25.5	30.7	0.21	0.21
3	5.6	3.7	0.20	0.21
4	2.7	2.0	0.49	0.35
sum	**100.0**	**100.0**		

Despite the large effect of the photolysis on the molecular composition, the *average* properties of MG/AS BrC did not change significantly. For example, there was a very small net decrease in the average DBE (double bound equivalent, Figure 3.7), almost no change in the average atomic ratios (Table 3.3), and almost no change in the N-atom distribution between the BrC compounds (Table 3.4). The average molecular formula of MG/AS BrC remained essentially the same after photolysis:

$$C_{10.0}H_{14.6}O_{5.1}N_{1.4} \ + \ h\nu \ \rightarrow \ C_{10.1}H_{15.4}O_{5.0}N_{1.6}$$
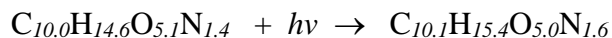
The formulas for the peaks that appeared during photolysis were not qualitatively different (in terms of the average size and average atomic ratios) from the formulas of compounds that disappeared during photolysis. These observations suggest that the average properties, such as the <O/C> and <N/C> ratios, are not good indicators of the extent of photolysis-driven molecular changes in the MG/AS BrC system. This conclusion is similar to that reached in our recent study of aqueous photolysis of SOA generated from different precursors[28] and in the photolysis of alpha-pinene SOA particles.[29]

3.4.5. NaBH₄ Reduction of Carbonyls

Adding a small amount of NaBH₄ (~0.6 mg) to MG/AS BrC resulted in a slight red shift

in the absorption peak, as shown in Figure 3.8(a); then, over about 20 hours, the absorbance

continuously increased. This was not expected because the selective reduction of carbonyl

groups to alcohols by NaBH₄ is supposed to eliminate CT complexes, decreasing the absorbance

at longer wavelengths.[18] Once this increase in the absorbance slowed down, an excess amount of

NaBH₄ (4.7 mg) was added; this led to the anticipated decrease in absorbance after about 3 hours

(Figure 3.8(a)). These observations suggest that the effect of NaBH₄ on the MG/AS BrC is not

limited to selective reduction of carbonyl groups; more complex chemistry must be occurring.

Although the exact mechanism is unclear, the eventual decrease in the absorbance suggests that

the carbonyl groups in MG/AS BrC are essential parts of the chromophores (e.g., IC shown in

Figure 3.1 is known to have a high extinction coefficient). The results of these experiments were

the same under both O_2 and N_2 purging conditions, suggesting that oxygen does not play a

significant role in the borohydride reduction chemistry.
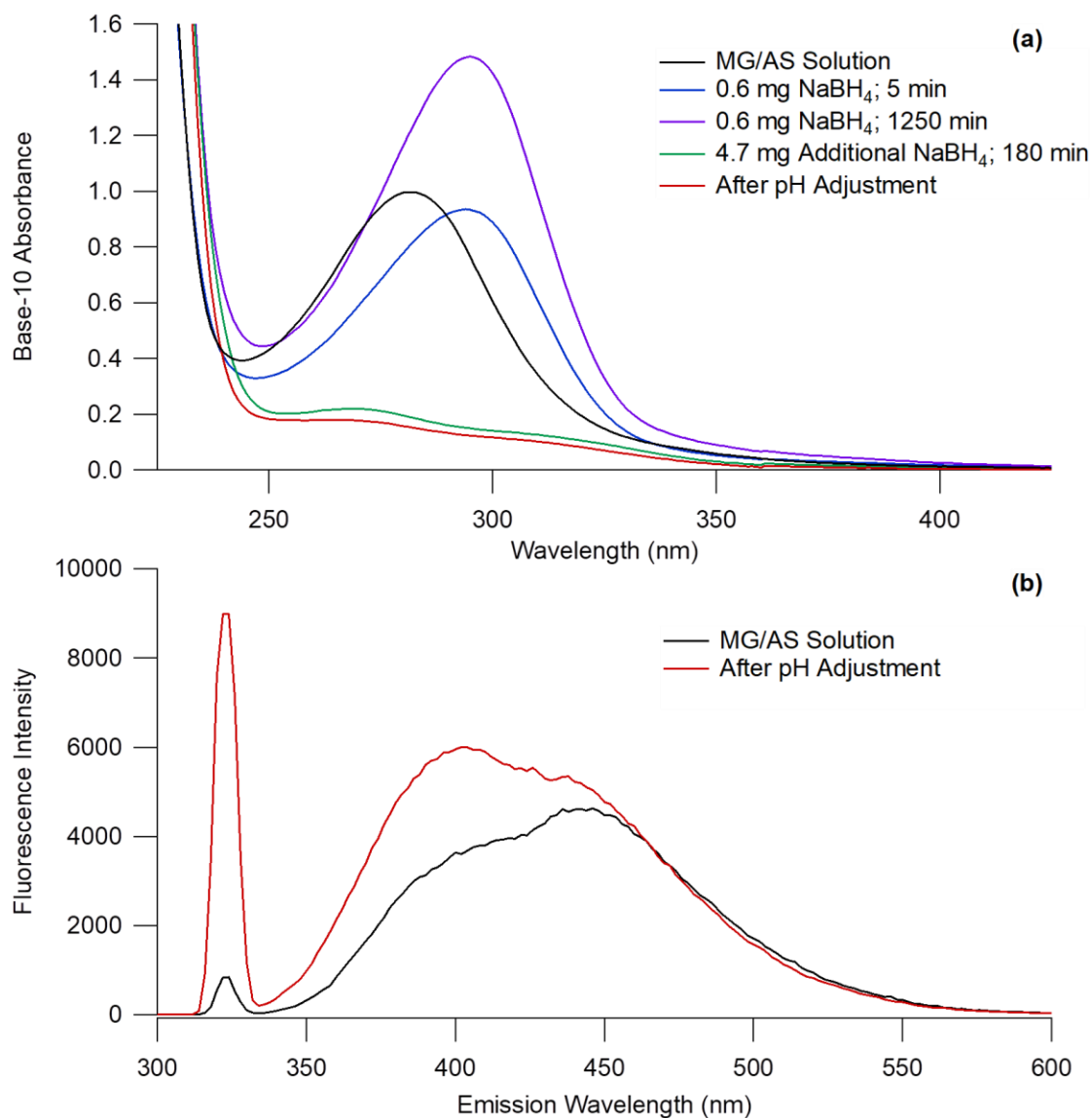
Figure 3.8: The effect of the MG/AS BrC + NaBH$_4$ reduction in an O$_2$-containing solution on the: (a) absorption spectrum and (b) fluorescence spectrum excited at 325 nm. Similar results were obtained in a duplicate study under conditions of N$_2$ bubbling through the solution.

We note that the increase in the pH of the MG/AS solution upon addition of NaBH$_4$ may have side effects on the reaction mechanism, complicating the interpretation of the results. The pH of the solution increased from 4 to about 9 as a result of adding the excess amount of NaBH$_4$. Re-adjusting the pH to match the pH of the initial MG/AS BrC solution after evaporation and dilution, further decreased the absorbance (Figure 3.8(a)). The change in pH from the addition of

NaBH$_4$ may shut down the acid-catalyzed and/or enable base-catalyzed aldol condensation reactions. The aldol condensation mechanism is known to be important for the formation of light-absorbing products in the MG/AS system, as demonstrated by Sareen et al. (2010).[8] Therefore, the reduction of the carbonyls by NaBH$_4$ may have to compete with pH-induced changes in the aldol formation equilibria.

While the absorption at 280 nm decreased with the addition of the excess NaBH$_4$, the fluorescence intensity increased slightly (Figure 3.8(b)). In contrast, both the absorption and fluorescence decreased during photolysis (Figure 3.3 and Figure 3.4). This difference in behavior suggests that the primary chromophores responsible for the 280 nm absorption, which are removed by both methods, are different from the fluorophores, which decrease with photolysis and increase with NaBH$_4$ reduction. In other words, the molecular subsets of the chromophores and fluorophores in MG/AS BrC do not fully overlap.

3.4.6. HPLC-PDA-HRMS

Figure 3.9 shows PDA chromatograms for the dark control (a), photolysis (b), and NaBH$_4$ reduction (c) MG/AS BrC samples. The wavelength range is limited to 250-400 nm in

Figure 3.9 in order to emphasize the chromophores contributing to the near-UV range. For each peak in the PDA chromatograms, we used the approach of Lin et al.[17] to find molecular formulas that give well-defined peaks in the selected ion chromatogram (SIC) at the same time that the absorbing species are eluting in the PDA chromatogram (after accounting for a known time delay between the PDA and ESI-MS detectors). While this approach worked for a few of the PDA peaks, we could not unambiguously assign formulas to all of them because of the dominating abundance of ions that did not correspond to any of the chromophores and eluted

over a broad range of elution times. For example, the mass spectra for retention times below 6 minutes were very complex, and included peaks from various ionic complexes built from ammonium, sulfate, bisulfate, and organic ions. Furthermore, most of the PDA peaks correlated to more than one candidate ion, and conversely SICs for many candidate ions had peaks at more than one retention time.
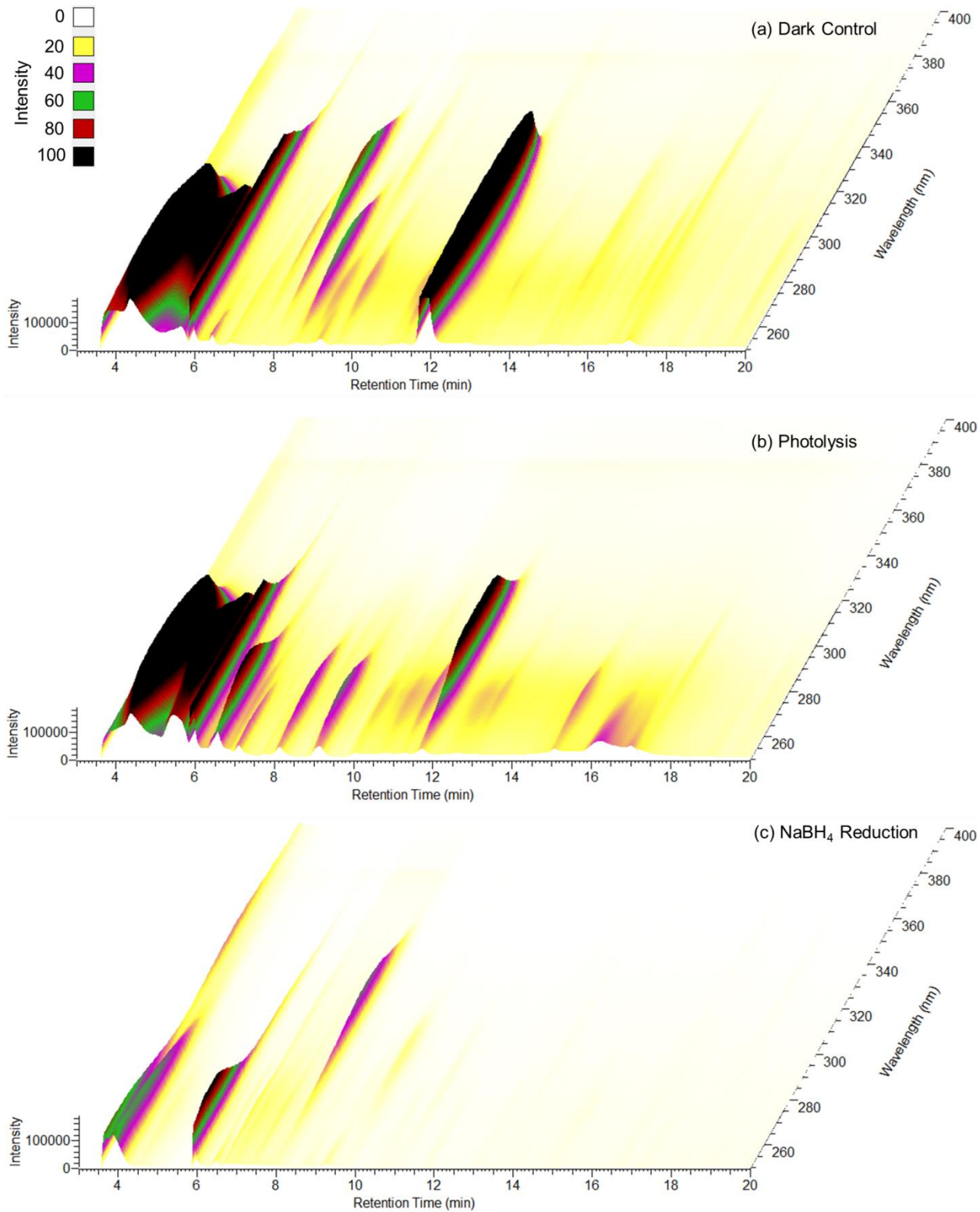
Figure 3.9: HPLC-PDA chromatograms for the MG/AS (a) dark control, (b) photolyzed sample, and (c) NaBH$_4$ reduction sample after excess NaBH$_4$ was added. The PDA absorbance is indicted by the color (darker color = higher absorbance).

The largest PDA peak occurred at 12 minutes in the chromatogram for the dark control sample in

Figure 3.9(a). It correlated well with the *m/z* 125.0709 SIC, and was assigned to the protonated IC. This *m/z* was also the largest peak in the direct infusion ESI mass spectrum of the unphotolyzed MG/AS BrC sample shown in Figure 3.5. The 12 minute UV/Vis absorption spectrum acquired by the PDA had a broad peak near 290 nm, in qualitative agreement with the absorption spectra reported previously [9-11] for the related IC formed from glyoxal. The PDA chromatogram had additional peaks at shorter retention times in the *m/z* 125.0709 SIC (Figure 3.10) suggesting possible structural isomers of IC or in-source fragmentation. Figure 3.11 shows that the MG + AS reaction may potentially produce two structural isomers of IC. The isomer IC2 should have its carbonyl group converted into a gem-diol in an aqueous solution, and it is expected to be more polar and elute at earlier times. The isomer IC1 should be more stable than IC2 because of the aromatic stabilization of IC1, and more stable with respect to hydration. Therefore, IC1 must be the chromophoric species eluting at 12 min. Larger compounds, such as the IC + MG oligomers shown in Figure 3.1, could potentially undergo fragmentation in the ion source to produce the protonated IC giving rise to additional smaller peaks in the *m/z* 125.0709 SIC at longer retention times shown in Figure 3.10.
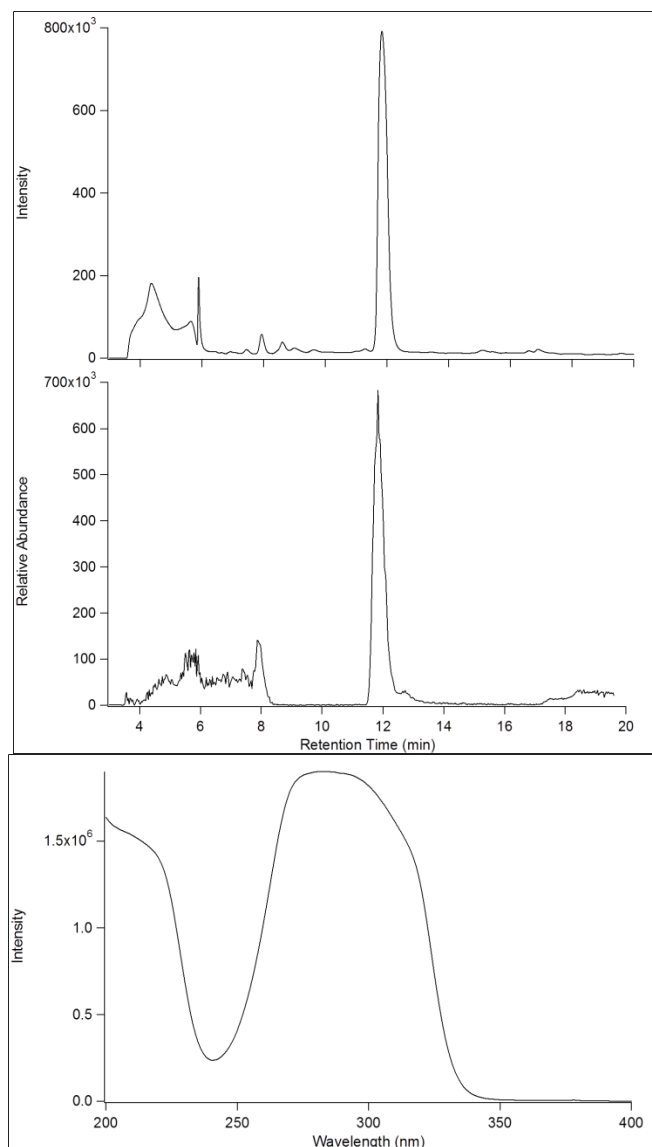
Figure 3.10: The selected Ion Chromatogram (SIC) for the *m/z* 125.0709 ion (mass range 125.00-125.10) corresponding to protonated IC is shown in the bottom of the first panel. The 12.2 min peak in SIC (bottom) correlates with the 11.8 min peak of the major chromophore in the PDA chromatogram (top). Other peaks in SIC may be due to less stable isomers of IC (see Scheme 2 in the text) or fragmentation of larger compounds into protonated IC. The second panel shows the full absorption spectrum of the peak at 11.8 minutes in the PDA with a broad peak centered around 290 nm.
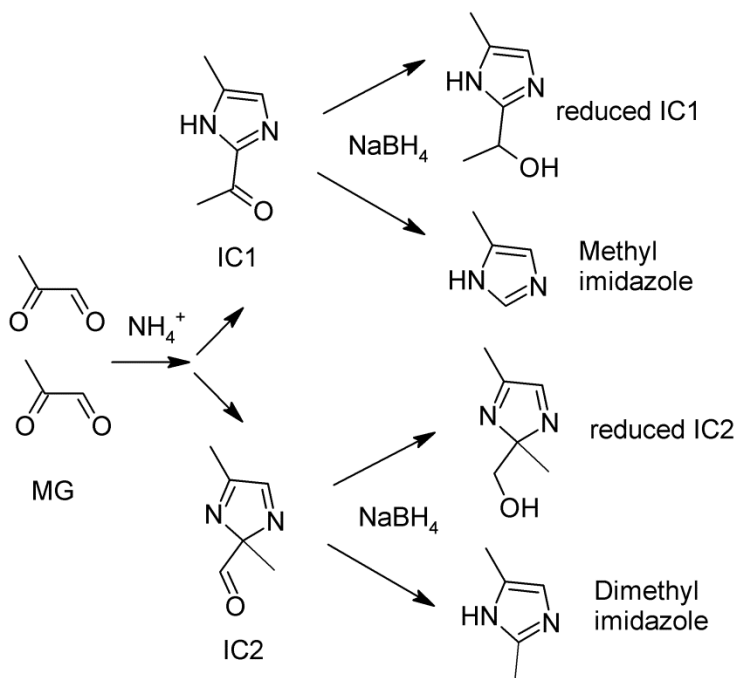
Figure 3.11: Two possible structural isomers of the imidazole carbonyl (IC) and processes involved in their reaction with NaBH₄.

Lin et al. (2015) carried out analyses of a similar MG/AS BrC system in which bulk aqueous solutions containing MG and AS were aged over several days.[17] Figure 3.12 compares the PDA chromatogram from that work with the one recorded in this study. The slow aging method used by Lin et al. (2015) produced 30 chromophores with assignable formulas,[17] as opposed to the evaporation method in this study that produced BrC within minutes but only resulted in a dominant major absorbing species (IC). Another difference is that Lin et al. (2015) had higher concentrations of MG and AS, and desalted the sample before the analysis.[17] In our work here, the concentrations were lower and no desalting was done. The dramatic difference in the resulting chromatograms of these two MG/AS systems indicates that various pathways of atmospheric aging may have significant effects on the molecular structures of BrC chromophores.
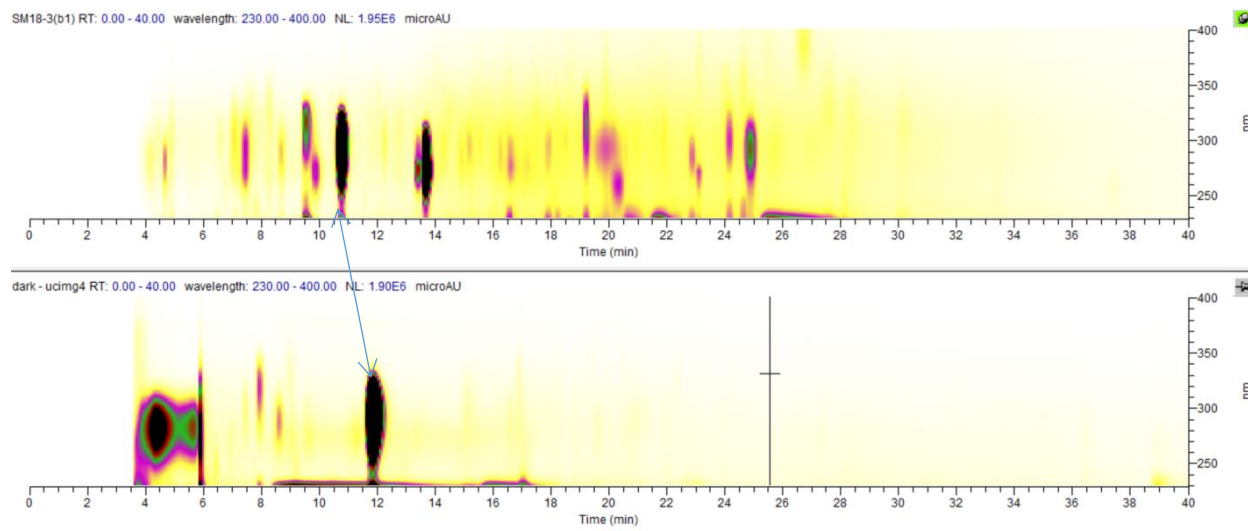
Figure 3.12: The top PDA chromatogram corresponds to a BrC sample obtained by Lin et al.[17] by a reaction of MG with AS in water for four days followed by desalting to remove excess AS. The bottom chromatogram was obtained for an evaporation MG/AS BrC sample, with no desalting used. While the major peak of IC is the same in both cases, there are very significant differences between the distributions of eluting BrC chromophores in the two samples.

The IC peak at 12 min greatly decreased in intensity upon exposure to UV irradiation, as shown in

Figure 3.9(b). Exposure to radiation can cause the IC to undergo different photochemical reactions. One example is a Norrish Type I reaction causing cleavage at the carbonyl carbon and leading to two free radical fragments that can then undergo secondary processes to form a variety of products.[30] Norrish Type I photolysis processes generally have high photolysis quantum yields, in agreement with the large observed effective QY values reported in Table 3.1. The irradiation can also generate an electronically excited IC, which can react with a hydrogen donor (such as another IC, alcohols, or aldehydes) to form an aromatic alkoxy radical, also leading to a different set of products.[30]

NaBH$_4$ is expected to reduce IC to the corresponding alcohol (neutral formula C$_6$H$_{10}$ON$_2$, protonated ion *m/z* 127.0866) as shown in Figure 3.11. An abundant ion with this *m/z* generated two peaks around 8 min in the NaBH$_4$ reduction sample.

Figure 3.9(c) also shows a co-eluting chromophoric species at 8 minutes with an absorption peak at 320 nm. Based on the structure of the reduced IC, we do not expect it to have any absorption bands at 320 nm. Thus, the 8 minute peak in the PDA chromatogram must be from another co-eluting compound (which we could not identify). We also found that methyl imidazole (C$_4$H$_6$N$_2$) was a major new species in the NaBH$_4$ reduction sample. Methyl imidazole does not absorb in the near-UV and therefore does not show up in the PDA chromatogram in

Figure 3.9, but it does absorb strongly at 220 nm and results in a large peak eluting near this wavelength at 7.5 minutes. Dimethyl imidazole was also detected in the NaBH$_4$ reduction sample, presumably resulting from the IC2 isomer (Figure 3.11). These results indicate that the action of NaBH$_4$ is not simply a reduction of the carbonyl groups and that the addition of NaBH$_4$ to the MG/AS BrC solution initiates more complex processes that cleave C-C bonds.

A few other major ions were detected in the initial MG/AS BrC sample that did not correlate to any of the PDA peaks of the BrC chromophores. For example, there was a prominent group of peaks that eluted at a variety of retention times in both the dark control and photolysis samples. The *m/z* values of these species and corresponding neutral formulas were 306.1183 (C$_{12}$H$_{19}$NO$_8$), 324.1289 (C$_{12}$H$_{21}$NO$_9$), and 342.1395 (C$_{12}$H$_{23}$NO$_{10}$). Each of these species is produced by combining four MG units and one NH$_3$, with added hydration and dehydration steps. Other observed species that follow a similar formation pattern occurred at *m/z* 252.1078 (C$_9$H$_{17}$NO$_7$) and 234.0972 (C$_9$H$_{15}$NO$_6$), both comprised of three MG units. Figure 3.13 illustrates plausible formation mechanisms of these compounds. However, while these open-chain

compounds are prominent in the mixture, they are not sufficiently conjugated to absorb in the

near-UV and visible range.
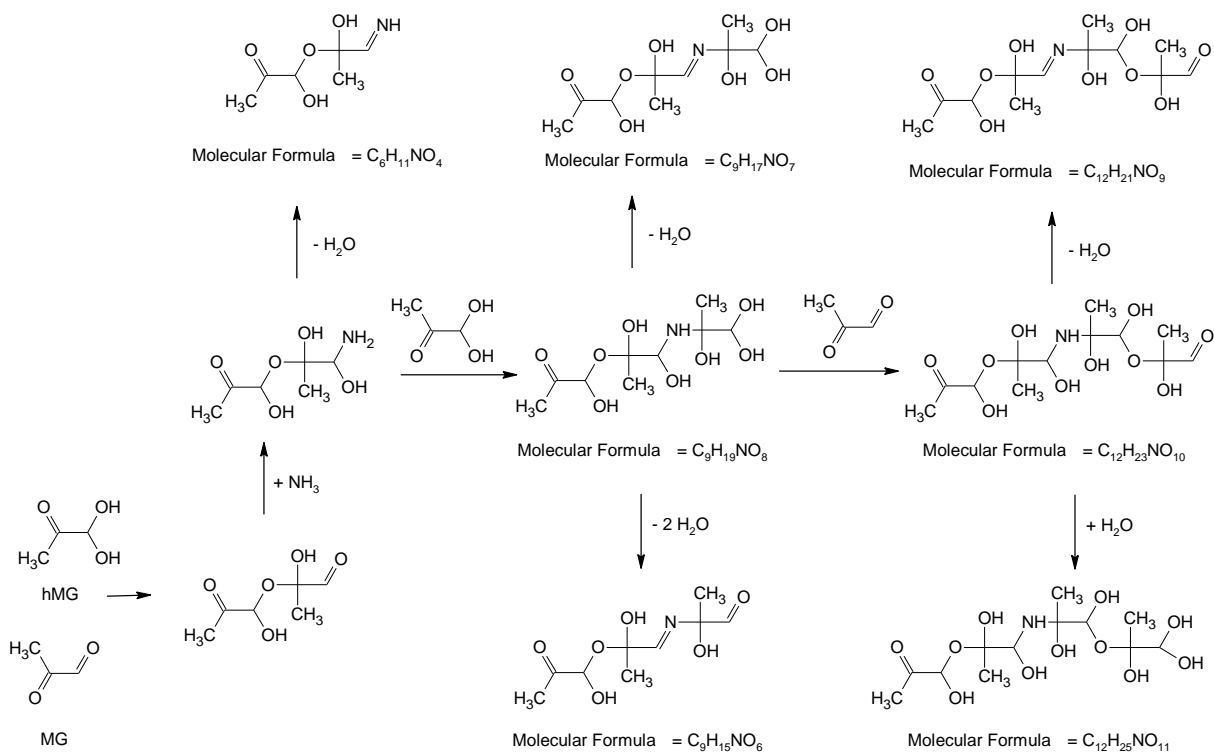
Figure 3.13: Possible mechanism for the formation of the observed products that are not derived from imidazole. MG and hMG stand for methylglyoxal and hydrated methylglyoxal, respectively.

3.5. Summary

The products of the G + AS and MG + AS reactions, and aged LIM/O₃ SOA, attracted

much attention as model BrC systems.[2] Our results, as well as previous experiments on the

photochemistry of MG/AS system[12, 15] suggest that MG/AS BrC has a low photochemical

stability. For example, with the QY from Table 3.1 and the measured *MAC* from Figure 3.3, we

estimate a photolysis lifetime for MG/AS BrC of about 13 minutes at zero-solar zenith angle at

sea level. This estimated lifetime is comparable to that determined by Sareen et al. (2013)[12] and

Zhao et al. (2012).[15] The lifetime for the photobleaching of the aged-LIM/O₃ SOA is also

relatively short, of the order of 1 hour.[22] While the lifetimes will increase somewhat under cloudy conditions and at lower solar zenith angles, the potential impact of these photolabile BrC species on climate may be limited. Even if a sufficient amount of BrC were produced during the night it would be readily photobleached upon sunrise and make minor contribution to the absorption of solar radiation for the rest of the day.

Another implication of this work is that the results of NaBH$_4$ addition to BrC or any other environmental mixture for the purpose of selective reduction of carbonyl groups to hydroxyl groups should be interpreted with care. This reaction is routinely used as a test for the presence of CT complexes in atmospheric BrC.[18, 31] However, in the MG/AS BrC system, the addition of small amount of NaBH$_4$ had complex effects on the absorption and fluorescence spectra. The excess amount of NaBH$_4$ did remove the major UV absorber, the imidazole carbonyl, as expected. However, the imidazole carbonyl is a small molecule that does not require intermolecular CT to absorb radiation. Furthermore, NaBH$_4$ appeared to lead to additional reactions other than simple reduction of carbonyls groups, which broke C-C bonds in the compounds. We can conclude that the reduction by NaBH$_4$ can lead to a decrease in the absorption of the mixture, but it has little to do with the removal of CT complexes. Recent results relying on HPLC-PDA-HRMS data show that, at least in some BrC systems, including MG/AS BrC, the overall absorption of the mixture is dominated by spectra of isolated chromophores and not CT complexes.[17, 32]

The last conclusion of this work is that processes accelerated by evaporation of water can produce very different results compared to slow reactions in aqueous solution. We previously showed that evaporation of water from a solution of limonene ozonolysis SOA and ammonium sulfate accelerated BrC formation by a large factor.[20] This work, as well as work by Zhao et al.

(2012),[15] showed that evaporation not only accelerated BrC formation in the MG/AS system but also resulted in a completely different distribution of the chromophores. The evaporation conditions used in this work (bulk solution evaporated for ~ 20 min at 30 °C) may not fully replicate the much faster evaporation of water from cloud and fog droplets or from aerosol particles containing liquid water. However, the available data strongly suggest that the evaporative pathway for producing BrC should be relevant to the atmospheric environment because of the frequent changes in relative humidity and high frequency of fog and cloud droplet formation followed by evaporation. We recommend that future studies of secondary BrC formation in water should always include an evaporation test to check if BrC formation is enhanced (with the experiments ideally carried out with aerosolized droplets instead of a bulk solution).

3.6. References

1.   Fu, T. M.; Jacob, D. J.; Wittrock, F.; Burrows, J. P.; Vrekoussis, M.; Henze, D. K., Global budgets of atmospheric glyoxal and methylglyoxal, and implications for formation of secondary organic aerosols. *J. Geophys. Res.* **2008**, *113*, D15303, doi:10.1029/2007jd009505.

2.   Laskin, A.; Laskin, J.; Nizkorodov, S. A., Chemistry of atmospheric brown carbon. *Chem. Rev.* **2015**, *115*, (10), 4335-4382.

3.   Grimmett, M. R.; Richards, E. L., 686. Imidazolic compounds from the reaction of pyruvaldehyde with ammonia. *J. Chem. Soc. (Resumed)* **1965**, 3751-3754.

4.   Freedman, M. A.; Hasenkopf, C. A.; Beaver, M. R.; Tolbert, M. A., Optical properties of internally mixed aerosol particles composed of dicarboxylic acids and ammonium sulfate. *J. Phys. Chem. A* **2009**, *113*, (48), 13584-13592.

5.   Hawkins, L. N.; Baril, M. J.; Sedehi, N.; Galloway, M. M.; De Haan, D. O.; Schill, G. P.; Tolbert, M. A., Formation of semisolid, oligomerized aqueous SOA: lab simulations of cloud processing. *Environ. Sci. Technol.* **2014**, *48*, (4), 2273-2280.

6.   De Haan, D. O.; Corrigan, A. L.; Tolbert, M. A.; Jimenez, J. L.; Wood, S. E.; Turley, J. J., Secondary organic aerosol formation by self-reactions of methylglyoxal and glyoxal in evaporating droplets. *Environ. Sci. Technol.* **2009**, *43*, (21), 8184-8190.

7.   De Haan, D. O.; Hawkins, L. N.; Kononenko, J. A.; Turley, J. J.; Corrigan, A. L.; Tolbert, M. A.; Jimenez, J. L., Formation of nitrogen-containing oligomers by methylglyoxal and amines in simulated evaporating cloud droplets. *Environ. Sci. Technol.* **2011**, *45*, (3), 984-991.

8.   Sareen, N.; Schwier, A. N.; Shapiro, E. L.; Mitroo, D.; McNeill, V. F., Secondary organic material formed by methylglyoxal in aqueous aerosol mimics. *Atmos. Chem. Phys.* **2010**, *10*, (3), 997-1016.

9.   Maxut, A.; Noziere, B.; Fenet, B.; Machakra, H., Formation mechanisms and yields of small imidazoles from reactions of glyoxal with NH_4^+ in water at neutral pH. *Phys. Chem. Chem. Phys.* **2015**, *17*, (31), 20416-20424.

10.   Kampf, C. J.; Filippi, A.; Zuth, C.; Hoffmann, T.; Opatz, T., Secondary brown carbon formation via the dicarbonyl imine pathway: nitrogen heterocycle formation and synergistic effects. *Phys. Chem. Chem. Phys.* **2016**, *18*, (27), 18353-18364.

11.   Kampf, C. J.; Jakob, R.; Hoffmann, T., Identification and characterization of aging products in the glyoxal/ammonium sulfate system-implications for light-absorbing material in atmospheric aerosols. *Atmos. Chem. Phys.* **2012**, *12*, (14), 6323-6333.

12.   Sareen, N.; Moussa, S. G.; McNeill, V. F., Photochemical aging of light-absorbing secondary organic aerosol material. *J. Phys. Chem. A* **2013**, *117*, (14), 2987-2996.

13.   Woo, J. L.; Kim, D. D.; Schwier, A. N.; Li, R.; McNeill, V. F., Aqueous aerosol SOA formation: impact on aerosol physical properties. *Faraday Discuss.* **2013,** *165*, 357-367.

14.   McNeill, V. F.; Woo, J. L.; Kim, D. D.; Schwier, A. N.; Wannell, N. J.; Sumner, A. J.; Barakat, J. M., Aqueous-phase secondary organic aerosol and organosulfate formation in atmospheric aerosols: a modeling study. *Environ. Sci. Technol.* **2012,** *46*, (15), 8075-8081.

15.   Zhao, R.; Lee, A. K.; Abbatt, J. P. D., Investigation of aqueous-phase photooxidation of glyoxal and methylglyoxal by aerosol chemical ionization mass spectrometry: observation of hydroxyhydroperoxide formation. *J. Phys. Chem. A* **2012,** *116*, (24), 6253-6263.

16.   Lee, A. K.; Zhao, R.; Li, R.; Liggio, J.; Li, S. M.; Abbatt, J. P., Formation of light absorbing organo-nitrogen species from evaporation of droplets containing glyoxal and ammonium sulfate. *Environ. Sci. Technol.* **2013,** *47*, (22), 12819-12826.

17.   Lin, P.; Laskin, J.; Nizkorodov, S. A.; Laskin, A., Revealing brown carbon chromophores produced in reactions of methylglyoxal with ammonium sulfate. *Environ. Sci. Technol.* **2015,** *49*, (24), 14257-14266.

18.   Phillips, S. M.; Smith, G. D., Light absorption by charge transfer complexes in brown carbon aerosols. *Environ. Sci. Technol. Lett.* **2014,** *1*, (10), 382-386.

19.   Sharpless, C. M.; Blough, N. V., The importance of charge-transfer interactions in determining chromophoric dissolved organic matter (CDOM) optical and photochemical properties. *Environ. Sci.: Processes Impacts* **2014,** *16*, (4), 654-671.

20.   Nguyen, T. B.; Lee, P. B.; Updyke, K. M.; Bones, D. L.; Laskin, J.; Laskin, A.; Nizkorodov, S. A., Formation of nitrogen- and sulfur-containing light-absorbing compounds accelerated by evaporation of water from secondary organic aerosols. *J. Geophys. Res.* **2012,** *117*, D01207, doi:10.1029/2011JD016944.

21.   Epstein, S. A.; Shemesh, D.; Tran, V. T.; Nizkorodov, S. A.; Gerber, R. B., Absorption spectra and photolysis of methyl peroxide in liquid and frozen water. *J. Phys. Chem. A* **2012,** *116*, (24), 6068-6077.

22.   Lee, H. J.; Aiona, P. K.; Laskin, A.; Laskin, J.; Nizkorodov, S. A., Effect of solar radiation on the optical properties and molecular composition of laboratory proxies of atmospheric brown carbon. *Environ. Sci. Technol.* **2014,** *48*, (17), 10217-10226.

23.   Bunce, N. J.; LaMarre, J.; Vaish, A. P., Photorearrangement of azoxybenzene to 2-hydroxyazobenzene: a convenient chemical actinometer. *Photochem. Photobiol.* **1984,** *39*, (4), 531-533.

24.   Nguyen, T. K. V.; Zhang, Q.; Jimenez, J. L.; Pike, M.; Carlton, A. G., Liquid water: ubiquitous contributor to aerosol mass. *Environ. Sci. Technol. Lett.* **2016,** *3*, (7), 257-263.

25.   Chen, Y.; Bond, T. C., Light absorption by organic carbon from wood combustion. *Atmos. Chem. Phys.* **2010,** *10*, (4), 1773-1787.

26.   Powelson, M. H.; Espelien, B. M.; Hawkins, L. N.; Galloway, M. M.; De Haan, D. O., Brown carbon formation by aqueous-phase carbonyl compound reactions with amines and ammonium sulfate. *Environ. Sci. Technol.* **2013,** *48*, (2), 985-993.

27.   Hawkins, L. N.; Lemire, A. N.; Galloway, M. M.; Corrigan, A. L.; Turley, J. J.; Espelien, B. M.; De Haan, D. O., Maillard chemistry in clouds and aqueous aerosol as a source of atmospheric humic-like substances. *Environ. Sci. Technol.* **2016,** *50*, (14), 7443-7452.

28.   Romonosky, D. E.; Laskin, A.; Laskin, J.; Nizkorodov, S. A., High-resolution mass spectrometry and molecular characterization of aqueous photochemistry products of common types of secondary organic aerosols. *J. Phys. Chem. A* **2015,** *119*, (11), 2594-2606.

29.   Epstein, S. A.; Blair, S. L.; Nizkorodov, S. A., Direct photolysis of alpha-pinene ozonolysis secondary organic aerosol: effect on particle mass and peroxide content. *Environ. Sci. Technol.* **2014,** *48*, (19), 11251-11258.

30.   George, C.; Ammann, M.; D'Anna, B.; Donaldson, D. J.; Nizkorodov, S. A., Heterogeneous photochemistry in the atmosphere. *Chem. Rev.* **2015,** *115*, (10), 4218-4258.

31.   Phillips, S. M.; Smith, G. D., Further evidence for charge transfer complexes in brown carbon aerosols from excitation-emission matrix fluorescence spectroscopy. *J. Phys. Chem. A* **2015,** *119*, (19), 4545-4551.

32.   Lin, P.; Aiona, P. K.; Li, Y.; Shiraiwa, M.; Laskin, J.; Nizkorodov, S. A.; Laskin, A., Molecular characterization of brown carbon in biomass burning aerosol particles. *Environ. Sci. Technol.* **2016,** *50*, (21), 11815-11824.

Chapter 4   Effect of Solar Radiation on the Optical Properties and Molecular Composition of Laboratory Proxies of Atmospheric Brown Carbon

4.1. Abstract

Sources, optical properties, and chemical composition of atmospheric brown carbon (BrC) aerosol are uncertain, making it challenging to estimate its contribution to radiative forcing. Furthermore, optical properties of BrC may change significantly during its atmospheric aging. We examined the effect of photolysis on the molecular composition, mass absorption coefficient, and fluorescence of secondary organic aerosol (SOA) prepared by high-NO_x photooxidation of naphthalene (NAP SOA). Our experiments were designed to model photolysis processes of NAP SOA compounds dissolved in cloud or fog droplets. Aqueous solutions of NAP SOA were observed to photobleach (i.e., lose their ability to absorb visible radiation) with an effective half-life of ~15 h (with sun in its zenith) for the loss of near-UV (300-400 nm) absorbance. The molecular composition of NAP SOA was significantly modified by photolysis, with the average SOA formula changing from $C_{14.1}H_{14.5}O_{5.1}N_{0.085}$ to $C_{11.8}H_{14.9}O_{4.5}N_{0.023}$ after 4 h of irradiation. However, the average O/C ratio did not change significantly, suggesting that it is not a good metric for assessing the extent of photolysis-driven aging in NAP SOA (and in BrC in general). In contrast to NAP SOA, the photobleaching of BrC material produced by the reaction of limonene + ozone SOA with ammonia vapor (aged LIM/O_3 SOA) was much faster, but it did not result in a significant change in molecular composition. The characteristic absorbance of the aged LIM/O_3 SOA in the 450-600 nm range decayed with an effective half-life of < 0.5 h. This result emphasizes the highly variable and dynamic nature of different types of atmospheric BrC.

4.2. Introduction

Atmospheric aerosols affect the Earth's radiative balance by direct and indirect mechanisms.[1] The direct radiative forcing is typically negative (cooling) because light scattering dominates over absorption for most types of aerosols. However, aerosols that strongly absorb visible radiation, such as black carbon (BC), mineral dust, and brown carbon (BrC),[2] may either reduce the cooling effect or result in positive radiative forcing (warming).[3] In contrast to well characterized BC, the sources, optical properties, and chemical composition of BrC are not well understood, making it challenging to estimate the contribution of BrC to global forcing.[2, 4, 5]

Biomass burning and fossil-fuel combustion serve as important primary sources of BrC and BC. In addition, BrC may also have secondary sources related to gas-phase and aqueous processes involved in the formation and aging of secondary organic aerosols (SOA). For example, ammonium sulfate has been shown to react with glyoxal and methyl glyoxal in aqueous solutions producing imidazole-based light-absorbing compounds.[6-12] SOA produced from certain biogenic precursors, such as limonene (LIM), have been found to produce BrC in the presence of ammonia.[13-17] Aqueous oxidation of phenols and gas-phase oxidation of certain aromatic compounds also produce BrC material.[18-20] The multitude of poorly-characterized secondary sources contributes to the challenge of constraining the properties of BrC aerosols in climate modeling.

Several studies demonstrated that optical properties of BrC may evolve significantly as a result of atmospheric aging. For example, Rincon et al. analyzed the absorption spectra of irradiated solutions of pyruvic acid and showed that the spectra change significantly depending on temperature, irradiation history, and other conditions.[21] Sareen et al. examined the properties of methyl glyoxal + ammonium sulfate reaction products, and found that the near-UV

absorbance of these products drops on a time scale of minutes in reactions with ozone and during photolysis.[11] Lambe et al. demonstrated that optical properties of SOA are strongly affected by extensive OH oxidation.[22] Zhong and Yang demonstrated that biomass burning BrC undergoes reactions that both produce light-absorbing compounds and remove them on time scales of hours.[23] Therefore, it is not sufficient to know the initial absorption properties of BrC; it is also important to predict how they may evolve during various aging scenarios.

The goal of this study is to explore the effect of photolysis on the optical properties of laboratory generated proxies of BrC in aqueous solutions, as a model for cloud/fog processing of BrC. The model BrC used in this study is SOA produced by high-NO_x photooxidation of naphthalene (NAP). NAP is the most abundant and simplest polycyclic aromatic hydrocarbon found in highly-populated urban areas,[23, 24] with fossil-fuel combustion serving as its major source.[25-29] Gas-phase reaction with OH ($k = 2\times10^{-11}$ cm^3 molecules^{-1} s^{-1})[25] is the primary sink for NAP resulting in a lifetime of about 6 h at [OH] $= 2\times10^6$ molecules cm^{-3}. This reaction forms a multitude of secondary pollutants in both the particle and gas phase. Figure 4.1 shows the initial processes involved in NAP photooxidation and Table 4.1 lists some of the products previously reported in literature.[27-31] Some of the products shown in Figure 4.1, such as aromatic aldehydes, nitroaromatic compounds, and quinones are expected to absorb light in the near-UV range and be photochemically active. Therefore, photolysis is expected to have a strong effect on NAP SOA composition.
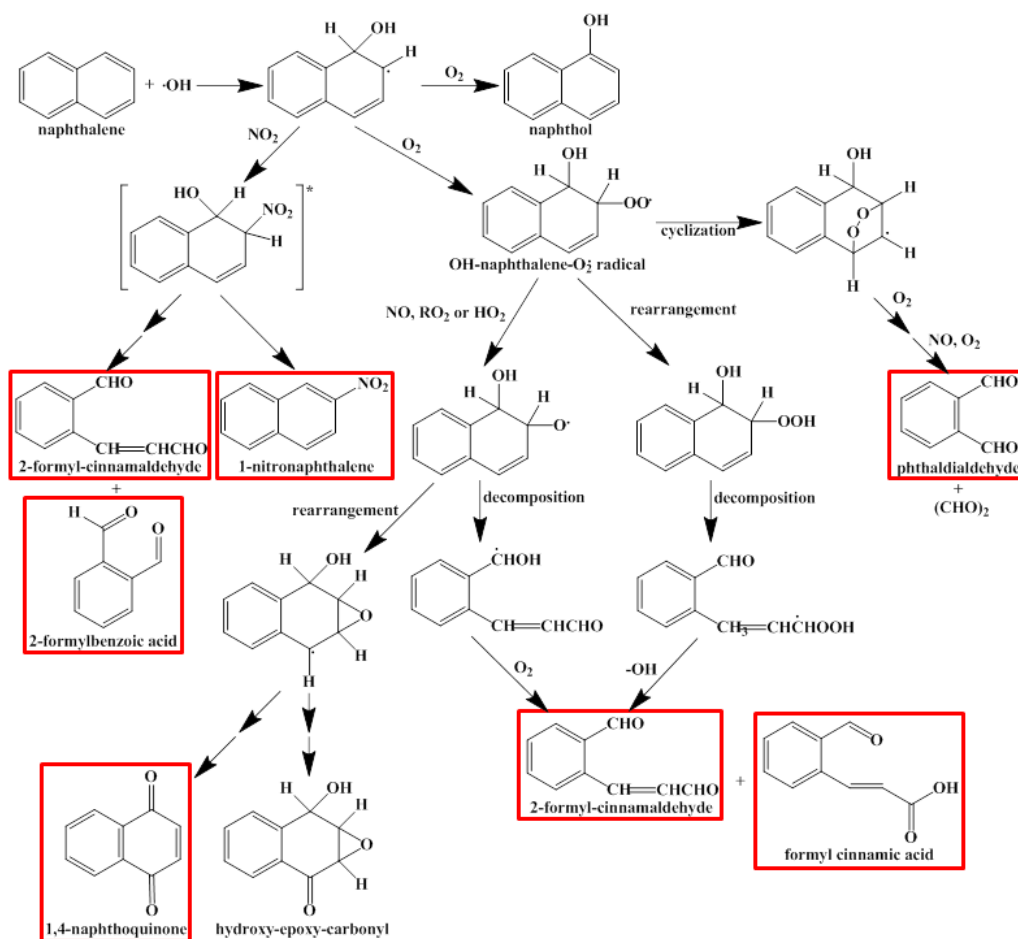
Figure 4.1: Initial processes involved in atmospheric oxidation of NAP adapted and modified from Nishino et al.[29] In addition to the products retaining the NAP skeleton (naphthols and nitro compounds), a number of ring-opening benzene derivatives can also be produced. A partial list of possible products is provided in **Table 4.1**. Formulas corresponding to the boxed compounds have been observed in the HR-MS spectra reported in this work.

Table 4.1: A partial list of known products of NAP photooxidation.

Name*	Formula	Peak abundance (%) $[M+H]^+$	$[M+Na]^+$	Effect of photolysis
benzoic acid	$C_7H_6O_2$	-	-	-
Phthaldialdehyde	$C_8H_6O_2$	-	37	↑
2-hydroxy benzoic acid	$C_7H_6O_3$	-	-	-
phthalic anhydride	$C_8H_4O_3$	-	-	-
2-formylbenzoic acid	$C_8H_6O_3$	-	13	↑
2-formyl-cinnamaldehyde	$C_{10}H_8O_2$	1.9	20	↓
formyl cinnamic acid	$C_{10}H_8O_3$	3.1	23	↑
Naphthol	$C_{10}H_8O$	-	-	-
1,4-naphthoquinone	$C_{10}H_6O_2$	-	2.4	↓
2,3-epoxy-1,4-quinone	$C_{10}H_6O_3$	-	6.4	↓
4-hydroxy-2,3-epoxy-carbonyl	$C_{10}H_7O_3$	-	-	-
1-nitronaphthalene	$C_{10}H_7NO_2$	-	12	↓

*This table lists common names and chemical formulas of the products reported in Refs. [27-31]. If the formula is detected in the unphotolyzed NAP SOA sample by ESI/HR-MS, the relative abundances (in % relative to the largest peak in the mass spectrum) of the corresponding protonated $[M+H]^+$ and sodiated $[M+Na]^+$ species are also included. The last column indicates whether the peaks corresponding to these compounds increase (↑) or are removed (↓) upon photolysis.

NAP SOA can be considered a prototype of BrC material because of its relatively large absorption coefficient[17, 22] and because its absorption spectrum is similar in shape to the absorption spectra of ambient organic and biomass burning aerosols.[23, 32, 33] In this work, we attempted to correlate the photolysis-driven changes in the optical properties of NAP SOA to changes in its molecular composition probed by high-resolution mass spectrometry (HR-MS). Photolysis produced significant changes in the molecular composition of NAP SOA, but only had a modest effect on its wavelength-dependent mass absorption coefficient (MAC). To demonstrate that this is not universally applicable to all types of BrC, we also examined photolysis of BrC material produced by chemical aging of LIM/O$_3$ SOA with ammonia vapor (NH$_3$).[13, 15-17] The aged LIM/O$_3$ SOA displayed the completely opposite behavior, with

relatively small changes in the composition, but dramatic changes in the absorption spectrum. The contrast between NAP SOA and aged LIM/O_3 SOA emphasizes the highly variable and dynamic nature of different types of BrC materials.

4.3. Experimental Method

4.3.1. SOA Preparation

Photooxidation of NAP was carried out in a 5 m^3 Teflon chamber under dry, high-NO_x conditions. The chamber was purged overnight with 60 L min^{-1} of dry clean air resulting in residual levels of particulate matter, O_3 and NO_y that were below the detection limits of the corresponding analyzers. Approximately 2–4 ppm (10^{-6} by volume) of H_2O_2 was introduced to the chamber by evaporating 40–80 µL of H_2O_2 (Sigma-Aldrich, 30% by volume in water). This was followed by adding 450–900 ppb (10^{-9} by volume) of NAP by evaporating 25–50 µL of 0.5 g mL^{-1} NAP (Fisher, 99% purity) dissolved in dichloromethane (Fisher, 99.9% purity) and 500–800 ppb of NO from a premixed gas-bottle (Praxair, 5000 ppm NO in N_2). The precursors were thoroughly mixed in the chamber using a fan, which was later turned off once photolysis began to minimize particle wall losses. Photooxidation was driven by 35 UV-B lamps (FS40T12/UVB, Solarc Systems, Inc.) with emission centered at 310 nm. The real-time concentrations of NO/NO_y and O_3 were monitored by Thermo Scientific 42i-Y and 49i analyzers, respectively. Relative humidity and temperature of the chamber were monitored by a Vaisala HMP233 probe; the temperature typically increased by 3-5 °C during photooxidation. The particle size distribution was monitored with a TSI model 3936 scanning mobility particle sizer (SMPS). Volatile compounds were monitored with a proton-transfer-reaction time-of-flight mass spectrometer, PTR-ToF-MS (IONICON Analytik GmbH, Innsbruck, Austria). The steady-state OH concentration in the chamber was estimated from the rate of decay of NAP, observed by

PTR-ToF-MS as its protonated ^{13}C–isotope at m/z 130.16, and the known bimolecular rate constant (2×10^{-11} cm^3 molecules^{-1} s^{-1}) for the NAP + OH reaction.[25] The estimated steady-state concentration of OH was ~5×10^6 molecules cm^{-3}.

After 3 h of photooxidation, the resulting SOA was collected on two PTFE filters (Millipore 0.2 µm pore size) in parallel at a constant flow rate of about 16 L min^{-1} per filter. An activated carbon denuder (Sunset Laboratory) was installed between the chamber and the filters to help remove excess volatiles and O_3. The amount of SOA collected on each filter was estimated from the SMPS data assuming 100% collection efficiency by the filters and known NAP SOA density of 1.55 g cm^{-3}.[30] Typically, 800–1300 µg of SOA material was collected on each filter. The filter samples were either used immediately or were stored in a freezer at -20 °C before photolysis experiments and/or HR-MS analysis.

In addition to the NAP SOA samples, SOA from ozonolysis of LIM (LIM/O_3 SOA) was generated and aged with NH_3 to produce BrC as described in Lee et al.[16] This type of aged SOA has a distinctive, well-characterized absorption spectrum in the visible range,[13, 16, 17, 34] making it a convenient model system for studying photochemistry of BrC. We will refer to this material as "aged LIM/O_3 SOA."

4.3.2. Optical Properties and Photolysis of Aqueous SOA

SOA was extracted from filters by sonication in 1.8-2 mL of deionized water for 10-15 minutes to achieve a concentration of 0.58 ± 0.07 mg mL^{-1} of dissolved SOA material. The completeness of the extraction was verified by first extracting the filter with water and then extracting the residual material on the filter with acetonitrile. By comparing the UV absorbance of the primary water extract and secondary acetonitrile extract we estimate that water extracted more than 80% of the organic material for both NAP and aged LIM/O_3 SOA. A dual-beam

spectrometer (Shimadzu UV-2450) was used to record UV/Vis absorption spectra of the SOA extracts in the 200-700 nm range. Three-dimensional excitation-emission matrix (EEM) spectra of SOA extracts were acquired with a Hitachi F-4500 fluorescence spectrometer as described in Lee et al.[16] The excitation wavelength spanned the 200–500 nm range in 5 nm steps, and the emission was recorded over the 300–600 nm range in 2 nm increments. Deionized water served as the background for the absorption and EEM measurements.
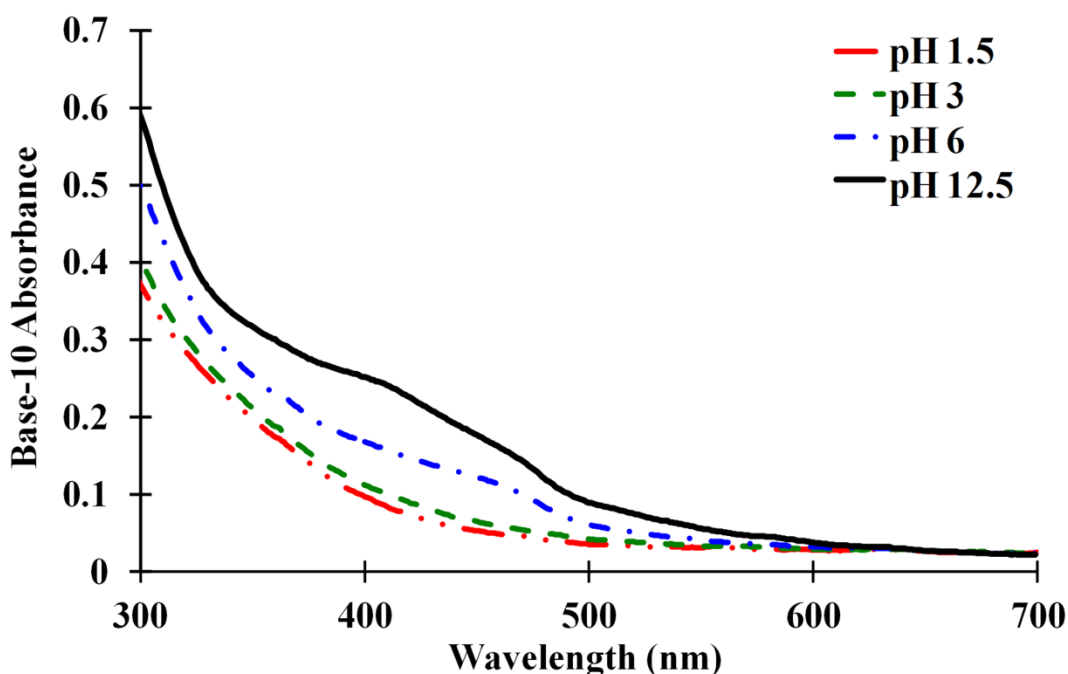
Figure 4.2: Absorption spectra of a NAP SOA sample measured at different pH levels.

We investigated the effect of the solution pH on the absorption spectrum by adding few drops of 0.1 M KOH or HCl to the solution to make it more basic or acidic. We observed that the absorption spectra of the NAP SOA extracts were pH dependent; Figure 4.2 shows that the absorbance increased significantly between 400-500 nm with the increase of pH. We attribute the pH dependence to acid-base equilibria of nitrophenols, which are important products of high-NO_x photooxidation of aromatics (see Vione et al.[35] and references therein). In addition, ionization of SOA compounds, such as carboxylic acids, may also contribute to the red-shift, as

109

shown by other authors.[36-40] Spectra of nitrophenols are known to experience a significant red-shift upon ionization in solution.[37, 40] For example, 2,4-dinitrophenol does not strongly absorb radiation above 300 nm, while its anion has distinctive absorption bands between 300 and 450 nm. As shown in Figure 4.2, an increase in pH above pH = 6 resulted in the appearance of absorption bands between 400-500 nm suggesting that nitrophenols contributed significantly to absorbance by NAP SOA. The measured pH values of the NAP SOA extracts were around 5-6, similar to the pH of cloud droplets.[41, 42] Under these conditions, the degree of ionization of nitrophenols should be relatively small. All the photolysis experiments described in this work have been carried out at pH = 5-6 (obtained when an SOA sample was extracted in water).

The procedure for the photolysis of aqueous SOA extracts was similar to that described by Epstein et al.[43] for photolysis of aqueous methyl hydroperoxide (CH_3OOH). A standard 1.0 cm quartz cuvette containing the extract was placed in a temperature controlled cuvette holder. A small magnetic stir bar mixed the sample during photolysis. The absorbance at a selected wavelength (300 nm for NAP SOA and 500 nm for the aged LIM/O_3 SOA) was continuously recorded to determine the photolysis rate. In addition, a complete absorption spectrum was periodically taken (the stir bar was stopped during these measurements to avoid noise from solution turbulence). Radiation from a xenon arc lamp in a Newport Optics Photomax housing was reflected with a 90-degree dichroic mirror, filtered with a U-330 band-pass filter (Edmund optics 46-438), and coupled into a 1 m long, 0.95 cm diameter light-guide. The light guide delivered the radiation into the UV/Vis spectrometer and irradiated the cuvette from above. The radiant flux density was determined by photolyzing a 0.1 M solution of azoxybenzene (Fisher Scientific, 98 %) in ethanol in the presence of 0.1 M potassium hydroxide.[43, 44] Azoxybenzene is a convenient actinometer for relatively slow photolysis processes in SOA because its quantum

yield is relatively low ($QY_{azo} \sim 0.020$) and does not strongly depend on temperature and concentration.[44] The actinometer measurements were carried out both before and after SOA photolysis. The photolysis rate was determined from the rate of increase in absorbance due to the azoxybenzene's photoisomer, using its known molar extinction coefficient of 7600 L mol^{-1} cm^{-1} at 458 nm (Figure 4.3).[44]

4.3.3. Calculation of Radiant Flux Density from the Actinometry Measurements

In the experiments described in this paper, the SOA or actinometer solution of volume $V_{solution}$ is irradiated from the top in a standard $b = 1.0$ cm cuvette with a collimated beam of radiation with cross-section $Area$. The effective, solution-volume-normalized rate with which photons are absorbed by the sample can be described with the following equation,

$$Rate_{absorption}\left(\frac{photons}{cm^3 s}\right) = \frac{Area}{V_{solution}}\int_{\lambda} D_0(\lambda)\left(1 - 10^{-A_{vertical}(\lambda)}\right)d\lambda \qquad \textbf{(Equation 4.1)}$$

where $D_0(\lambda)$ is the spectral flux density of the photolyzing radiation (in photons cm^{-2} s^{-1}), and $A_{vertical}$ is the base-10 absorbance of the solution over the vertical path length of the photolyzing radiation, $h_{solution}$. We measure the absorption spectrum of the solution in a normal way, i.e., perpendicular to the cuvette over path length b. This gives absorbance $A(\lambda)$, which is directly proportional to $A_{vertical}(\lambda)$ under conditions when the Beer-Lambert law holds.

$$A_{vertical}(\lambda) = \frac{h_{solution}A(\lambda)}{b} \qquad \textbf{(Equation 4.2)}$$

However, for the purposes of actinometry, it is more convenient to make the absorbance of the actinometer reasonably high so that all of the incoming radiation is absorbed by the solution (it is important in this case to mix the solution during photolysis). In this case, Eq. 4.1 simplifies to:

$$Rate_{absorption} = \frac{Area}{V_{solution}}\int_{\lambda} D_0(\lambda)d\lambda \qquad \textbf{(Equation 4.3)}$$

111

We assume that $D_0(\lambda)$ is directly proportional to the intensity of the radiation measured with a USB4000 Ocean Optics spectrometer:

$$D_0(\lambda) = \alpha \times OO(\lambda)$$

<div align="right">**(Equation 4.4)**</div>

In this formula, $OO(\lambda)$ is a baseline-corrected dimensionless function of wavelength returned by the USB4000 spectrometer. The constant α, which has the same units as D_0, has to be determined for each specific set of experimental conditions. In order to do so, we measure the rate of photolysis of the actinometer from the time-dependent rise in absorbance of the photolysis product of azoxybenzene.

$$azoxybenzene + h\nu \rightarrow azoxybenzene\ photoisomerization\ product$$

In the strong actinometer absorbance limit, the absorbance by the product, $A_{product}$, grows linearly as shown in Figure 4.3a. This can be converted into the actual photolysis rate using the known molar extinction coefficient of the product, $\varepsilon_{product} = 7600$ L mol^{-1}cm^{-1} at 458 nm.
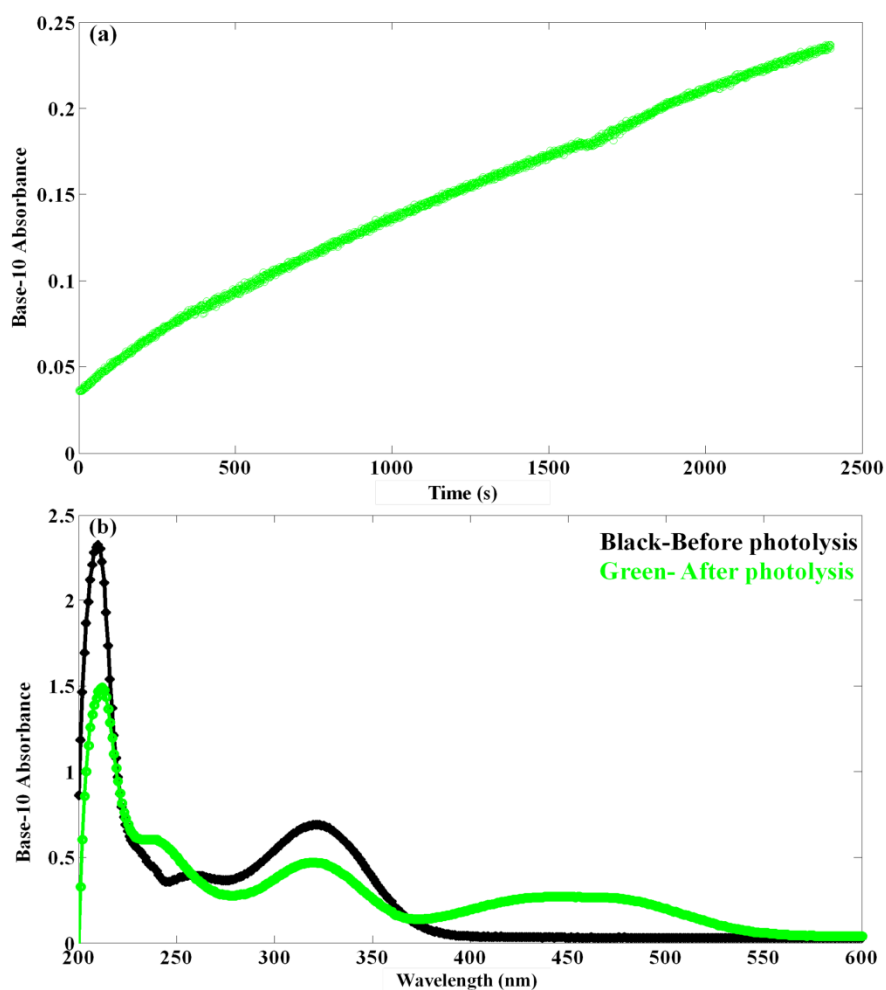
Figure 4.3: (a) Absorbance of the product at 458 nm versus time. (b) Absorption spectrum of the actinometer before and after photolysis.

Expressed in molecular units, the photolysis rate is directly proportional to the initial slope in Figure 4.3a.

$$Rate_{photolysis}\left(\frac{molec}{cm^3 s}\right) = \frac{N_A}{1000}\frac{d[\text{product}]}{dt} = \frac{N_A}{1000b\varepsilon_{product}}\frac{dA_{product}}{dt} \qquad \textbf{(Equation 4.5)}$$

The ratio of the rate of photolysis from Eq. 4.5 and the rate of absorption from Eq. 4.3 are equal to the quantum yield of azoxybenzene ($\phi_{azo} \sim 0.020$).[44] Combining all the equations together, we obtain Eq. 4.6 to determine constant α:

$$a = \frac{\dfrac{N_A}{1000b\varepsilon_{product}}\dfrac{dA_{product}}{dt}}{\phi_{AZO}\left(\dfrac{Area}{V_{solution}}\right)\displaystyle\int_\lambda OO(\lambda)d\lambda}$$ **(Equation 4.6)**

Finally, in a case where the entire cross-section of the cuvette is illuminated (which

approximately applies to our measurements), all dimension-related terms cancel out, leading to:

$$a = \frac{\dfrac{N_A}{1000\varepsilon_{product}}\dfrac{dA_{product}}{dt}}{\phi_{AZO}\displaystyle\int_\lambda OO(\lambda)d\lambda}$$ **(Equation 4.7)**

This is the equation we used in calibrating the spectral flux density. A typical result for $D_0(\lambda)$ is

shown in Figure 4.4.
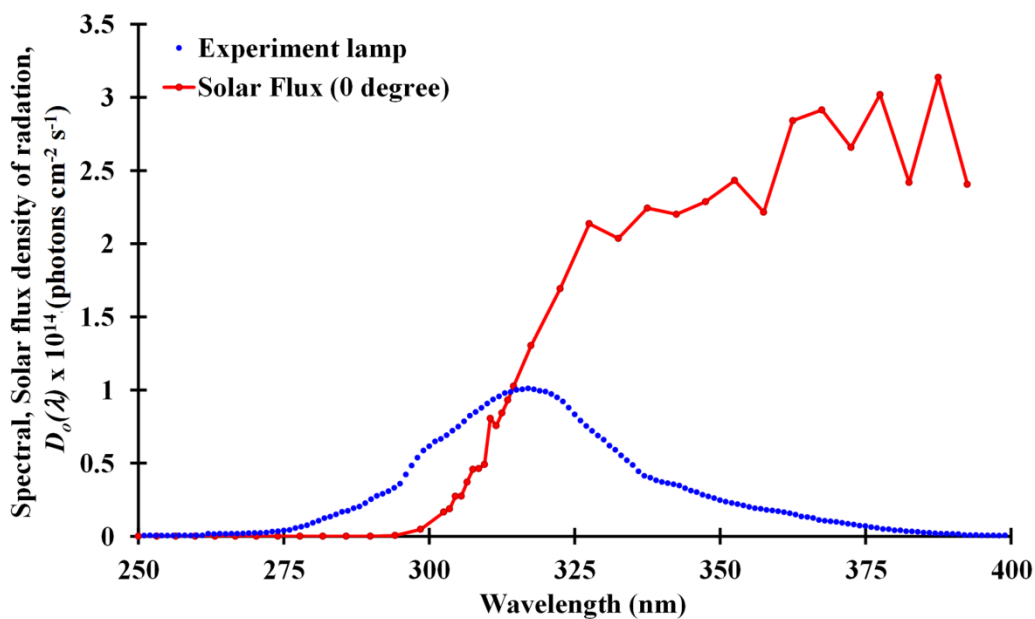
Figure 4.4: A typical solar and spectral flux density of radiation, $D_0(\lambda)$, from the irradiation
source compared to that from a sun in zenith.

4.3.4. Procedure for Calculating the Effective Photolysis Rate

We calculate the effective rate of NAP SOA photolysis under realistic atmospheric conditions from the experimentally determined rate. Since the wavelength-dependent photolysis quantum yield information is not available from our experiments, we make the following approximations:

1. Photolysis is limited to wavelengths below 400 nm (visible photons are not expected to be energetic enough to result in photolysis). This assumption prevents the overestimation of the atmospheric photolysis rate when convoluting the absorption spectrum of SOA and solar flux.

2. Photolysis quantum yields for the absorbing NAP SOA compounds do not strongly depend on wavelength over the range of the photolysis source (shown in Figure 4.4).

These assumptions make it possible to re-scale the experimental photolysis time scale into an effective photolysis time relevant to the atmospheric environment as follows:

$$\frac{J(EXP)}{J(ATM)} = \frac{\int_{250}^{400} D_{lamp}(\lambda)\Phi(\lambda)\sigma_{SOA}(\lambda)d\lambda}{\int_{250}^{400} D_{solar}(\lambda)\Phi(\lambda)\sigma_{SOA}(\lambda)d\lambda} \approx \frac{\int_{250}^{400} D_{lamp}(\lambda)\sigma_{SOA}(\lambda)d\lambda}{\int_{250}^{400} D_{solar}(\lambda)\sigma_{SOA}(\lambda)d\lambda} \qquad \textbf{(Equation 4.8)}$$

In this equation, F represents the actinic flux from the lamp or from the sun, and σ represents the effective absorption cross section of NAP SOA, which is proportional to the measured absorbance of the NAP SOA solution. The photolysis quantum yields cancel out from this equation because of the second assumption. The spectral flux density of the photolyzing radiation, $D_{lamp}(\lambda)$, is obtained using the methods described above (a typical result is shown in Figure 4.4). The solar actinic flux, $D_{solar}(\lambda)$, was obtained from a TUV calculator provided by

NCAR,[45] at one kilometer ground elevation and surface albedo of 0.10 (the result is also shown in Figure 4.4).

The effective photolysis time at zero solar zenith angle, *t(effective)*, can now be calculated from the experimental photolysis time in the lab, *t(laboratory)*, using Eq. 4.9.

$$t(effective) = t(laboratory) * \frac{J(EXP)}{J(ATM)} \qquad \textbf{(Equation 4.9)}$$

For the LIM/O_3 SOA + NH_3 data, the integration range for Eq. 4.8 was from 250–400, due to the optically active region shown in Figure 4.7. The *J*(ratio), ~ 0.56, was slightly higher than NAP SOA.

4.3.5. Electrospray Ionization High-Resolution Mass Spectrometry (ESI/HR-MS)

Three separate sets of SOA samples were analyzed with a high–resolution (m/Δm ~ 10^5 at *m/z* 450) linear-ion-trap (LTQ) Orbitrap^{TM} mass spectrometer (Thermo Corp.) equipped with an electrospray ionization (ESI) source operating in the positive ion mode. In each set of experiments, two identical SOA filter samples were separately extracted to obtain 0.34 ± 0.07 mg mL^{-1} SOA solutions in water. One of the solutions was photolyzed while the other was kept in the dark as a control. The exposure was equivalent to about 3-4 h under a solar zenith angle (SZA) of 0°.

After photolysis and immediately prior to analysis, the aqueous solutions were mixed with acetonitrile (Aldrich, HPLC grade) in a 1:1 ratio to improve the ESI source stability. Mass spectra of a blank sample corresponding to a 1:1 mixture of acetonitrile and water, and of a calibration mixture of caffeine MRFA and Ultramark 1621 (LTQ ESI Positive Ion Calibration Solution, Thermo Scientific, Inc.) were also recorded. The combination of the external calibration and an internal re-calibration of each spectrum with respect to the expected products of NAP oxidation resulted in an estimated peak position accuracy of better than $\pm$ 0.0005 Da

over the *m/z* 100-500 range of interest where more than 95% of the detected peaks were found. The compounds were detected as sodiated $[M + Na]^+$ and/or protonated $[M + H]^+$ species. For clarity, the formulas discussed in this paper will correspond to the neutral analytes. The data analysis was carried out as discussed in Nizkorodov et al.[46, 47] Briefly, peaks that appeared in the blank sample and peaks corresponding to ^{13}C isotopes were discarded. The peaks were assigned to formulas $C_{1-40}H_{2-80}O_{0-35}N_{0-2}Na_{0-1}^+$ with 0.00075 *m/z* tolerance while constraining the H/C and O/C ratios to 0.4–2.5 and 0–1.0 and only permitting closed-shell ions (no ion-radicals). Most of the peaks could be assigned unambiguously with these constraints. However, for a subset of peaks, either N_0 or N_2 assignments were possible for a single *m/z*. In these cases, preference was given to the N_0 assignment based on analysis of the N-atom distribution for the unambiguously assigned peaks.

4.4. Results and Discussion

4.4.1. Mass Absorption Coefficients of NAP SOA

The measured absorption spectra presented in this work are in the form of wavelength-dependent *MAC*, which is calculated from the base-10 absorbance, A_{10}, of the SOA solution with known mass concentration, C_{mass} (g cm^{-3}), and path length, *b* (cm).[48]

$$MAC(\lambda) = \frac{A_{10}^{solution}(\lambda) \times \ln(10)}{b \times C_{mass}} \qquad \textbf{(Equation 4.10)}$$

Examples of the *MAC* spectra taken at different photolysis times are shown in Figure 4.5. The shape of the spectra are characteristic of a typical atmospheric BrC material[33] and consistent with previous measurements for NAP SOA.[17, 22] The absorption coefficient is highest in the UV range, but there is a broad tail in the visible range. The absolute *MAC* values (0 – 6000 cm^2 g^{-1} between 300–700 nm) are qualitatively consistent with previous measurements by Updyke et al. (0–5000 cm^2 g^{-1} in the same wavelength range).[17] The differences are likely due to uncertainties

in estimating the mass of collected SOA from the SMPS data. A power law is customarily used to describe the wavelength dependence of the mass absorption coefficient of BrC, $MAC(\lambda) = MAC_o \times \lambda^{-AAE}$, where *AAE* stands for the absorption Angstrom exponent. Values of *AAE* in excess of 1, which are typical for BC-dominated aerosol, indicate strong contribution of BrC to aerosol absorption. The *AAE* for NAP SOA studied here is ~ 6.2 for the visible wavelength range of 400– 630 nm. It is slightly smaller than the value of 6.5 reported by Updyke et al. but closer to the range of reported *AAE* values for BrC, ranging from 2 to 7, measured in the field studies.[22, 49-52] In summary, NAP SOA can be regarded as an example of a moderately–absorbing type of BrC.
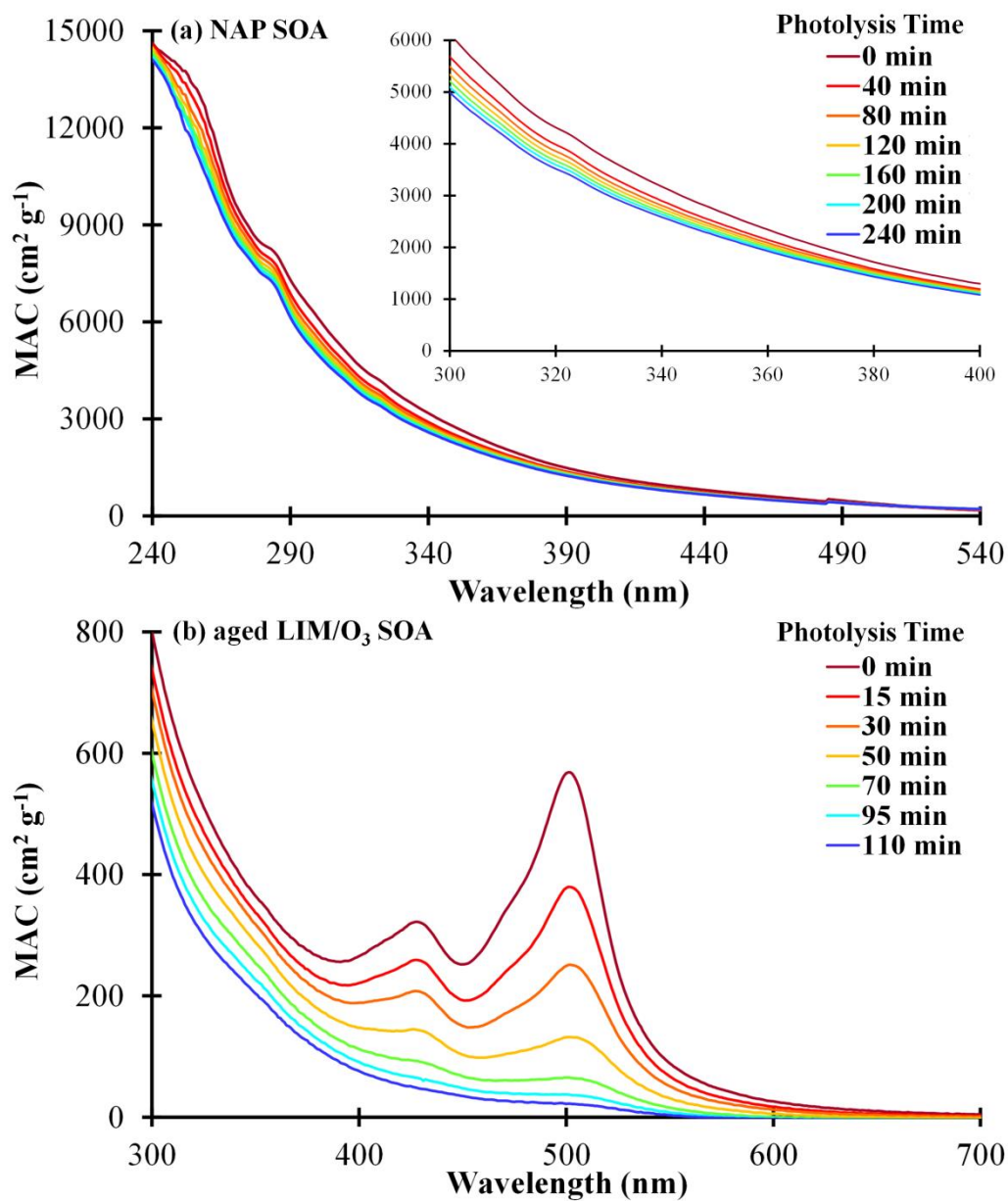
Figure 4.5: UV-Vis absorption spectra recorded during photolysis of: (a) an aqueous solution of NAP SOA and (b) an aqueous solution of LIM/O₃ SOA aged through reaction with ammonia vapor. The vertical axis corresponds to the mass absorption coefficient (*MAC*) calculated from Eq. 4.10. The inset in panel (a) zooms in on the 300-400 nm range.

4.4.2. Effective Rate of NAP SOA Photolysis

As Figure 4.5a demonstrates, the exposure of aqueous NAP SOA to actinic radiation

slightly reduces its MAC, presumably as a result of photodegradation of BrC chromophores.

Although omitted from Figure 4.5a, the *MAC* continues to decline at approximately the same rate upon further photolysis. Quantitative interpretation of these measurements is rather complicated because of the unknown and likely very large number of individual chromophores in the SOA solution. We approximate the *MAC* decay as a first-order kinetic process with an effective rate constant k.

$$MAC_t = MAC_0 \times \exp(-kt)$$ **(Equation 4.11)**

To facilitate the discussion of the atmospheric relevance of these results, we converted the laboratory photolysis time into an equivalent time in the atmosphere at SZA = 0°. This procedure converts the photolysis rate resulting from irradiation by the UV source (shown in Figure 4.4) to that resulting from solar irradiation (also shown in Figure 4.4). We stress that this approach is approximate as it neglects wavelength dependence of the photolysis quantum yields for NAP SOA compounds.

Figure 4.6a shows the dependence of the average *MAC* in the near-UV (300-400 nm) and visible (450-600 nm) regions on the effective atmospheric photolysis time. The effective rate constant, k, appears to be larger in the near-UV range ($k = 0.052$ h^{-1}) than in the visible range ($k = 0.011$ h^{-1}). These rates can be converted into empirical half-lives, $\tau = \ln(2)/k$, which are listed in

Table 4.2. The half-life suggests that NAP SOA loses its ability to absorb near-UV and visible radiation on a time scale of days, with the fastest changes on the blue end of the spectrum. We verified in a separate set of experiments that NAP SOA can be completely photobleached (i.e., lose its yellow color) upon prolonged irradiation (after many effective days of photolysis).
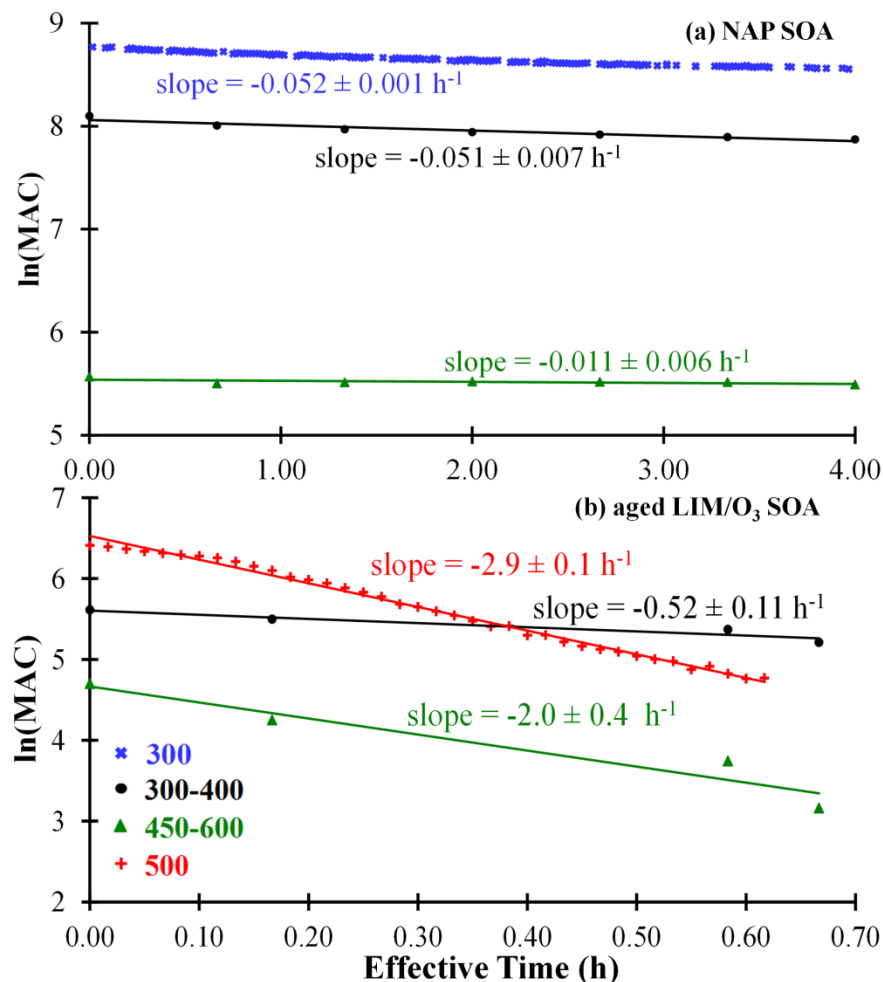
Figure 4.6: Decay of absorbance during irradiation of SOA aqueous solutions. (a) For NAP SOA, the average ln(*MAC*) is plotted against the effective photolysis time at 300 nm (blue x), in the near-UV region (300-400 nm, black points), and in the visible region (450-600 nm, green triangle). (b) For LIM/O$_3$ SOA + ammonia vapor reaction products, the data are plotted for the near-UV region, visible region, and at 500 nm (red +). The solid lines correspond to linear fits to the data. Numbers next to the lines correspond to the slopes $\pm$ 1σ, SD. The 300 nm measurement for NAP SOA and the 500 nm measurement for LIM/O$_3$ SOA were continuous single wavelength observation, while the rest were extracted from the individual absorption spectrum.

Table 4.2: Effective half-life (in h) for the disappearance of absorbance at different wavelengths.

Wavelength (nm)*	NAP SOA	Aged LIM/O_3 SOA
300	13	3.0
near-UV	14	1.3
Visible	64	0.35
500	43	0.24

*The half-lives, $\tau = \ln(2)/k$, are calculated for NAP SOA and aged LIM/O_3 SOA at different regions: at 300 nm, in the near-UV region (300-400 nm), in the visible region (450-600 nm), and at 500 nm where the aged LIM/O_3 SOA has its characteristic absorption peak.

To demonstrate that not all BrC is as resilient to photolysis as NAP SOA, we also include data on photodegradation of BrC produced by the reaction of LIM/O_3 SOA with NH_3.[5, 16, 17, 47] Figure 4.5b shows the initial absorption spectrum of the aged LIM/O_3 SOA and its evolution during irradiation. The distinctive 500 nm peak is almost completely removed after 2 h of photolysis and the brown color of the solution almost disappears in the process. The decay of *MAC* approximated by the first-order kinetics (Figure 4.6b) indicates an effective atmospheric photolysis time on the order of 1 h (

Table 4.2). In contrast to NAP SOA, *MAC* changes faster in the visible range ($k = 2.0$ h^{-1}) than in the near-UV range ($k = 0.52$ h^{-1}).

4.4.3. Effect of Photolysis on Molecular Composition of Photolyzed NAP SOA

Table 4.1 lists known products of NAP photooxidation observed by gas chromatography-mass spectrometry,[27-29, 31] proton-transfer-reaction mass spectrometry,[30] and aerosol mass spectrometry,[30, 53, 54] while Figure 4.1 shows an abridged mechanism of their formation. Seven out of the twelve compounds listed in Table 4.1 appeared in the ESI/HR-MS spectra of NAP SOA, detected mostly as sodiated species. The expected major products[27-31, 53, 54] (phthaldialdehyde, formyl cinnamic acid, 2-formyl-cinnamaldehyde, 2-formylbenzoic acid, and 1-nitronaphthalene) were abundant in the mass spectra (10-40% of the largest observed peak). Other expected products were not detected, presumably because of relatively high volatility and low abundance in SOA (e.g., benzoic acid), lower ionization efficiencies, or possible hydrolysis in water extracts. For example, phthalic anhydride, a secondary oxidation product of phthaldialdehyde,[29, 55] may have hydrolyzed in the aqueous solution.

Figure 4.7 compares the ESI high-resolution mass spectra acquired before and after photolysis of aqueous NAP SOA. For ease of comparison, the peak abundances are normalized to that of the largest peak in the corresponding mass spectrum. The initial mass spectrum had a bimodal peak distribution featuring the monomeric and dimeric groups of SOA constituents. Photolysis resulted in a significant change in the spectrum with the marked decline of the relative abundance of the dimeric compounds and parallel formation of new compounds at lower *m/z* values. Overall, before photolysis, 244 peaks were reproduced in all three NAP SOA samples (we only include peaks in our analysis that appeared in all three of the mass spectra of independently prepared samples). Of those, 150 peaks were removed by photolysis. In photolyzed samples, 108 peaks reproducibly appeared in all of the mass spectra. Of those, 14 peaks correspond to newly formed compounds, and 94 peaks correspond to compounds present

in the initial sample. Clearly, photolysis affects the molecular composition of SOA in a profound way.

For an individual compound, $C_cH_hO_oN_n$, that contains c carbon, h hydrogen, o oxygen, and n nitrogen atoms, the double bond equivalent (DBE, the total number of double bonds and rings) can be calculated as follows:

$$DBE = 1 + \frac{n-h}{2} + c \qquad \textbf{(Equation 4.12)}$$

This formula assumes a valence of 3 for nitrogen, and therefore it underestimates the DBE for nitrocompounds (-NO$_2$) and organonitrates (-ONO$_2$) by 1. Figure 4a shows the distribution of DBE values, which indicates a substantial decline in the DBE values upon photolysis presumably driven by the preferential destruction of larger, oligomeric compounds.
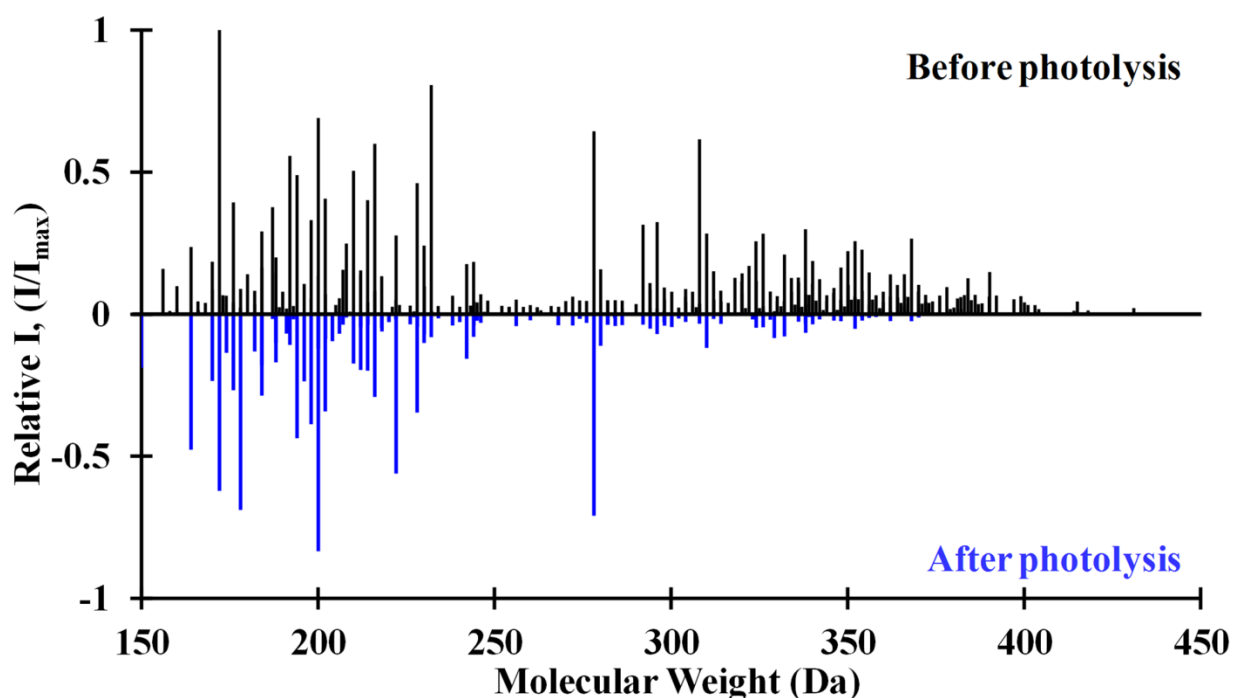
Figure 4.7: High-resolution positive ion mode mass spectra of NAP SOA before and after photolysis plotted as positive and negative signals, respectively. The spectra are normalized with respect to the largest detected peak. The preferential removal of larger compounds in photolysis is clearly evident from the spectra.
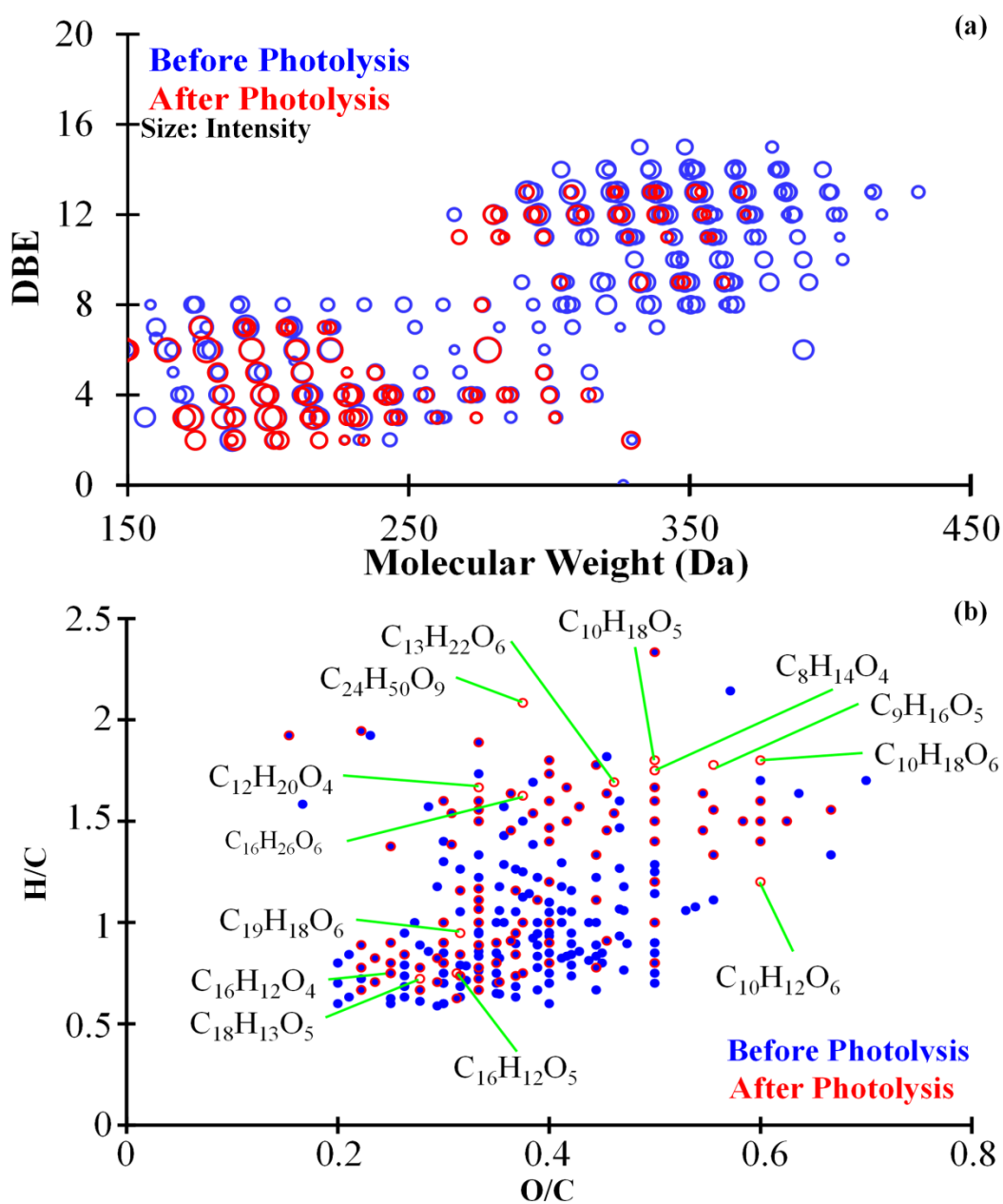
Figure 4.8: Comparison of molecular characteristics of the NAP SOA constituents before and after photolysis plotted as: (a) DBE versus molecular weight (Da) and (b) Van Krevelen plot of H/C versus O/C.

There is no clear effect of photolysis on the O/C or H/C ratios as evident from the lack of obvious patterns in the van Krevelen (VK) diagram (H/C vs O/C for individual compounds) in Figure 4.8b. In view of the molecular complexity of SOA, it is common to express its bulk composition as averaged elemental ratios. The average elemental composition and ratios (C, N, O, H/C, O/C, C/N and O/N), and the average DBE can be estimated from the assigned molecular formulas:[56]

$$\langle Y \rangle = \frac{\sum_i x_i Y_i}{\sum_i x_i} \quad \text{where } Y = c, h, o, n, \text{ or } DBE \qquad \textbf{(Equation 4.13)}$$

$$\left\langle \frac{Y}{Z} \right\rangle = \frac{\sum_i x_i Y_i}{\sum_i x_i Z_i} \quad \text{where } Y/Z = H/C, O/C, N/C, \text{ and } N/O \qquad \textbf{(Equation 4.14)}$$

These formulas use peak abundances, x_i, as weighing factors. Strictly speaking, Eq. 4.14 calculates <Y>/<Z>, but we designate it as <Y/Z> to simplify the notation. Table 4.3 lists the elemental composition of NAP SOA before and after photolysis calculated using Eq. 4.13 and 4.14. Based on these results, the 3-4 h of atmospheric photolysis of NAP SOA can be represented by an effective chemical equation:

$$C_{14.1}H_{14.5}O_{5.1}N_{0.085} \; + \; hv \; \rightarrow \; C_{11.8}H_{14.9}O_{4.5}N_{0.023} \qquad \textbf{(Equation 4.15)}$$

The average carbon number, <C>, as well as the overall molecular size, are reduced by photolysis. There is also a significant decrease in <DBE> implying a preferential breakdown of more unsaturated compounds. The average atomic ratios <N/C> and <O/N> drop in magnitude, while <H/C> increases. The small increase in <H/C> suggests a decrease in the level of unsaturation upon photolysis. It is noteworthy that the change in <O/C> is small (from 0.36 to 0.38). The <O/C> ratio, a measure of the degree of oxidation, is frequently used in the literature as an indicator of photochemical aging of SOA. Our results indicate that <O/C> may not be an

informative parameter for tracking the age of SOA in cases when photolysis is the primary

mechanism of aging.

Table 4.3: Average elemental composition, elemental ratios, and double bond equivalents (DBE) before and after photolysis of NAP SOA solution.

	<C>*	<H>	<O>	<N>	<H/C>	<O/C>	<N/C>	<N/O>	<DBE>
Before	14.1	14.5	5.1	0.085	1.02	0.36	0.0060	0.017	7.9
(SD)	(0.7)	(0.4)	(0.1)	(0.017)	(0.06)	(0.02)	(0.0012)	(0.003)	(0.9)
After	11.8	14.9	4.5	0.023	1.27	0.38	0.0020	0.0053	5.3
(SD)	(0.4)	(0.6)	(0.3)	(0.003)	(0.07)	(0.03)	(0.0002)	(0.0007)	(0.2)
After - Before	-2.4	0.4	-0.7	-0.06	0.3	0.02	-0.0041	-0.012	-2.6

*Data collected from three independent measurements were averaged. Errors in are reported as 1σ standard deviation (SD) between the measurements.

Table 4.4 lists fractions of compounds containing 0 and 1 nitrogen atoms (0N and 1N

compounds). The decrease in <N> and in the <N/C> ratio indicates a significant reduction in the

fraction of 1N compounds during photolysis. Photolysis is known to be the dominant loss

process for gas-phase nitronaphthalenes.[57] Our observations suggest that photolysis remains an

important loss mechanism for these compounds in the aqueous phase. Indeed, the peak

corresponding to nitronaphthalene (Table 4.1) disappears from the mass spectrum upon

photolysis. Although nitroaromatic compounds have been shown to photodegrade very slowly in

water,[58, 55] they can be efficiently photoreduced in the presence of suitable hydrogen atom

donors, such as alcohols and aldehydes,[59, 60] which are abundant in SOA. Photoreduction of

nitroaromatics is consistent with the observed decline in the O/N ratio of the products.

Table 4.4: Distribution of N-atoms in the products before and after photolysis. Breakdown of the observed ions by nitrogen content. 0N and 1N refer to compounds containing 0 and 1 nitrogen atoms, respectively. As shown in this table, ~13% of the 1N compounds are removed, and ~13%, of the 0N compounds are formed by photolysis, suggesting that one of the mechanism of photolysis involves removal of $-NO_2$ groups from the nitroaromatic compounds or $-ONO_2$ groups from nitric acid esters.

N-compound	Before Photolysis		After Photolysis		In Both	
	#	%	#	%	#	%
0N	193	79.1	99	91.7	86	91.5
1N	51	20.9	9	8.3	8	8.5
Total	244	100	108	100	94	100

Another contribution to the loss of nitrogen-containing organics may come from photolysis of organonitrates, $RONO_2$, which are known to photolyze by breaking the weak O-N bond. Nguyen et al.[61] observed a significant reduction of organonitrates in the photolysis of aqueous solutions of high-NO_x isoprene SOA, as well as formation of 2N species. In contrast to the isoprene SOA, we do not observe a buildup of 2N compounds after photolysis of NAP SOA. In fact, the fraction of 2N species both before and after photolysis was very small. This suggests that production of 2N compounds may be unique to the photolysis of high-NO_x isoprene SOA.

The known products of NAP photooxidation that do not contain nitrogen atoms (e.g., the ones shown in Table 4.1 and Figure 4.1) were also strongly affected by photolysis. 2-formyl-cinnamaldehyde was removed by photolysis in agreement with the expected reactivity of α,β-unsaturated aldehydes. Formyl cinnamic acid increased, presumably as a result of photooxidation of 2-formyl-cinnamaldehyde and similar compounds. Aromatic aldehydes, phthaldialdehyde and 2-formylbenzoic acid, both increased with photolysis. In summary, photolysis of NAP SOA introduces rather significant changes in its molecular composition.

To study the extent of compositional changes in aged LIM/O_3 SOA induced by photolysis, we carried out LC-ESI/HR-MS (reverse phase separation by liquid chromatography

on a C18 column with the ESI/HR-MS detector) analysis before and after photolysis. After 2 h

photolysis of aged LIM/O$_3$ SOA, which was sufficient to completely change its absorption

spectrum as shown in Figure 4.5b, the effective average chemical composition of SOA changed

as follows:

$$C_{13.4}H_{19.1}O_{3.5}N_{0.62} + hv \rightarrow C_{14.2}H_{20.4}O_{4.3}N_{0.72}$$ **(Equation 4.16)**

Since a different technique was used to analyze the aged LIM/O$_3$ SOA and NAP SOA mixtures,

a direct comparison to Eq. 4.15 cannot be made. However, this result shows that the extent of

photolysis-driven changes in the mass spectra were smaller in the aged LIM/O$_3$ SOA than in

NAP SOA. This result can be explained by the low relative abundance of the chromophores in

aged LIM/O$_3$ SOA, which makes it difficult to detect them within a complex matrix of the much

more abundant non-absorbing compounds.[34]

4.4.4. Fluorescence of NAP SOA

The EEM plots in Figure 4.9 show that NAP SOA was moderately fluorescent both

before and after photolysis. The fluorescence quantum yield (QY), measured as described in Lee

et al. [16], increased from ~0.2% to ~0.3%. Although photolysis reduced the overall absorption

coefficient of NAP SOA compounds (Figure 4.6), there was a slight increase in their

fluorescence intensity as shown in Figure 4.9b. This is an unexpected result, considering that the

photolysis of NAP SOA also reduced the average number of double bonds (inferred from DBE

values) in the NAP SOA sample (Figure 4.8 and Table 4.3), thus preferentially removing highly

unsaturated molecules that are more likely to fluoresce. One possible contribution to the

increased fluorescence intensity is the loss of nitroaromatic compounds during photolysis. Such

compounds undergo highly efficient intersystem crossing (ISC) into the triplet manifold,

followed by thermal relaxation.[62] Shutting down the ISC pathway could make the effective QY

higher. Another possibility is that the photolysis may create carboxylic acids and reduce the

solution pH. This was observed as the typical starting NAP SOA pH of about 5–6 decreased by

0-1 units during photolysis. When we carried out fluorescence measurements on unphotolyzed

samples at intentionally lowered pH values, we also observed higher emissions intensities.

Therefore, some of the observed increase in the fluorescence intensity may be attributed to the

pH effects. We note that the observed increase in the intensity of fluorescence in the photolyzed

NAP SOA is in stark contrast with the aged LIM/O_3 SOA system, which loses its ability to

fluoresce upon photolysis. Figure 4.10 the shows a typical EEM plot for the aged LIM/O_3 SOA

solution before and after photolysis.
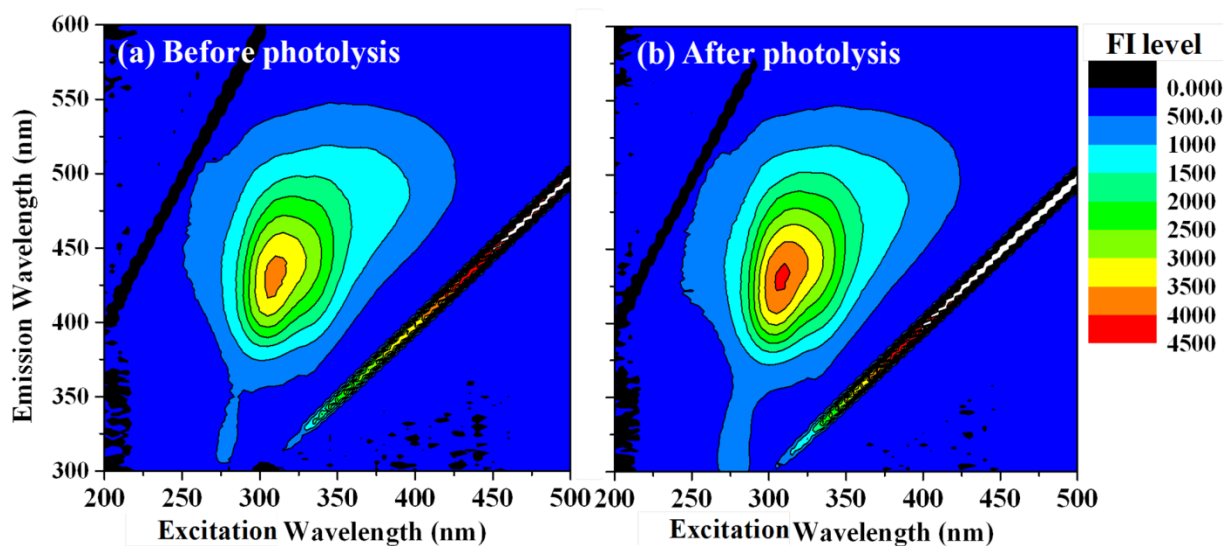
Figure 4.9: EEM plot recorded (a) before and (b) after photolysis. After 120 minutes of photolysis the fluorescence intensity (FI, color coded as shown on the right) increased somewhat (while the solution absorbance decreased, as shown in Figure 4.5).
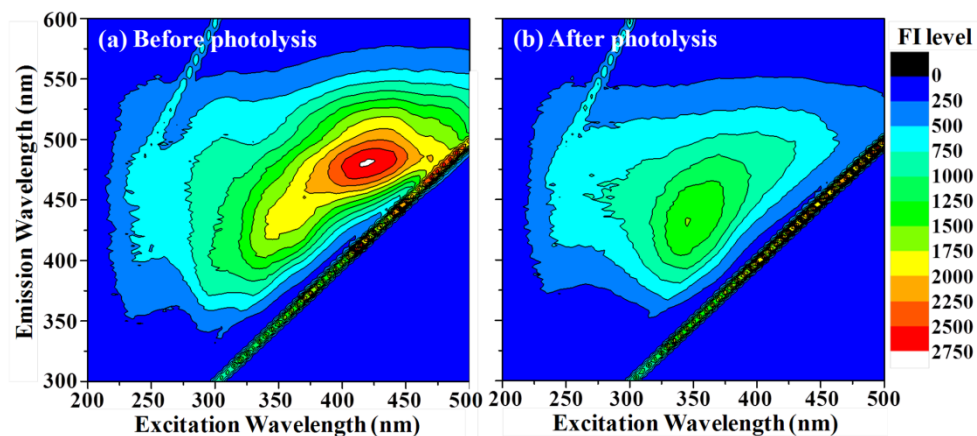
Figure 4.10: Aged LIM/O$_3$ SOA EEM plot recorded (a) before and (b) after photolysis of solution of aged LIM/O$_3$ SOA. After 110 minutes of photolysis the fluorescence intensity (FI, color coded as shown on the right) increased somewhat (while the solution absorbance decreased, as shown in Figure 4.5).

4.5.   Atmospheric Implications

We examined the photolysis of aqueous solutions of NAP SOA, a prototypical BrC aerosol, as a model of photochemical processing of BrC compounds in cloud and fog droplets. Photolysis had a modest effect on the wavelength-dependent *MAC* of NAP SOA, but produced significant changes in the molecular composition as determined by ESI/HR-MS methods. To demonstrate that this is not universally applicable to all types of BrC, we also presented results on the photolysis of BrC produced by reaction of LIM/O$_3$ SOA aged with NH$_3$. This system displayed an opposite behavior to NAP SOA, with relatively little change in the overall composition, but more dramatic and faster changes in the absorption spectrum. These results highlight the great diversity of properties of different types of BrC, and imply that the chemical nature of the light-absorbing compounds in different types of BrC can be quite different.

An important conclusion of this work is that chemical composition and optical properties of BrC cannot be viewed as static. Light-absorbing compounds responsible for the color of BrC can potentially photobleach in sunlight (i.e., lose their ability to absorb visible radiation). This

photobleaching can be quite fast, as in the case of light-absorbing products of reactions of LIM/O_3 SOA + NH_3 (a couple of hours of irradiation, Figure 4.6) and methyl glyoxal + ammonium sulfate(a few minutes of irradiation according to the estimation in Sareen et al.[10]). It can also be considerably slower, as in the case of NAP SOA examined in this work. Our conclusions corroborate the results of Zhong and Jang, who found that the absorption spectrum of biomass-burning aerosol changed significantly over the course of a day due to a competition between formation and photobleaching of light-absorbing organics.[23]

Even in the case of the relatively resilient NAP SOA, the *MAC* decays with an estimated effective half-life of ~ 15 h. Therefore, in addition to the wavelength-dependent *MAC* values of various BrC samples, the effective rate with which *MAC* evolves under typical atmospheric conditions should also be quantified and reported. A strongly absorbing BrC sample will not produce much direct radiative forcing if it photolyzes in minutes, as reported, for example, for the chromophores in methyl glyoxal + ammonium sulfate solutions.[10]

The average O/C ratio, is a parameter that can be derived from aerosol mass spectrometry measurements.[63, 64] In many reports, O/C is used as a convenient indicator of the degree of oxidation in SOA and a number of studies have attempted to correlate O/C with the aerosol type, chemical age, and even its properties, such as viscosity, optical properties,[22] hygroscopicity,[65, 66] etc. Our results suggest that the O/C ratio is not a fundamental characteristic that can uniquely describe these SOA properties. The chemical composition and *MAC* of NAP SOA undergoes significant changes during photolysis. However, these changes cannot be adequately captured by bulk measurements of the O/C ratio. Therefore, this type of photolysis-driven aging would likely be missed by measurements of integrated O/C values.

Although this work focused on aqueous solutions of NAP SOA, we also briefly examined photolysis of NAP SOA material directly on the filter. The photolysis also resulted in efficient photobleaching (photographs of NAP SOA filters before and after photolysis are shown on the Table of Contents image in the abstract). Moreover, the molecular composition of NAP SOA photolyzed on the filter changed in a qualitatively similar manner to that in an aqueous NAP SOA solution. Therefore, the scope of our results is not limited to aqueous photolysis of SOA; photolysis is likely to be just as important in organic particles (although the mechanism of photolysis in the aerosol may be very different from that in the aqueous solution of SOA). This is consistent with our previous observations of efficient photochemistry of biogenic SOA material.[67-69]

Finally, a significant fluorescence level of NAP SOA, with QY of ~0.2-0.3% is worth noting. Many studies have reported strong fluorescence emission produced by primary biological aerosol particles (PBAP).[70-72] Lee et al. suggested that SOA may interfere with detection of PBAP with fluorescence–based techniques. The wide excitation (250–425 nm) and emission (350–550 nm) range for NAP SOA further supports this concern. In fact, the emission of NAP SOA overlaps even better with the EEM peak for PBAP than that of the biogenic SOA reported previously in Lee et al.[16]

4.6.   References

1.   Solomon, S. Q., D.; Manning, M.; Chen, Z.; Marquis, M.; Averyt, K.; Tignor, M.; Miller, H. L., *Contribution of Working Group I to the Fourth Assessment Report of the Intergovernmental Panel on Climate Change*. In New York, 2007.

2.   Andreae, M. O.; Gelencsér, A., Black carbon or brown carbon? The nature of light-absorbing carbonaceous aerosols. *Atmos. Chem. Phys.* **2006,** *6*, (10), 3131-3148.

3.   Ramanathan, V.; Carmichael, G., Global and regional climate changes due to black carbon. *Nature Geoscience* **2008,** *1*, (4), 221-227.

4.   Alexander, D. T. L.; Crozier, P. A.; Anderson, J. R., Brown carbon spheres in east asian outflow and their optical properties. *Science* **2008,** *321*, (5890), 833-836.

5.   Bond, T. C.; Bergstrom, R. W., Light Absorption by Carbonaceous Particles: An Investigative Review. *Aerosol Science and Technology* **2006,** *40*, (1), 27-67.

6.   Aregahegn, K. Z.; Noziere, B.; George, C., Organic aerosol formation photo-enhanced by the formation of secondary photosensitizers in aerosols. *Faraday Discussions* **2013**.

7.   De Haan, D. O.; Corrigan, A. L.; Tolbert, M. A.; Jimenez, J. L.; Wood, S. E.; Turley, J. J., Secondary Organic Aerosol Formation by Self-Reactions of Methylglyoxal and Glyoxal in Evaporating Droplets. *Environmental Science & Technology* **2009,** *43*, (21), 8184-8190.

8.   Kampf, C. J.; Jakob, R.; Hoffmann, T., Identification and characterization of aging products in the glyoxal/ammonium sulfate system-implications for light-absorbing material in atmospheric aerosols. *Atmos. Chem. Phys.* **2012,** *12*, (14), 6323-6333.

9.   Noziere, B.; Cordova, A., A kinetic and mechanistic study of the amino acid catalyzed aldol condensation of acetaldehyde in aqueous and salt solutions. *The Journal of Physical Chemistry A* **2009b,** *112*, (13), 2827-2837.

10.   Sareen, N.; Schwier, A. N.; Shapiro, E. L.; Mitroo, D.; McNeill, V. F., Secondary organic material formed by methylglyoxal in aqueous aerosol mimics. *Atmos. Chem. Phys.* **2010,** *10*, (3), 997-1016.

11.   Shapiro, E. L.; Szprengiel, J.; Sareen, N.; Jen, C. N.; Giordano, M. R.; McNeill, V. F., Light-absorbing secondary organic material formed by glyoxal in aqueous aerosol mimics. *Atmos. Chem. Phys.* **2009,** *9*, 2289-2300.

12.   Trainic, M.; Abo Riziq, A.; Lavi, A.; Flores, J. M.; Rudich, Y., The optical, physical and chemical properties of the products of glyoxal uptake on ammonium sulfate seed aerosols. *Atmos. Chem. Phys.* **2011,** *11*, (18), 9697-9707.

13.   Bones, D. L.; Henricksen, D. K.; Mang, S. A.; Gonsior, M.; Bateman, A. P.; Nguyen, T. B.; Cooper, W. J.; Nizkorodov, S. A., Appearance of strong absorbers and fluorophores in limonene-O$_3$

secondary organic aerosol due to NH_4^+-mediated chemical aging over long time scales. *J. Geophys. Res.* **2010,** *115*, (D5), 10.1029/2009JD012864.

14.   Flores, J. M.; Washenfelder, R. A.; Adler, G.; Lee, H. J.; Segev, L.; Laskin, J.; Laskin, A.; Nizkorodov, S. A.; Brown, S. S.; Rudich, Y., Complex refractive indices in the near-ultraviolet spectral region of biogenic secondary organic aerosol aged with ammonia. *Physical Chemistry Chemical Physics* **2014,** *16*, (22), 10629-10642.

15.   Laskin, J.; Eckert, P. A.; Roach, P. J.; Heath, B. S.; Nizkorodov, S. A.; Laskin, A., Chemical analysis of complex organic mixtures using reactive nanospray desorption electrospray ionization mass spectrometry. *Analytical Chemistry* **2012,** *84*, (16), 7179-7187.

16.   Lee, H. J.; Laskin, A.; Laskin, J.; Nizkorodov, S. A., Excitation–emission spectra and fluorescence quantum yields for fresh and aged biogenic secondary organic aerosols. *Environmental Science & Technology* **2013,** *47*, (11), 5763-5770.

17.   Updyke, K. M.; Nguyen, T. B.; Nizkorodov, S. A., Formation of brown carbon via reactions of ammonia with secondary organic aerosols from biogenic and anthropogenic precursors. *Atmospheric Environment* **2012,** *63*, 22-31.

18.   Chang, J. L.; Thompson, J. E., Characterization of colored products formed during irradiation of aqueous solutions containing H_2O_2 and phenolic compounds. *Atmospheric Environment* **2010,** *44*, (4), 541-551.

19.   Gelencsér, A.; Hoffer, A.; Kiss, G.; Tombácz, E.; Kurdi, R.; Bencze, L., In-situ formation light-absorbing organic matter in cloud water. *Journal of Atmospheric Chemistry* **2003,** *45*, (1), 25-33.

20.   Jacobson, M. Z., Isolating nitrated and aromatic aerosols and nitrated aromatic gases as sources of ultraviolet light absorption. *J. Geophys. Res.* **1999,** *104*, (D3), 3527-3542.

21.   Rincón, A. G.; Guzmán, M. I.; Hoffmann, M. R.; Colussi, A. J., Thermochromism of model organic aerosol matter. *The Journal of Physical Chemistry Letters* **2009,** *1*, (1), 368-373.

22.   Lambe, A. T.; Cappa, C. D.; Massoli, P.; Onasch, T. B.; Forestieri, S. D.; Martin, A. T.; Cummings, M. J.; Croasdale, D. R.; Brune, W. H.; Worsnop, D. R.; Davidovits, P., Relationship between oxidation level and optical properties of secondary organic aerosol. *Environmental Science & Technology* **2013,** *47*, (12), 6349-6357.

23.   Zhong, M.; Jang, M., Dynamic light absorption of biomass-burning organic carbon photochemically aged under natural sunlight. *Atmos. Chem. Phys.* **2014,** *14*, (3), 1517-1525.

24.   Desyaterik, Y.; Sun, Y.; Shen, X.; Lee, T.; Wang, X.; Wang, T.; Collett, J. L., Speciation of "brown" carbon in cloud water impacted by agricultural biomass burning in eastern China. *Journal of Geophysical Research: Atmospheres* **2013,** *118*, (13), 7389-7399.

25.   Atkinson, R.; Arey, J., Atmospheric chemistry of gas-phase polycyclic aromatic hydrocarbons: formation of atmospheric mutagens. *Environ Health Perspect* **1994,** *102 Suppl 4*, 117-26.

26.   Atkinson, R.; Arey, J., Mechanisms of the gas-phase reactions of aromatic hydrocarbons and PAHs with OH and NO₃ radicals. *Polycyclic Aromatic Compounds* **2007,** *27*, (1), 15-40.

27.   Bunce, N. J.; Liu, L.; Zhu, J.; Lane, D. A., Reaction of naphthalene and its derivatives with hydroxyl radicals in the gas phase. *Environmental Science & Technology* **1997,** *31*, (8), 2252-2259.

28.   Nishino, N.; Arey, J.; Atkinson, R., 2-Formylcinnamaldehyde formation yield from the OH radical-initiated reaction of naphthalene: effect of NO₂ concentration. *Environmental Science & Technology* **2012,** *46*, (15), 8198-8204.

29.   Wang, L.; Atkinson, R.; Arey, J., Dicarbonyl products of the OH radical-initiated reactions of naphthalene and the C1- and C2-alkylnaphthalenes. *Environmental Science & Technology* **2007,** *41*, (8), 2803-2810.

30.   Chan, A. W. H.; Kautzman, K. E.; Chhabra, P. S.; Surratt, J. D.; Chan, M. N.; Crounse, J. D.; Kürten, A.; Wennberg, P. O.; Flagan, R. C.; Seinfeld, J. H., Secondary organic aerosol formation from photooxidation of naphthalene and alkylnaphthalenes: implications for oxidation of intermediate volatility organic compounds (IVOCs). *Atmos. Chem. Phys.* **2009,** *9*, (9), 3049-3060.

31.   Sasaki, J.; Aschmann, S. M.; Kwok, E. S. C.; Atkinson, R.; Arey, J., Products of the gas-phase OH and NO3 radical-initiated reactions of naphthalene. *Environmental Science & Technology* **1997,** *31*, (11), 3173-3179.

32.   Hecobian, A.; Zhang, X.; Zheng, M.; Frank, N.; Edgerton, E. S.; Weber, R. J., Water-soluble organic aerosol material and the light-absorption characteristics of aqueous extracts measured over the Southeastern United States. *Atmos. Chem. Phys.* **2010,** *10*, (13), 5965-5977.

33.   Sun, H.; Biedermann, L.; Bond, T. C., Color of brown carbon: A model for ultraviolet and visible light absorption by organic carbon aerosol. *Geophysical Research Letters* **2007,** *34*, (17), L17813.

34.   Laskin, J.; Laskin, A.; Roach, P. J.; Slysz, G. W.; Anderson, G. A.; Nizkorodov, S. A.; Bones, D. L.; Nguyen, L. Q., High-Resolution Desorption Electrospray Ionization Mass Spectrometry for Chemical Characterization of Organic Aerosols. *Analytical Chemistry* **2010,** *82*, (5), 2048-2058.

35.   Vione, D.; Maurino, V.; Minero, C.; Duncianu, M.; Olariu, R.-I.; Arsene, C.; Sarakha, M.; Mailhot, G., Assessing the transformation kinetics of 2- and 4-nitrophenol in the atmospheric aqueous phase. Implications for the distribution of both nitroisomers in the atmosphere. *Atmospheric Environment* **2009,** *43*, (14), 2321-2327.

36.   Biggs, A. I., A spectrophotometric determination of the dissociation constants of p-nitrophenol and papaverine. *Transactions of the Faraday Society* **1954,** *50*, 800-802.

37.   Hayon, E.; Ibata, T.; Lichtin, N. N.; Simic, M., Electron and hydrogen atom attachment to aromatic carbonyl compounds in aqueous solution. Absorption spectra and dissociation constants of ketyl radicals. *The Journal of Physical Chemistry* **1972,** *76*, (15), 2072-2078.

38.   Laws, W. R.; Brand, L., Analysis of two-state excited-state reactions. The fluorescence decay of 2-naphthol. *The Journal of Physical Chemistry* **1979,** *83*, (7), 795-802.

39.   van Stam, J.; Lofroth, J.-E., The protolysis of singlet excited beta-naphthol: A two-day laboratory experiment to introduce photophysics. *Journal of Chemical Education* **1986,** *63*, (2), 181.

40.   Zhu, D.; Hyun, S.; Pignatello, J. J.; Lee, L. S., Evidence for π−π electron donor−acceptor interactions between π-donor aromatic compounds and π-acceptor sites in soil organic matter through pH effects on sorption. *Environmental Science & Technology* **2004,** *38*, (16), 4361-4368.

41.   Brantner, B.; Fierlinger, H.; Puxbaum, H.; Berner, A., Cloudwater chemistry in the subcooled droplet regime at Mount Sonnblick (3106 M A.S.L., Salzburg, Austria). *Water, Air, and Soil Pollution* **1994,** *74*, (3-4), 363-384.

42.   Marinoni, A.; Parazols, M.; Brigante, M.; Deguillaume, L.; Amato, P.; Delort, A.-M.; Laj, P.; Mailhot, G., Hydrogen peroxide in natural cloud water: Sources and photoreactivity. *Atmospheric Research* **2011,** *101*, (1–2), 256-263.

43.   Epstein, S. A.; Shemesh, D.; Tran, V. T.; Nizkorodov, S. A.; Gerber, R. B., Absorption spectra and photolysis of methyl peroxide in liquid and frozen water. *The Journal of Physical Chemistry A* **2012,** *116*, (24), 6068-6077.

44.   Bunce, N. J.; Lamarre, J.; Vaish, S. P., Photorearrangment of azoxybenzene to 2-hydroxyazobenezene: A convenient chemical actinometer*. *Photochemistry and Photobiology* **1984,** *39*, (4), 531-533.

45.   Madronich, S. T., X. X.; Barth, M.; D., M. Tropospheric Ultraviolet and Visible (TUV) Radiation Model.

46.   Nizkorodov, S. A.; Laskin, J.; Laskin, A., Molecular chemistry of organic aerosols through the application of high resolution mass spectrometry. *Physical Chemistry Chemical Physics* **2011,** *13*, (9), 3612-3629.

47.   Nguyen, T. B.; Lee, P. B.; Updyke, K. M.; Bones, D. L.; Laskin, J.; Laskin, A.; Nizkorodov, S. A., Formation of nitrogen- and sulfur-containing light-absorbing compounds accelerated by evaporation of water from secondary organic aerosols. *Journal of Geophysical Research: Atmospheres* **2012,** *117*, (D1), 10.1029/2011JD016944.

48.   Chen, Y.; Bond, T. C., Light absorption by organic carbon from wood combustion. *Atmos. Chem. Phys.* **2010,** *10*, 1773-1787.

49.   Bergstrom, R. W.; Pilewskie, P.; Russell, P. B.; Redemann, J.; Bond, T. C.; Quinn, P. K.; Sierau, B., Spectral absorption properties of atmospheric aerosols. *Atmos. Chem. Phys.* **2007,** *7*, (23), 5937-5943.

50.   Pöschl, U., Aerosol particle analysis: challenges and progress. *Analytical and Bioanalytical Chemistry* **2003,** *375*, (1), 30-32.

51.   Hoffer, A.; Gelencsér, A.; Guyon, P.; Kiss, G.; Schmid, O.; Frank, G. P.; Artaxo, P.; Andreae, M. O., Optical properties of humic-like substances (HULIS) in biomass-burning aerosols. *Atmos. Chem. Phys.* **2006,** *6*, (11), 3563-3570.

52.   Kirchstetter, T. W.; Thatcher, T. L., Contribution of organic carbon to wood smoke particulate matter absorption of solar radiation. *Atmos. Chem. Phys. Discuss.* **2012,** *12*, (2), 5803-5816.

53.   Chhabra, P. S.; Ng, N. L.; Canagaratna, M. R.; Corrigan, A. L.; Russell, L. M.; Worsnop, D. R.; Flagan, R. C.; Seinfeld, J. H., Elemental composition and oxidation of chamber organic aerosol. *Atmos. Chem. Phys.* **2011,** *11*, (17), 8827-8845.

54.   McWhinney, R. D.; Zhou, S.; Abbatt, J. P. D., Naphthalene SOA: redox activity and naphthoquinone gas–particle partitioning. *Atmos. Chem. Phys.* **2013,** *13*, (19), 9731-9744.

55.   J. G. Calvert, A. M., J. J. Orlando, M. J. Pilling and T. J. Willington, *The Mechanisms of Atmospheric Oxidation of The Oxygenates*. Oxford university Press, Inc. : New York, 2011.

56.   Bateman, A. P.; Laskin, J.; Laskin, A.; Nizkorodov, S. A., Applications of high-resolution electrospray ionization mass spectrometry to measurements of average oxygen to carbon ratios in secondary organic aerosols. *Environmental Science & Technology* **2012,** *46*, (15), 8315-8324.

57.   Atkinson, R.; Aschmann, S. M.; Arey, J.; Barbara, Z.; Schuetzle, D., Gas-phase atmospheric chemistry of 1- and 2-nitronaphthalene and 1,4-naphthoquinone. *Atmospheric Environment (1967)* **1989,** *23*, (12), 2679-2690.

58.   Lipczynska-Kochany, E., Degradation of nitrobenzene and nitrophenols in homogeneous aqueous solution. Direct photolysis versus photolysis in the presence of hydrogen peroxide and the Fenton reagent. *Water Poll. Res. J. Canada* **1992,** *27*, (1), 97-122.

59.   Barltrop, J. A.; Bunce, N. J., Organic photochemistry. Part VIII. The photochemical reduction of nitro-compounds. *Journal of the Chemical Society C: Organic* **1968**, (0), 1467-1474.

60.   Hashimoto, S.; Kano, K., The photochemical reduction of nitrobenzene and its reduction intermediates. X. The photochemical reduction of the monosubstituted nitrobenzenes in 2-propanol. *Bulletin of the Chemical Society of Japan* **1972,** *45*, (2), 549-553.

61.   Nguyen, T. B.; Laskin, A.; Laskin, J.; Nizkorodov, S. A., Direct aqueous photochemistry of isoprene high-NOx secondary organic aerosol. *Physical Chemistry Chemical Physics* **2012,** *14*, (27), 9702-9714.

62.   Takezaki, M.; Hirota, N.; Terazima, M., Nonradiative relaxation processes and electronically excited states of nitrobenzene studied by picosecond time-resolved transient grating method. *The Journal of Physical Chemistry A* **1997,** *101*, (19), 3443-3448.

63.   Aiken, A. C.; DeCarlo, P. F.; Jimenez, J. L., Elemental analysis of organic species with electron ionization high-resolution mass spectrometry. *Analytical Chemistry* **2007,** *79*, (21), 8350-8358.

64.   Aiken, A. C.; DeCarlo, P. F.; Kroll, J. H.; Worsnop, D. R.; Huffman, J. A.; Docherty, K. S.; Ulbrich, I. M.; Mohr, C.; Kimmel, J. R.; Sueper, D.; Sun, Y.; Zhang, Q.; Trimborn, A.; Northway, M.; Ziemann, P. J.; Canagaratna, M. R.; Onasch, T. B.; Alfarra, M. R.; Prevot, A. S. H.; Dommen, J.; Duplissy, J.; Metzger, A.; Baltensperger, U.; Jimenez, J. L., O/C and OM/OC ratios of primary, secondary, and ambient organic aerosols with high-resolution time-of-flight aerosol mass spectrometry. *Environmental Science & Technology* **2008,** *42*, (12), 4478-4485.

65.   Duplissy, J.; DeCarlo, P. F.; Dommen, J.; Alfarra, M. R.; Metzger, A.; Barmpadimos, I.; Prevot, A. S. H.; Weingartner, E.; Tritscher, T.; Gysel, M.; Aiken, A. C.; Jimenez, J. L.; Canagaratna, M. R.; Worsnop, D. R.; Collins, D. R.; Tomlinson, J.; Baltensperger, U., Relating hygroscopicity and composition of organic aerosol particulate matter. *Atmos. Chem. Phys.* **2011,** *11*, (3), 1155-1165.

66.   Stock, M.; Cheng, Y. F.; Birmili, W.; Massling, A.; Wehner, B.; Müller, T.; Leinert, S.; Kalivitis, N.; Mihalopoulos, N.; Wiedensohler, A., Hygroscopic properties of atmospheric aerosol particles over the Eastern Mediterranean: implications for regional direct radiative forcing under clean and polluted conditions. *Atmos. Chem. Phys.* **2011,** *11*, (9), 4251-4271.

67.   Mang, S. A.; Henricksen, D. K.; Bateman, A. P.; Andersen, M. P. S.; Blake, D. R.; Nizkorodov, S. A., Contribution of carbonyl photochemistry to aging of atmospheric secondary organic aerosol. *The Journal of Physical Chemistry A* **2008,** *112*, (36), 8337-8344.

68.   Pan, X.; Underwood, J. S.; Xing, J. H.; Mang, S. A.; Nizkorodov, S. A., Photodegradation of secondary organic aerosol generated from limonene oxidation by ozone studied with chemical ionization mass spectrometry. *Atmos. Chem. Phys.* **2009,** *9*, (12), 3851-3865.

69.   Walser, M. L.; Desyaterik, Y.; Laskin, J.; Laskin, A.; Nizkorodov, S. A., High-resolution mass spectrometric analysis of secondary organic aerosol produced by ozonation of limonene. *Physical Chemistry Chemical Physics* **2008,** *10*, (7), 1009-1022.

70.   Ammor, M., Recent advances in the use of intrinsic fluorescence for bacterial identification and characterization. *Journal of Fluorescence* **2007,** *17*, (5), 455-459.

71.   Hill, S. C.; Pinnick, R. G.; Niles, S.; Pan, Y.-L.; Holler, S.; Chang, R. K.; Bottiger, J.; Chen, B. T.; Orr, C.-S.; Feather, G., Real-time measurement of fluorescence spectra from single airborne biological particles. *Anal. Chem. Technol.* **1999,** *3*, (4-5), 221-239.

72.   Pöhlker, C.; Huffman, J. A.; Pöschl, U., Autofluorescence of atmospheric bioaerosols – fluorescent biomolecules and potential interferences. *Atmos. Meas. Tech.* **2012,** *5*, 37-71.

Chapter 5   Effects of Humidity, NOx, and Ammonia on the Optical Properties and Molecular Composition of Photo-oxidized Naphthalene Secondary Organic Aerosols

5.1. Abstract

Light-absorbing aerosols, referred to as "brown carbon" (BrC), have a significant effect on climate. Primary sources of BrC are reasonably well-known, but BrC can also be formed by less constrained secondary atmospheric reactions, such as photooxidation of aromatic volatile organic compounds (VOCs) and reactions of carbonyl compounds in secondary organic aerosols (SOA) with ammonia (NH_3). As NH_3 and VOC emissions increase globally, it is critical to examine these poorly understood BrC production pathways. This study investigates how the optical and molecular characteristics of photooxidized naphthalene (NAP) SOA are affected by the presence of NH_3, NO_x, and relative humidity (RH). NAP was oxidized with hydroxyl radicals in a smog chamber at high and low levels of NO_x and humidity, and in the absence and presence of NH_3. The reaction was monitored using a scanning mobility particle sizer (SMPS) and SOA were collected on filters for offline analysis. UV-Vis spectroscopy and high-resolution mass spectrometry were used to determine mass absorption coefficients and molecular composition, respectively. The results show that RH, NO_x, and NH_3 each have some effect on the molecular composition and optical properties of NAP SOA.

5.2. Introduction

There is much uncertainty in the radiative forcing produced by atmospheric aerosols. The majority of aerosols produce negative forcing, resulting in net cooling, by scattering incoming solar radiation and modifying cloud properties. However, certain aerosols, including black carbon (BC), brown carbon (BrC), and mineral dust, absorb visible radiation and convert it into trapped heat thus reducing this cooling effect.[1-3] Of these light-absorbing aerosols, BrC have the highest chemical complexity and mechanisms of chemical aging. BrC is composed of organic molecules that are capable of absorbing both visible and near-ultraviolet radiation, such as nitrophenols, which give BrC a characteristic yellow-brown color.[4-7] BrC comes from primary sources such as fossil fuel combustion and biomass-burning,[4, 5, 8-10] but BrC can also be produced by secondary processes.[1, 11] Examples of secondary BrC formation processes include high-NO_x (=$NO+NO_2$) photooxidation of aromatic volatile organic compounds (VOCs) resulting in secondary organic aerosols (SOA),[12-19] reactive uptake of oxygenated VOCs on highly-acidic particles,[20-25] aqueous-phase OH oxidation of aromatic compounds,[26-29] and the reaction of ammonia (NH_3) and other nitrogen-containing species with carbonyl compounds.[30-43]

The interest in BrC has resulted in multiple measurements of their optical properties, including extinction and absorption coefficients, single scattering albedo, absorption spectra and fluorescence spectra. Different mass spectrometry methods have also been used to investigate the chemical composition of BrC in order to identify the primary chromophores responsible for its the brown color.[11] From these measurements, nitroaromatics, or more specifically nitrophenols, have been identified as primary contributors to light absorption by BrC.[44] These compounds are readily produced during photooxidation of aromatics. For example, Updyke *et al.* (2012) produced NAP and trimethylbenzene SOA under high- and low-NO_x conditions and found that

for both SOA high-NO_x conditions resulted in higher overall mass absorption coefficient (MAC) across the 300-700 nm wavelength range.[31] Nakayama *et al.* (2013) found that increasing NO_x concentration during toluene photooxidation increases its imaginary and real refractive indices at 405 and 532 nm, using photoacoustic and cavity ring-down spectroscopy.[15] Liu *et al.* (2015) also measured the real and imaginary refractive indices of toluene, as well as m-xylene, secondary organic material, using spectroscopic ellipsometry and UV-Vis spectroscopy. Both indices increased as a function of increasing NO_x concentration, while decreasing with increasing wavelength. Using infrared spectroscopy they also showed that the presence of NO_x resulted in the production of organonitrogen species.[45] Lin *et al.* (2015) also found that elevated NO_x conditions drastically increase MAC of toluene photooxidation SOA, while simultaneously altering the chemical composition by producing more nitrogen-containing compounds.[12] Liu *et al.* (2016) worked with SOA formed by photooxidation of toluene and trimethylbenzene in order to determine how light absorption of SOA is affected by precursor type, NO_x levels, photolysis time, and RH. The presence of NO_x increased SOA absorptions, with moderate humidity and short photolysis times resulting in the highest MAC.[13] Lastly, Aiona *et al.* (2018) determined absorption coefficients of BrC produced by high-NO_x photooxidation of naphthalene (NAP), toluene, p-xylene, and benzene and found a pH-dependent decrease in absorption coefficients across visible wavelengths.[18]

Reduced nitrogen compounds, most prominently NH_3 and amines, have been found to alter the optical properties of BrC by converting carbonyl compounds into more strongly absorbing imines and nitrogen-containing heterocyclic compounds. Updyke *et al.* (2012) observed an increase in MAC during exposure of various types of absorbing and non-absorbing SOA to gaseous NH_3. For example white low-NO_x trimethylbenzene SOA gained a beige color

upon exposure, while NAP SOA characteristic yellow color became more saturated.[31] Liu et al. (2018) observed formation of nitrogen-containing organics and increase in the absorption coefficient during exposure of low-NOx toluene SOA to ammonia.[46] Extensive studies have been done exploring the mechanism of the NH_3-driven browning reactions. The general mechanism appears to involve reactions of dicarbonyls with NH_3 resulting in nitrogen-containing heterocyclic compounds, but the exact details depend on the specific system. For example, 1,2 dicarbonyls, such as glyoxal and methylglyoxal form oligomeric compounds derived from imidazole,[36, 37, 47, 48] whereas 1,4 dicarbonyls, such as ketolimonoaldehyde (a secondary limonene ozonolysis product) and 4-oxopentanal, produce light-absorbers based on pyrroles.[49, 50]

Relative humidity has been found to affect the chemical composition of some SOA systems, and therefore is expected to also have an effect on optical properties. Song *et al.* (2013) found that high RH caused a decrease in light-absorption in high-NO$_x$ α-pinene ozonolysis SOA formed on seed particles.[24] In contrast, Liu *et al.* (2016) found that toluene and trimethylbenzene photooxidation SOA formed under dry conditions had a significantly lower MAC than those formed in under humid conditions. In humid conditions the percent humidity did not cause a dramatic difference, with 30, 50, and 80% RH all resulting in similar absorption.[13] Moderately humid conditions (30%) resulted in more CHON species than dry conditions, implicating the nitrogen-containing species contribute to increased MAC, as seen with toluene in Lin *et al.* (2015).[12, 13] Finally, in the recent study by Liu et al. (2018), the extent of browning of low-NOx toluene SOA was reduced under dry conditions, when high viscosity of SOA particles placed a diffusion limitation on the rate of reaction between SOA carbonyls and ammonia.[46]

In this study, we are investigating the effect of RH, and the presence of NH_3 and nitrogen oxides (NO$_x$) on the production, optical properties, and molecular composition of BrC formed by

the photooxidation of NAP. High-NO_x NAP SOA can be regarded as prototypical secondary BrC with a high MAC,[19] approaching that for primary BrC produced by burning of biomass. SOA are formed under either wet or dry and high- or low-NO_x conditions, in the presence and absence of NH_3. UV-Vis spectroscopy is used to investigate differences in optical properties based on reaction conditions. Nanospray desorption ionization mass spectrometry (nano-DESI MS) is used to find how these conditions affect the SOA chemical composition. We find that RH, NO_x, and NH_3 all affect the characteristics of NAP SOA that were investigated. NO_x levels were found to have the most influence on both molecular and optical properties. RH has some effect on both, while NH_3 affects composition more than absorption.

5.3. Experimental

5.3.1. NAP SOA Formation

SOA were produced by the photooxidation of NAP in a 5 m^3 Teflon aerosol smog chamber. The environmental variables included high- and low-NO_x levels, high and low RH, and absence and presence of ammonia (NH_3). Prior to each study the chamber was flushed with purge air overnight for cleaning purposes. The RH for all dry studies was <2%. For elevated RH studies, humidification to >80% was accomplished by flowing air through a Nafion multichannel humidifier. Approximately 40 µL of H_2O_2 (Aldrich; 30% by volume in water), which serves as the OH precursor, was evaporated into the chamber to achieve mixing ratios of 2 ppm. For high-NO_x studies, 200-400 ppb of NO was added to the chamber from a premised gas cylinder (Praxair, 5000 ppm NO in N_2). About 11-23 µL of a solution of 0.5 g/mL of NAP in dichloromethane was the evaporated into the chamber to reach a mixing ratio of 200-400 ppb. No seed aerosol was used. All precursors were mixed by a fan inside the chamber, which was turned off before the start of photooxidation. Photooxidation was initiated by UV-B lamps (Solar

Tec Systems model FS40T12/UVB) with emissions centered at 310 nm and ranged from 1.5-2.5 hours. As SOA was forming in the chamber, a variety of instruments were sampling it simultaneously. Real time temperature and RH were measured with a Vaisala HMT330 probe and concentrations of ozone (model 49i) and NO/NO$_y$ (model 42i-Y) were measured with ThermoScientific monitors. Particle size distribution was monitored using a scanning mobility particle sizer (SMPS, TSI Model 3936), which was then used to estimate the mass of NAP SOA collected on the filters used for offline analysis.

Table 5.1 summarizes the conditions in different experiments done in this work. For chamber runs 1 – 4 in Table 5.1, after photooxidation, NH$_3$ was incrementally added to the chamber by evaporation of NH$_4$OH solution aiming for a mixing ratio of 1000 ppb. It was later determined using an ammonia monitor installed at a later time that most of the injected ammonia may have been quickly removed by the chamber walls, so the actual mixing ratio ammonia could be up to an order of magnitude lower. Runs 5 – 16 aimed to determining the effects of ammonia on the composition or optical properties. The mixing ratios of NAP and NO doubled for these runes in order to obtain more material for mass spectrometric analysis, but the ratio of NAP to NO$_x$ remained consistent (1:1). In runs 10-13, NH$_4$OH was evaporated into the chamber to reach 1000 ppb NH$_3$ in a single injection, prior to photooxidation. Runs 5 – 9 and 14 – 16 in Table 5.1 were done without the addition of ammonia. In all cases, SOA was collected after the experiment by passing particles through an activated charcoal denuder and onto a PTFE filter at 15-20 standard liters per minute for 3-4.5 hours.

Table 5.1: Summary of conditions for chamber experiments.

Run #	NAP (ppm)	H$_2$O$_2$ (ppm)	NO$_x$ (ppm)	RH (%)	NH$_3$ (ppm)[a]	Photo-oxidation (h)	Instrumentation Used [b]
1	0.2	2.0	0.2	2	1.0	1.5	SMPS, nano-DESI
2	0.2	2.0	0.0	85	1.0	2.5	SMPS, nano-DESI
3	0.2	2.0	0.2	84	1.0	2.0	SMPS, nano-DESI
4	0.2	2.0	0.0	1	1.0	2.0	SMPS, nano-DESI
5	0.4	2.0	0.0	0	-	2.0	SMPS, nano-DESI
6	0.4	2.0	0.4	0	-	2.0	SMPS, nano-DESI
7	0.4	2.0	0.0	99	-	2.0	SMPS, nano-DESI
8	0.4	2.0	0.4	86	-	2.0	SMPS, nano-DESI
9	0.4	2.0	0.0	0	-	2.0	SMPS, UV-Vis
10	0.4	2.0	0.0	87	1.0	2.0	SMPS, UV-Vis
11	0.4	2.0	0.0	0	1.0	2.0	SMPS, UV-Vis
12	0.4	2.0	0.4	0	1.0	2.0	SMPS, UV-Vis
13	0.4	2.0	0.4	87	1.0	2.5	SMPS, UV-Vis
14	0.4	2.0	0.0	89	-	2.0	SMPS, UV-Vis
15	0.4	2.0	0.4	0	-	2.0	SMPS, UV-Vis
16	0.4	2.0	0.4	94	-	2.0	SMPS, UV-Vis

[a] The actual concentration of NH$_3$ in the chamber was lower because of the rapid loss of ammonia to the chamber walls.
[b] Runs 1-4 involved both on-line (not discussed in this thesis) and offline characterization of SOA. Runs 6-17 were only done with offline methods.

5.3.2. Nano-DESI HRMS Experiments

Filters were analyzed at the Environmental Molecular Science Laboratory at PNNL using nanospray desorption electrospray ionization high-resolution mass spectrometry (nano-DESI-HRMS) in the positive ion mode. Mass spectra for each sample were obtained using a LTQ-Orbitrap masa spectrometer (Thermo Electron, Bremen, Germany) with a nano-DESI source in both positive and negative ion mode. Before analysis filters were taken out of the freezer and brought to room temperature and cut in half. One half was taped to a microscope slide for analysis. A mixture of 70 % acetonitrile and 30% DI water was dropped onto the surface of the filter through a primary silica capillary to dissolve the NAP SOA, which was then transferred into the mass spectrometer via a nanospray capillary. The spray voltage for these runs was 3-5 kV, the heated capillary temperature was 250°C, and the mass resolving power was 10^5 m/Δm at

m/z 400. In order to obtain background spectra the probe was placed over the area of the filter

that did not contain any sample for 2-3 minutes, and then was moved to the center of the filter for

3 to 6 minutes to collect sample data. The sample was moved underneath the capillary bridge to

expose fresh spots on the filter to the droplet, with about 10 mm distance travelled by the droplet

by the end of the scan. The flow rate in positive mode ranged from 600 to 800 nL/min and 800 to

1200 nL/min in negative mode.

Peaks in the sample and background mass spectra with a peak to background ratio greater

than 5 were extracted using Decon2LS software developed at PNNL. Peaks were then aligned

and assigned using LabView with a tolerance of ±0.001 *m/z* units, with constraints applied on the

number of specified elements (C: 1-40, H: 2-80, O: 0-35; N: 0-3, and Na: 0-1), and elemental

ratios (H/C: 0.3 to 2.50 and O/C: 0.0 to 2.30). All solvent peaks were removed, as well as any

peaks containing ^{13}C atoms. Using the remaining peaks an internal calibration was done to

achieve better mass precision and refine the assignments. Observed peaks were either protonated

(H^+) or sodiated (Na^+) species, but neutral formulas will be used throughout the discussion

portion of the paper.

5.3.3. Spectrophotometry Experiments

Runs 9 – 16 in Table 5.1 are for chamber studies that were done to produce NAP SOA

for offline UV-Vis absorption spectroscopy studies. NAP SOA collected on filters was extracted

three times in succession, using 4 mL of DI water for each extraction. Filters were shaken for 10

minutes during each extraction. Three milliliters of the dissolved NAP SOA was then transferred

to a 1.0 cm quartz cuvette and analyzed using a dual-beam spectrometer (Shimadzu UV-2450)

with a DI water blank. Absorption spectra were taken for each of the extracts for all 8 samples.

Mass absorption coefficients (MAC) are used to quantify the browning of BrC samples and used

as a comparison of different sources. The MAC of each sample was calculated using equation

(5.1)

$$MAC(\lambda) = \frac{A_{10}(\lambda)*\ln(10)}{b*C_{mass}}$$ **(Equation 5.1)**

We used the following procedure to estimate the completeness of the extraction at each

step using absorbance data from each of the three extractions. This procedure made it possible to

correct for the incomplete dissolution of the SOA material during the first extraction. We know

the total mass of SOA, m, sitting on the filter from a separate measurement, specifically from the

SMPS measurements. When we extract the SOA material from the filter we dissolve a certain

portion of it (m_1) in a volume of solvent (V_1) in the first extraction, and a certain portion (m_2) in a

volume of solvent (V_2) in the 2nd extraction. We do not know the SOA masses that went into

extracts 1 and 2 but we are going to assume that the two extractions fully extract all soluble SOA

material (this treatment can easily be extended to 3 or more extractions):

$$m = m_1 + m_2$$ **(Equation 5.2)**

The corresponding (unknown) mass concentrations in the extracts are:

$$C_1 = \frac{m_1}{V_1}$$ **(Equation 5.3)**

$$C_2 = \frac{m_2}{V_2}$$ **(Equation 5.4)**

If extract # 2 has no measurable absorbance ($A_1 \gg A_2 \sim 0$), the calculations are simple. It means

that everything extracted on the first trial, so we can assume $m = m_1$ and (b is the cell path

length):

$$MAC(\lambda) = \frac{A_1(\lambda) \times \ln(10)}{b \times C_1} = \frac{A_1(\lambda) \times \ln(10) \times V_1}{b \times m_1}$$ **(Equation 5.5)**

However, we find the absorbance of extract #2, while small, is not negligible. Assuming that absorbance has a linear dependence on concentration (verified below), we can relate the absorbance in extracts 1 and 2 to MAC as follows.

$$m = m_1 + m_2 = \frac{A_1(\lambda) \times \ln(10) \times V_1}{b \times MAC(\lambda)} + \frac{A_2(\lambda) \times \ln(10) \times V_2}{b \times MAC(\lambda)}$$ **(Equation 5.6)**

Or equivalently:

$$MAC(\lambda) = \frac{\ln(10)}{b \times m} \left(A_1(\lambda) \times V_1 + A_2(\lambda) \times V_2 \right)$$ **(Equation 5.7)**

If the volumes used at each step are the same ($V = V_1 = V_2$), this simplifies to:

$$MAC(\lambda) = \frac{\ln(10) \times V}{b \times m} \left(A_1(\lambda) + A_2(\lambda) \right)$$ **(Equation 5.8)**

Equivalently, we can calculate MAC from the results of the first measurement only

$$MAC(\lambda) = \frac{\ln(10) \times V}{b \times m_1} A_1(\lambda)$$ **(Equation 5.9)**

Where the unknown mass of m_1 is estimated from

$$m_1 = m \times \frac{\langle A_1(\lambda) \rangle}{\langle A_1(\lambda) \rangle + \langle A_2(\lambda) \rangle}$$ **(Equation 5.10)**

Equations (5.9) and (5.10) are the ones we used in this chapter, wherein the absorbances were averaged over the wavelength range 285 to 585 nm. The MAC reported below represent values that have been corrected by this method.
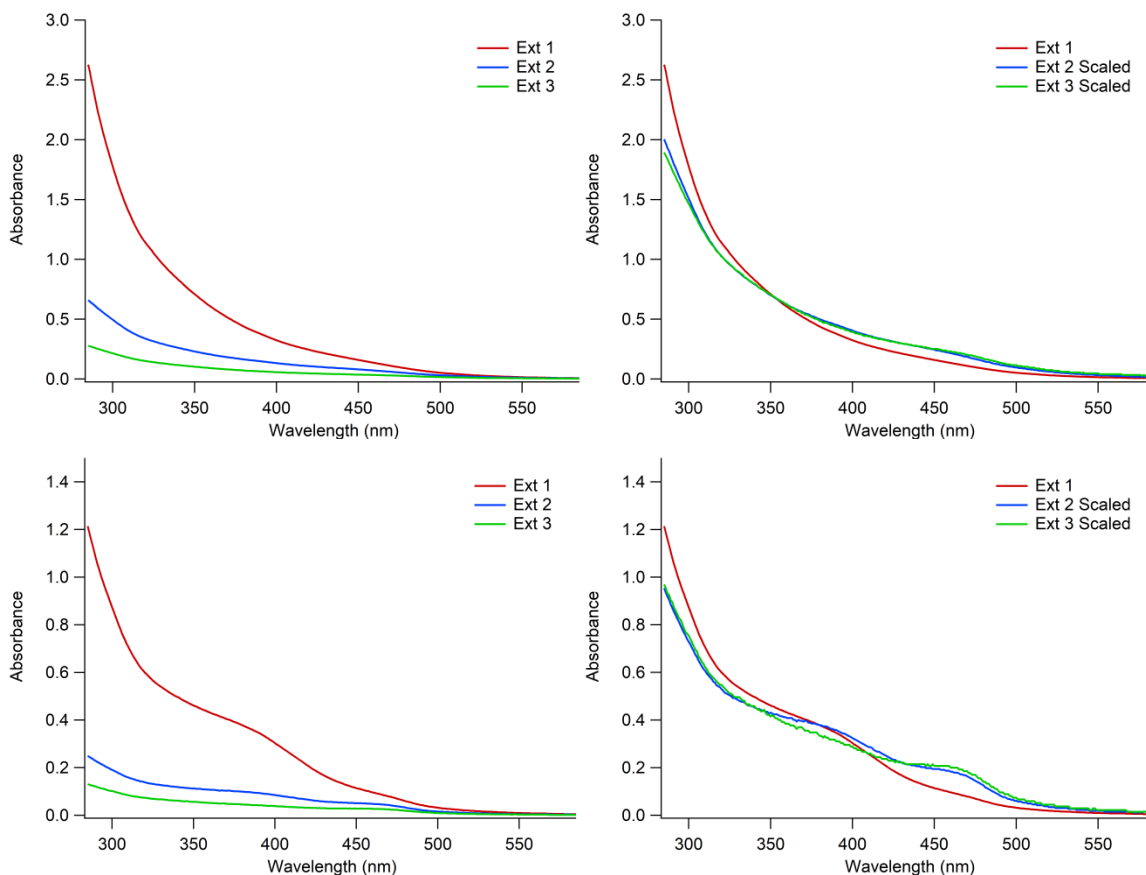
Figure 5.1: A typical result for our experiment plotting absorbances A_1, A_2, A_3 for three successive extractions of the NAP SOA sample, using absorbance data from the high NO_x dry (top) and high NO_x wet (bottom) studies, both with NH_3 present. In the 2nd panel of this figure, we scaled all of them to the same maximum value to show that the absorption spectra of the 1st and 2nd extract have the same wavelength dependence making it possible for us to assume the same MAC values in the denominators of equation (5.6).

5.4. Results and Discussion

5.4.1. Molecular Composition

Mass spectra were generated for the 8 samples that underwent nano-DESI analysis (runs 1 – 8 in Table 5.1), and average molecular formulas ($C_cH_hO_oN_n$), and elemental ratios (<H/C>, <O/C>, and <N/C>) were calculated for each compared subset. The mass spectra collected in positive ion mode can be found in Figure 5.2 to Figure 5.5, and average formulas and atomic ratios can be found in Table 5.2. In all cases, the mass spectra featured well-defined monomeric and dimeric regions, with molecular weights ranging from 100-270 Da and 270-500 Da,

respectively. This is consistent with the mass spectrum of NAP SOA reported in our previous work.[19] While the overall shape of the mass spectra was similar, the distribution of peak intensities changed from one mass spectrum to another depending on the conditions. SOA composition and the corresponding mass spectra were found to depend on all three variables (presence of NO_x, presence of NH_3, and RH) varied in this work, making the task of isolating specific influences somewhat challenging.

Table 5.2: Summary of average molecular data.

Study Subset	Average Formula	<H/C>	<O/C>	<N/C>
High RH	$C_{16.4}H_{14.9}O_{5.4}N_{0.30}$	0.92	0.33	0.019
Low RH	$C_{14.6}H_{13.2}O_{5.3}N_{0.32}$	0.90	0.36	0.022
High NO_x	$C_{15.3}H_{13.7}O_{5.3}N_{0.40}$	0.90	0.35	0.027
Low NO_x	$C_{15.7}H_{14.4}O_{5.4}N_{0.20}$	0.92	0.34	0.014
With NH_3	$C_{15.0}H_{13.9}O_{5.2}N_{0.40}$	0.93	0.35	0.026
Without NH_3	$C_{16.0}H_{14.2}O_{5.4}N_{0.20}$	0.89	0.34	0.015

Figure 5.2 to Figure 5.5 compare the effect of changing RH on the mass spectra of NAP SOA. When all the wet and dry samples were averaged, the presence of water increased both <C>, <H>, and <H/C>, while decreasing <O/C>. The average molecular formula of all samples collected under high RH was $C_{16.4}H_{14.9}O_{5.4}N_{0.30,}$ and for all dry samples was $C_{14.6}H_{13.2}O_{5.3}N_{0.32}$. In a recent study of the effect of RH on the low-NO_x SOA from toluene, Hinks *et al.* (2018) observed suppression of oligomeric compounds under humid conditions. For NAP SOA, the situation is reversed with the relative intensity of the dimer peaks increasing under humid conditions. Figure 5 specifically shows this trend under low-NO_x conditions with no nitrogen influence from NH_3. Perhaps this is due to the difference in structure between toluene, which has a single aromatic ring, and naphthalene with two aromatic rings. The additional conjugation may lead to more oligomerization. Additionally, wet samples tend to have more N=0 peaks and dry

samples have more N=1 and N=2 peaks, but the difference is minimal, especially in studies with

no nitrogen species.
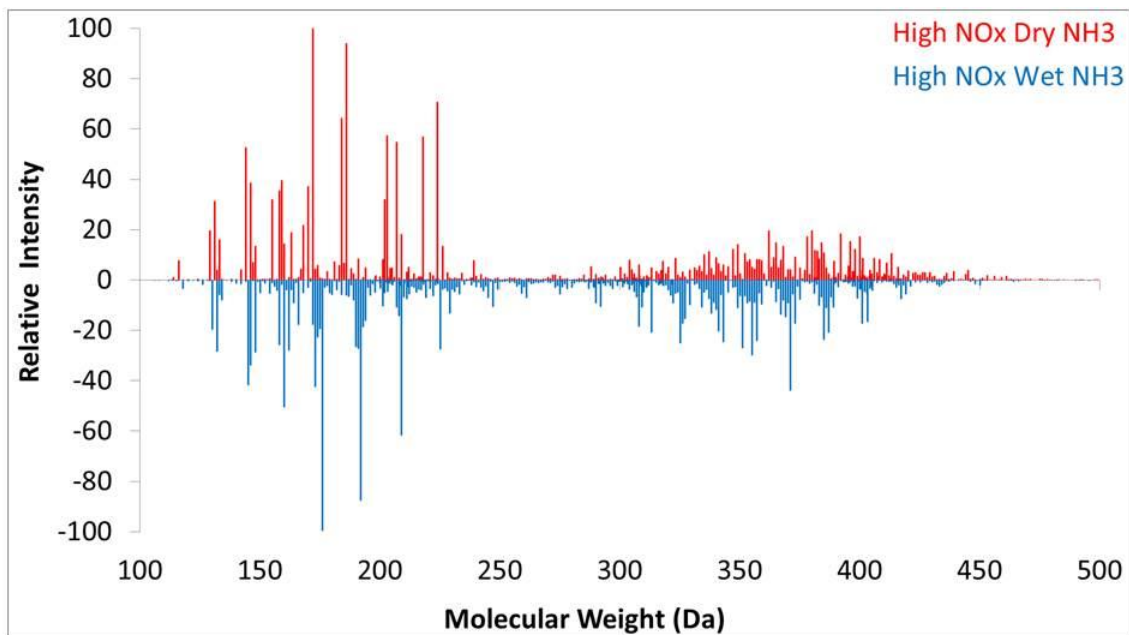
Figure 5.2: Mass spectra comparing wet and dry conditions of high-NO$_x$ studies done in the presence of NH$_3$.
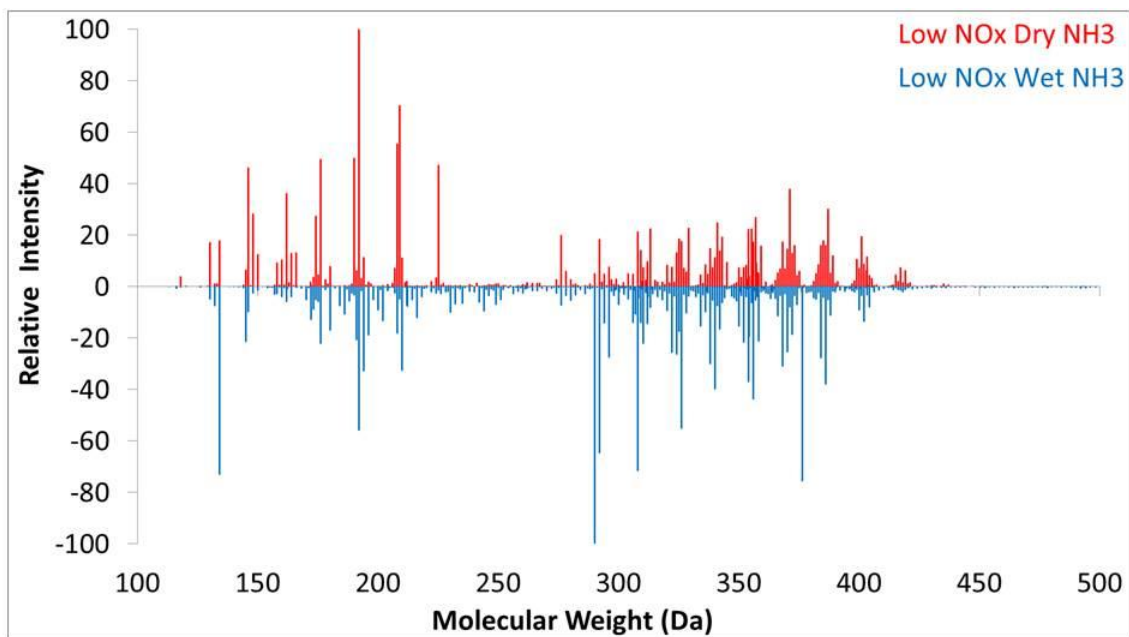
Figure 5.3: Mass spectra comparing wet and dry conditions of low-NO$_x$ studies done in the presence of NH$_3$.
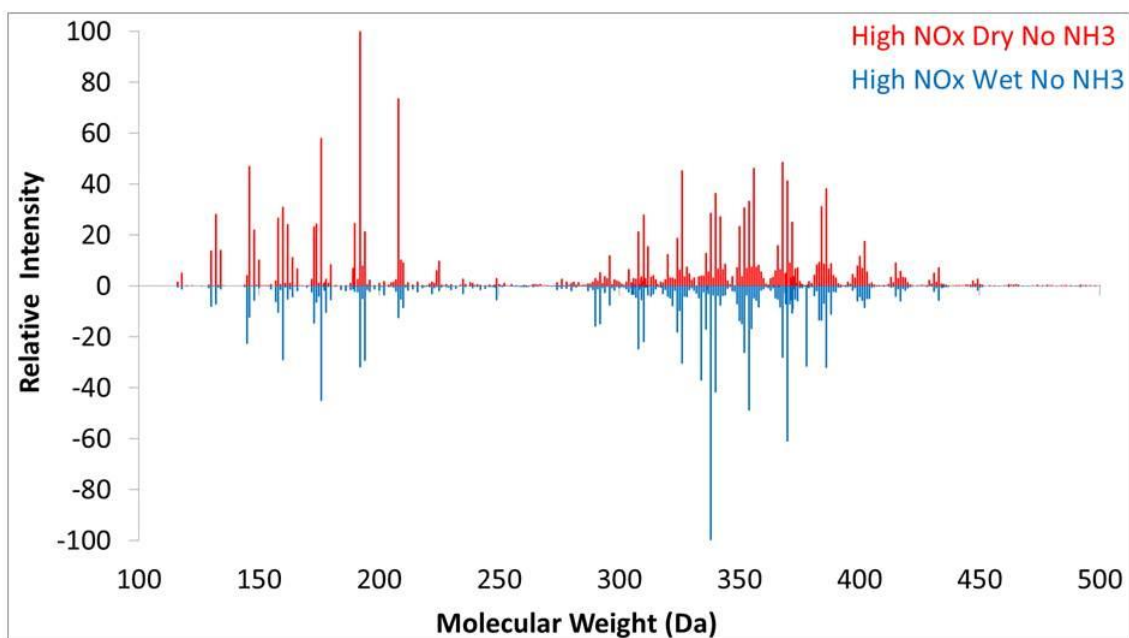
Figure 5.4: Mass spectra comparing wet and dry conditions of high-NO_x studies done in the without NH_3.
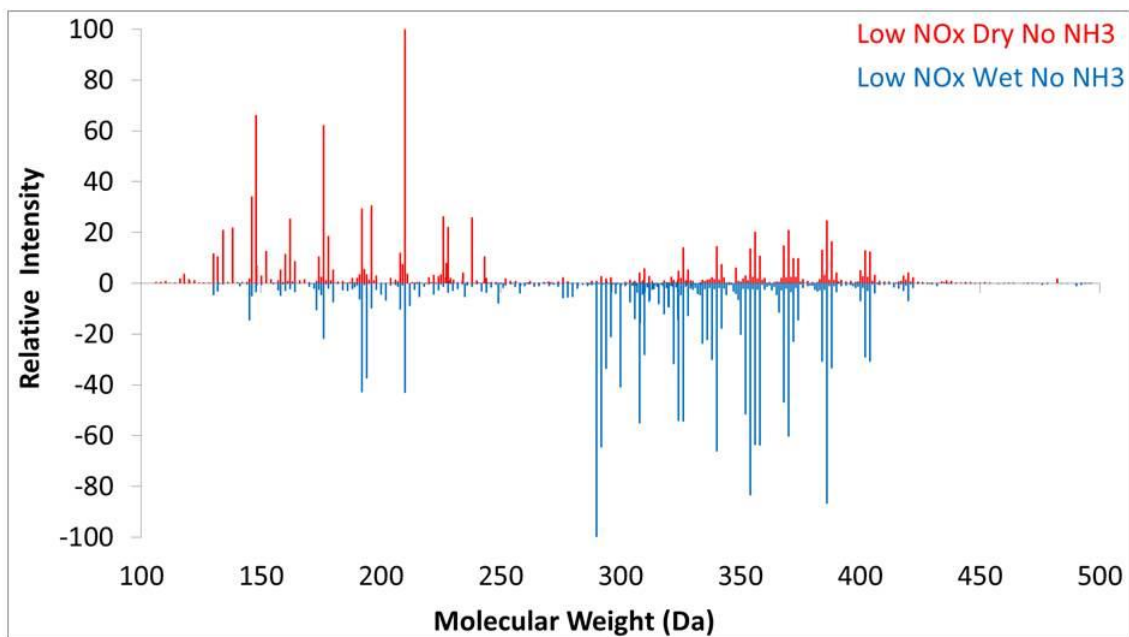
Figure 5.5: Mass spectra comparing wet and dry conditions of low-NO_x studies done in the without NH_3.

Comparisons were also done for high- vs low-NO_x and with and without NH_3. Upon

comparing NO_x and NH_3 conditions, it was found that both high-NO_x and the presence of NH_3

resulted in a decrease in <H> and in increased in <N> (Figure 5.6a) and <N/C>. The average

formula of all high-NO_x studies is $C_{15.3}H_{13.7}O_{5.3}N_{0.40}$ and $C_{15.7}H_{14.4}O_{5.4}N_{0.20}$ for all low-NO_x studies. The value of $<C>$ was found to decrease when NH_3 was present, with the average formula of $C_{15.0}H_{13.9}O_{5.2}N_{0.40}$ for samples with NH_3 and $C_{16.0}H_{14.2}O_{5.4}N_{0.20}$ without it. Figure 5.6b shows that the presence of NO_x and NH_3 increases the number of times the difference of mass of NH_3 (17.0256 Da) occurs between peaks in the mass spectra. Under high-NO_x conditions the reaction of peroxy radicals (RO_2) with NO produces more carbonyl compounds than the RO_2/HO_2 chemistry occurring in low-NO_x samples.[51] These carbonyls likely react with the NH_3, resulting in the increased occurrence seen for its mass difference. There was also a decrease in assignments where N=0, while N=1 and N=2 assignments increased under both conditions, as seen in Figure 5.7. This is consistent with previous nano-DESI studies of toluene photooxidation SOA produced under high-and low-NO_x conditions. High-NO_x studies resulted in 68% CHON species in comparison to low-NO_x studies that produced mostly CHO products with some low intensity CHON species thought to be due to NH_3 present in room air. The O/N ratio of high-NO_x samples was greater than two, indicating the presence of nitro groups such as nitrophenols, nitrates, and nitro acids.[12] Liu *et al.* (2015) also observed organonitrogen compounds ($-ONO_2$ and $-NO_2$) in the IR spectra for high-NO_x toluene and *m*-xylene SOM.[45] These types of nitrogen-containing species are likely those seen in the high-NO_x/NH_3 studies and are may be responsible for high MAC values discussed in the next section.
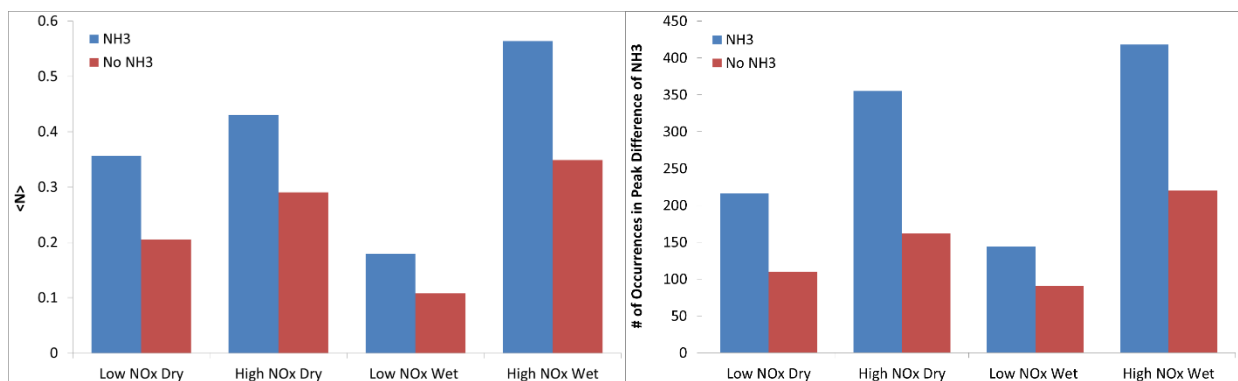
Figure 5.6: Comparison of studies with and without NH_3; (a) is a comparison of $\langle N \rangle$ all for studies of done under the same NO_x and RH conditions and (b) compares the occurrences of the difference of 17.0265 Da (mass of NH_3).
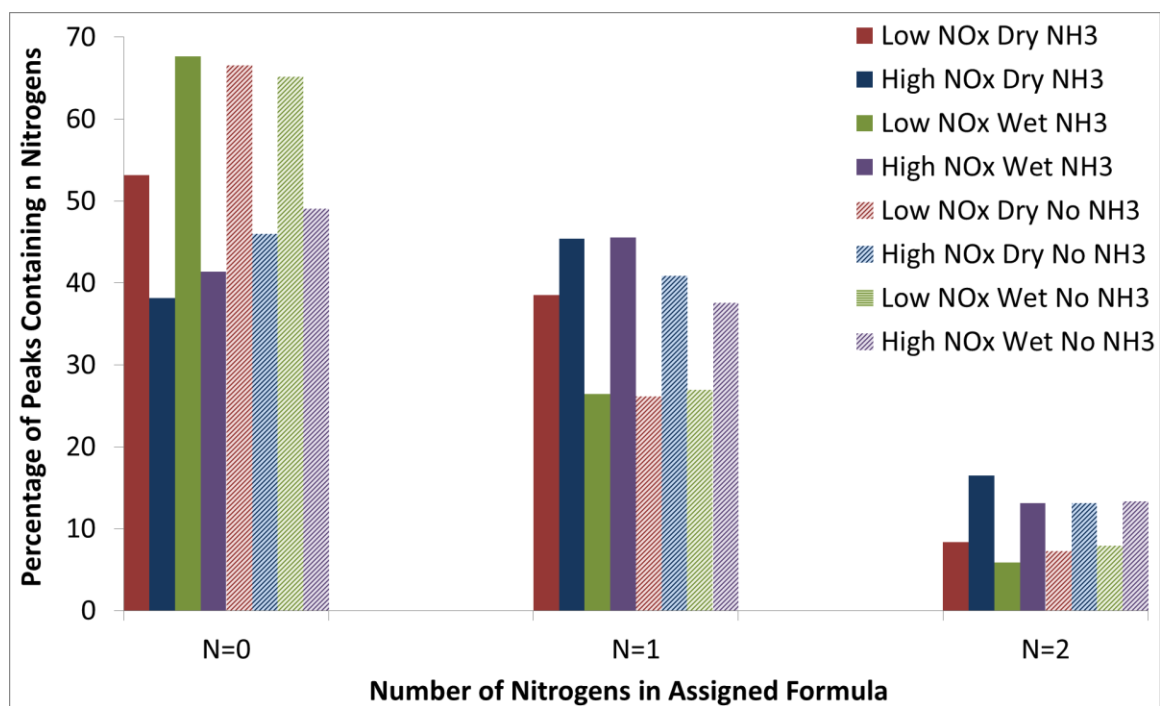
Figure 5.7: Percentage of assigned peaks that contain N = 0, 1, or 2 nitrogen atoms for each study.

5.4.2. Optical Properties

Figure 5.8a and 8b compare the effect of the NH_3 and RH on the MAC of NAP SOA under high- and low-NO_x conditions, respectively. The observed MAC values have comparable magnitudes and wavelength dependence under all conditions but there are several noteworthy

differences. First, each high-NO_x sample on average has a higher MAC than its corresponding low-NO_x sample. This is consistent with the previous observations of increased absorption from high-NO_x aromatic SOA. However, the contrast between high-NO_x and low-NO_x samples is not as large as for toluene SOA (in which the low-NOx sample was essentially non-absorbing).[12] Secondly, high-NO_x and high-RH conditions results in a distinct peak in MAC near 400 nm. In the sample with NH_3 this peak results in the wet conditions having a higher MAC than dry samples after 350 nm, while the MAC of the sample with no NH_3 remains similar in both samples after 400 nm. This peak can be assigned to compounds in which aromatic ring(s) are substituted with both phenol and nitro groups.[45] HPLC-PDA-MS data has shown that high-NO_x toluene SOA produces spectra with distinct light-absorbing fractions between 300-500 nm, compared to low-NO_x samples that only contained a few absorbing features above the background level. The corresponding mass spectra showed that the light-absorbing species were likely aromatic rings or nitro groups.[12] Under low-NO_x conditions RH results in an increase in MAC across all wavelengths and the peak seen at 400 nm in the high-NO_x conditions is not present. This is likely due to the lack of production of organonitrogen compounds in the absence of NO_x chemistry.
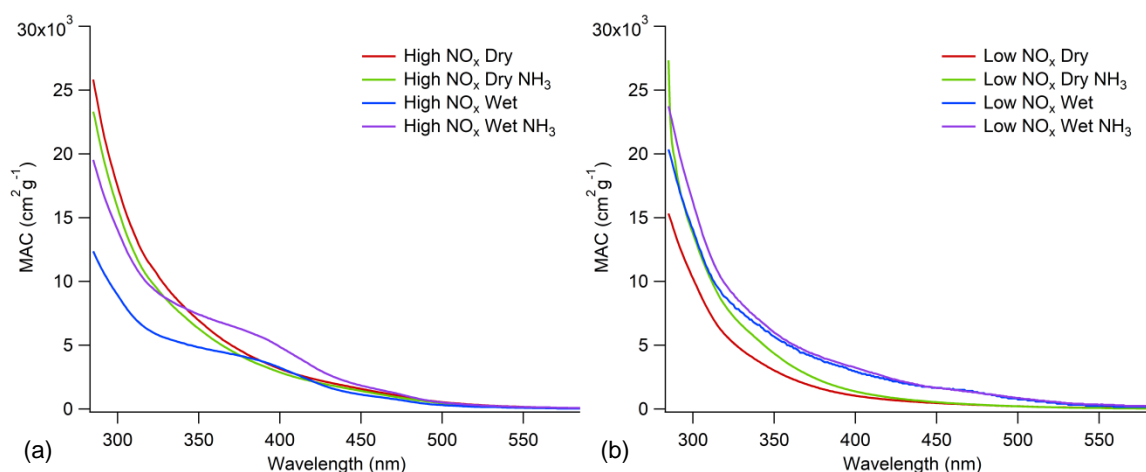
Figure 5.8: Comparison of relative humidity and the presence of NH_3 of the MAC of NAP SOA in (a) high- and (b) low-NO_x conditions.

Figure 5.8 shows a clear and consistent increase in MAC under humid conditions at both NO$_x$ levels. Liu *et al.* (2016) observed the RH above 30% caused MAC to increase by a factor of 1.33 at 365 nm for toluene and trimethylbenzene SOA.[13] Previous studies show that dry conditions can prevent nitrogen-containing compounds from forming.[12, 15, 52, 53] A reduction in these light-absorbing compounds may be responsible for the difference in MAC seen between dry and humid conditions. The effect of NH$_3$ appears to be minimal; however, the MAC values increase on average in the presence of ammonia.

5.5.   Conclusions

All of the environmental influences tested in this study had some sort of influence on the overall composition of NAP SOA and/or its optical properties. Elevated RH resulted in the production of more dimer products upon comparison of mass spectra from wet and dry studies (Figure 5.2 to Figure 5.5). The humid samples were also found to have increased MAC compared to their dry counterparts. The level of NO$_x$ seemed to have the most influence on both molecular characteristics and optical properties. High-NO$_x$ levels resulted in an increase in <N>, <O/C>, and <N/C>, as well as in the number of peaks with assigned formulas containing one or two nitrogen atoms. The also resulted in more peaks occurring with a mass difference equivalent to NH$_3$ between them, likely do to carbonyls produced by RO$_2$ + NO chemistry reacting with NH$_3$. Optically, there was an overall increase in MAC under high-NO$_x$ conditions, along with the growth of a distinct peak at 400 nm. This peak is likely due to the production of organonitrogen species. Lastly, NH$_3$ was found to have some effect on the resulting mass spectra. Like NO$_x$, NH$_3$ increased <N>, <N/C>, <O/C>, nitrogen-containing formulas, and NH$_3$ peak differenced. There was also a decrease in <C> and <H>, but an increased <H/C>. The optical influence was minimal, with only a slight MAC elevation. Since all of these parameters were tested

simultaneously, the exact cause and effect of each is difficult to determine. Overall this study

shows that atmospheric conditions can alter the characteristics of NAP SOA.

5.6.   References

1.   Boucher, O.; Randall, D.; Artaxo, P.; Bretherton, C.; Feingold, G.; Forster, P.; Kerminen, V.-M.; Kondo, Y.; Liao, H.; Lohmann, U.; Rasch, P.; Satheesh, S. K.; Sherwood, S.; Stevens, B.; Zhang, X. Y., Clouds and Aerosols. In *Climate Change 2013: The Physical Science Basis. Contribution of Working Group I to the Fifth Assessment Report of the Intergovernmental Panel on Climate Change*, Stocker, T. F.; Qin, D.; Plattner, G.-K.; Tignor, M.; Allen, S. K.; Boschung, J.; Nauels, A.; Xia, Y.; Bex, V.; Midgley, P. M., Eds. Cambridge University Press: Cambridge, United Kingdom and New York, NY, USA, 2013.

2.   Twomey, S., Aerosols, clouds and radiation. *Atmos. Environ., Part A: General Topics* **1991,** *25A*, (11), 2435-42.

3.   Charlson, R. J.; Schwartz, S. E., Climate forcing by anthropogenic aerosols. *Science* **1992,** *255*, (5043), 423-30.

4.   Andreae, M. O.; Gelencser, A., Black carbon or brown carbon? The nature of light-absorbing carbonaceous aerosols. *Atmos. Chem. Phys.* **2006,** *6*, (10), 3131-48.

5.   Bond, T. C., Spectral dependence of visible light absorption by carbonaceous particles emitted from coal combustion *Geophys. Res. Lett.* **2001,** *28*, (21), 4075-78.

6.   Bond, T. C.; Bergstrom, R. W., Light absorption by carbonaceous particles: an investigative review. *Aerosol Sci. Technol.* **2006,** *40*, (1), 27-67.

7.   Bond, T. C.; Charlson, R. J.; Heintzenberg, J., Quantifying the emission of light-absorbing particles: Measurements tailored to climate studies. *Geophys. Res. Lett.* **1998,** *25*, 337-40.

8.   Hopkins, R. J.; Lewis, K.; Desyaterik, Y.; Wang, Z.; Tivanski, A. V.; Arnott, W. P.; Laskin, A.; Gilles, M. K., Correlations between optical, chemical and physical properties of biomass burn aerosols. *Geophys. Res. Lett.* **2007,** *34*.

9.   Saleh, R.; Robinson, E. S.; Tkacik, D. S.; Ahern, A. T.; Liu, S.; Aiken, A. C.; Sullivan, R. C.; Presto, A. A.; Dubey, M. K.; Yokelson, R. J.; Donahue, N. M.; Robinson, A. L., Brownness of organics in aerosols from biomass burning linked to their black carbon content. *Nat. Geosci.* **2014,** *7*, 647-50.

10.   Washenfelder, R. A.; Attwood, A. R.; Brock, C. A.; Guo, H.; Xu, L.; Weber, R. J.; Ng, N. L.; Allen, H. M.; Ayres, B. R.; Baumann, K.; Cohen, R. C.; Draper, D. C.; Duffey, K. C.; Edgerton, E.; Fry, J. L.; Hu, W. W.; Jimenez, J. L.; Palm, B. B.; Romer, P.; Stone, E. A.; Wooldridge, P. J.; Brown, S. S., Biomass burning dominates brown carbon absorption in the rural southeastern United States *Geophys. Res. Lett.* **2015,** *42*, (2), 653-64.

11.   Laskin, A.; Laskin, J.; Nizkorodov, S. A., Chemistry of atmospheric brown carbon. *Chem. Rev.* **2015,** *115*, (10), 4335-82.

12.   Lin, P.; Liu, J.; Shilling, J. E.; Kathmann, S. M.; Laskin, J.; Laskin, A., Molecular characterization of brown carbon (BrC) chromophores in secondary organic aerosol generated from photo-oxidation of toluene. *Phys. Chem. Chem. Phys.* **2015,** *17*, 23312-25.

13.   Liu, J.; Lin, P.; Laskin, A.; Laskin, J.; Kathmann, S. M.; Wise, M.; Caylor, R.; Imholt, F.; Selimovic, V.; Shilling, J. E., Optical properties and aging of light-absorbing secondary organic aerosol. *Atmos. Chem. Phys.* **2016,** *16*, 12815-27.

14.   Lambe, A. T.; Cappa, C. D.; Massoli, P.; Onasch, T. B.; Forestieri, S. D.; Martin, A. T.; Cummings, M. J.; Croasdale, D. R.; Brune, W. H.; Worsnop, D. R.; Davidovits, P., Relationship between oxidation level and optical properties of secondary organic aerosol. *Environ. Sci. Technol.* **2013,** *47*, (12), 6349-57.

15.   Nakayama, T.; Sato, K.; Matsumi, Y.; Imamura, T.; Yamazaki, A.; Uchiyama, A., Wavelength and NO_x dependent complex refractive index of SOAs generated from the photooxidation of toluene *Atmos. Chem. Phys.* **2013,** *13*, 531-45.

16.   Nakayama, T.; Matsumi, Y.; Sato, K.; Imamura, T.; Yamazaki, A.; Uchiyama, A., Laboratory studies on optical properties of secondary organic aerosols generated during the photooxidation of toluene and the ozonolysis of α-pinene *J. Geophys. Res. Atmos.* **2010,** *115*, (D24), D24204.

17.   Kim, H.; Paulson, S. E., Real refractive indices and volatility of secondary organic aerosol generated from photooxidation and ozonolysis of limonene, α-pinene and toluene *Atmos. Chem. Phys.* **2013,** *13*, 7711-23.

18.   Aiona, P. K.; Luek, J. L.; Timko, S. A.; Powers, L. C.; Gonsior, M.; Nizkorodov, S. A., Effect of photolysis on absorption and fluorescence spectra of light-absorbing secondary organic aerosols. *ACS Earth Space Chem.* **2018,** *2*, 235-45.

19.   Lee, H. J.; Aiona, P. K.; Laskin, A.; Laskin, J.; Nizkorodov, S. A., Effect of solar radiation on the optical properties and molecular composition of laboratory proxies of atmospheric brown carbon. *Environ. Sci. Technol.* **2014,** *48*, 10217-26.

20.   Noziere, B.; Esteve, W., Organic reactions increasing the absorption index of atmospheric sulfuric acid aerosols. *Geophys. Res. Lett.* **2005,** *32*, L03812, 10.1029/2004GL021942.

21.   Noziere, B.; Esteve, W., Light-absorbing aldol condensation products in acidic aerosols: spectra, kinetics, and contribution to the absorption index. *Atmos. Environ.* **2007,** *41*, (6), 1150-63.

22.   Noziere, B.; Voisin, D.; Longfellow, C. A.; Friedli, H.; Henry, B. E.; Hanson, D. R., The uptake of methyl vinyl ketone, methacrolein, and 2-methyl-3-butene-2-ol onto sulfuric acid solutions. *J. Phys. Chem. A* **2006,** *110*, (7), 2387-95.

23.   Lin, Y. H.; Budisulistiorini, S. H.; Chu, K.; Siejack, R. A.; Zhang, H.; Riva, M.; Zhang, Z.; Gold, A.; Kautzman, K. E.; Surratt, J. D., Light-absorbing oligomer formation in secondary organic aerosol from reactive uptake of isoprene epoxydiols. *Environ. Sci. Technol.* **2014,** *48*, (20), 12012–21.

24.   Song, C.; Gyawali, M.; Zaveri, R. A.; Shilling, J. E.; Arnott, W. P., Light absorption by secondary organic aerosol from α-pinene: effects of oxidants, seed aerosol acidity, and relative humidity. *J. Geophys. Res. Atmos.* **2013,** *118*, 11741-49.

25.   Limbeck, A.; Kulmala, M.; Puxbaum, H., Secondary organic aerosol formation in the atmosphere via heterogeneous reaction of gaseous isoprene on acidic particles. *Geophys. Res. Lett.* **2003,** *30*, (19), 1996, 10.1029/2003GL017738.

26.   Gelencser, A.; Hoffer, A.; Kiss, G.; Tombacz, E.; Kurdi, R.; Bencze, L., In-situ formation of light-absorbing organic matter in cloud water. *J. Atmos. Chem.* **2003,** *45*, (1), 25-33.

27.   Chang, J. L.; Thompson, J. E., Characterization of colored products formed during irradiation of aqueous solutions containing H_2O_2 and phenolic compounds. *Atmos. Environ.* **2010,** *44*, (4), 541-51.

28.   Li, Y. J.; Huang, D. D.; Cheung, H. Y.; Lee, A. K. Y.; Chan, C. K., Aqueous-phase photochemical oxidation and direct photolysis of vanillin – a model compound of methoxy phenols from biomass burning *Atmos. Chem. Phys.* **2014,** *14*, 2871-85.

29.   Sun, Y. L.; Zhang, Q.; Anastasio, C.; Sun, J., Insights into secondary organic aerosol formed via aqueous-phase reactions of phenolic compounds based on high resolution mass spectrometry *Atmos. Chem. Phys.* **2010,** *10*, 4809-22.

30.   Shapiro, E. L.; Szprengiel, J.; Sareen, N.; Jen, C. N.; Giordano, M. R.; McNeill, V. F., Light-absorbing secondary organic material formed by glyoxal in aqueous aerosol mimics. *Atmos. Chem. Phys.* **2009,** *9*, (7), 2289-2300.

31.   Updyke, K. M.; Nguyen, T. B.; Nizkorodov, S. A., Formation of brown carbon via reactions of ammonia with secondary organic aerosols from biogenic and anthropogenic precursors. *Atmos. Environ.* **2012,** *63*, 22-31.

32.   Lin, P.; Laskin, J.; Nizkorodov, S. A.; Laskin, A., Revealing brown carbon chromophores produced in reactions of methylglyoxal with ammonium sulfate. *Environ. Sci. Technol.* **2015,** *49*, (24), 14257-66.

33.   De Haan, D. O.; Hawkins, L. N.; Welsh, H. G.; Pednekar, R.; Casar, J. R.; Pennington, E. A.; de Loera, A.; Jimenez, N. G.; Symons, M. A.; Zauscher, M.; Pajunoja, A.; Caponi, L.; Cazaunau, M.; Formenti, P.; Gratien, A.; Pangui, E.; Doussin, J. F., Brown carbon production in ammonium- or amine-containing aerosol particles by reactive uptake of methylglyoxal and photolytic cloud cycling. *Environ. Sci. Technol.* **2017,** *51*, (13), 7458-66.

34.   De Haan, D. O.; Tapavicza, E.; Riva, M.; Cui, T.; Surratt, J. D.; Smith, A. C.; Jordan, M. C.; Nilakantan, S.; Almodovar, M.; Stewart, T. N.; de Loera, A.; De Haan, A. C.; Cazaunau, M.; Gratien, A.; Pangui, E.; Doussin, J. F., Nitrogen-containing, light-absorbing oligomers produced in aerosol particles exposed to methylglyoxal, photolysis, and cloud cycling. *Environ. Sci. Technol.* **2018,** *52*, (7), 4061-71.

35.   Kwon, D.; Or, V. W.; Sovers, M. J.; Tang, M.; Kleiber, P. D.; Grassian, V. H., Optical property measurements and single particle analysis of secondary organic aerosol produced from the aqueous-phase reaction of ammonium sulfate with methylglyoxal. *ACS Earth Space Chem.* **2018,** *2*, (4), 356-65.

36.   Sareen, N.; Schwier, A. N.; Shapiro, E. L.; Mitroo, D.; McNeill, V. F., Secondary organic material formed by methylglyoxal in aqueous aerosol mimics. *Atmos. Chem. Phys.* **2010,** *10*, (3), 997-1016.

37.   De Haan, D. O.; Corrigan, A. L.; Tolbert, M. A.; Jimenez, J. L.; Wood, S. E.; Turley, J. J., Secondary organic aerosol formation by self-reactions of methylglyoxal and glyoxal in evaporating droplets. *Environ. Sci. Technol.* **2009,** *43*, (21), 8184-90.

38.   Bones, D. L.; Henricksen, D. K.; Mang, S. A.; Gonsior, M.; Bateman, A. P.; Nguyen, T. B.; Cooper, W. J.; Nizkorodov, S. A., Appearance of strong absorbers and fluorophores in limonene-O_3 secondary organic aerosol due to NH_4^+-mediated chemical aging over long time scales. *J. Geophys. Res.* **2010,** *115*, D05203, 10.1029/2009jd012864.

39.   Nguyen, T. B.; Lee, P. B.; Updyke, K. M.; Bones, D. L.; Laskin, J.; Laskin, A.; Nizkorodov, S. A., Formation of nitrogen- and sulfur-containing light-absorbing compounds accelerated by evaporation of water from secondary organic aerosols. *J. Geophys. Res.* **2012,** *117*, D01207, 10.1029/2011jd016944.

40.   Lee, H. J.; Laskin, A.; Laskin, J.; Nizkorodov, S. A., Excitation-emission spectra and fluorescence quantum yields for fresh and aged biogenic secondary organic aerosols. *Environ. Sci. Technol.* **2013,** *47*, (11), 5763-70.

41.   Flores, J. M.; Washenfelder, R. A.; Adler, G.; Lee, H. J.; Segev, L.; Laskin, J.; Laskin, A.; Nizkorodov, S. A.; Brown, S. S.; Rudich, Y., Complex refractive indices in the near-ultraviolet spectral region of biogenic secondary organic aerosol aged with ammonia. *Phys. Chem. Chem. Phys.* **2014,** *16*, (22), 10629-42.

42.   Yu, G.; Bayer, A. R.; Galloway, M. M.; Korshavn, K. J.; Fry, C. G.; Keutsch, F. N., Glyoxal in aqueous ammonium sulfate solutions: products, kinetics and hydration effects. *Environ. Sci. Technol.* **2011,** *45*, (15), 6336-42.

43.   Powelson, M. H.; Espelien, B. M.; Hawkins, L. N.; Galloway, M. M.; De Haan, D. O., Brown carbon formation by aqueous-phase carbonyl compound reactions with amines and ammonium sulfate. *Environ. Sci. Technol.* **2014,** *48*, (2), 985-93.

44.   Xie, M.; Chen, X.; Hays, M. D.; Lewandowski, M.; Offenberg, J.; Kleindienst, T. E.; Holder, A. L., Light absorption of secondary organic aerosol: composition and contribution of nitroaromatic compounds *Environ. Sci. Technol.* **2017,** *51*, (20), 11607-16.

45.   Liu, P. F.; Abdelmalki, N.; Hung, H. M.; Wang, Y.; Brune, W. H.; Martin, S. T., Ultraviolet and visible complex refractive indices of secondary organic material produced by photooxidation of the aromatic compounds toluene and m-xylene. *Atmos. Chem. Phys.* **2015,** *15*, 1435-45.

46.   Liu, P.; Li, Y. J.; Wang, Y.; Bateman, A. P.; Zhang, Y.; Gong, Z.; Bertram, A. K.; Martin, S. T., Highly viscous states affect the browning of atmospheric organic particulate matter. *ACS Cent. Sci.* **2018,** *4*, (2), 207-15.

47.   De Haan, D. O.; Hawkins, L. N.; Kononenko, J. A.; Turley, J. J.; Corrigan, A. L.; Tolbert, M. A.; Jimenez, J. L., Formation of nitrogen-containing oligomers by methylglyoxal and amines in simulated evaporating cloud droplets. *Environ. Sci. Technol.* **2011,** *45*, (3), 984-91.

48.   Aiona, P. K.; Lee, H. J.; Leslie, R.; Lin, P.; Laskin, A.; Laskin, J.; Nizkorodov, S. A., Photochemistry of products of the aqueous reaction of methylglyoxal with ammonium sulfate. *ACS Earth Space Chem.* **2017,** *1*, (522-32).

49.   Aiona, P. K.; Lee, H. J.; Lin, P.; Heller, F.; Laskin, A.; Laskin, J.; Nizkorodov, S. A., A role for 2-methyl pyrrole in the browning of 4-oxopentanal and limonene secondary organic aerosol. *Environ. Sci. Technol.* **2017,** *51*, 11048-56.

50.   Nguyen, T. B.; Laskin, A.; Laskin, J.; Nizkorodov, S. A., Brown carbon formation from ketoaldehydes of biogenic monoterpenes. *Faraday Discuss.* **2013,** *165*, 473-94.

51.   Finlayson-Pitts, B. J.; Pitts, J. N. J., *Finlayson-Pitts BJ, Pitts Jr JN. Chemistry of the upper and lower atmosphere: theory, experiments, and applications*. Elsevier: 1999.

52.   Liu, Y.; Liggio, J.; Staebler, R.; Li, S.-M., Reactive uptake of ammonia to secondary organic aerosols: kinetics of organonitrogen formation. *Atmos. Chem. Phys.* **2015,** *15*, 13569-84.

53.   Zhang, X.; Lin, Y. H.; Surratt, J. D.; Zotter, P.; Prevot, A. S. H.; Weber, R. J., Light-absorbing soluble organic aerosol in Los Angeles and Atlanta: A contrast in secondary organic aerosol. *Geophys. Res. Lett.* **2011,** *38*, L21810.

Chapter 6   Effect of Photolysis on Absorption and Fluorescence Spectra of Light-Absorbing Secondary Organic Aerosols

6.1. Abstract

Excitation-emission matrices (EEMs) constructed from fluorescence measurements are increasingly used for the characterization of chromophoric dissolved organic matter (CDOM) and light-absorbing atmospheric organic aerosol known as brown carbon (BrC). There is a high uncertainty in the effect of BrC aerosols on climate because their optical properties depend on the amount of time they spent in the atmosphere. In order to aid in the quantification of BrC aerosols' contribution to radiative forcing, we investigated the effect of solar radiation on the fluorescence, expressed as EEMs, and absorption spectra of the water-soluble fraction of BrC species formed by the high-NOx photooxidation of benzene, toluene, p-xylene, and naphthalene. The BrC samples were prepared in a smog chamber, extracted in water, and irradiated in a solar simulator at a fixed pH of 3, representative of aerosol liquid water, or at a fixed pH of 6, representative of cloud water. Semi-continuous fluorescence and absorbance measurements were carried out during the irradiation at 20 minute intervals for 48 hours. The absorption coefficients depended on the solution pH, with the solutions at pH 6 absorbing stronger than solutions at pH 3. All samples underwent a decrease in absorption coefficient at all visible wavelengths, while fluorescence intensities showed both increases and decreases in different regions of the EEMs. Upon comparison with CDOM samples, the fluorescence intensity of all secondary organic aerosol (SOA) samples decreased in the region of the EEMs where the characteristic terrestrial humic-like C peak occurs. These experimental observations suggest that: (i) this type of BrC will have different effects on climate depending on whether it ends up in an acidic or neutral environment; (ii) exposure to UV radiation will diminish the ability of this type of BrC to affect climate on a time scale of about a day; (iii) fluorescence by BrC compounds has a minimal effect

on aerosol radiative forcing; (iv) photooxidized aromatics may be closely related, in terms of

optical properties, to CDOM found in fresh waters.

6.2. Introduction

Fluorescence spectroscopy is commonly used to characterize different types of chromophoric dissolved organic matter (CDOM) in water samples from different systems.[1-3] Low levels of CDOM and small variation in its composition can be measured using fluorescence spectroscopy and excitation-emission matrices (EEMs) because these methods are much more sensitive than absorption spectroscopy.[4, 5] Specific peaks in EEM spectra correspond to different chemical compositions of CDOM. Table 6.1 adapted from Coble (1996 and 2007) lists the location of particular humic-, protein-, and pigment-like peaks due to fluorophores that are commonly found in natural water samples.[4, 5] However, it should be noted here that other fluorophores have been suggested to give similar fluorescence than those described in Table 6.1.[6]

Table 6.1: List of commonly observed peaks in EEMs spectra of CDOM found in natural water systems as described in Coble (1996 and 2007).

Component	Peak Name	Ex_{max} (nm)	Em_{max} (nm)
Tyrosine-like, protein-like	B	275	305-310
Tryptophan-like, protein-like	T	275	340
UVC terrestrial humic-like	A	260	380-460
UVA terrestrial humic-like	C	320-360	420-480
UVA terrestrial humic-like	-	250 (385)	504
UVA marine humic-like	M	290-312	370-420
Pigment-like	P	398	660

These peaks are subject to change due to environmental stress from mixing, biological degradation and production, and photochemical processes.[5] CDOM exposed to solar radiation is known to undergo photobleaching, which is accompanied by changes in its fluorescent properties.[1, 2, 7] Irradiation leads to a decrease in the fluorescence of the photolabile species in

CDOM, but some materials such as tyrosine, tryptophan, and low molecular weight aromatic compounds may actually produce CDOM when exposed to irradiation.[2]

In contrast to the large number of fluorescence measurements for CDOM found in a variety of water systems, applications of fluorescence-based methods to describe organic compounds found in atmospheric aerosols remain limited.[8-14] Hawkins *et al*. (2016) compared fluorescence maps of aldehydes reacted with ammonium sulfate and glycine to those of water-soluble organic carbon extracts.[10] Matos *et al*. (2015) performed parallel factor analysis (PARAFAC) of EEMs collected for water-soluble and alkaline-soluble organic matter in extracts of urban aerosols.[9] Phillips and Smith (2014 and 2015) used fluorescence measurements to explore the role of charge transfer complexes in absorption by organic compounds in particulate matter.[11, 12] These fluorescence studies help distinguish different components of brown carbon (BrC) and allow for a more in depth understanding of its chemical and optical properties.

BrC is a subset of atmospheric particles containing molecules that strongly absorb visible and near ultraviolet (UV) radiation. Upon deposition, BrC finds its way into ground waters and becomes part of CDOM. BrC can be produced by both primary sources, such as biomass burning and by secondary reactions in the atmosphere.[15] Secondary organic aerosol (SOA) is formed by photooxidation of volatile organic compounds (VOCs), and for certain VOCs, the oxidation products have a characteristic brown color. Examples include SOA produced by gas-phase photooxidation of naphthalene,[16] toluene,[17] xylene,[18] indole,[19] as well as by aqueous phase photooxidation of phenolic compounds[20, 21] and other aromatic compounds.[22] In addition, reactive uptake of carbonyls and other organic compounds can also lead to BrC.[23-26] Some of these types of BrC are fluorescent and have been previously examined using EEMs.[9, 15, 27, 28]

BrC SOA is a highly oxidized and complex system that may contain components that are similar to CDOM. These BrC species contain both water-soluble and insoluble components, with the water-soluble portion accounting for up to 70%.[15] Between 20-50% of water-soluble organic components in aerosols can be categorized as "humic-like substances" (HULIS).[29-32] The compositions of HULIS and CDOM found in natural water systems are similar, with both containing heterogeneous mixtures of water-soluble, light-absorbing components.[29, 33] Duarte *et al.* (2004) found the EEMs of water-soluble organic compounds in atmospheric aerosols produced fluorescence peaks similar to those of aquatic humic substances, with a shift to shorter wavelengths.[27]

Applications of fluorescence-based methods to BrC have provided valuable information about the effect of irradiation on its optical properties and composition. Lee *et al*. (2014) observed loss of absorption coefficient but gain in fluorescence from BrC produced from photooxidation of naphthalene.[16] Aiona *et al*. (2017) observed rapid removal of both chromophores and fluorophores from BrC produced by reaction between methyl glyoxal and ammonium sulfate.[34] Zhong and Jang (2013) reported a decrease in the fluorescence emission of extracts of wood smoke upon exposure to natural sunlight.[35] Within these studies the effect of photolysis on fluorescent characteristics of different types of BrC SOA has not been systematically investigated. None of the previous studies controlled the pH of the solution during irradiation, making it difficult to attribute changes solely to photolysis due to the high pH dependency of optical properties.[7]

In this study, EEM spectra, absorption spectra, and fluorescence quantum yields of BrC SOA are measured using a novel system that photolyzes aqueous extracts of BrC and simultaneously measures absorption and fluorescence spectra, while actively controlling the

solution pH.[2, 7] Benzene, toluene, p-xylene, and naphthalene are selected as representative secondary BrC precursors. We find that absorption coefficients for all BrC SOA decrease upon exposure to irradiation. In comparison, fluorescence decreases in certain regions of the EEMs, specifically in the area of the humic-like C peak, and increases in others. These changes in the humic region of the EEMs are characteristic of CDOM found in fresh water systems with terrestrial plant matter as the ultimate source.

6.3. Experimental Methods

6.3.1. Formation of Secondary Organic Aerosols

SOA samples were generated in a ~5 m^3 aerosol smog chamber via photooxidation under high-NO$_x$ (NO$_x$ refers to the sum of NO and NO$_2$) conditions for four different precursors: benzene, toluene, p-xylene, and naphthalene (abbreviated as BEN, TOL, XYL, and NAP, respectively). The chamber was flushed with clean air overnight and humidified to the desired level by filling it with air through a Nafion multichannel humidifier. Samples were prepared at 40% relative humidity (RH) in the chamber, except for a preliminary NAP SOA sample prepared under dry conditions (RH<2%). The photochemical reactor (described below) required several milligrams of SOA material, so elevated concentrations of H$_2$O$_2$, NO$_x$, and each organic precursor had to be used in order to obtain 1.5-2 mg of SOA sample (Table 6.2). H$_2$O$_2$ (Aldrich; 30% by volume in water) was evaporated into the chamber with zero air in mixing ratios ranging from 2-15 ppm to serve as a photochemical precursor to hydroxyl radicals. NO was added from a premixed cylinder to achieve initial NO$_x$ concentrations ranging from 0.4-1.5 ppm. For NAP SOA samples, ~23 µL of a 0.5 g/mL solution of naphthalene in dichloromethane was evaporated into the chamber to produce 0.4 ppm. Microliter volumes of pure toluene, benzene, or p-xylene were evaporated directly into the chamber to achieve initial mixing ratios of 7.5, 15.0, and 0.8

ppm, respectively. These concentrations are quite high by smog chamber standards, but they were necessary to produce sufficient amounts of material needed for the optical measurements described below. Chamber contents were mixed with a fan after addition before photooxidation, which was then initiated using UV-B lamps (Solar Tec Systems model FS40T12/UVB) with an emission centered at 310 nm. Photooxidation time ranged from 2-3.5 hours. ThermoScientific monitors were used to monitor real time concentrations of NO/NO_y (model 42i-Y, NO_y refers to the sum of NO, NO_2, and other nitrogen containing compounds that can be catalytically reduced to NO) and ozone (model 49i), while temperature and RH were monitored with a Vaisala HMT330 probe enclosed in the chamber. Particle size distribution was monitored using a scanning mobility particle sizer (SMPS) (TSI Model 3936). The particle chemical composition was not tracked during the preparation. However, for NAP SOA prepared by Lee et al. (2014)[16] using a similar method, the average formula determined by high-resolution mass spectrometry was $C_{14.1}H_{14.5}O_{5.1}N_{0.085}$, corresponding to an average O/C of 0.36.

Photooxidation lasted for 2-4 hours (Table 6.2) and was stopped when the particle mass concentration in the chamber stopped growing. Particles were then collected for 4 hours onto a PTFE filter at 15-20 standard liters per minute (SLM) after passing through an activated carbon denuder. Collected SOA mass ranged from 1.5-2 mg, estimated from SMPS data assuming 100% collection efficiency by the filter (the actual mass was probably smaller since filters do not capture all the particles). Filters were then vacuum sealed and stored, before being sent to the University of Maryland for analysis. Due to the time consuming nature of the measurements and data analysis, only one sample was prepared and examined for each of the SOA types.

Table 6.2: Summary of SOA preparation conditions.[a]

Precursor mixing ratio (ppm)	H_2O_2 (ppm)	NO_x (ppm)	RH (%)	Photo-oxidation (h)	Collection Time (h)	Mass Collected (mg)	pH Control	Irradiation Time (h)	C_{mass}[b] (mg/L)
NAP [0.4][c]	2.0	0.4	0	2	4	2	None	46	40
NAP [0.4]	2.0	0.4	40	2.3	4	1.8	3 and 6	44	36
TOL [1.5]	7.5	1.5	40	3.3	4	1.7	3 and 6	44	34
BEN [5.0]	15.0	0.5	40	3.7	4	1.7	3 and 6	44	34
p-XYL [2.0]	8.0	0.6	40	3.5	4	1.5	3 and 6	44	30

a) Precursor abbreviations: "NAP" – naphthalene, "TOL" – toluene, "BEN" – benzene, and "p-XYL" – p-xylene; H_2O_2 and NO_x concentrations and relative humidity (RH) are listed before photooxidation.

b) Mass concentration of the SOA material in the solution assuming the SOA material could be fully extracted in 50 mL of water.

c) This sample was prepared under dry conditions to test the photolysis system without pH control.

6.3.2. Photolysis Experiments

All photolysis experiments, calculations, and plots were done by Jenna Luek, Stephen Timko, Leanne Powers, and Michael Gonsior at the University of Maryland Center for Environmental Science, Chesapeake Biological Laboratory in Solomons, MD. A custom-built photolysis system was used to irradiate the SOA samples while simultaneously collecting absorbance and fluorescence data. SOA samples were extracted from filters using 50 mL of water and sonicated for two minutes, resulting in solution mass concentrations of the SOA compounds ranging from 30 to 40 mg/L (Table 6.2). We need to emphasize that this procedure only extracts water-soluble BrC components. However, the fraction of the water-insoluble compounds that remained on the filter is likely to be small because the brown-colored filter became white after the extraction. Indeed, NAP SOA prepared by a similar method by Lee et al. (2014) remained soluble to at least 0.6 g/L,[16] which is more than an order of magnitude higher than the concentrations used in this study. Samples were pumped through a spiral flow cell

located underneath a solar simulator using an inert micro gear pump. An Oriel Sol2A Class ABA solar simulator (Newport Corporation, Irvine, CA) with a 1000 W Xe arc lamp equipped with an AM 1.5 filter was used for irradiations. The solar spectrum of the lamp was set up to simulate the sun at a 48.2° solar zenith angle and an intensity of one sun (1 "sun" = 1000 W/m^2). Lamp power was controlled with a Newport 68951 Digital Exposure controller and its power was measured before each experiment with a Newport 91150 V Reference Cell. The spiral flow cell was custom built using SCHOTT Borofloat borosilicate glass (Hellma Analytics, 70 to 85% transmission between 300 and 350 nm, and 85% transmission at wavelengths >350), with a 2 mm wide by 1 mm deep flow path (total surface area of 101 cm^2).[7] The irradiation cell was temperature controlled to 25 °C using Peltier units and a recirculating water bath. Upon irradiating the photo reactor flow cell, the solution was injected into a 10 mL round bottom flask with three necks, where the pH of the solution was monitored with a Thermo Orion 8220BNWP microelectrode. The pH was automatically adjusted as needed with a J-Kem Infinity II reaction controller coupled with a dual syringe pump using 0.1 M HCl or NaOH solutions. After passing through the air equilibrator, the sample was then drawn into the 4x10 mm flow cell of a Horiba Aqualog spectrofluorometer before being recirculated through the irradiation cell.

The NAP SOA sample prepared under dry conditions was used in the initial tests of the system. It was irradiated for 46 hours with no pH control, and a small change in pH (0.25 SU increase) was observed over the course of irradiation. Therefore, the rest of the experiments were done with active pH control of the irradiated solution. The SOA samples prepared at 40% RH were all irradiated for 44 hours at two different controlled pH values. The irradiation time of 44 hours under one sun (equivalent to a dose of 6.9 Einstein/m^2 in the 330-380 nm window) is comparable to the typical lifetime of aerosol particles in the atmosphere (a few days).

Furthermore, the rate of change in the absorption coefficients became small after 44 h, and further irradiation was deemed unnecessary. A pH of 6 was tested to represent SOA compounds dissolved in cloud water, while a pH of 3 was tested to simulate the more acidic environment of aerosol liquid water or polluted cloud.[36] Even lower pH values have been reported in aerosol particles,[36] but achieving pH below 3 would be problematic with this photolysis system. Excitation-emission matrices (EEMs) and absorption spectra were collected for each sample in 20 minute intervals using a 0.4 second integration time. Excitation scans and absorption spectra were collected from 230 to 600 nm in 3 nm intervals. Emission spectra were collected from 210 to 618 nm in 3.27 nm intervals. Fluorescence intensities were converted into Quinine Sulfate Units (QSU), after correcting for the Rayleigh and Raman scattering and inner filter effects using previously described methods.[2, 37] The absorption data were used to create kinetics plots at 260, 365, 405, and 532 nm. The change in fluorescence apparent quantum yield (AQY) over the course of irradiation was calculated using fluorescence intensities and values given by Brouwer (2011) for quinine sulfate in 0.1 M $HClO_4$.[38, 39]

6.4. Results and Discussion

6.4.1. Effect of Photolysis on the Absorption Spectra

Figure **6.1** shows the initial values of $\alpha_{solution}$ for all samples before the irradiation. Figure 6.2 and Figure 6.3 compare absorption coefficients ($\alpha_{solution}$ in m^{-1}) for the solutions of BEN, TOL, XYL and NAP SOA when irradiated for 44 hours at pH 3 and pH 6, respectively. To produce these figures, the measured base-10 absorbance values (A_{10}) were converted into base-e solution absorption coefficients by normalizing to the cell pathlength (l).

$$\alpha_{solution}(\lambda) = \frac{A_{10}(\lambda) \times \ln(10)}{l}$$ (**Equation 6.1**)

Because of the low mass concentration of SOA in the solution (C_{mass}, given in the last column of Table 6.1) we can safely assume complete extraction of the SOA material into solution. Therefore, we can get the bulk mass absorption coefficient (MAC_{bulk} in m^2/kg) of the SOA material by normalizing $\alpha_{solution}$ to C_{mass}:

$$MAC_{bulk}(\lambda) = \frac{\alpha_{solution}(\lambda)}{C_{mass}}$$
(Equation 6.2)

The observed MAC_{bulk} values are comparable to values reported in previous studies. For example, Lee et al. (2014) reported $MAC_{bulk} = 0.6$ m^2/g for NAP SOA at 300 nm,[16] and the corresponding value estimated from the data in

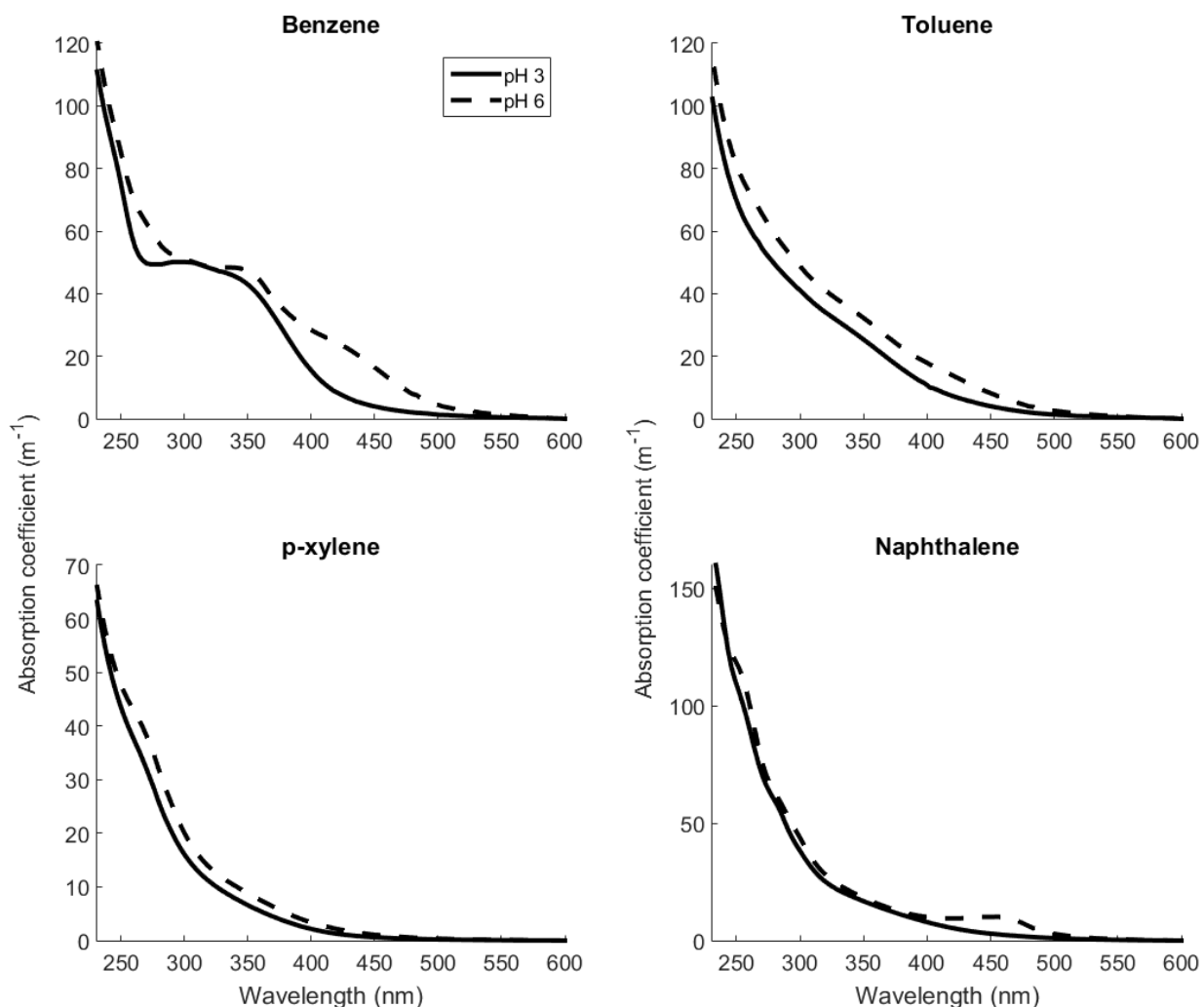Figure **6.1** is $MAC_{bulk} \sim 1$ m^2/g.

Figure 6.1: Comparison of solution absorption coefficients at t=0. Plots shown for all four SOA types and two different pH values (pH 3 is a solid line and pH 6 is a dotted line). If desired, these solution absorption coefficients can be converted into bulk mass absorption coefficients (MAC) of the SOA material using equation 6.2.

The solution absorption coefficients generally decreased during photolysis. To see the changes more clearly, panels B, D, F, H of Figure 6.2 and Figure 6.3 show differences in the absorption coefficient relative to the value before photolysis. Both the initial absorption coefficient and the difference in absorption coefficient depend on pH.

Figure **6.1** provides a comparison of the absorption spectra of each SOA at pH 3 and pH 6 at t=0 to show that the solution are absorbing stronger at pH 6 across the entire absorption

177

spectrum. Photooxidation of aromatic compounds under high-NO_x conditions is known to produce nitrophenols, which make the dominant contribution to the absorption coefficient.[17] The acid-base equilibria of nitrophenols are well-known to cause a strong pH dependence in absorption spectra.[16, 40] With a typical pK_a of ~7, the fraction of nitrophenols ionized at pH 3 is very small. However, at pH 6, nitrophenols will be partially ionized and the absorption spectrum will have a contribution from the anions, which have red-shifted absorption spectra compared to the non-ionized nitrophenols.[41-45] As a result, the absorption coefficient is enhanced at pH 6 (

Figure **6.1**). These are important characteristics because depending on the atmospheric environment where these compounds end up they can have different effects on the absorption of solar radiation. In an acidic environment, which is representative of aerosol liquid water,[36] BrC would absorb less visible sunlight than it would under more neutral conditions in cloud and fog droplets.[46, 47]

In all the SOA samples, there was a decrease in the measured absorption coefficients over the irradiation time at all visible wavelengths (Figure 6.2 and Figure 6.3). For BEN and TOL SOA, the decrease was the largest at 350 nm, where nitrophenols are known to absorb. In addition to nitrophenols, quinones in NAP SOA can also absorb at visible wavelengths (for example, 1,4-naphthoquinone is yellow). The absorption coefficient around 260 nm was less affected by radiation, and in fact, a distinct absorption band grew at this wavelength in some of the samples. This effect was the strongest in BEN SOA at pH 6, which showed an initial increase in absorption coefficient at 260 nm, while XYL SOA at pH 3 showed a weaker increase after 20 h of irradiation. Other experiments, such as TOL SOA at pH 3 and pH 6, did not show an increase in absorption coefficient, but rather a decreased rate of absorption loss at 260 nm, resulting in the same distinct band. This suggests the presence of photo-stable compounds in the

SOA, which are produced during irradiation in some samples and absorb at 260 nm. These observations are consistent with results of aqueous photooxidation of 4-nitrocatechol and related compounds in experiments by Zhao *et al.* (2015).[48] Direct photolysis and aqueous reaction by the hydroxyl radical led to rapid photobleaching of the nitrophenols, as well as a decrease in absorption coefficient at 350 nm and increase at 260 nm.[48]
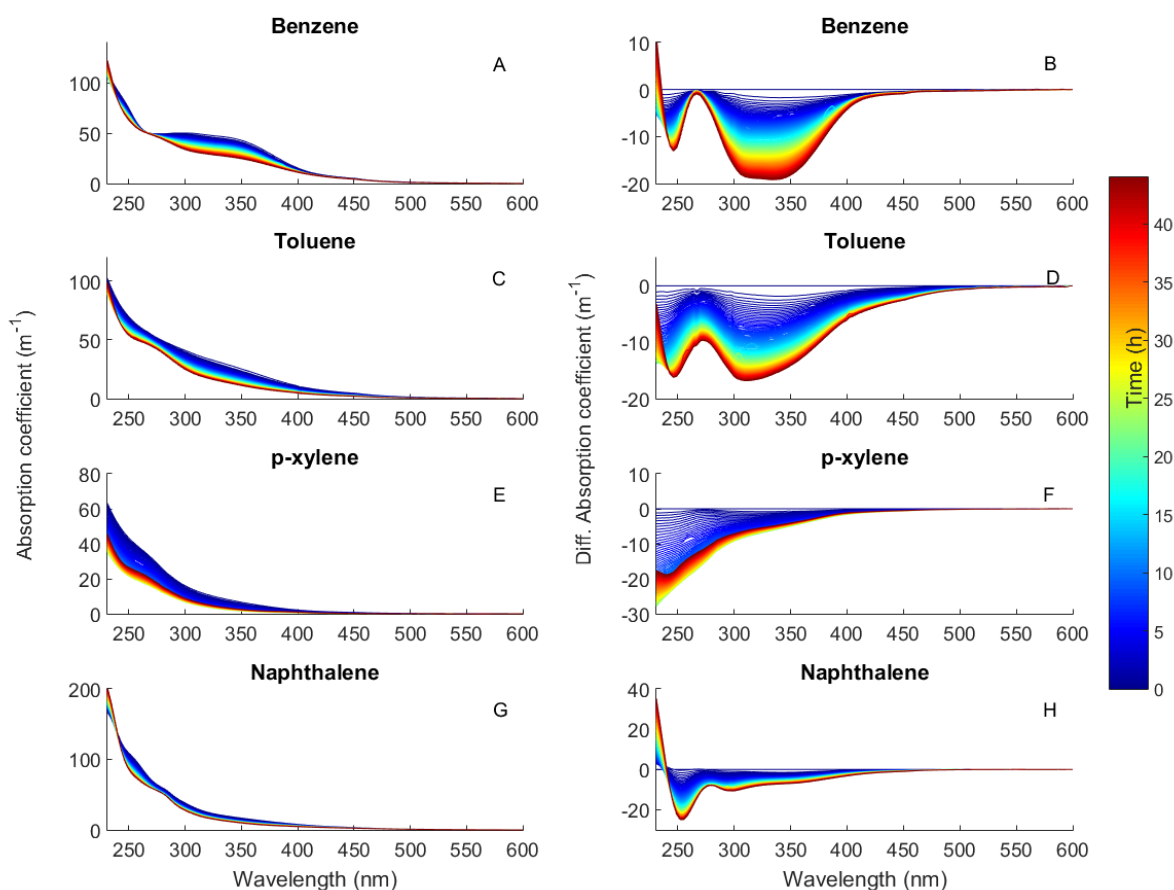

Figure 6.2: Comparison of solution absorption coefficients (m^{-1}, panels: A – BEN SOA, C – TOL SOA, E – XYL SOA, and G – NAP SOA) and the change in absorption coefficient (panels: B – BEN SOA, D – TOL SOA, F – XYL SOA, and H – NAP SOA) for each SOA over 44 h of irradiation at pH 3. If desired, these solution absorption coefficients can be converted into bulk mass absorption coefficients (MAC) of the SOA material using equation 6.2.
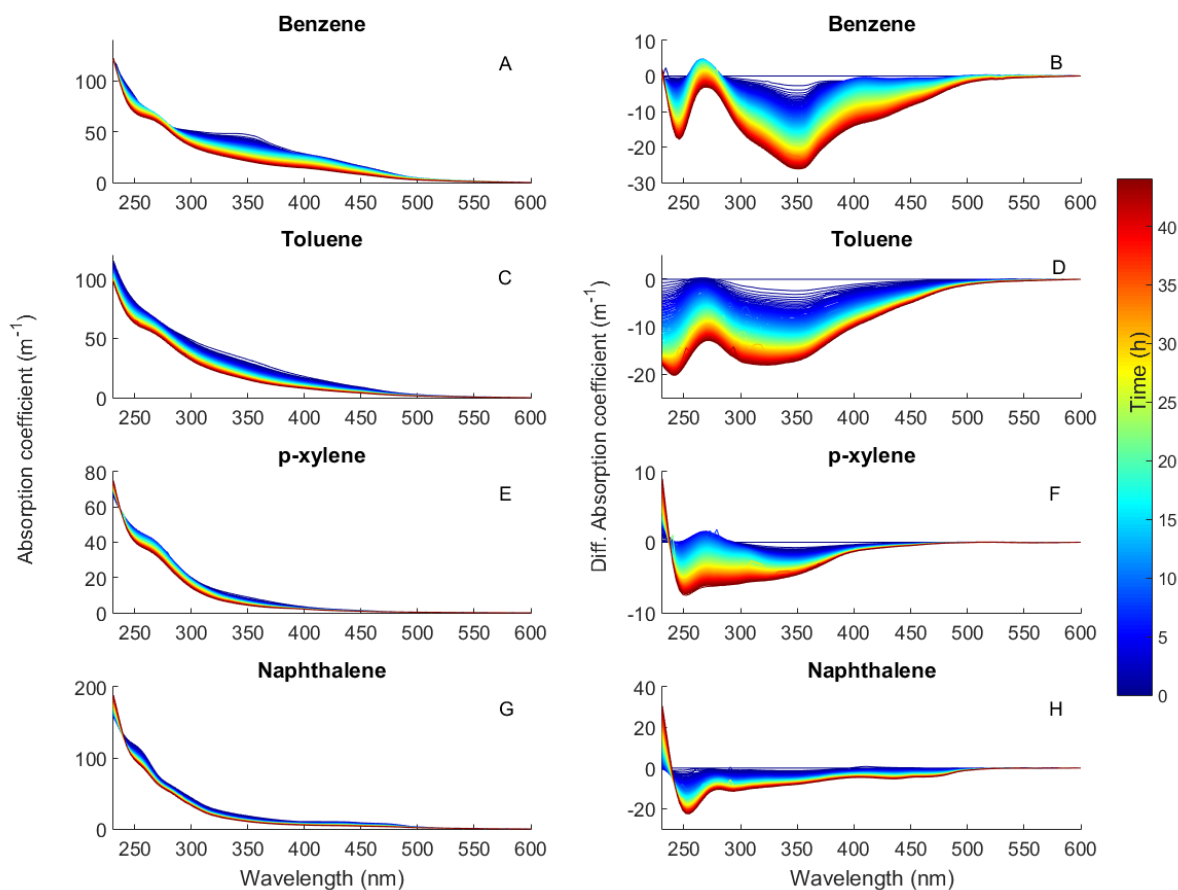
Figure 6.3: Comparison of solution absorption coefficients (m^{-1}, panels: A – BEN SOA, C – TOL SOA, E – XYL SOA, and G – NAP SOA) and the change in absorption coefficient (panels: B – BEN SOA, D – TOL SOA, F – XYL SOA, and H – NAP SOA) for each SOA over 44 h of irradiation at pH 6.

The rate at which absorption coefficients of BrC change is an important parameter for predicting radiative forcing by BrC. If BrC photobleaches rapidly, it will have less of an overall effect on climate. Figure 6.4 and Figure 6.5 show the kinetics plots for each SOA at pH 3 and pH 6, respectively. The chosen wavelengths include 260 nm (where an absorption band appears during irradiation), 365 nm, 405 nm, and 532 nm (wavelengths at which optical properties of aerosols are commonly measured). The 365 nm and 405 nm wavelengths represent shorter wavelengths in the solar spectrum, where BrC has been found to contribute 10-30% of total

absorption by fine particles, while 532 nm falls in the visible region where BrC contributes about 10% of the total absorption.[49] The peak of the solar spectrum also occurs close to 532 nm. The kinetics at 365 and 405 nm follow similar trends in all samples, with the absorption coefficients of SOA decreasing by more than a factor of 2 over 44 h (Figure 6.4 and Figure 6.5) in a majority of samples. In the TOL and BEN SOA at pH 3 and 6 and XYL at pH 3, the trace at 532 nm also decreases significantly. These observations indicate that as these SOA in the atmosphere are exposed to sunlight, their radiative forcing will diminish.

Figure 6.4: Kinetics plots for samples photolyzed at pH 3 (panels: A – BEN SOA, B – TOL SOA, C – XYL SOA, D – NAP SOA) showing the effect of UV radiation on relative absorption coefficients (normalized to zero time) at 260, 365, 405, and 532 nm. The 532 nm trace is noisier than the rest of the traces because the absorption coefficient at this wavelength is small.
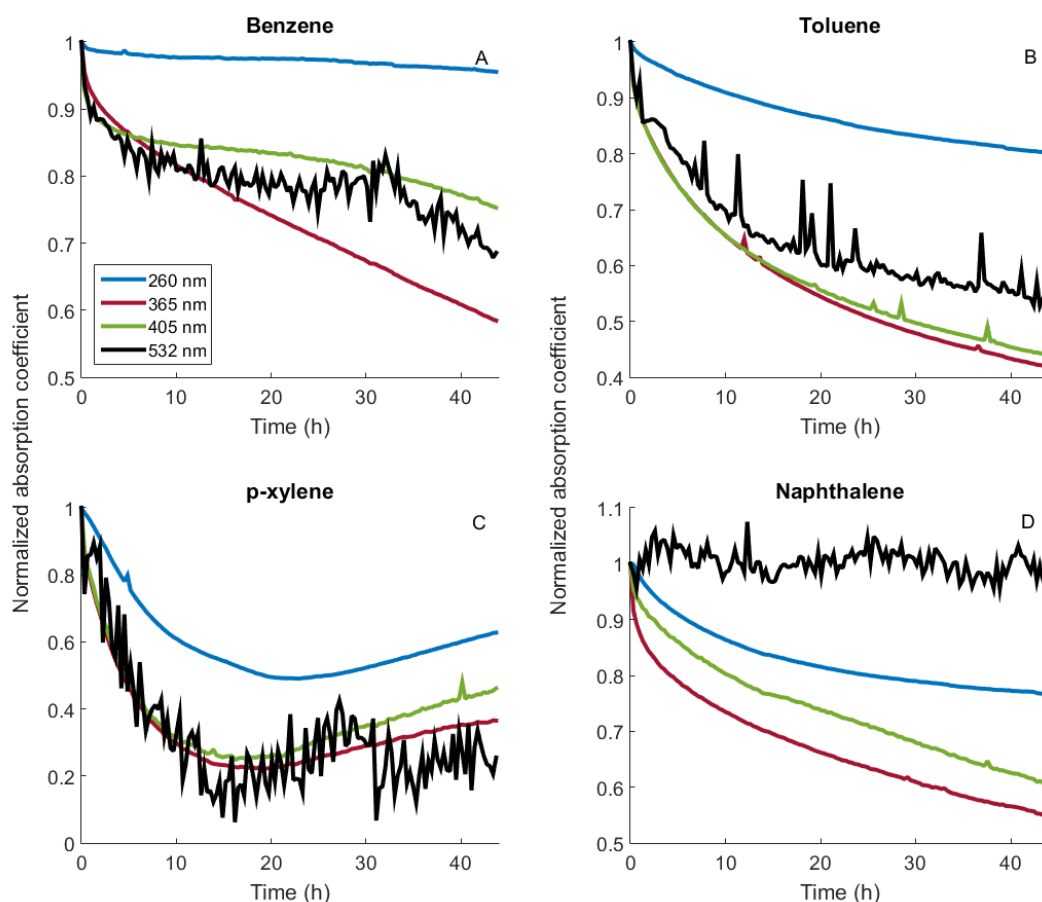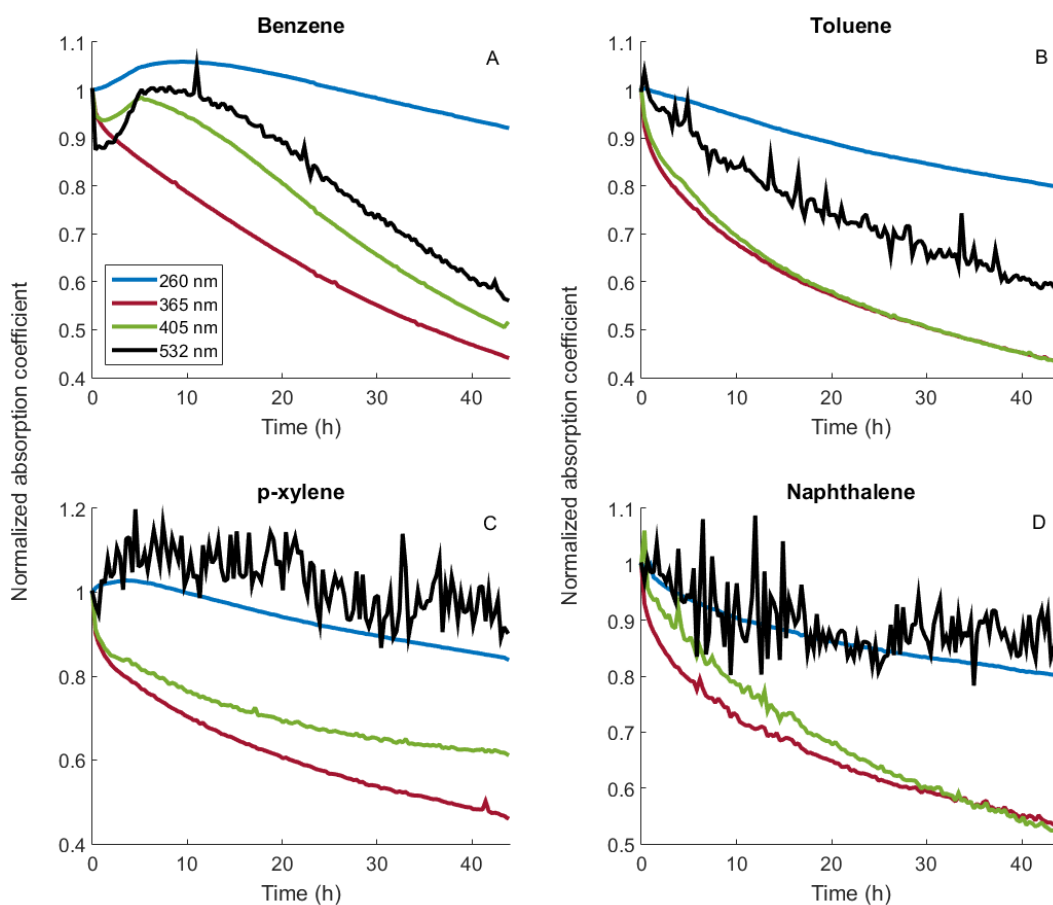
Figure 6.5: Kinetics plots for samples photolyzed at pH 6 (panels: A – BEN SOA, B – TOL SOA, C – XYL SOA, D – NAP SOA) showing the effect of UV radiation on relative absorption coefficients (normalized to zero time) at 260, 365, 405, and 532 nm.

6.4.2. Effect of Photolysis on Excitation-Emission Matrix Spectra

Figure 6.6 to Figure 6.9 show the EEM data for all four SOA samples irradiated at both pH 3 and 6 for 44 hours. Unlike the reduction in the visible absorption coefficient across all SOA samples, the fluorescence intensity decreased for some excitation-emission wavelength pairs but increased for others. Increases in fluorescence may indicate the formation of new fluorophores or the loss of quenching compounds/moieties, leading to a higher observed quantum yield of fluorescence.[50] There were also small differences between samples irradiated at pH 3 and pH 6, but again, the differences were not uniform amongst the four SOA samples.

BEN SOA displayed two distinct peaks in the EEM spectrum at ex/em = 220/430 and 320/430 at both pH 3 (Figure 6.6a) and pH 6 (Figure 6.6d). After the irradiation, there was a broad region around 220-300/400 nm where the fluorescence increased. This region showed no distinct peaks when irradiated at pH 3 (Figure 6.6c), but irradiation at pH 6 resulted in the increase of a more defined peak centered around 300/400 nm (Figure 6.6f). Fluorescence decreased at both pH 3 and pH 6 centered at 375/450 nm, similar to component C4 in Timko *et al.* (2015a), generally attributed to terrestrial humic-like components of CDOM. [2, 4, 5] The rate of fluorescence loss increased with pH, similar to previous reports on terrestrial CDOM.[7]

Figure 6.6: Fluorescence data for BEN SOA sample before (A and D) and after (B and E) 44 h of irradiation at pH 3 (top) and pH 6 (bottom), as well as the overall change in fluorescence (C and F). Common CDOM peaks listed in Table 6.1 are labeled with boxes in subfigure C.

The EEM spectra of TOL SOA shown in Figure 6.7a for pH 3 and Figure 6.7d for pH 6 were similar to those of BEN SOA before the irradiation. However, the EEM spectra after

irradiation showed greater change at pH 6 than at pH 3. There was a large increase in

fluorescence intensity at 250/325 nm at pH 6, but almost no change at pH 3. The fluorescence

decreased at 220/450 and at 330/450 nm, and the decrease was stronger in the pH 6 sample.

While the peak at 250/325 nm is often attributed to autochthonous sources when found in

CDOM, small aromatic molecules such as p-cresol fluoresce in this region.[5, 39, 51] The longer-

wavelength peaks that decreased during irradiation were similar to the decreasing terrestrial

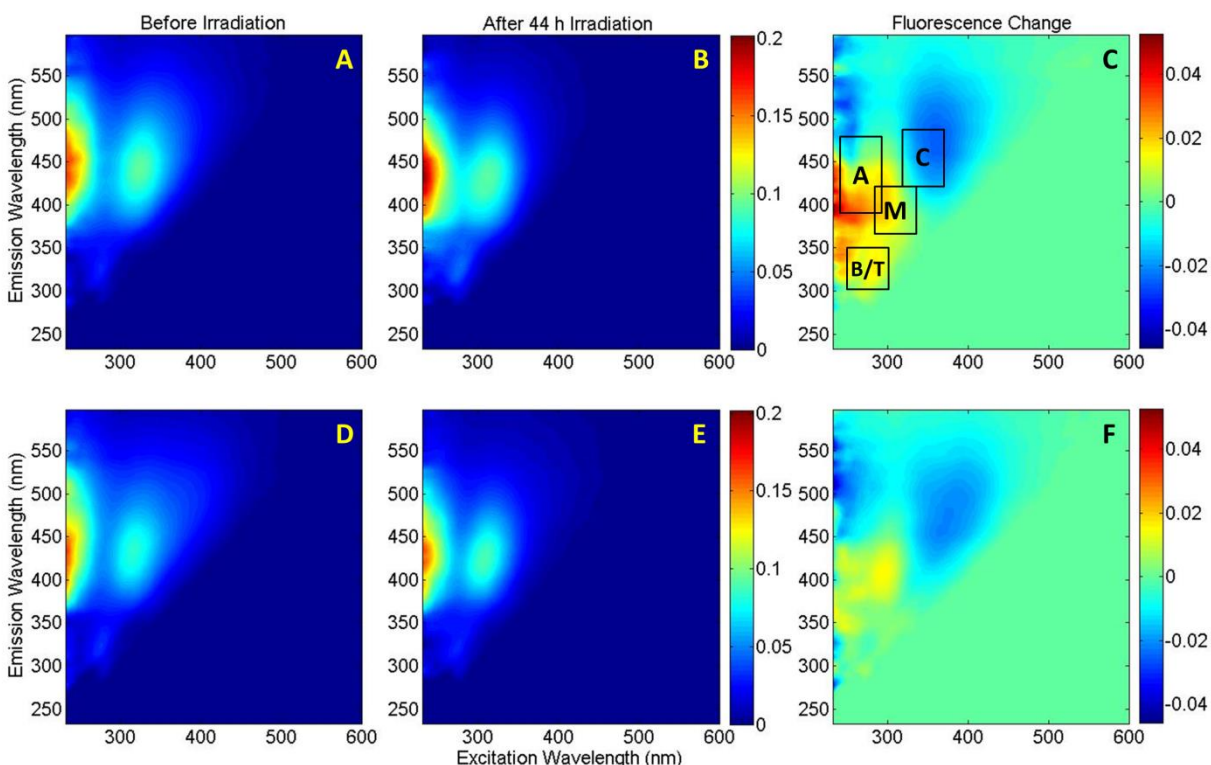humic-like peaks seen in the BEN SOA.

Figure 6.7: Fluorescence data for TOL SOA sample before (A and D) and after (B and E) 44 h of irradiation at pH 3 (top) and pH 6 (bottom), as well as the overall change in fluorescence (C and F). Common CDOM peaks listed in Table 6.1 are labeled with boxes in subfigure C.

The initial EEM spectra of XYL SOA shown in Figure 6.8a and Figure 6.8d were also

similar to the corresponding spectra of BEN SOA and TOL SOA. However the effect of

irradiation on the EEM spectrum of XYL SOA was considerably stronger, with fluorescence

decreasing by more than a factor of two at some fluorescence wavelengths. This is a little easier to see in one dimensional fluorescence spectra at ex =250 nm and 330 nm shown in Figure 6.10 and Figure 6.11, respectively. The EEM peak at 220/325 nm had a minimal increase at pH 6, but decreased at pH 3. XYL SOA also has peaks that decrease in intensity centered at 220/450 nm and 330/450 nm at both pH values. These are once again terrestrial humic-like peaks, which fall in the photo-labile region.[2, 7]
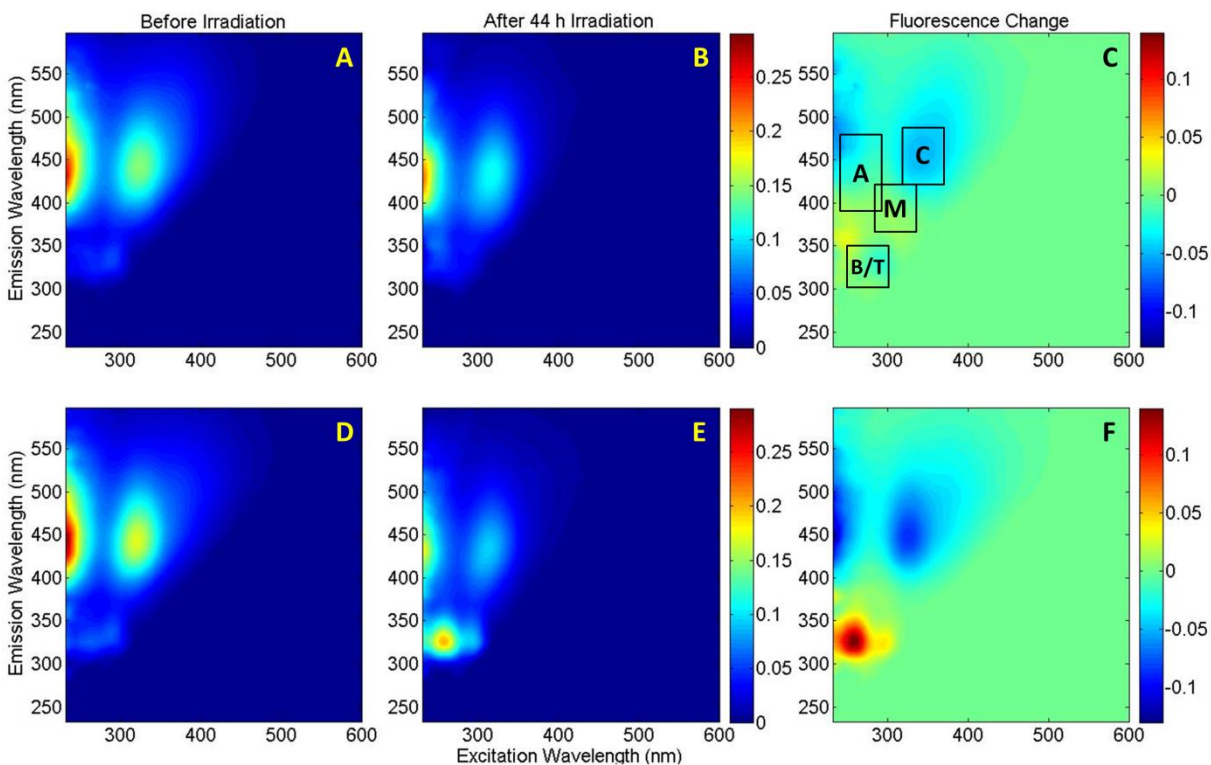

Figure 6.8: Fluorescence data for XYL SOA sample before (A and D) and after (B and E) 44 h of irradiation at pH 3 (top) and pH 6 (bottom), as well as the overall change in fluorescence (C and F). Common CDOM peaks listed in Table 6.1 are labeled with boxes in subfigure C.

Fluorescence of the NAP SOA samples was quite different from that in BEN, XYL, and TOL samples. The maximum fluorescence intensity was greater for NAP SOA than for the rest of the SOA samples. The spectrum was dominated by a strong peak at 220/300 nm, characteristic of low molecular weight aromatic compounds (Figure 6.9). This peak increased in intensity by

~50% during irradiation, with a greater fluorescence increase at pH 3 than pH 6. There were two weaker peaks at 275/300 nm and 310/430 nm both of which showed similar increases of ~50% in intensity. Lee *et al*. (2014)[16] recorded an EEM spectrum of NAP SOA at a higher solution concentration, and they only reported the 310/430 nm peak, which also increased in intensity after UV irradiation.
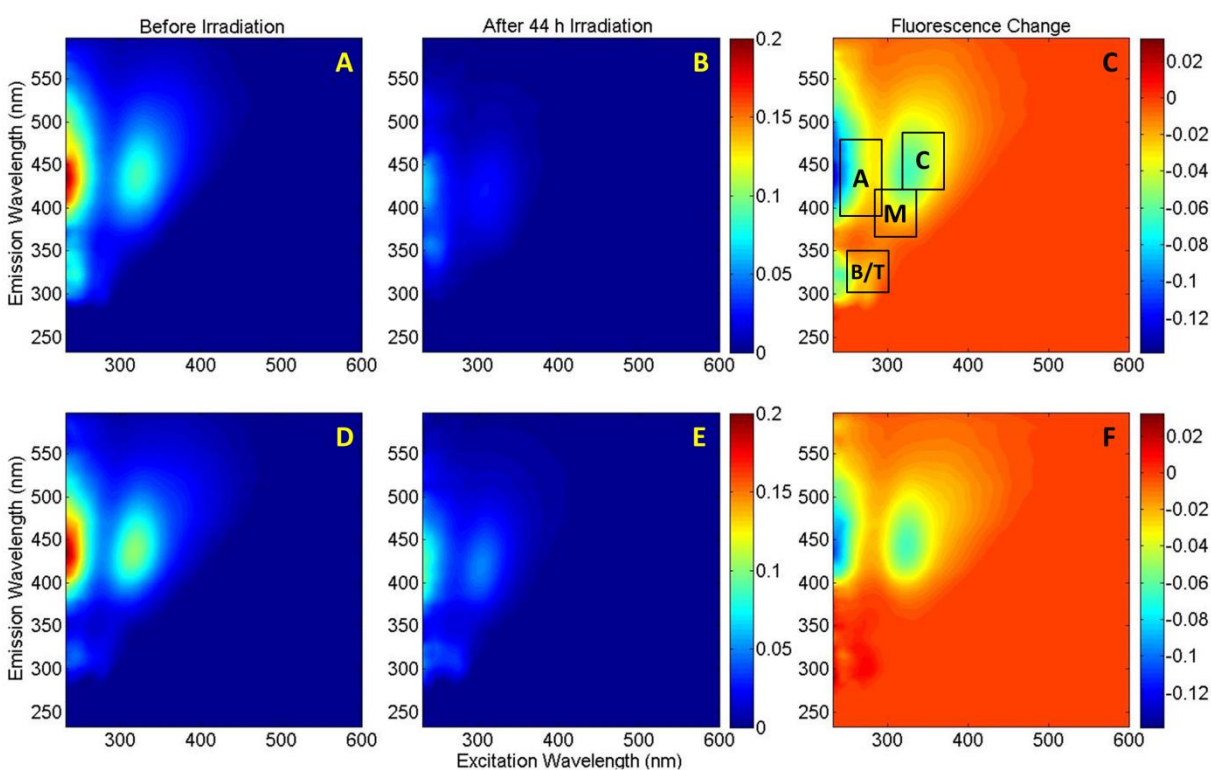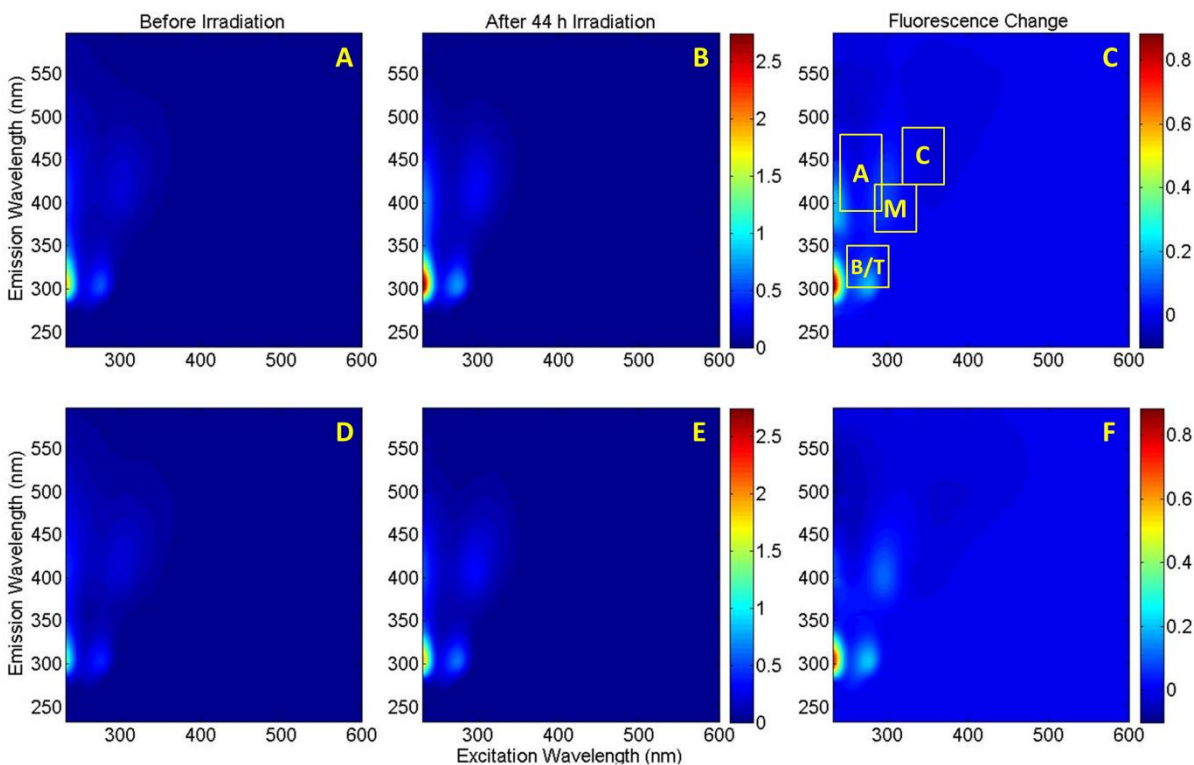

Figure 6.9: Fluorescence data for NAP SOA sample before (A and D) and after (B and E) 44 h of irradiation at pH 3 (top) and pH 6 (bottom), as well as the overall change in fluorescence (C and F). Common CDOM peaks listed in Table 6.1 are labeled with boxes in subfigure C.
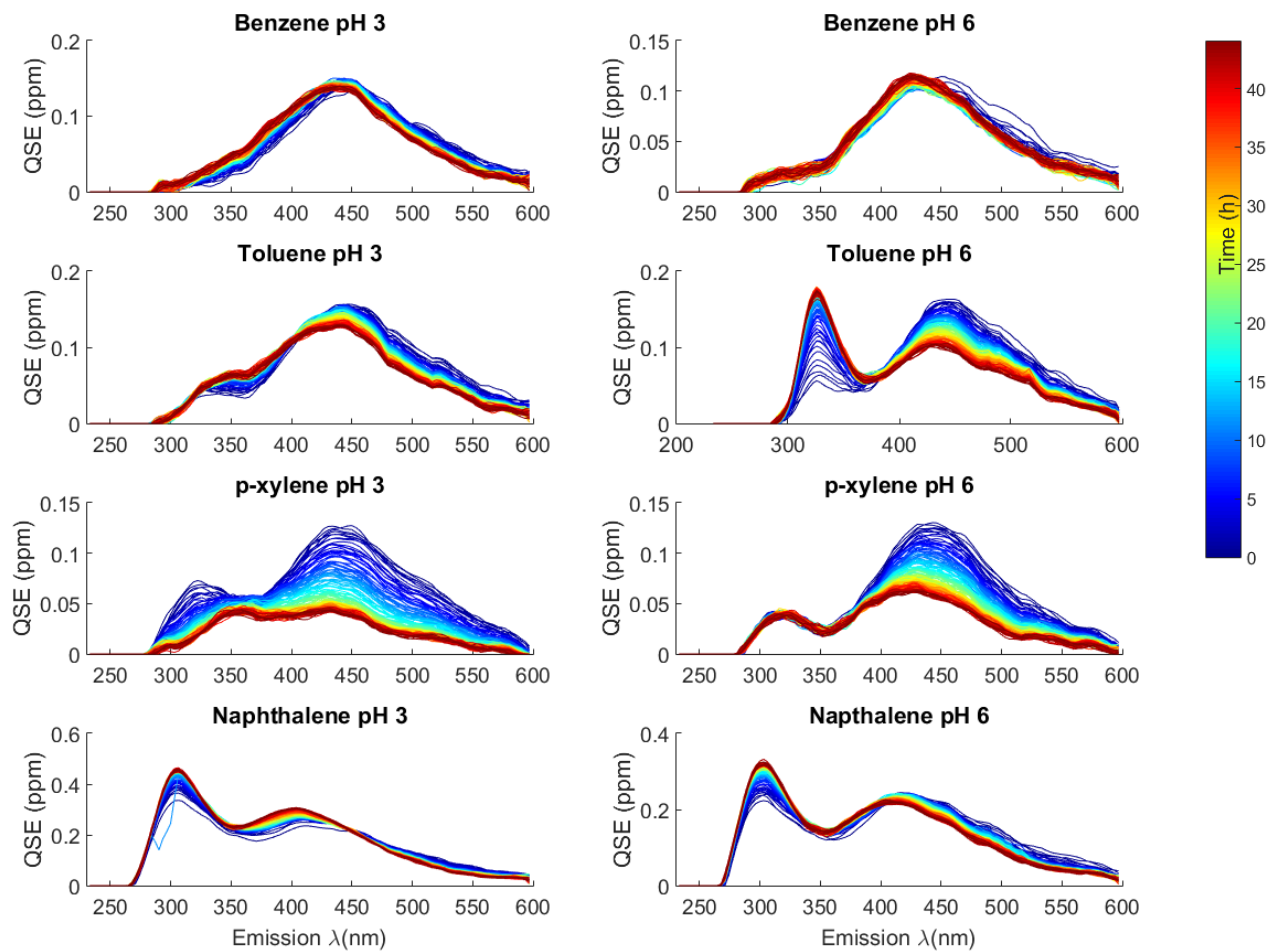
Figure 6.10: Fluorescence spectra at λ_{ex} = 250 nm. Plots shown for each SOA sample at pH 3 (left) and pH 6 (right). The excitation wavelength chosen for this plot (λ_{ex} = 330 nm) corresponds to one of the observed maxima in the EEM spectra (Figure 6.6 to Figure 6.9).
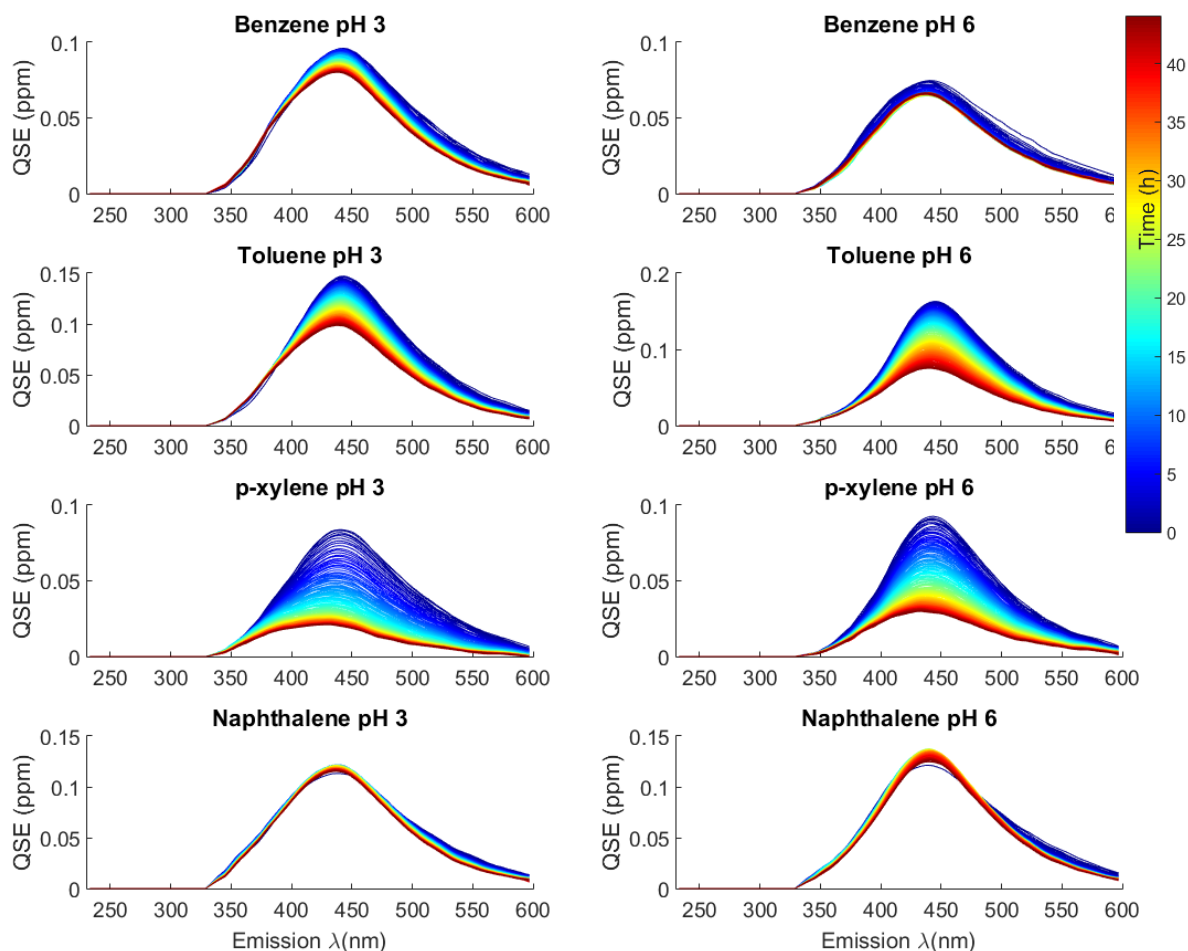
Figure 6.11: Fluorescence spectra at λ_{ex} = 330 nm. Plots shown for each SOA sample at pH 3 (left) and pH 6 (right). The excitation wavelength chosen for this plot (λ_{ex} = 330 nm) corresponds to one of the observed maxima in the EEM spectra (Figure 6.6 to Figure 6.9).

Although the fluorescence intensity changes are not as consistent as the absorption coefficient change, there is a decrease for all samples in the 325-375 nm excitation and 425-475 nm emission range, which corresponds to the C peak, often attributed to terrestrial humic-like components of CDOM in natural water samples.[4, 5] Chen *et al.* (2016) found that water soluble organic material found in aerosols tend to fluoresce in this region when the species are highly oxygenated with terrestrial and marine origins.[52] Duarte *et al.* (2004) also produced EEMs of water soluble organic components in aerosols that were similar to those produced for BrC formed by BEN SOA, TOL SOA, and XYL SOA, although the peaks were slightly shifted.[27]

This component was found to be photo-labile, as seen in the decrease in fluorescence intensity here and in component C4 in Timko *et al*. (2015a).[2] Additionally, Yamashita *et al.* (2015) found that there is a strong correlation between lignin derived phenols and this peak.[53] Therefore, nitrophenols responsible for the pH dependence seen in absorption coefficient may also be responsible for the decrease in fluorescence at this peak.

The difference in the location of fluorescence peaks and their response to irradiation shows that, although all of these samples are considered to be types of BrC SOA, each precursor produces compounds with different fluorescent properties. Overall, BrC SOA samples seem to have similar characteristics to CDOM found in fresh water with contributions from terrestrial plant material. Additionally, TOL, XYL, and NAP SOA all showed fluorescence changes in the UVA (320 to 400 nm) portion of the EEM. While peaks in this region are often associated with autochthonous, protein-like material due to the fluorescence of tryptophan and tyrosine, fluorescence changes in these samples are more likely the result of production/destruction of small aromatic molecules.[39]

Information about the fluorescence apparent quantum yield (AQY) for BrC aerosols is important for understanding the effect of BrC on climate. If BrC compounds fluoresce with high efficiency only a fraction of the absorbed radiative energy will be converted into heat, diminishing the heating effect of BrC. At the present time, only a few studies reported AQY for BrC. For example, Lee *et al*. (2014) reported AQY of 0.2% for BrC produced from photooxidation of NAP SOA and 2% for BrC from the methyl glyoxal and ammonium sulfate reaction.[16] Using the fluorescence data in Figure 6.6 to Figure 6.9, the change in AQY over the 44 hour irradiation period was calculated and plotted in Figure 6.12. In all of the SOA samples, both the initial AQY and photo-induced changes are wavelength- and pH-dependent. For

example, for TOL SOA at pH=3, AQY grows with photolysis below 350 nm, but is reduced above 350 nm. However, for all of these SOA samples, the AQY values are generally quite small, with the peak value of 4% for XYL SOA. This means that fluorescence by this type of BrC is not likely to affect the radiative forcing by aerosols because most of the absorbed solar energy will not be re-radiated but available for heating the atmosphere.

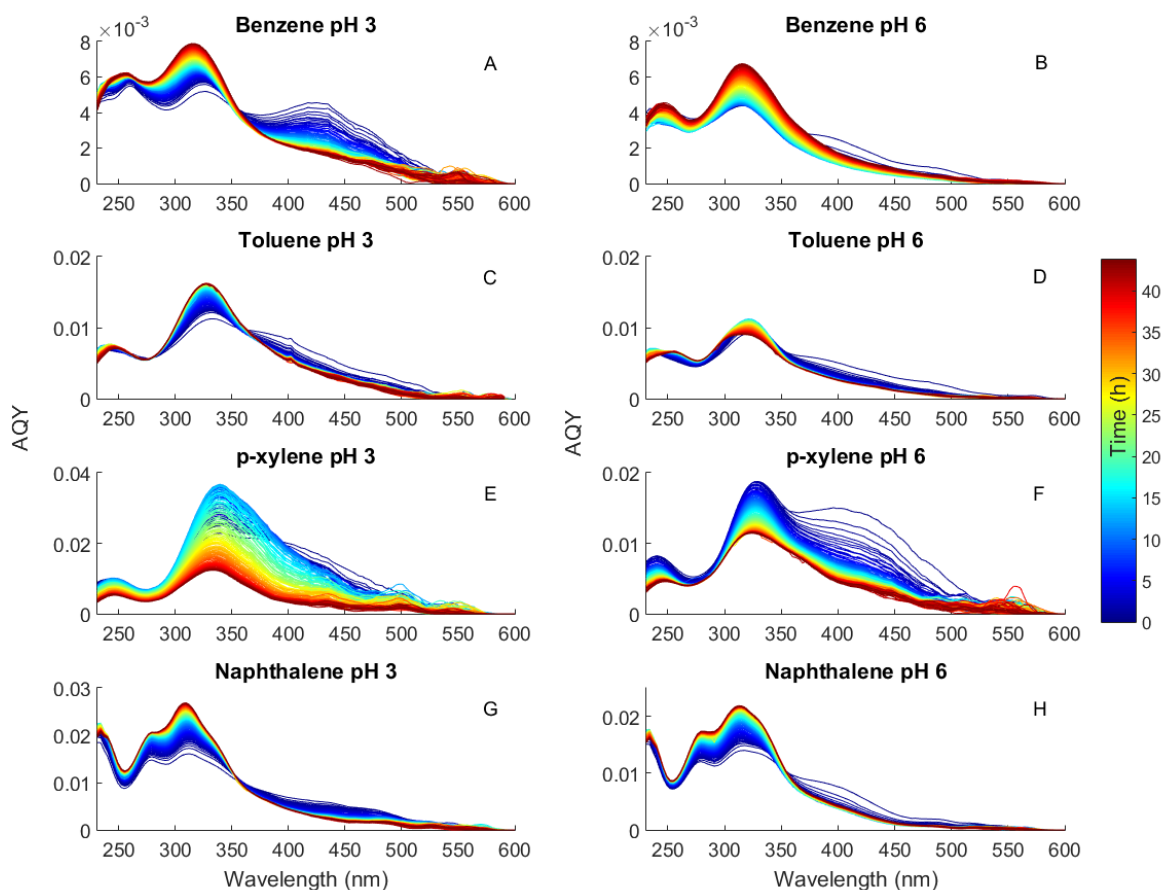**Figure 6.12:** Plots showing the change in apparent quantum yield (AQY) for each SOA sample (BEN SOA – A and B, TOL SOA – C and D, XYL SOA – E and F, and NAP SOA – G and H) over the course of 44 hours at pH 3 (left) and pH 6 (right).

6.5. Conclusions

In this study we examined how the absorption coefficient and fluorescence spectra of BrC aerosols prepared by high-NOx photooxidation of common aromatic compounds are

190

affected by solar radiation. The aqueous extracts of SOA prepared from benzene, toluene, p-xylene, and naphthalene were found to absorb radiation in the near-UV and visible ranges of the spectrum. The absorption coefficients depended on the solution pH, with the solutions at pH 6 (representative of cloud water) absorbing stronger than solutions at pH 3 (representative of aerosol and polluted fog water). The change in the absorption coefficient with pH is due to the acid-base ionization equilibria of phenols, which have very different absorption spectra in ionized and non-ionized forms. The absorption coefficients were reduced upon exposure to solar irradiation, especially at visible wavelengths. The photolysis-induced changes in the absorption coefficient and fluorescence spectra mean that the climate effect of these types of BrC SOA will be evolving as the aerosols are aging in the atmosphere. Variations in fluorescence intensity were also observed in several regions of EEM spectra for all four SOA samples. The apparent fluorescence quantum yield was small, of the order of a few percent, which is in agreement to previous fluorescence quantum yield measurements. This indicates that fluorescence is not likely to affect the strength of radiative forcing by this type of BrC. Lastly, the EEM spectra of BrC could be related to EEM spectra of CDOM found in different water systems. The humic characteristics of BrC SOA appeared to be similar to the organic matter found in fresh water with contributions from terrestrial plants. This suggests that deposition of BrC into water systems could contribute to the pool of CDOM in fresh water.

6.6. References

1.   Sharpless, C. M.; Blough, N. V., The importance of charge-transfer interactions in determining chromophoric dissolved organic matter (CDOM) optical and photochemical properties. *Environ. Sci.: Processes Impacts* **2014,** *16*, 654-71.

2.   Timko, S. A.; Maydanov, A.; Pittelli, S. L.; Conte, M. H.; Cooper, W. J.; Koch, B. P.; Schmitt-Kopplin, P.; Gonsior, M., Depth-dependent photodegradation of marine dissolved organic matter. *Front. Mar. Sci.* **2015a,** *2*, (66), 1-13.

3.   Hudson, N.; Baker, A.; Reynolds, D., Fluorescence analysis of dissolved organic matter in natural, waste and polluted waters-a review. *River Res. Applic.* **2007,** *23*, (6), 631-49.

4.   Coble, P. G., Characterization of marine and terrestrial DOM in seawater using excitation-emission matrix spectroscopy. *Mar. Chem.* **1996,** *51*, (4), 325-46.

5.   Coble, P. G., Marine optical biogeochemistry: The chemistry of ocean color. *Chem. Rev.* **2007,** *107*, (2), 402-18.

6.   Zhao, Z.; Gonsior, M.; Luek, J.; Timko, S.; Ianiri, H.; Hertkorn, N.; Schmitt-Kopplin, P.; Fang, X.; Zeng, Q.; Jiao, N.; Chen, F., Picocyanobacteria and deep-ocean fluorescent dissolved organic matter share similar optical properties. *Nat. Commun.* **2017,** *8*, 15284, 10.1038/ncomms15284.

7.   Timko, S. A.; Gonsior, M.; Cooper, W. J., Influence of pH on fluorescent dissolved organic matter photo-degradation. *Water Res.* **2015b,** *85*, 266-74.

8.   Pinnick, R. G. E.; Frernandez, E.; Rosen, J. M.; Hill, S. C.; Wang, Y.; Pan, Y. L., Fluorescence spectra and elastic scattering characteristics of atmospheric aerosol in Las Cruces, New Mexico, USA: Variability of concentrations and possible constituents and sources of particles in various spectral clusters. *Atmos. Environ.* **2013,** *65*, 195-204.

9.   Matos, J. T.; Freire, S. M.; Duarte, R. M.; Duarte, A. C., Natural organic matter in urban aerosols: Comparison between water and alkaline soluble components using excitation–emission matrix fluorescence spectroscopy and multiway data analysis. *Atmos. Environ.* **2015,** *102*, 1-10.

10.   Hawkins, L. N.; Lemire, A. N.; Galloway, M. M.; Corrigan, A. L.; Turley, J. J.; Espelien, B. M.; De Haan, D. O., Maillard chemistry in clouds and aqueous aerosol as a source of atmospheric humic-like substances, . *Enviro. Sci. Technol.* **2016,** *50*, (14), 7443-52.

11.   Phillips, S. M.; Smith, G. D., Light absorption by charge transfer complexes in brown carbon aerosols. *Environ. Sci. Technol. Lett.* **2014,** *1*, (10), 382-86.

12.   Phillips, S. M.; Smith, G. D., Further evidence for charge transfer complexes in brown carbon aerosols from excitation–emission matrix fluorescence spectroscopy. *J. Phys. Chem. A* **2015,** *119*, (19), 4545-51.

13.   Lee, H. J.; Laskin, A.; Laskin, J.; Nizkorodov, S. A., Excitation-emission spectra and fluorescence quantum yields for fresh and aged biogenic secondary organic aerosols. *Enviro. Sci. Technol.* **2013,** *47*, (11), 5763-70.

14.   Pöhlker, C. J.; Huffman, J. A.; Pöschl, U., Autofluorescence of atmospheric bioaerosols – fluorescent biomolecules and potential interferences. *Atmos. Meas. Tech.* **2012,** *5*, 37-71.

15.   Laskin, A.; Laskin, J.; Nizkorodov, S. A., Chemistry of atmospheric brown carbon. *Chem. Rev.* **2015,** *115*, 4335-82.

16.   Lee, H. J.; Aiona, P. K.; Laskin, A.; Laskin, J.; Nizkorodov, S. A., Effect of solar radiation on the optical properties and molecular composition of laboratory proxies of atmospheric brown carbon. *Enviro. Sci. Technol.* **2014,** *48*, 10217-26.

17.   Liu, J. M.; Lin, P.; Laskin, A.; Laskin, J.; Kathmann, S. M.; Wise, M.; Caylor, R.; Imholt, F.; Selimovic, V.; Shilling, J. E., Optical properties and aging of light-absorbing secondary organic aerosol. *Atmos. Chem. Phys.* **2016,** *16*, (19), 12815-27.

18.   Romonosky, D. E.; Ali, N. N.; Saiduddin, M. N.; Wu, M.; Lee, H. J.; Aiona, P. K.; Nizkorodov, S. A., Effective absorption cross sections and photolysis rates of anthropogenic and biogenic secondary organic aerosols. *Atmos. Environ.* **2016,** *130*, 172-79.

19.   Montoya-Aguilera, J.; Horne, J. R.; Hinks, M. L.; Fleming, L. T.; Perraud, V.; Lin, P.; Laskin, A.; Laskin, J.; Dabdub, D.; Nizkorodov, S. A., Secondary organic aerosol from atmospheric photooxidation of indole. *Atmos. Chem. Phys.* **2017,** *17*, 11605-21.

20.   Smith, J. D.; Kinney, H.; Anastasio, C., Phenolic carbonyls undergo rapid aqueous photodegradation to form low-volatility, light-absorbing products. *Atmos. Environ.* **2016,** *126*, 36-44.

21.   Chang, J. L.; Thompson, J. E., Characterization of colored products formed during irradiation of aqueous solutions containing H_2O_2 and phenolic compounds. *Atmos. Environ.* **2010,** *44*, (4), 541-51.

22.   Gelencser, A.; Hoffer, A.; Kiss, G.; Tombacz, E.; Kurdi, R.; Bencze, L., In-situ formation of light-absorbing organic matter in cloud water. *J. Atmos. Chem.* **2003,** *45*, (1), 25-33.

23.   Kampf, C. J.; Filippi, A.; Zuth, C.; Hoffmann, T.; Opatz, T., Secondary brown carbon formation via the dicarbonyl imine pathway: nitrogen heterocycle formation and synergistic effects. *Phys. Chem. Chem. Phys.* **2016,** *18*, (27), 18353-64.

24.   Lin, Y. H.; Budisulistiorini, S. H.; Chu, K.; Siejack, R. A.; Zhang, H.; Riva, M.; Zhang, Z.; Gold, A.; Kautzman, K. E.; Surratt, J. D., Light-absorbing oligomer formation in secondary organic aerosol from reactive uptake of isoprene epoxydiols. *Enviro. Sci. Technol.* **2014,** *48*, (20), 12012-21.

25.   De Haan, D. O.; Hawkins, L. N.; Welsh, H. G.; Pednekar, R.; Casar, J. R.; Pennington, E. A.; de Loera, A.; Jimenez, N. G.; Symons, M. A.; Zauscher, M. D.; Pajunoja, A., Brown carbon production in ammonium-or amine-containing aerosol particles by reactive uptake of methylglyoxal and photolytic cloud cycling. *Enviro. Sci. Technol.* **2017,** *51*, (13), 7458-66.

26.   Kroll, J. H.; Ng, N. L.; Murphy, S. M.; Varutbangkul, V.; Flagan, R. C.; Seinfeld, J. H., Chamber studies of secondary organic aerosol growth by reactive uptake of simple carbonyl compounds. *J. Geophys. Res.: Atmos.* **2005,** *110*, (D23, 10.1029/2005JD006004).

27.   Duarte, R. M.; Pio, C. A.; Duarte, A. C., Synchronous scan and excitation-emission matrix fluorescence spectroscopy of water-soluble organic compounds in atmospheric aerosols. *J. Atmos. Chem.* **2004,** *48*, (2), 157-71.

28.   Bones, D. L.; Henricksen, D. K.; Mang, S. A.; Gonsior, M.; Bateman, A. P.; Nguyen, T. B.; Cooper, W. J.; Nizkorodov, S. A., Appearance of strong absorbers and fluorophores in limonene-O_3 secondary organic aerosol due to NH_4^+-mediated chemical again over long time scales. *J. Geophys. Res.* **2010,** *115*, D05203, 10.1029/2009JD012864.

29.   Graber, E. R.; Rudich, Y., Atmospheric HULIS: How humic-like are they? A comprehensive and critical review. *Atmos. Chem. Phys.* **2006,** *6*, 729-53.

30.   Limbeck, A.; Kulmala, M.; Puxbaum, H., Secondary organic aerosol formation in the atmosphere via heterogeneous reaction of gaseous isoprene on acidic particles. *Geophys. Res. Lett.* **2003,** *30*, (19), 1996, 10.1029/2003GL017738.

31.   Mukai, H.; Ambe, Y., Characterization of a humic acid-like brown substance in airborne particulate matter and tentative identification of its origin. *Atmos. Environ.* **1986,** *20*, 813-19.

32.   Zappoli, S.; Andracchio, A.; Fuzzi, S.; Facchini, M. C.; Gelencser, A.; Kiss, G.; Krivacsy, Z.; Molnar, A.; Meszaros, E.; Hansson, H. C.; Rosman, K.; Zebuhr, Y., Inorganic, organic and macromolecular components of fine aerosol in different areas of Europe in relation to their water solubility. *Atmos. Environ.* **1999,** *33*, (17), 2733-43.

33.   Santos, P. S.; Otero, M.; Duarte, R. M.; Duarte, A. C., Spectroscopic characterization of dissolved organic matter isolated from rainwater. *Chemosphere* **2009,** *74*, (8), 1053-61.

34.   Aiona, P. K.; Lee, H. J.; Leslie, R.; Lin, P.; Laskin, A.; Laskin, J.; Nizkorodov, S. A., Photochemistry of products of the aqueous reaction of methylglyoxal with ammonium sulfate. *ACS Earth Space Chem.* **2017,** *1*, 522-32.

35.   Zhong, M.; Jang, M., Dynamic light absorption of biomass-burning organic carbon photochemically aged under natural sunlight. *Atmos. Chem. Phys.* **2014,** *14*, 1517-25.

36.   Herrmann, H.; Schaefer, T.; Tilgner, A.; Styler, S. A.; Weller, C.; Teich, M.; Otto, T., Tropospheric Aqueous-Phase Chemistry: Kinetics, Mechanisms, and Its Coupling to a Changing Gas Phase. *Chem. Rev.* **2015,** *115*, 4259-334.

37.   Zepp, R. G.; Sheldon, W. M.; Moran, M. A., Dissolved organic fluorophores in southeastern US coastal waters: correction method for eliminating Rayleigh and Raman scattering peaks in excitation-emission matrices. *Mar. Chem.* **2004,** *89*, (1-4), 15-36.

38.   Brouwer, A. M., Standards for photoluminescence quantum yield measurements in solution (IUPAC Technical Report)*. *Pure Appl. Chem.* **2011,** *83*, (12), 2213-28.

39.   Wünsch, U. J.; Murphy, K. R.; Stedmon, C. A., Fluorescence quantum yields of natural organic matter and organic compounds: Implications for the fluorescence-based interpretation of organic matter composition. *Front. Mar. Sci.* **2015,** *2*, (98), 1-15.

40.   Vione, D.; Maurino, V.; Minero, C.; Duncianu, M.; Olariu, R. I.; Arsene, C.; Sarakha, M.; Mailhot, G., Assessing the transformation kinetics of 2- and 4-nitrophenol in the atmospheric aqueous phase.Implications for the distribution of both nitroisomers in the atmosphere. *Atmos. Environ.* **2009,** *43*, (14), 2321-27.

41.   Biggs, A. I., A spectrophotometric determination of the dissociation constants of p-nitrophenol andpapaverine. *Trans. Faraday Soc.* **1954,** *50*, 800-02.

42.   Hayon, E.; Ibata, T.; Lichtin, N. N.; Simic, M., Electron and hydrogen atom attachment to aromaticcarbonyl compounds in aqueous solution. Absorption spectra and dissociation constants of ketylradicals. *J. Phys. Chem.* **1972,** *76*, (15), 2072-78.

43.   Zhu, D.; Hyun, S.; Pignatello, J. J.; Lee, L. S., Evidence for $\pi-\pi$ electron donor$-$acceptor interactionsbetween π-donor aromatic compounds and π-acceptor sites in soil organic matter through pH effectson sorption. *Enviro. Sci. Technol.* **2004,** *38*, (16), 4361-68.

44.   Laws, W. R.; Brand, L., Analysis of two-state excited-state reactions. The fluorescence decay of 2-naphthol. *J. Phys. Chem.* **1979,** *83*, (7), 795-802.

45.   van Stam, J.; Lofroth, J. E., The protolysis of singlet excited beta-naphthol: A two-day laboratoryexperiment to introduce photophysics. *J. Chem. Educ.* **1986,** *63*, (2), 181-84.

46.   Marinoni, A.; Parazols, M.; Brigante, M.; Deguillaume, L.; Amato, P.; Delort, A. M.; Laj, P.; Mailhot, G., Hydrogen peroxide in natural cloud water: Sources and photoreactivity. *Atmos. Res.* **2011,** *101*, (1-2), 256-63.

47.   Brantner, B.; Fierlinger, H.; Puxbaum, H.; Berner, A., Cloudwater chemistry in the subcooled dropletregime at Mount Sonnblick (3106 M A.S.L., Salzburg, Austria). *Water, Air, Soil Pollut.* **1994,** *74*, (3-4), 363-84.

48.   Zhao, R. A.; Lee, K. Y.; Huang, L.; Li, X.; Yang, F.; Abbatt, J. P. D., Photochemical processing of aqueous atmospheric brown carbon. *Atmos. Chem. Phys.* **2015,** *15*, 6087-100.

49.   Yuan, J. F.; Huang, X. F.; Cao, L. M.; Cui, J.; Zhu, Q.; Huang, C. N.; Lan, Z. J.; He, L. Y., Light absorption of brown carbon aerosol in the PRD region of China. *Atmos. Chem. Phys.* **2016,** *16*, 1433-43.

50.   Wang, Z.; Cao, J.; Meng, F., Interactions between protein-like and humic-like components in dissolved organic matter revealed by fluorescence quenching. *Water Res.* **2015,** *68*, 404-13.

51.   Stedmon, C. A.; Nelson, N. B., The Optical Properties of DOM in the Ocean. In *Biogeochemistry of Marine Dissolved Organic Matter* Hansell, D. A.; Carlson, C. A., Eds. Academic Press: New York, 2015; pp 481-508.

52.   Chen, Q.; Miyazaki, Y.; Kawamura, K.; Matsumoto, K.; Coburn, S.; Volkamer, R.; Iwamoto, Y.; Kagami, S.; Deng, Y.; Ogawa, S.; Ramasamy, S.; Kato, S.; Ida, A.; Kajii, Y.; Mochida, M., Characterization of chromophoric water-soluble organic matter in urban, forest, and marine aerosols by HR-ToF-AMS analysis and excitation−emission matrix spectroscopy. *Enviro. Sci. Technol.* **2016,** *50*, 10351-60.

53.   Yamashita, Y.; Fichot, C. G.; Shen, Y.; Jaffé, R.; Benner, R., Linkages among fluorescent dissolved organic matter, dissolved amino acids and lignin-derived phenols in a river-influenced ocean margin. *Front. Mar. Sci.* **2015,** *2*, (92), 1-14.